Towards a GIS-based Multiscale Visibility Assessment Method for Solar Urban Planning

PAR

Pietro FLORIO

ÉCOLE POLYTECHNIQUE
FÉDÉRALE DE LAUSANNE

Suisse
2018

Acknowledgements

I am extremely grateful to the numerous people who made the completion of this PhD thesis possible and to the institutions providing funding and exchange opportunities:

Keywords

Solar energy

Urban planning

Visibility

Visual impact assessment

BIPV

Building integrated solar technologies

Architectural integration of renewables

Résumé

On constate dans les zones urbaines une recrudescence des technologies solaires thermiques et photovoltaïques sur l'enveloppe des bâtiments, qui comprend à la fois des toitures et des façades, conséquence de la Stratégie Énergétique 2050. Cette transformation du parc immobilier s'opère souvent sans considération pour la qualité d'intégration architecturale, souhaitable dans un contexte urbain donné, dépendant de sa sensibilité socio-culturelle propre et de la visibilité des installations solaires depuis l'espace public. Visibilité et impact visuel se sont révélés être des facteurs décisionnels récurrents dans le domaine de la planification territoriale, du fait de leurs implications pratiques sur la promotion touristique et immobilière, le confort urbain, l'orientation, la sensation de sécurité et la publicité.

La notion de visibilité est explorée du point de vue physique et psycho-physiologique, plusieurs indicateurs quantitatifs ayant été suggérés et testés dans le cadre de ce travail. L'objectif est de fournir une méthodologie applicable à toutes échelles, centrée sur l'évaluation de la visibilité des surfaces d'enveloppe de bâtiments dans les zones urbaines, qui pourraient être recouvertes de modules solaires. Un indice de visibilité a été développé dans le but d'inclure ce dernier dans une méthode de décision multicritères, allant de l'échelle territoriale jusqu'au niveau du quartier, de l'îlot ou d'un groupe de bâtiments. La thèse inclut l'évaluation de l'intérêt visuel du public au moyen de bases de photographies numériques participatives en ligne, qui complètent des paramètres géométriques typiques, tels que les « bassins visuels cumulatifs » et les angles solides. A chaque échelle, l'indice de visibilité est systématiquement superposé à une carte de sensibilité urbaine issue du plan d'affectation et à une représentation du potentiel de production d'énergie solaire, à un niveau de détail variable. Les résultats indiquent qu'il est possible d'employer des modules solaires intégrés aux bâtiments sans impact visuel significatif sur la perception publique. Dans les cas d'étude considérés en ville de Genève (Suisse), plus de 50 m^2 / bâtiment de surfaces non visibles sont disponibles pour la moitié des bâtiments, qui reçoivent une irradiation solaire suffisante pour justifier une installation viable économiquement. Les capteurs solaires thermiques ou photovoltaïques, installés essentiellement sur les surfaces à faible visibilité, pourraient produire près de 10% des besoins en chaleur ou la même fraction environ des besoins en électricité d'un quartier. Les surfaces faiblement visibles se situent, en majorité, dans des cours intérieures, loin de la rue ou dans des canyons urbains profonds ; en parallèle, beaucoup de surface visible reste disponible pour des rénovations solaires de qualité élevée, ayant un caractère exemplaire et/ou de démonstration.

Mots-clés : énergie solaire, planification urbaine, visibilité, impact visuel, BIPV, technologies solaires intégrées aux bâtiments, intégration architecturale des renouvelables

Sintesi

Le zone urbane sono dominate dallo sviluppo delle tecnologie solari termiche e fotovoltaiche sulle superfici esterne degli edifici, tra cui le coperture e le facciate, come conseguenza della Strategia Energetica 2050. Tale trasformazione si verifica spesso senza considerare la qualità d'integrazione architettonica esigibile in un contesto urbano specifico, che dipende dalla sua sensibilità socio-culturale e dalla visibilità degli impianti solari dallo spazio pubblico. Visibilità e impatto visivo si annoverano tra i fattori di decisione più ricorrenti nell'ambito della pianificazione territoriale, con le loro implicazioni pratiche tra cui la promozione turistica e immobiliare, il confort urbano, l'orientamento, la sensazione di sicurezza e la pubblicità.

La nozione di visibilità è esplorata da un punto di vista fisico e psico-fisiologico; diversi indicatori quantitativi sono descritti e testati in questa tesi. L'intento è di fornire una metodologia multi-scala, al fine di valutare la visibilità delle superfici d'involucro degli edifici in contesto urbano, che potrebbero accogliere un'installazione solare. Ci si propone di sviluppare un indice di visibilità da includere in un modello decisionale multi-criteri, dalla scala territoriale fino a quella del quartiere, dell'isolato o dell'insieme di edifici. La tesi presenta la stima dell'interesse visivo attraverso database fotografici partecipativi sul web, a completare parametri geometrici tipici come i "bacini visivi cumulativi" e gli angoli solidi. Ad ogni scala, l'indice di visibilità è sistematicamente sovrapposto ad una carta di sensibilità urbana ricavata dal piano regolatore e ad una rappresentazione del potenziale di generazione di energia solare, ad un livello di dettaglio variabile. I risultati indicano la possibilità di impiegare moduli solari integrati agli edifici, privi d'impatto significativo sulla percezione dallo spazio pubblico. Nei casi considerati nella città di Ginevra (Svizzera), la metà degli edifici dispone di più di 50 m² / edificio di superficie non visibile, caratterizzata contemporaneamente da un'irradiazione solare sufficiente per l'installazione di un impianto economicamente sostenibile. I moduli solari termici o fotovoltaici, installati unicamente sulla superficie a bassa visibilità, compenserebbero circa il 10% del fabbisogno termico o una frazione equivalente del fabbisogno elettrico di un quartiere. La superficie debolmente visibile si affaccia principalmente verso i cortili interni, lontano dalla strada oppure in corrispondenza dei "canyon urbani" profondi: parallelamente, una superficie visibile consistente rimane disponibile per un retrofit solare di qualità, dal carattere dimostrativo ed esemplare.

Parole chiave: energia solare, pianificazione urbana, visibilità, impatto visivo, BIPV, tecnologie solari integrate all'edificio, integrazione architettonica delle rinnovabili

Abstract

Urban areas are facing a growing deployment of solar photovoltaic and thermal technologies on building envelopes, both on roofs and on façades, essential for the realization of the Swiss Energy Strategy 2050. This process often occurs regardless of the desirable architectural integration quality in a given urban context, which depends on socio-cultural sensitivity and on the visibility of the solar modules from the public space. Visibility and visual impact are recurrent decisional factors in spatial planning processes, with practical implications including touristic and real estate promotion, outdoor human comfort, way finding, public feeling of security and advertisement.

In this thesis, the definition of visibility under a geometrical, physical and psycho-physiological perspective is explored, several quantitative indicators being described and tested. The objective is to provide a scale-dependent methodology to assess the visibility of building envelope surfaces exposed to solar radiation, which could host solar modules, in urban areas. A visibility index is determined for inclusion as a variable in a multi criteria method, covering areas from the strategic broad territorial scale to the district level, including neighborhoods and clusters of buildings. Accomplished research includes the estimation of public visual interest on the basis of crowd-sourced photographic databases, complementing geometry-based parameters such as cumulative viewsheds and solid angles. At each scale, the visibility index is systematically overlapped on an urban sensitivity layer issued from land use and on a spatial representation of the solar energy generation potential, at an variable level of detail. Results indicate that stakeholders can reasonably expect to employ building integrated solar systems without crucially affecting public perception. In the study area located in the city of Geneva (Switzerland), more than 50 m^2 / building of non-visible envelope surface receiving sufficient solar radiation for an economically viable solar refurbishment is available over half of the buildings. Solar thermal collectors or PV panels installed on scarcely visible surfaces, mainly situated in courtyards, far from the streets or in deep urban canyons, could cover about 10% of the annual heating demand or alternatively, the same share of electricity needs on a district basis. At the same time, plenty of highly visible areas remain available for high-end solar deployments, which could also serve pilot and demonstration purposes.

Keywords: solar energy, urban planning, visibility, visual impact assessment, BIPV, building integrated solar technologies, architectural integration of renewables

Nomenclature

Symbol	Unit	Designation
θ	[deg]	Visual angle
ds	[-]	Just noticeable difference
s	[-]	Perceptual stimulus
k	[-]	Weber's-Fechner's constant of perception proper of a sense
p	[-]	Fechner's perception
s_0	[-]	Threshold stimulus
VA	[-] [LogMAR]	Visual Acuity (when comparing observers' perception of a common object) or Visual Amplitude (when comparing objects' magnitude for a common observer)
MAR	[arcmin]	Minimum Angle of Resolution
d	[m]	Distance from viewpoint to character, in Snellen's fraction
$d_{1'}$	[m]	Distance from viewpoint to character subtending 1 minute of arc, in Snellen's fraction
C_w	[-]	Weber's contrast
L_o	[cd/m^2]	Luminance of a target object
L_b	[cd/m^2]	Luminance of the background surrounding an object
CS	[-]	Contrast sensitivity
C_0	[-]	Threshold contrast
MOR	[m]	Meteorological Optical Range
F_ξ	[lm]	Luminous flux after a length of path ξ in the atmosphere
C_ξ	[-]	Contrast after a length of path ξ in the atmosphere
F_0	[lm]	Luminous flux
σ	[1/m]	Atmospheric extinction coefficient
ξ	[m]	Distance from viewpoint to target
ΔE^*	[-]	CIELAB Color difference distance
L^*	[-]	Color lightness coordinate (black/white) in CIELAB color space
a^*	[-]	Color opponent coordinate (green/red) in CIELAB color space

b^*	[-]	Color opponent coordinate (blue/yellow) in CIELAB color space
S_P	[m]	Perceived linear size of an object
K	[1/m]	Emmert's constant
R	[m]	Linear size of retinal image
D_P	[m]	Perceived distance of an object
r_k	[m]	Kernel's search radius
SD	[m]	Standard distance
D_m	[m]	Median of the distances from each point in a kernel set to their mean center
n	[-]	Number of points in a kernel set
x_i, y_i, z_i	[-]	Coordinates of a given point in a kernel set
X, Y, Z	[-]	Coordinates of the mean center relative to points in a kernel set
d_{lim}	[m]	Limit distance of a rectangular feature perception (detection threshold)
A_p	[m^2]	Projected area of a feature on the visual plane or on the spherical field of view
S_0	[arcmin^2]	Minimal perceptible visual size corrected with lightness contrast
$VISRATIO$	[-]	Ratio of visible pixels (> 1 viewpoint) and total pixels per building roof
$RADRATIO$	[-]	Ratio of viably solar radiated pixels (> 800 kWh/m^2 yr) and total pixels per building roof
A_i	[m^2]	Area of a building envelope cell
α_i	[deg]	Slope of a building envelope cell
$\Omega(A)$	[sr]	Solid angle subtended by the surface A
A	[m^2]	Target surface
r	[m]	Radius of a sphere, i.e. a spherical field of view
$\Omega(\hat{A})$	[sr]	Solid angle subtended by the triangular surface A
$\vec{a}, \vec{b}, \vec{c}$	[-]	Vectors connecting the viewpoint to the vertices of a triangular surface Â
a, b, c	[m]	Magnitude of vectors connecting the viewpoint to the vertices of a triangular surface Â
E	[lx]	Illuminance
I	[cd]	Luminous intensity
d_A	[m]	Distance from the luminous source to the illuminated surface, in Inverse Square Law of light propagation

ϕ	[lm]	Luminous flux
L	[cd/m^2]	Luminance
A_S	[m^2]	Emitting area of a luminous source
Ω_0	[sr]	Threshold solid angle
$A_{p,0}$	[m^2]	Projected area of the threshold feature on the spherical field of view
r_0	[m]	Radius of the sphere on which the threshold feature is projected
C_l	[%]	Lightness contrast ratio
l_o	[-]	Pixel lightness (0-255) of a target object
l_b	[-]	Pixel lightness (0-255) of the background surrounding an object
l_{max}	[-]	Maximal pixel lightness (255)
θ_{crit}	[deg]	Brewster's angle between two optical media
n_1	[-]	Refractive index of medium 1
n_2	[-]	Refractive index of medium 2
ω	[deg]	View angle
$\bar{\Omega}_{av}$	[sr]	Average solid angle subtended by multiple viewpoints
Ω_p	[sr]	Solid angle subtended by the point p
b_p	[-]	Boolean visibility viewshed index (0 or 1)
x	[-]	Number of viewpoints in a multiple viewpoints configuration
y	[-]	Number of subdivisions of the target surface
E_w	[lx]	Weighted illuminance induced on a target surface from a non-spherical gazing model, accounting for distribution along possible directions in the field of view
E_s	[lx]	Illuminance induced on a target surface from a spherical gazing model, with even attention distribution along possible directions in the field of view
H	[-]	Shannon's entropy
P_i	[-]	Probability of occurrence of item i in the entropy set
a	[m]	Major axis of an ellipsoid
b	[m]	Minor axis of an ellipsoid
$r(\varphi, \nu)$	[m]	Radius of an ellipsoid as a function of azimuthal and zenithal angles
φ	[deg]	Azimuthal angle
ν	[deg]	Zenithal angle

List of Figures

Table of contents

Chapter 1   Introduction

Following the Swiss Federal Council decision of 25 May 2011, ratified by the Federal Assembly, Switzerland is planning a phasing-out of its nuclear power plants, producing around 40% of the national electricity demand in 2013. This means that, as many other European countries, Switzerland is facing an energy transition at a short as well as mid-term. In 2012, the "Energy Strategy 2050" was launched accordingly, mainly targeting a more efficient use of energy, the increase of renewable energy production as well as fostering research and development in energy [1].

Concerning renewable energy in particular, the revision of the Energy Act 1998 [2] embedded in the Annex of the Energy Supply Act 2007 [3], imposes a minimal increase of the average annual renewable production of 5.4 TWh by 2030 compared to the year 2000. The Action Plan set up in 2008 [4] announces by 2020 a renewable energy coverage ratio of 24% over the total national consumptions, in line with the corresponding engagement of the European Union [5]. According to the Swiss Federal Office of Statistics [6], this share was equal to 22% in 2016. Within the renewable energy production, solar energy accounts for 2.3% of the electricity demand and for 4.3% of the end use heat in Switzerland, a larger fraction of renewable electricity being issued from hydroelectric power. Nevertheless, over the period 2015-2016 solar energy production has grown of 5% for solar thermal and 20% for photovoltaics [7]. Some of the reasons of this significant growth are briefly explained herein.

Residential buildings are responsible for 28% of the total energy consumption in Switzerland [7]. The "Energy Strategy 2050" is promoting the implementation of the "Net Zero Energy Building" concept (NZEB) by stating that by 2020 "all new buildings should be self-sufficient throughout one year in terms of thermal energy produced by renewable sources and partially by electricity produced on site"[1], in line with the same objective expressed at European level [8]. The importance of energy savings in the building sector has also been outlined by the Swiss Confederation in the most recent revisions of the Energy Act [2], which requires the Cantons to fix

minimal renewable production targets for new buildings. Solar energy is accordingly a key factor to meet these goals, as well as the one imposed by the CO2 Emission Reduction Ordinance [9].

The achievement of an annual "net zero energy balance" for a building implies, among others, to combine an energy efficient building envelope with a large solar collectors and photovoltaic modules area. This is far easier to implement in a sprawled urban context, where extensive sun-exposed surfaces are available in relation with the heated volume of building; this is not the case for an urban environment, especially in Switzerland, where a habitat densification is foreseen in cities due to the population growth. One of the suggested approaches consists to consider the building and its neighborhood as an 'Energy-Hub': such *unit where multiple energy carriers can be converted, conditioned and stored* [10] allows promoting an energy exchange at a larger scale among different buildings. This implies a practical shift from the building to the urban level, which can be more easily implemented at the supply side (energy production) than at the demand side (energy consumption) due to financial reasons [11]. Consequently, a larger flexibility is required at the grid level (the so called "Smart Grid") and a novel energy distribution network must be envisaged, involving an urban dimension and a debate at the city planning level (e.g. stakeholders, municipalities, etc.). In the electricity domain for instance, Switzerland is currently restructuring the market by opening the latter to the European electricity trading system, with implications on the electricity network transmission capacity within and beyond the national borders [12].

Within this framework, there is a large interest of both Switzerland and EU countries in exploring the development and dissemination of solar energy at an urban level.

1.1   Solar energy integration in urban contexts

In most developed countries, urban areas are already consolidated [13]: the largest share of energy consumptions due to the building sector is accounted to the existing stock. With the greater benefits in addressing energy savings in existing buildings, a bigger effort is requested in modifying the built infrastructure. Currently, most of the attention is devoted to the mitigation of energy demand, but in the future, more comprehensive refurbishments involving localized energy production are envisioned.

According to a research dating back to 2011, buildings are covering 25 000 million of m^2 of useful floor space in the EU27, Switzerland and Norway; 75% are residential buildings, and

more than one third were built before 1960, when no energy saving policy was conceived [14]. Much of the effort, especially in Europe, has been concentrated in renovating the whole building stock that accounts for almost 40% of the total energy use [14]. Benefits coming from the urgent retrofit of this amount of existing buildings are remarkable, even if the reduction of energy needs should be coupled with a distributed renewable energy production. A report of 2002 highlights how the solar power production potential from photovoltaic roofs and façades could cover between 15% and 60% of the electricity demand in IEA countries [15]. It is foreseen that more than half of the global PV capacity from now to 2050 will be installed on buildings, producing a little less than half of the total PV electricity needed [16]. This is also enhanced by the continuous reduction in price of solar technologies [17].

Nevertheless, this process remains quite challenging: as a consequence of the above-mentioned cost reduction, public incitation like feed-in-tariffs or fiscal rebates are diminishing [17] and the entire financial burden (and risk) is shifted more and more on the private initiative. This encompasses a "renewable refurbishment expenditure" that in some occasions is translated into higher tenants rents or a filtering-up of wealthier households in freshly solar-equipped buildings, or sometimes even discourages potential investors. One general effect is the critical optimization of energy production to cover the investment, which is probably more dramatic on existing buildings than for new urban developments, where solar design can be implemented at the beginning of the whole design process.

As a result, most of solar plants in existing urban areas are installed on roofs where the prevalent amount of solar radiation is available, targeting the highest production and often disregarding the architectural integration quality of the system, which should be coherent with the urban context. Public institutions and local authorities, on the other hand, have to balance the will of installing more solar systems on buildings and the protection of their territory and cultural heritage. This can be sometimes contradictory and raises conflicts between energy planning and cultural heritage preservation.

Similarly, the imposition of solar energy production targets has to be conciliated with limited economic resources available for affordable developments, such as social housing complexes: an urban developer might face the dilemma of equipping residential settlements with solar technologies versus keeping the costs within a reasonable range for low-income households. Community involvement is essential in setting up effective renewable refurbishments: citizens

should be aware of the opportunities offered by solar energy and be part of the negotiations to settle energy goals. Purchase groups, community engagement, capacity building, participatory design and local actions are some of the solutions.
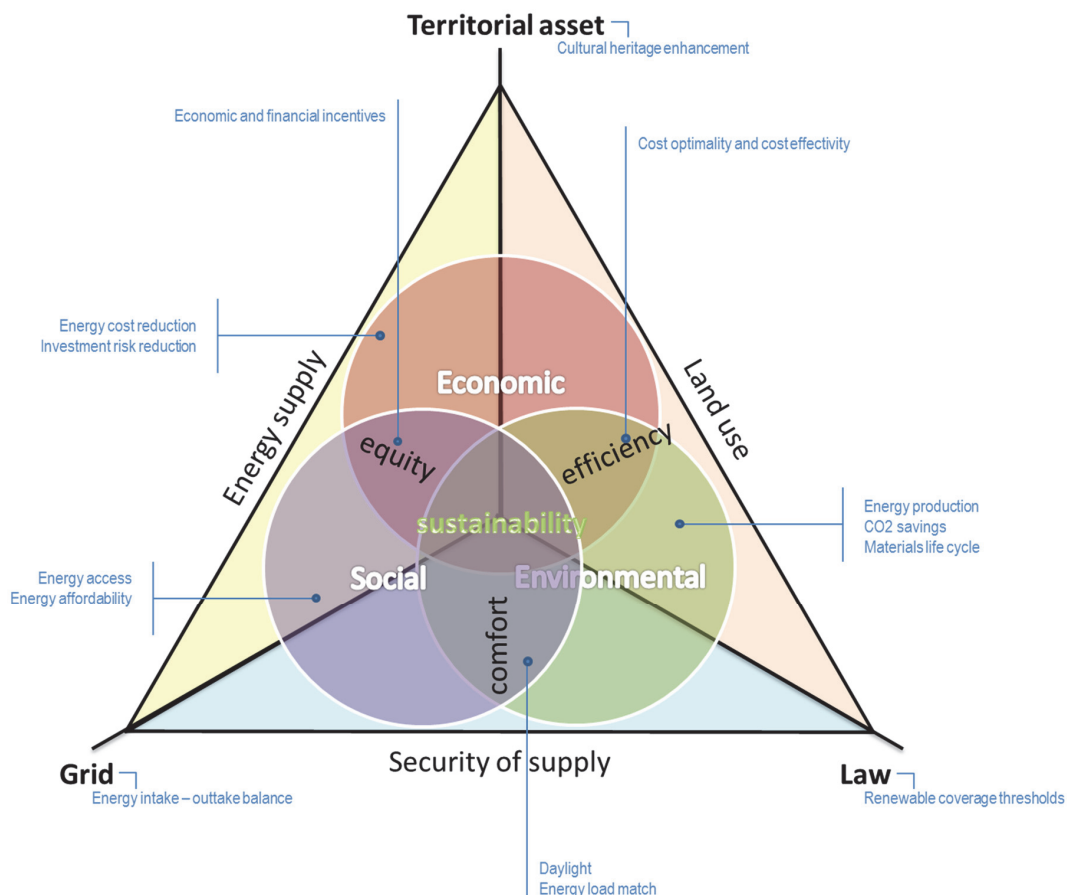
Figure 1.1 Proposition for a holistic representation of solar energy planning challenges

(Author's own elaboration)

Other typical trade-offs competing against the maximization of solar energy yield are the daylight access and the densification of the built environment. In fact, solar modules can cover most of the building envelope: as such, they should be arranged in a way that lets a sufficient amount of sunlight and daylight reach the interior environment, depending on the use of adjacent indoor spaces. In particular cases such airports or other infrastructures though, luminous reflections produced by large solar production plants can locally provide visual discomfort and/or glare, the problem being an excessive luminosity.

On the other hand, if solar panels are not the cause of unwanted shading they might suffer from shadows cast by neighboring buildings, vegetation or other urban furniture. In this sense,

densification of existing sites or new developments may compromise the insolation and the consequent energy generation. Nevertheless, effective spaces for integrating solar panels can be explored in urban voids, i.e. courtyards, parking sites or even roads, bike lanes, rivers, lakes; novel technologies based on translucent light transmission will allow the exploitation of windows for solar energy generation.

(a) solar energy meets cultural heritage protection. Paul VI Hall, Vatican city. Credits: arsliberalis, Wikimedia commons

(b) solar energy meets affordable housing design. Colorado Court, Santa Monica, US. Credits: limelightpower, Flickr

(c) solar energy enhances visual and thermal comfort. SolarFabrik, Freiburg, Germany. Credits: Joergens.mi, Wikimedia commons

(d) new spaces for solar energy in dense urban environment. Blackfriars station bridge, London, UK. Credits: AlisonW (Alison M Wheeler), Wikimedia commons

Figure 1.2 Challenges for solar energy deployment at the urban scale

All the previous consideration can lead to the conclusion that the adoption of solar energy in cities is a complex task, having to mediate among many different and articulated priorities, sometimes in conflict (Figure 1.1 and Figure 1.2). The decisional process affects the strategic development of cities and affects significantly inhabitants' everyday life. The responsibility of such a process relies and has to rely on political decisions: researcher's duty is to make it an informed decision, with appropriate supportive instruments. Some of them are listed in the following paragraphs.

1.2 Multi-Criteria Decision Making in energy planning

Multi-Criteria Decision Making (MCDM) techniques provide solutions to problems involving conflicting and multiple objectives. Several methods based on weighted averages, priority setting, outranking, fuzzy principles and their combinations are employed for energy planning decisions [18].

After the first energy crises in 1970s, reliable models to support fossil fuel extraction were needed. In particular, single parameter approaches were developed to identify efficient supply options and were subsequently extended from industry to the public sector. Since that period, decision analysis is largely applied to the energy domain [19], often exploring relations between energy demand and economic viability. The following decades brought a growing awareness in climate issues and the emerging definition of sustainable development [20] claimed the importance of environmental and social factors in planning procedures, raising the necessity for comprehensive multi-criteria decisions among sometimes conflicting goals. Usually, a MCDM workflow includes the formulation of alternatives according to a set of selected criteria, as a result of a compromise among stakeholders, criteria weighting, evaluation of the outcomes by different models and the final aggregation of results.

Between the 1990s and the 2000s, MCDM methods and energy-related environmental studies increased substantially from around 5% in the period 1985-1995 to 20% in the period 1995-2005,with a growing interest for renewable energy sources [21]. The increasing popularity of these methods led to the use of different models to validate the results and meet the variegate composition of decision makers, more and more assisted by interactive decision support tools [22]. The subtended uncertainties have to be tackled by discussing among stakeholders; fuzzy methods were encouraged, since the use of different techniques can lead to dissimilar conclusions [22], [23].

Coming to the last decade, the complexity of the analyses improved; it became evident that more than one energy carrier should be taken into account for various options, especially when dealing with renewables. A shift from the prevailing national or regional scale to the urban dimension has been pointed out as a necessity [24]. In fact, cities play a very significant role as decision makers at the interface between policy elaboration and enabling action: "*Cities, not only as local authorities but also as local ecosystem of inhabitants, companies, public utilities and local governments, are today recognized at the international level for their key role in the*

fight against climate change" [25]. Supportive tools specifically addressed to municipalities aiming to foster "Smart cities", i.e. to their political, administrative and technical staff such as urban planners, are dramatically needed.

As a consequence, a debate regarding which decision criteria are relevant for an effective planning leaning towards sustainable cities is legitimate. A survey highlights that the investment cost and CO2 emission are in absolute terms the most significant and adopted criteria across the majority of available methodologies, thus confirming the specific interest for economic viability in MCDM [18]. The same enquiry though, identifies social parameters, aside from environmental and economical ones, as non-negligible for the selection of the energy supply systems. In particular, social acceptability appraises the reaction of the local population regarding the hypothesized realization of the plan and is essential since "the opinion of the population and of pressure groups may heavily influence the amount of time needed to go ahead with and complete an energy project" [26]. Nevertheless, social acceptance is often expressed as a qualitative criterion, thus limiting its use due to subjective appreciation and weight.

Coming to the subject of this thesis, the use of solar technologies in existing urban environments has been sometimes assessed as impacting negatively, in absolute, on social acceptance [27]. In spite of this, established research states that a high architectural integration quality can be even a driving force for solar development, when coherent refurbishment strategies are put in place by setting appropriate requirements within homogeneous zones of intervention [28].

1.3 Site identity and landscape preservation for a coherent solar deployment

One of the most evident conflicts in urban and large-scale solar energy diffusion relies between site identity preservation and renewable energy targets. In Switzerland, this is regulated by Art. 18a of the Land Use Act [29] (author's own translation), stating that:

«In new development areas and agricultural areas, solar power plants which are sufficiently adapted to roofs do not require authorization [...]. Such projects should be simply announced to the competent authority. Cantonal law may designate specific types of new development areas where aesthetics is a minor concern, and solar power plants may also be exempted from authorization; [Cantonal law may] state an authorization commitment for determinate areas to be protected. Solar power plants on cultural heritage or natural sites with cantonal or national

relevance are always subject to a building permit. They should not largely affect the asset or the site. Nevertheless, the interest in employing solar energy in new and existing buildings prevails over the principle related to the aesthetic aspects.»

Figure 1.3 The listed village of Rivaz as it is (left) and how it could become under an uncontrolled solar deployment (photo simulation, right)

(Edited image from deepakhere.mypixels on Flickr. Photo editing by the author)

In this case the legislator provides a specific reference for solar energy, clarifies when the setting of a solar power plant requires an authorization and which institution is in charge of it (cantonal law prevails for building construction in Switzerland). Nevertheless, some concepts remain inexplicit or subject to interpretation:

1. *Adaptability of solar power plants and relative impact on site identity*. It seems essential to find an objective method to assess the quality of integration and judge its adaptation to the context. The degree of impact generated on site perception and identity has to be evaluated.

2. *Classification of territories concerned by different levels of aesthetics.* It is evident that not all settlements require the same attention to aesthetics and architectural integration quality. Some criteria or guidelines identifying areas that are concerned, and to what extent, are needed.

3. *Suitability of façades to the application of solar technologies*. Roofs remain the most used substrate to host solar devices and the best exposed to the sun at the majority of latitudes. Nevertheless, future scenarios cannot neglect the integration of solar panels on façades, which needs to be disciplined.

4. *Prevalence of solar energy employment on aesthetic aspects*. The interest of using solar energy is of great relevance and may go beyond aesthetic aspects. This general statement is not in accordance with local land use and building regulations, which are in charge of protecting the territorial identity and often block the deployment of solar production plants. The conflict between energy targets and built environment preservation becomes a conflict of priorities and administrative prerogatives, to the detriment of the end user. This situation often occurs both in Switzerland and abroad [30].

The massive use of solar technologies in existing built environments can modify the public perception of cities or villages from the current one (Figure 1.3). Such a change is either accepted as an evolution of the construction techniques and building equipment or opposed as an aggression to the traditional image of urban landscapes. A multi-criteria decision tool and a targeted methodology to overcome this apparent incompatibility of goals has to come helping to identify appropriate solar energy deployment strategies in accordance with the vocation of the territory.

1.4   LESO-QSV method

New energy regulations, together with mandatory solar fractions for electricity and Domestic Hot Water are introducing new materiality and geometries in buildings, resulting in new forms of architectural expression, which are slowly modifying our city landscapes. The increased use of active solar collectors in buildings is clearly necessary and welcome, but brings major challenges in already existing environments. The large size of solar systems at the building scale asks for a thoughtful planning, as these systems may end up compromising the quality of the building, threatening the identity of entire contexts.

Sacrificing architectural quality to promote solar spread can be counterproductive, leading straight to the opposite effect in the long term. Intense discussions are already ongoing in most cities between the different involved parties. On one side "solar pros", concerned by the urgency of maximizing renewable energy use, ask for a total installation freedom; on the other side, architects and building heritage institutions express their worries about the urban impact of such systems and ask to restrict their use to certain urban contexts only. *De facto*, both concerns of maximizing solar energy spread and protecting the architectural quality of the built environment are justified, and both should possibly be satisfied at the same time. Furthermore, good architectural integrations can be possible also in the most critical situations, but they

clearly need appropriate design and cost investments (Figure 1.2a). If well-conceived, these examples can actually be very convincing and become strong driving forces for the energetic transition, repaying by far their extra design and cost.

1.4.1 LESO-QSV Method objectives

The question is no longer to be in favor or against the use of solar systems in cities, but becomes rather to define minimal local levels of integration quality, and to identify the factors needed to set smart solar energy policies, able to preserve the quality of pre-existing urban contexts while allowing solar energy use. The LESO-QSV approach gives clear and objective answers in this debate [28], [31]:

a) First it sets the innovative notion of architectural "Criticity" of city surfaces in relation to their need for integration quality (see Section 1.4.2).

b) Then it clarifies the notion of "Architectural integration quality" and proposes a simple evaluation method (see Section 1.4.2);

c) Based on a) and b) it helps authorities to set and implement precise local acceptability requirements (LESO-QSV acceptability) (see Section 1.4.3);

d) Finally it proposes a way to tailor solar energy policies to local urban specific contexts by mapping the architectural "criticity" of city surfaces, and crossing this map with the solar radiation map of the site (LESO-QSV-cross mapping) (see Section 1.4.4).

Integration quality is always desirable, but not always that crucial. In a concern to spread the use of solar energy, expectations toward integration quality may be reduced, for instance in industrial or commercial areas and/or on not visible envelope surfaces, like flat roofs.

The level of visibility of the surface from the public domain and the level of sensitivity of the urban context determine *de facto* the architectural "criticity" of a city surface, and the related need for integration quality. To structure the issue, a "criticity" grid is established by crossing the three identified levels of visibility (low-medium-high, Figure 1.4) with the three identified levels of sensitivity (low-medium-high, Figure 1.5), thus defining nine "criticity" situations for which quality expectations have to be set.
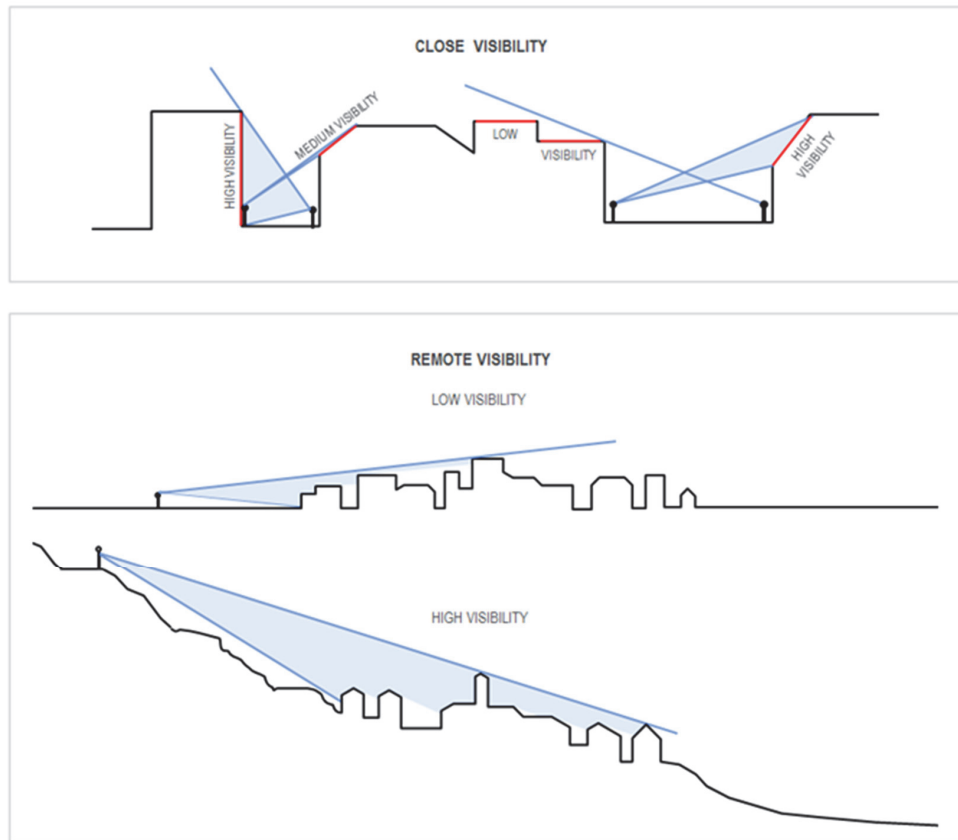
Figure 1.4 Different levels of visibility of city surfaces from the public domain

(Courtesy of Maria Cristina Munari Probst and Christian Roecker [28, Fig. 6])

Figure 1.5 Different degrees of sensitivity of existing urban contexts

(Courtesy of Maria Cristina Munari Probst and Christian Roecker [28, Fig. 7])

1.4.2 Assessing architectural integration quality

Requiring a certain level of integration quality implies being able to assess that quality. Often this is considered a matter of personal taste, but recent studies have confirmed the existence of implicit criteria shared by the community of architects and leading *de facto* the architectural integration quality perception [32]–[34].

To be perceived as integrated, the system has to be designed as an integral part of the building architecture, i.e. all the formal characteristics of the solar system (field size/position; visible materials; surface textures; colors; module shape/size; joints) have to be coherent with the global building design logic.

Based on these findings the LESO-QSV approach proposes a qualitative assessment method articulated into three simple steps, grouping the integration criteria to keep the procedure light and making the evaluation as objective as possible. The coherency of System geometry, System materiality, and System details, is evaluated using a three levels scale (fully - partly - not coherent). This being a qualitative evaluation, the partial results cannot be expressed by numbers and cannot be synthesized in a single mean value. Hence, the choice to represent each partial evaluation as a colored arc of a circle (green, yellow or red according to the level of coherency) to be combined with the others to form a complete circle made of three sectors. The global system quality is given by the number of sectors of each color (Figure 1.6).

The level of quality required for each "criticity" level is not absolute and constant, but depends on many temporal and local factors: in particular the energy supply strategy, the availability of other renewable energy sources, the general "integrability" of market products and the consequent difficulty in designing good integration solutions. Among others, also the city identity and image, its political orientation and economic structure, etc. Therefore, this method does not provide an absolute grid of quality requirements; it is rather conceived to support authorities in establishing local quality expectation grids, more or less severe depending on the local context (Figure 1.7).
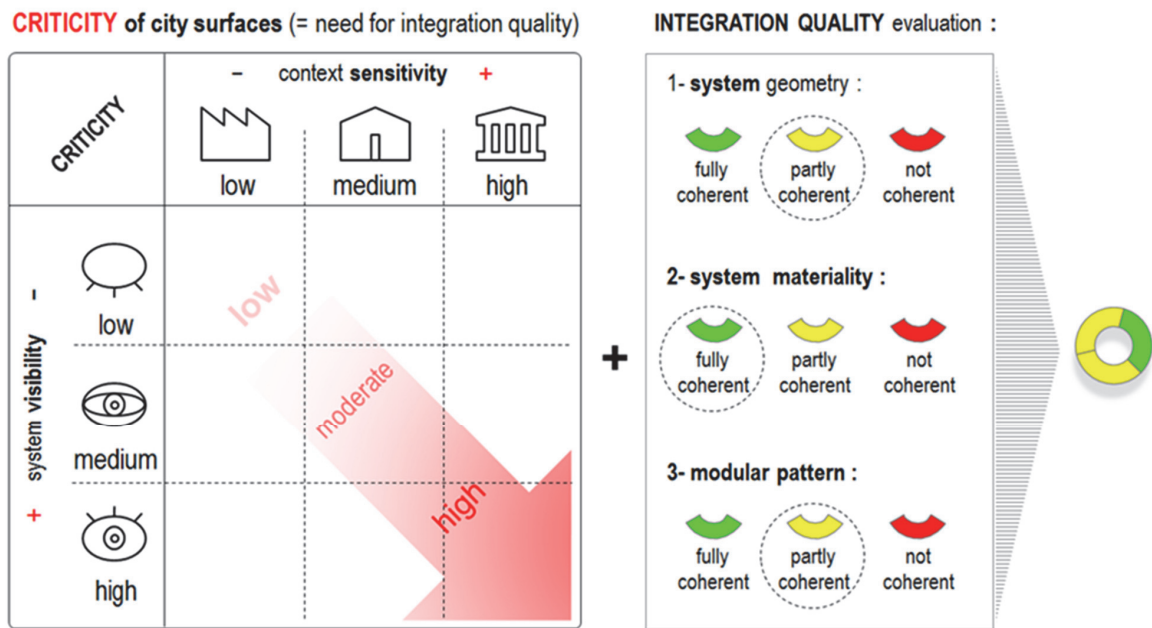
Figure 1.6 Left: architectural "criticiy"; Right: integration quality evaluation method based on three steps

(Courtesy of Maria Cristina Munari Probst and Christian Roecker [35])
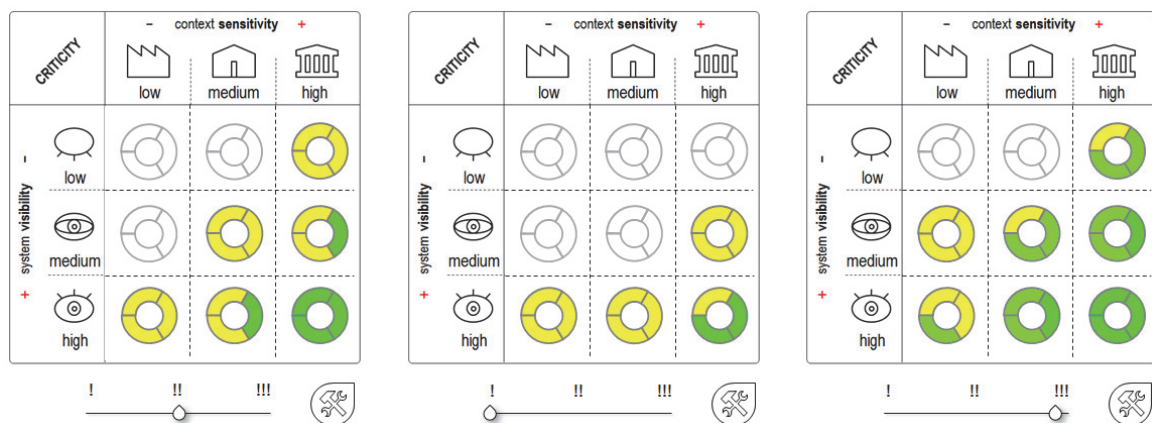
Figure 1.7 Local quality expectation grids, more or less severe depending on the local context.

(Courtesy of Maria Cristina Munari Probst and Christian Roecker [35])

1.4.3 LESO-QSV acceptability tool

To help authorities apply this method, a multi-purpose software tool has been developed, called LESO-QSV GRID (Figure 1.8). Quality expectations are represented by the same three circle sectors used to set the grid, ad described in Section 1.4.2. Three reference sets of quality requirements with increasing severity (permissive - standard - demanding) are made available to authorities ("choix de grille"), together with the additional option of setting a fully customized grid (Figure 1.7). To allow authorities choosing the most appropriate "acceptability grid", a large

collection of architectural integration case studies is displayed, showing which integrations would be acceptable in real time and which ones would have to be rejected according to the selected settings. This database of examples can be scrolled through, demonstrating the effect of the grid on a very extensive set of integration approaches and "criticity" situations.
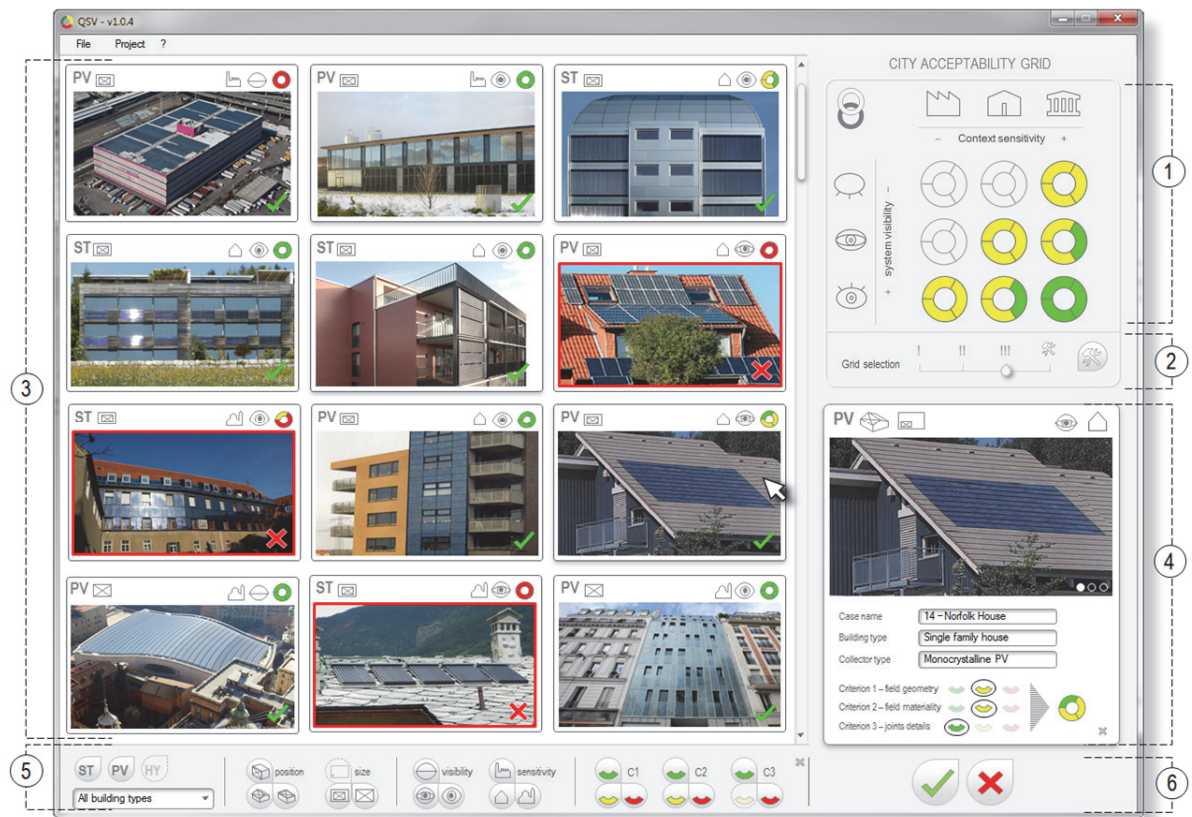
Figure 1.8 a screenshot of the LESO-QSV GRID software tool.

(Courtesy of Maria Cristina Munari Probst, Christian Roecker [28, p. 5])

The same software can also be used as an educational tool for architects, installers and building owners, with minor adaptations. The wide palette of examples provides inspiration based on the achieved refurbishments, shows mistakes to be avoided or suggests ideas on how to improve the quality of a project. It can also help city councils to explain the methodology in an interactive and visually convincing way and justify eventual project rejections to applicants (Figure 1.9). Filter buttons are available in the bottom part of the screen, to display a chosen subset of integration examples, in selected situations (visibility / context sensibility / type and size of solar systems, …) (Figure 1.8 section 5).
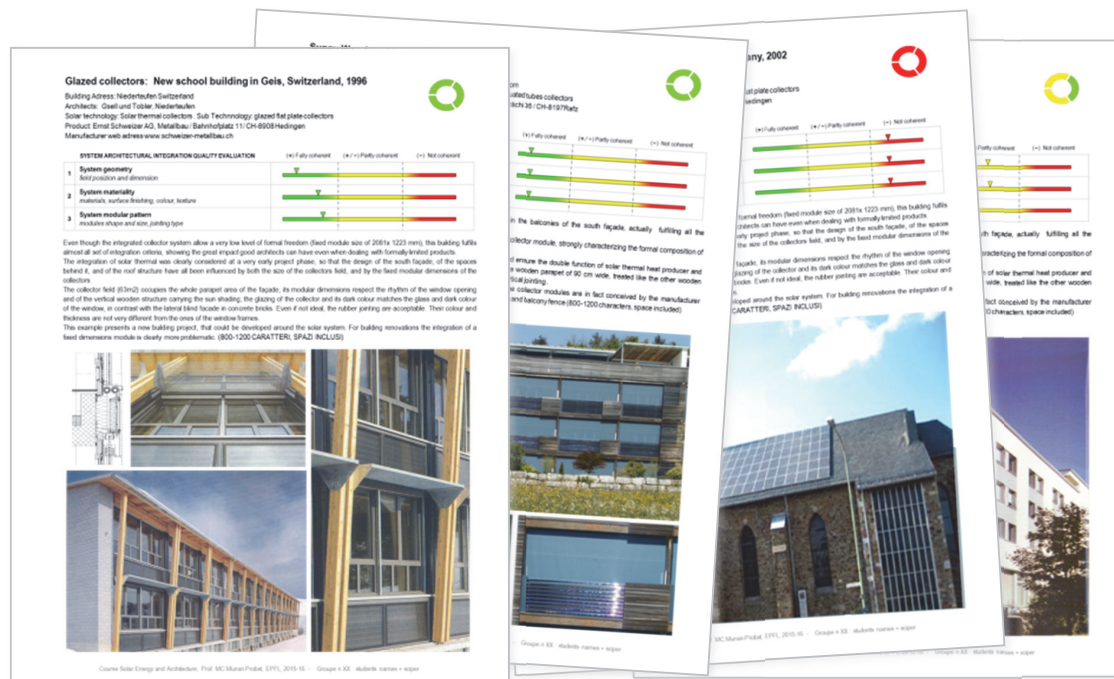
Figure 1.9 Quality evaluation sheets used to compile the case studies database of the QSV-Grid tool.

(Courtesy of Maria Cristina Munari Probst, Christian Roecker [35])

1.4.4 LESO-QSV cross-mapping tool

If the previously described acceptability tool is reactive and meant mainly for protection, the second tool derived from the "criticity" concept, called "LESO-QSV Crossmapping", is proactive and meant for energy planning. Presently, the only information available to planners and authorities to express decisions on solar promotion, regulations or financial incentives is the amount of solar radiation received by the various building envelope surfaces, displayed on interactive solar maps. These maps vary in accuracy and detail level (rough surfaces only, pitched roofs or not, façades…), their only goal being the assessment of building envelopes solar energy potential, with no concern for their urban specificities. As already explained, these specificities have a major impact on solar application strategies and should be made available to planners as well. To answer this need, the "Leso QSV-Crossmapping" tool suggests to map the architectural "criticity" of city surfaces, as defined in Section 1.4.2, and to superimpose this information over the solar radiation map. This allows weighting the solar potential of each surface with the expected architectural integration effort.

Different policies and aware decisions can be based on this more comprehensive information, keeping in mind that architectural integration of solar modules is possible also in delicate situations (Figure 1.2a). In these cases though, design effort and cost investment will probably be higher. If these extra efforts cannot be afforded, it might be preferable to postpone the refurbishment process, as poor integrations usually end up just discouraging new users. By contrast, well-designed interventions can be among the strongest driving forces for solar deployment, repaying by far their extra cost.

1.4.5 Conclusion

As more and more pressure is building up to increase the use of solar as a replacement for fossil energy carriers, there is an urgent need for new responsible ways to implement solar modules in urban contexts.

We strongly believe that the concept of "architectural criticity" at the basis of the LESO-QSV method offers valuable possibilities to develop such responsible policies. We do hope that the two inferred tools will contribute to finding valuable solutions to the problematic "Solar Energy promotion AND Urban Context Protection" equation.

This method is currently used within IEA SHC Task 51 ("Solar Energy in Urban Planning"), as a basis to assess the quality and acceptability of the different solar integration approaches proposed by a set of case studies. It represents also a core resource in three courses currently taught at EPFL (Ecole Polytechnique Fédérale de Lausanne, Switzerland) and Università IUAV in Venice (Italy). In November 2016, the method has been awarded with the Innovator of the year prize in Sweden [36].

1.5   Objectives

LESO-QSV method has been welcomed as an effective qualitative method suitable for urban planners' and architects' mindset. Further research is ongoing to characterize "criticity " metrics, i.e. visibility and sensitivity scales to compare different installation contexts. A thorough literature is available around the evaluation of architectural quality of solar modules integration in building envelopes. This subject is not addressed comprehensively in this doctoral thesis, except from the author's direct experience in the field.

The core of this work is the development of a comprehensive assessment method of visibility, which is a key factor for an extensive use of the LESO-QSV method. Visibility of solar modules

on a building component depends both on deterministic and stochastic variables. The deterministic part deals with the location of viewpoints in relation with the position and the size of the solar power plant. The stochastic part accounts for the visual contrast across the system boundaries due to atmospheric particulate or daylighting conditions, which can influence reflections and colors induced by the solar modules: as a consequence, viewer's perception is different. Certain fractions of buildings capture viewer's attention on priority, according to their shape, luminosity, color saturation and contrast.

The challenge of this thesis is to explore visual perception of building envelope components that could host solar technologies, before any eventual installation. Since the aim is to respond to a planning need, the "objects of interest" included in the assessment, are the building envelope surfaces and not the solar collectors themselves, which are not determined at this stage and are designed in a later phase.

1.6   Structure of this doctoral thesis

This doctoral thesis is articulated as follows. A review of biomechanical, physiological, physical, psychological and geometric principles at the basis of human visual perception are summarized in Chapter 2; Chapter 3 presents a detailed state-of-the art of visibility assessment techniques, from the territorial to the urban scale, with a dedicated focus on visibility and visual impact of renewable energy production plants. Subsequently, the research questions are detailed before outlining the developed multi-scale methodology in Chapter 4. Chapter 5 and Chapter 6 are devoted to the broad strategic scale and to the urban development scale respectively. Chapter 7 describes a novel index to assess visibility of building envelope surfaces at the detailed planning scale proper of the district, while Chapter 8 explores a possible implementation towards the architectural scale. General conclusions are drawn in Chapter 9. The appendix shows some outcomes of the assessment methodology on real projects, issued for architects and urban designers within their professional practice.

1.7   Acknowledgements

Chapter 2   Principles of Visual Perception

In the beginning when God created the heavens and the earth, the earth was a formless void and darkness covered the face of the deep, while a wind from God swept over the face of the waters. Then God said, "Let there be light"; and there was light.

<div align="right">

The Holy Bible, Genesis, 1-3

</div>

According to this excerpt of the Genesis book in the Bible, light was the first creation of God. Since the very beginning of human tradition, visual perception is linked with the physical properties of light and became later a symbol of knowledge. Even if there was no scientific measure of light intensity until the 20th century, the intuition that visual perception could be assessed through a lighting scale is innate in the humanity: it comes from the empirical evidence that no light means no visual perception. This intuition subtends also the work of this doctoral thesis, which tries to model the visual perception of an observer, as a light source. Before describing into detail the hypothesis underlying this research work, some definitions supporting the principles of visual perception in general and of vision in particular have to be specified in this chapter.

2.1   Visual field

Human vision is produced by light reflections from the environment into the eye. The light flux that is not stopped by obstacles, and reaches the sensing organ is influenced by biomechanics of the human body and geometrical features of the visual field.

The visual field is *the spatial array of visual sensations available to observation in introspectionist psychological experiments* [37]. Consequently, the visual field is typically the angular range from the line of sight in which stimuli from the external environment produce perception on an observer subject, when the eyes and the head are absolutely still. The line of sight connects the visual target with the viewpoint: the former is the point in the space focused by an observer in a steady position, the latter is assumed to coincide with the midpoint of the segment traced between the center of the two eyes retinas. The standard line of sight lies at the intersection between the horizontal and the vertical meridians of the sphere centered at the observer's

viewpoint. Actual line of sight varies slightly depending upon each individual and whether he/she is standing or sitting. In the first case, the line of sight is about 10 degrees below the horizontal and in the second one about 15 [38, p. 287] (Figure 2.1).

Generally, the monocular human visual field extends to circa 60-62 degrees nasally (toward the nose, or inward) from the vertical meridian in each eye, to 104 degrees temporally (away from the nose, or outwards) from the vertical meridian, and approximately 50 degrees above and 70 below the horizontal meridian. The binocular visual field results from the superimposition of the two monocular fields. The angular range around a given view direction, leading to the best visual perception is quite narrow: depending on the activity related with perception, this range becomes wider (Figure 2.1 and Figure 2.2). Finest details in shape and color can only be distinguished in a small portion of the visual field: the fovea, responsible for most complicated human tasks such as reading and driving, occupies an area of approximately 1.5 mm diameter in the center of the macula lutea on the eye retina [39] (Figure 2.3). As such, it covers circa 5 degrees of the visual field around the line of sight. Beyond this range, less precise tasks can be accomplished through vision, such as word recognition within a limit of 10-20 degrees from the line of sight, symbol recognition until 30 degrees, color discrimination until 60 degrees. Binocular vision is limited to 62 degrees. In the domain of luminous comfort, the angular range within 30 degrees from the line of sight is called ergorama and represents the most sensitive fraction of the visual field to luminance contrast; the angular range between 30 and 60 degrees is called panorama and coincides with the binocular field [40, p. 111].

The perceived environment can be increased by eye rotation, head or body movement (Figure 2.4), but attention will be less focused. Attention will be addressed further in this chapter, but it is useful to state from the beginning the movement limitation imposed by standard human anatomy, listed in Figure 2.1 and Figure 2.2. In case the observer is moving, the static visual field is not sufficient to explain his/her visual perception: as a result, a set of visual fields proper of different moments in time combine into a field of view. This terminology derives from optics and is adopted herewith to stress the accent on the cumulative aspect of visual perception in time, which equates human observers to sorts of "visual acquisition devices". When the observer displaces his/her gaze by effect of eyes, head or body movement, the field of view is also denominated gazing field, to highlight its dependence on the observer's attention.
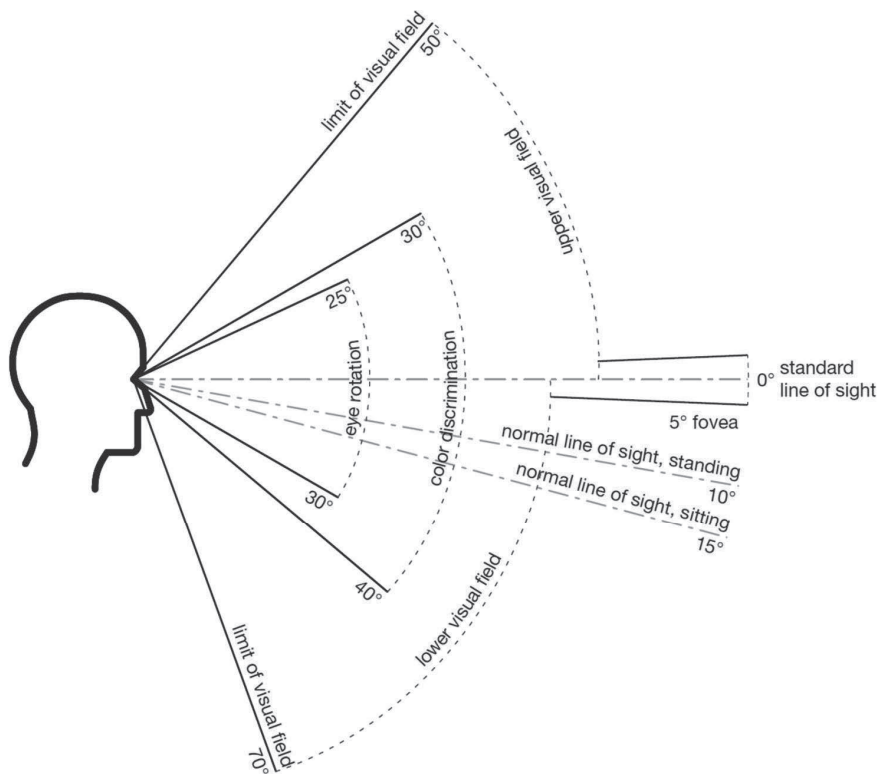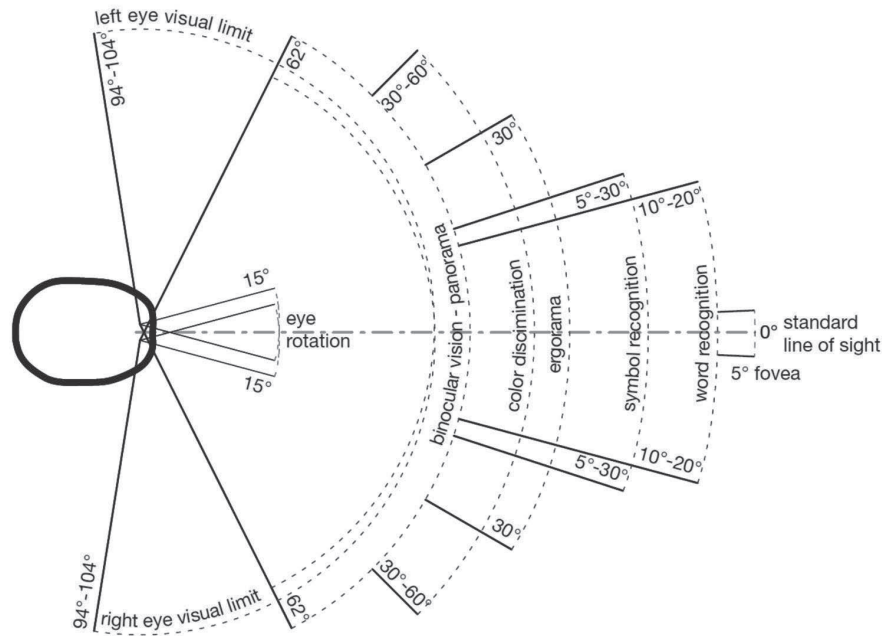
Figure 2.1 Visual field in the horizontal and vertical plane

(Author's re-elaboration from [38])
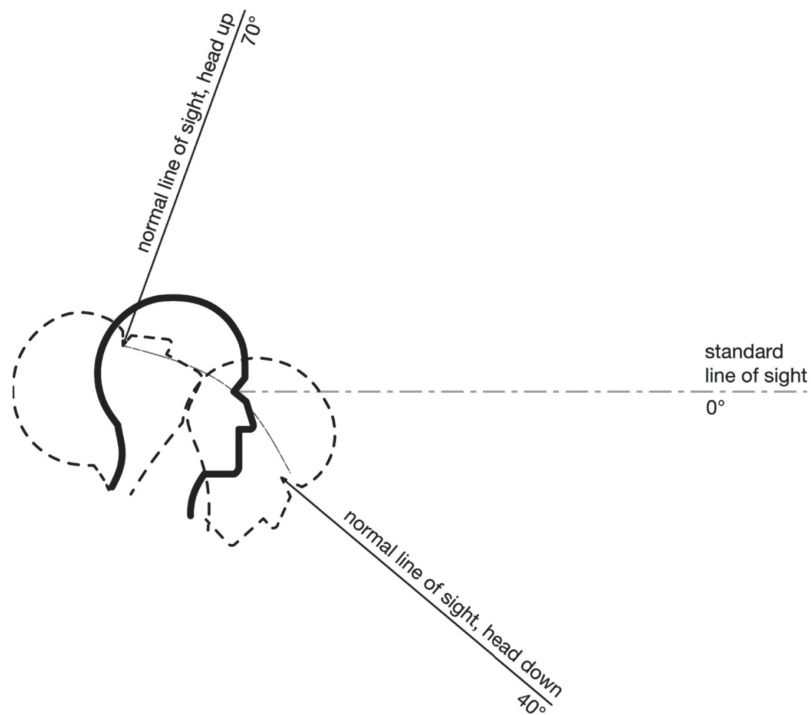
Figure 2.2 Range of head movement in the vertical plane

(Author's re-elaboration from [38])

(a) Diagram of the human eye. Credits: Rhcastilhos And Jmarchn, Wikimedia Commons

(b) Photograph of the retina of the human eye, with overlay diagrams. Credits: Danny Hope And Zyxwv99, Wikimedia Commons
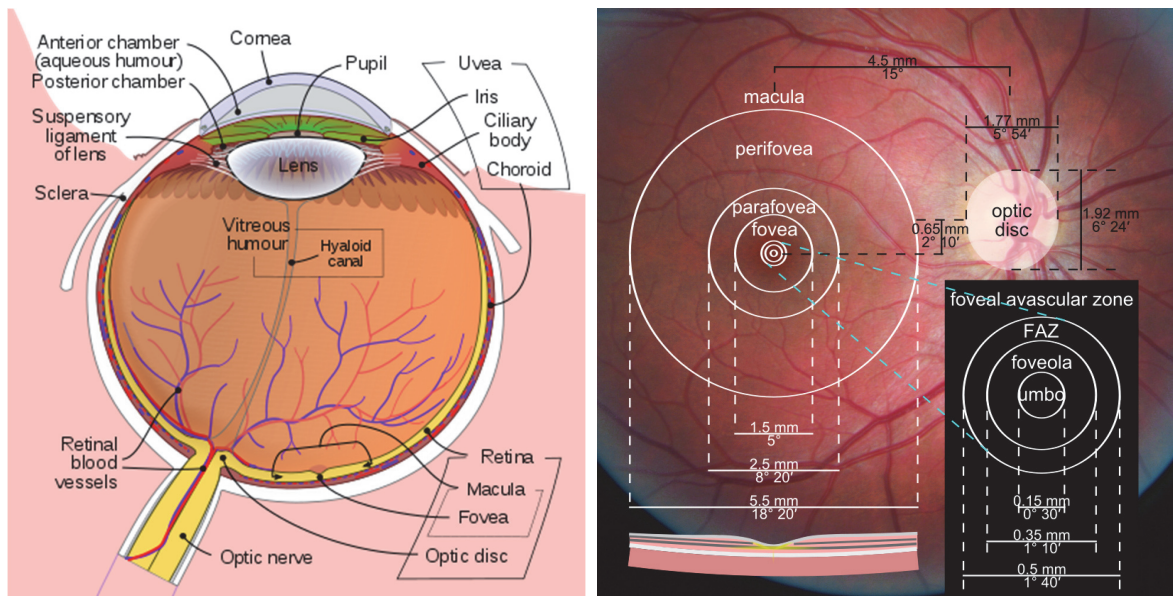
Figure 2.3 The human eye
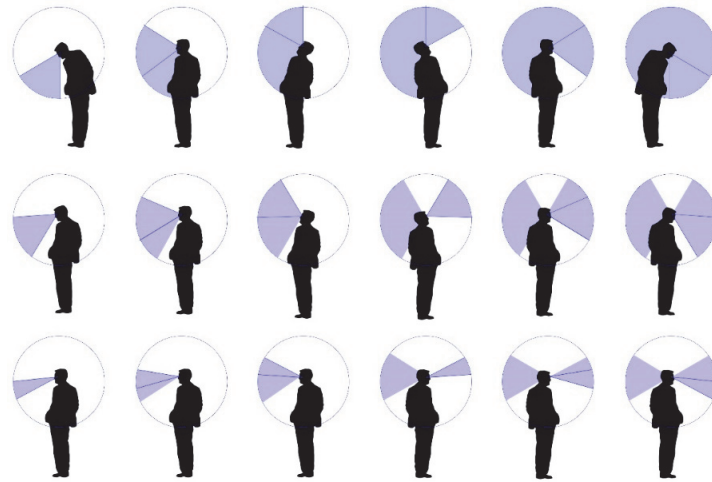
Figure 2.4 Qualitative schema of the gazing field by moving the head and rotating the eyes (1st row), by moving the head only (2nd row), or by rotating the eyes only (3rd row). See comments and further details in Section 7.1.4.

(Author's own elaboration)

2.2   Physiology of vision

For humans and some other animals, vision is entailed by a band of the electromagnetic spectrum redirected from the environment into the eye. This band, called visible light, ranges from 370 to 730 nm wavelength and is also responsible for color perception: a light ray is perceived as violet from 370 to 450 nm and as red from 620 to 730 nm wavelength [41] (Figure 2.5).

Figure 2.5 Samples of a commercial solar panel finishing glass that redirects a small portion of visible light to reproduce the color sensations while letting the rest of the solar spectrum transmitted through to produce energy.

(Credits Maria Cristina Munari Probst)

After a light ray passes through the pupil, it is refracted by the cornea and by the crystalline lens, then focused on the retina. Some common diseases like myopia or other deformations of the eyeball affect this process engendering a refraction error, usually corrected with lenses

whose refractive power is measured in diopters. At the bottom of the eye bulb, the retina is responsible for transduction of the light flux into an electric signal directed to the brain: this task is carried out by two kinds of receptors, the cones and the rods. The first are in charge of photopic vision (in well-lit conditions) and more concentrated in the central region of the retina, called fovea; the latter are implicated in scotopic vision (in conditions of dim light) (Figure 2.6). Cones are sensitive to slightly longer wavelengths in the visible light spectrum (peak at 560 nm), rods to shorter (peak at 500 nm) [42]; during dark adaptation from photopic to scotopic vision, highest color perception shifts from yellow-green to green-blue until it disappears in complete scotopic vision: color perception can be altered by the composition of visual pigments in diseases like daltonism or dichromatism. In fact, photons of light isomerize visual pigment molecules contained in rod and cone receptors; they trigger an enzyme cascade that stimulates an electrical response, transmitted to the bipolar and the ganglion cells [43]: fewer photons are sufficient to excite a rod receptor than a cone. Retinal degeneration diseases or traumas affect receptive tissues and their bio-chemical reactions at the base of transduction. The electric signal converges from many different receptors to a lower number of ganglion cells: on average, about 120 rods pool their signals to one ganglion cell but only 6 cones send signal to one of them, increasing to a one-to-one connection in the foveal zone [44, p. 58]. This results in a higher sensitivity of the rods and a better detail resolution and color vision by the cones. The detailed vision capability is called visual acuity and can be measured with different methods (see Section 2.4.1). Ganglion cells have a center-surrounding receptive field with antagonist excitatory-inhibitory neuron firing mechanism: this translates into a relative response of human perception to absolute light intensity [45]. After being processed by ganglion cells, the signal is sent through the fibers of the optic nerve to the lateral geniculate nucleus (LGN) in the thalamus, which regulates and sorts the neural information before sending it to the visual cortex. The receptive field of LGN cells is similar to the ganglion one and most sensitive to small light spots, while the visual cortex has three main types of receptors. Simple cortical cells, with excitatory and inhibitory areas arranged side by side, responding best to light bars of a given orientation; complex cortical cells, responding best to movement of a correctly oriented bar across the receptive field; end-stopped cortical cells, responding to corners, angles, or bars of a given length moving in a particular direction [44, p. 79] (Figure 2.7).
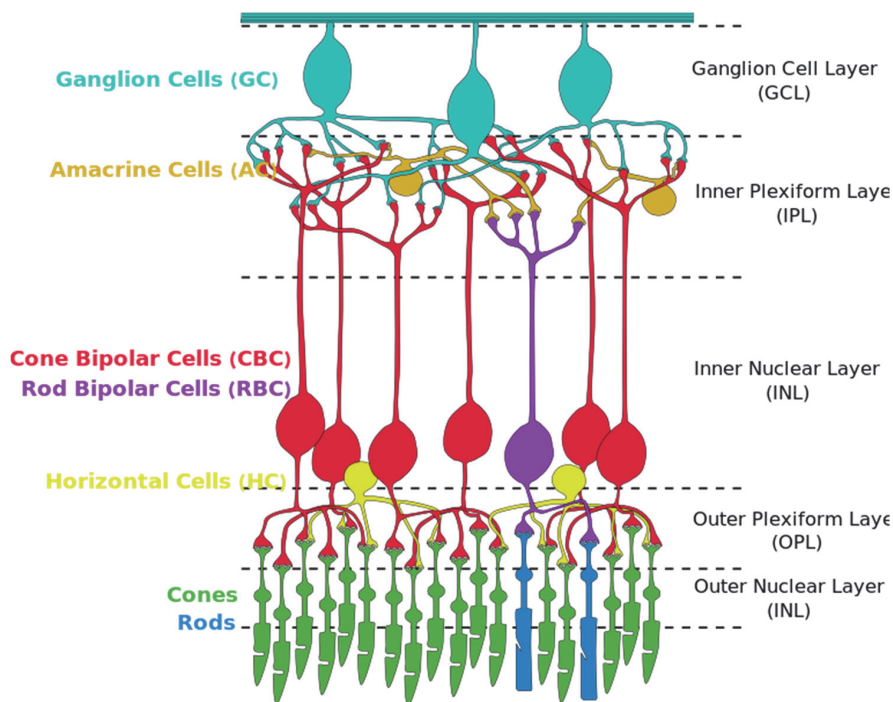
Figure 2.6 Schematic section of the eye receptors and neurons.

(Credits Jörg Encke, got from https://commons.wikimedia.org/)
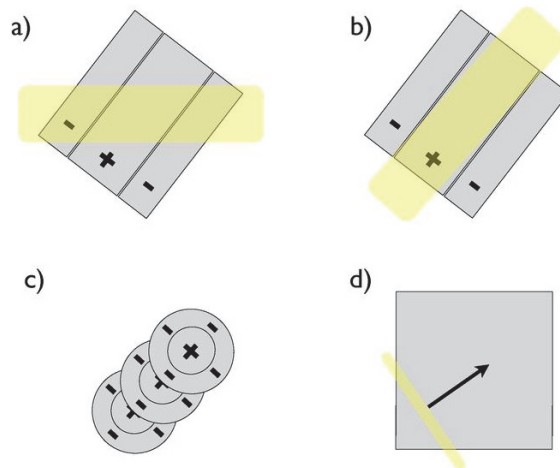
Figure 2.7 Receptive field of simple and complex cortical cells. Simple cortical cells respond better to light bars of a given orientation (b) than another (a); this selectivity is achieved through multiple centre-surround receptive fields aligned at a certain angle (c). Complex cortical cells respond to light bars with given orientation and motion direction (d).

(Credits Kyle.wg3139, got from https://commons.wikimedia.org/)

Travelling from the retina to the brain towards more sophisticated information processing, there is an increased complexity of the stimulus producing a neural response, from a simple light stimulus to more elaborated features: hence, cortical cells are generically denominated feature detectors. The cortical area devoted to vision corresponds univocally to given locations on the

retina, with a large portion allocated to signals from the fovea: this relationship can be mapped with brain monitoring and imaging techniques [46]. From the cortex, neural signals reach other zones of the brain, in relation with more specific perceptual tasks: for object discrimination and identification, they follow the ventral pathway to the temporal lobe; for directing an action with regard to the stimulus, they follow the dorsal pathway to the parietal lobe [47]. Neuropsychology investigates in depth brain activity in relation with perception and goes beyond the objectives of this work. In spite of this, object identification is decisive for the goals of this thesis dealing with the observation of solar modules. In the following paragraph, some clarifications on the perceptual tasks relevant for the current work are given.

2.3   Visual stimulus and threshold

While the previous paragraph focused on the physiological processes triggered by a visual stimulus, the aim here is to investigate perceptual responses to physical properties of stimuli, under a psychophysical approach. Stimuli can be defined as i) "incoming perceptual data", classified in a narrow-down hierarchy among available environmental stimuli, ii) focused stimuli filtered by attention and iii) stimuli that have passed through the environment-body interface to the receptor organ. After physiological processing, the latter generates a psychological response mediated by knowledge in a mutual influence; in fact, previous experience affects perception too. Psychological response is in accordance with the perceptual task that needs to be accomplished: detecting, resolving, recognizing, searching, sizing, describing an object are examples of such tasks.

For a standard observer who is not affected by particular pathologies [48], detection is usually the easiest task to achieve: it consists in the awareness of the presence of an object. Resolution is the smallest spatial separation between two nearby lines or points that can be distinguished by the observer. Recognition implies the ability of naming the object and categorizing it. For example, one may detect a dark spot on a sign without being able to resolve the graphic elements composing the letters printed on it, which allows the symbol recognition. In case of solar modules installed on a roof, one may detect a blinking reflection from the panel covering glazing on a faraway building, without recognizing it as a solar module, or even confusing it with a skylight.

Visual stimulus is usually measured in terms of visual angle, as the angle a viewed object subtends on the retina; such angle is formed by two lines, connecting the opposite edges of the

viewed object with the resultant edges of its representation on the retina. The two lines cross within the eye about 7 mm behind the vertex of the cornea: the visual angle is the angle formed at this crossing (Figure 2.8). In psychophysical studies, a threshold is the minimum stimulus needed to complete successfully a perceptual task; i.e. the character recognition threshold usually adopted by optometrists in the famous "reading the characters" test is about 5 minutes of arc, subtended by the whole pictogram (the character strokes subtend each an angle of 1 minute of arc). This means that a healthy subject not affected by refracting pathologies is able to recognize a letter subtending an arc of 5 minutes, which is centered in the subject's viewpoint (one minute, indicated with the apostrophe, is 1/60 of a degree) [49, p. 116] (Figure 2.9).
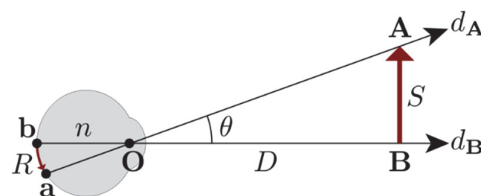
Figure 2.8 Visual angle θ [deg] of a stimulus S generating a retinal image R.

(Credits Melchoir, got from https://commons.wikimedia.org/)
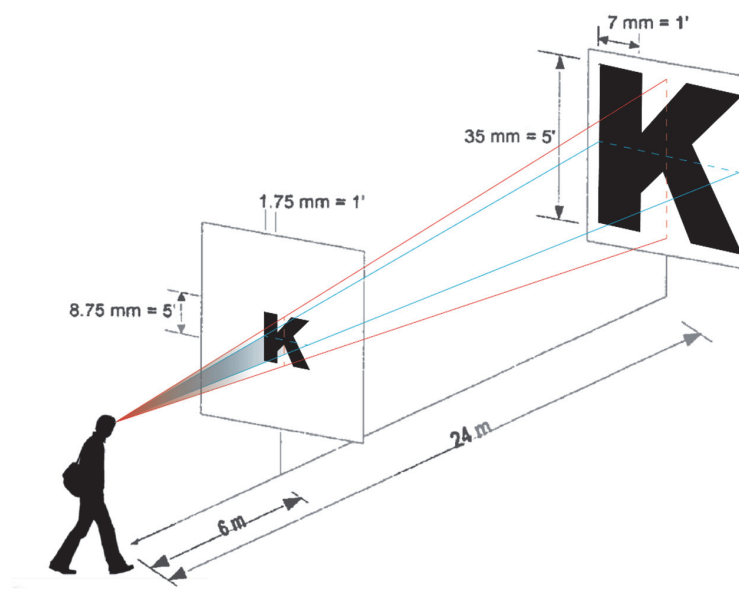
Figure 2.9 Visual acuity demonstration. Letter stroke subtends 1 min of arc, while the whole letter subtends 5 x 5 min of arc. The horizontal visual angle is highlighted in blue and the vertical visual angle is highlighted in red.

(Author's own elaboration)

Thresholds are usually experimentally determined with various techniques. Fechner distinguished between: i) method of limits, ii) method of adjustment and iii) method of constant stimuli

[50]. In the first, stimuli are presented to a subject by increasing or decreasing intensity and the "crossover point" between presence and absence of perception is marked down; in the second method stimulus intensity is adjusted either by the experimenter or by the subject until the threshold is reached. In the third method, which is the most reliable, stimuli are presented in random order for a number of trials: the threshold is the intensity that results in successful perception in 50% of trials. In addition to this formulation of absolute threshold a concept of relative or difference threshold was introduced: this corresponds to the smallest difference between two stimuli that a subject can detect. In the famous Weber's experiments, it is observed that this "just noticeable difference" is proportional to the stimulus and the constant of proportionality depends on the sense (light perception for vision, sound perception for hearing, etc.). The mathematical relationship shows that the ratio between the just noticeable difference ds and a given stimulus s is constant (Equation 2.1).

$$\frac{ds}{s} = k$$

Equation 2.1 – Weber's law

By integration of this fundamental formulation, it is possible to estimate the magnitude of perception: Fechner's law states that perception is proportional to the logarithm of the stimulus intensity times a constant proper to the sense, assuming that perceived stimulus becomes 0 at some threshold stimulus s_0 (Equation 2.2).

$$p = k \, \log \frac{s}{s_0}$$

Equation 2.2 – Fechner's law

From the previous statements, it becomes evident that to a linear increase in stimulus intensity does not correspond a linear increase in perception. Perceived electrical shock, for example, more than doubles by doubling the intensity of the current (response expansion); on the contrary, perceived brightness is lower than its double when doubling light intensity (response compression) [51]. This thesis relies on such quantification of perceptual magnitude: hence, stimulus expression in quantitative terms becomes essential. After having examined physiological and psychophysical aspects of vision, an overview of measurable physical phenomena and stimuli entailing particular visual capacities is given in the following paragraph.

2.4 Visual acuity and contrast

A mention of visual acuity as the ability to resolve details of the visual environment has been made in Section 2.3. Setting up a measuring unit and an assessment scale of visual acuity allows the designation of a threshold as defined in Section 2.3 and consequently, the quantification of visual perception. Intuitively, a visual stimulus generated by a given object depends on the size of the object and on the contrast between the object and its surrounding background. Hence, a threshold for visual acuity should be expressed by specifying these two variables: in other words, the minimum object size and contrast necessary to detect it.

2.4.1 Visual acuity

Size is usually defined as the visual angle, which is the angle of the arc, centered at the eye and subtending the object. Visual acuity is defined as follows in Equation 2.3 [49]:

$$VA_{(1)} = \frac{1}{MAR}$$

Equation 2.3 – Visual acuity definition in relation with the minimum angle of resolution (MAR)

In the above equation, MAR is the Minimum Angle of Resolution, measured in minutes of arc. From experimental evidence, it is assumed that the MAR of a standard observer is equal to 1 minute of arc in conditions of infinite luminance contrast, even if it can reach the theoretical value of 0.4 minutes of arc considering pupil diffraction and cones size limitations [49, p. 109]. Visual acuity tests are usually performed thanks to an eye chart showing different characters, designed to have an equal distribution of black and white space, i.e. of minimum and maximum luminance. In the reference line, characters' graphical strokes subtend 1 minute of arc (Figure 2.9). If the observer recognizes the letter, he resolves 1 minute of Minimum Angle of Resolution and has a visual acuity equal to 1, e.g. 10/10; if he needs to reduce the distance (or to read a bigger character) to increase the visual angle, he resolves bigger MAR and is characterized by lower visual acuity. Pathologies that affect visual acuity are the already cited refractive errors, traumas or corneal and retinal diseases. With regard to distance, another expression of visual acuity can be formulated, in Equation 2.4:

$$VA_{(1)} = \frac{d}{d_{1'}}$$

Equation 2.4 – Visual acuity definition in relation with distances (Snellen's fraction)

In this case, d is the minimum distance from the viewpoint to the character needed by the observer to recognize it, while $d_{1'}$ is the distance from the viewpoint to the character when the latter subtends a 1-minute arc centered in the viewpoint. It can be inferred that the absolute threshold for visual acuity at infinite luminance contrast is constituted by either the MAR or by the distance $d_{1'}$. In accordance with Fechner's law (Equation 2.2), a linear decrease in distance (or increase in character's size) does not correspond to a linear increase in character recognition. This can be observed in Snellen's eye charts where signs size increments more than linearly. Thus, a logarithmic scale can be introduced and visual acuity expressed as the logarithm base 10 of the MAR, as an alternative to the definition of Equation 2.3 [52]:

$$VA_{(2)} = \text{Log}_{10} MAR = \text{Log}_{10} \frac{d_{1'}}{d}$$

Equation 2.5 – Visual acuity definition in relation with the logarithm of the minimum angle of resolution (LogMAR)

Equation 2.5 explicates this relationship by combining both the MAR-based and the distance-based definitions. For clarity, a comparative table of visual acuity measures is presented in Table 2.1.

Table 2.1 Example of different visual acuity expressions

Decimal notation (1/MAR) (Equation 2.3)	Snellen's notation (Equation 2.4)	LogMAR (Equation 2.5)
2.000	6.00/3.00	-0.30
1.000	6.00/6.00	0.00
0.500	6.00/12.00	0.30
0.250	6.00/24.00	0.60
0.125	6.00/48.00	0.90
0.063	6.00/95.00	1.20

2.4.2 Visual contrast and color difference

As mentioned above, visual contrast is considered in the ideal situation as being infinite until this point. In reality, contrast attenuates over distance in outdoor environment where significant distances are covered by an observer's sight, as for the objectives of this study. In a broad sense, contrast is usually expressed as the ratio between the difference in luminance or color brightness, making an object discriminable, and the average luminance (or brightness) of the scene. This definition is compatible with Weber's law (Equation 2.1), since a smaller difference

becomes noticeable at a low luminance level. In its simplest formulation, visual contrast is given by Equation 2.6:

$$C_w = \frac{\Delta L_{o-b}}{L_b}$$

Equation 2.6 – Weber's contrast

At the numerator, there is the difference in luminance between the object and its surrounding background, while at the denominator the luminance of the background is used. The ability to discern between luminance of different levels is measured through contrast sensitivity that, similarly to visual acuity, is defined as the inverse of the threshold contrast C_0 (Equation 2.7).

$$CS = \frac{1}{C_0}$$

Equation 2.7 – Contrast sensitivity

Experimentally, it is determined by identifying the smallest luminance difference between the dark and light bars of a grating at which an observer can still detect the latter. As for characters reading, the angle subtended by the bars varies according to the size and the distance to them.

Conventionally, this variation is codified in spatial frequency, as the number of cycles of a dark and a light bar subtending a visual angle of one degree [41, Ch. 7]. Contrast sensitivity as a function of spatial frequency is plotted in form of a contrast sensitivity function (CSF), which can also be scaled logarithmically (Figure 2.10). Eye diseases like Glaucoma can affect contrast sensitivity.
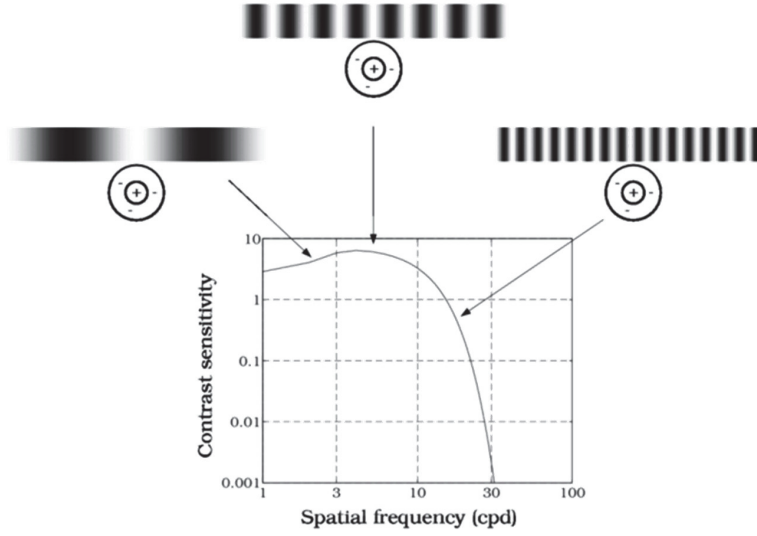
Figure 2.10 Contrast sensitivity function.

(Credits Star Whitt-Frousiakis, got from https://commons.wikimedia.org/)

The outdoor environment represents a certain level of complexity: light rays intensity attenuates over distance, mainly by effect of atmospheric particles absorbing, refracting or scattering the light beam. The atmospheric attenuation of a light ray can be measured objectively, and is represented by the Meteorological Optical Range (MOR), namely as:

"The length of the path in the atmosphere required to reduce the luminous flux in a collimated beam from an incandescent lamp, at a color temperature of 2 700 K, to 5 per cent of its original value" [53].

Light attenuation over distance follows Beer-Bouguer-Lambert's law (Equation 2.8), which describes the luminous flux F [lm] after a length of path x in the atmosphere. The latter is function of the luminous flux at the source F_0, [lm] the extinction coefficient proper to the atmosphere's composition σ [1/m] and the distance ξ .[m] The contrast between an object and its background at distance x respects this principles, as it is proportional to the contrast at distance 0 from the object [54] (Equation 2.9).

$$F_\xi = F_0 e^{-\sigma\xi}$$

Equation 2.8 – Luminous flux attenuation over distance (Beer-Bouguer-Lambert's law)

$$C_\xi = C_0 e^{-\sigma\xi}$$

Equation 2.9 – Contrast attenuation over distance (Koschmieder's law)

Laboratory experiments indicate that contrast ratios between 0.018 [-] and 0.03 [-] are perceptible for most daylight viewing conditions. Usually, a contrast ratio of C = 0.02 [-] corresponds to the detection threshold between large objects and the horizon sky for typical observers [55, p. 704] and is used for visual range calculations. Apart from the above-mentioned definitions, other formulations of contrast exist, taking into account color hue that has an influence on relative luminance (see for example [56]). In fact, color sensitivity varies as function of photopic or scotopic conditions (see paragraph 2.2) and the visible spectrum is characterized by different sensitivity response curves. A quantification of the difference in perception ΔE between two colors has been formulated by the International Commission on Illumination (CIE) in 1976, as shown in Equation 2.10 [57]:

$$\Delta E^* = \sqrt{(\Delta L^*)^2 + (\Delta a^*)^2 + (\Delta b^*)^2}$$

Equation 2.10 – CIELAB 1976 color difference formula

In this equation, color is expressed using the CIELAB color system coordinates, where L approximates the human perception of lightness as a nonlinear function of the relative luminance and ranges from 0 to 100, a is the coordinate between the color opponents green and red, with negative values indicating a shift to green and positive values to red, b is the coordinate between the color opponents blue and yellow, with negative values indicating a shift to blue and positive to yellow. In fact, according to the opponent process theory of color vision [58], opponent neurons in the retina and lateral geniculate nucleus respond with an excitatory response to a visual stimulus from one part of the spectrum and with an inhibitory response from another part, similarly to the process described in Section 2.2. Spatial distance in Equation 2.10 corresponds to difference in color perception. Nevertheless, such formulation has reported limitations for small color differences and highly saturated regions: it was therefore updated in 1994 and 2000. For the purposes of this work though, color differences between solar panels and the environment are significant and color saturation is attenuated in the atmosphere. Hence, Equation 2.10 is considered compliant with the objectives in accordance with the scientific literature [59, p. 848]. Threshold values for ΔE vary between 1 and 2.3 [60].

Figure 2.11 shows an example of solar modules installed on a building. The presence of the modules is evident from the difference in color between the panel and the host surface, which can be expressed in CIELAB coordinates. Simultaneously, there is a luminance difference between the module surface and its background. A reflectance edge stands along the perimeter

of the module, since it is made of a different material in comparison with the background; an illumination edge is generated by the shading of the panel, which is responsible for a higher illuminance on the surface of the panel compared to the shaded background.

Figure 2.11 Reflectance and illumination edges

(Author's own elaboration)

2.4.3 Relationship between visual acuity and contrast

Visual acuity and contrast thresholds are listed in the previous sections but the relationship between both and the existence of a common threshold has not been discussed yet. In an experimental study that is credited by other recent research [59], [61]–[65], Shang and Bishop inserted some bright objects in different black and white landscape pictures [66]. Size and contrast of these objects are close to the perceptual thresholds. After presenting the pictures to a set of observers, they marked down the thresholds resulting from a 50% successful perception (see Section 2.3), as a function of visual size and contrast. Visual size or magnitude is meant as the product of horizontal and vertical visual angles subtending the object (see Figure 2.9), representing the portion of visual field it occupies. A value of 5 x 5 square minutes is used as the smallest experimental object size in reason of display resolution limitations. Contrast is calculated as the difference between the average luminance of the object and the background border, divided by 256: the latter represents the total number of grey levels in a 24-bit Red Green Blue - RGB color space, used for visualization on digital monitors. In such space, each color results from the combination of the red, green and blue components by additive color mixing. First, it was found that the normalized object-background lightness contrast ranged from 8% to 26% with the most frequent value around 13% [66, p. 128]. More significantly, it is possible to plot a hyperbola expressing the relationship between visual size and contrast

thresholds (Figure 2.12). This allows the adjusting of a visual acuity threshold as a function of contrast and vice-versa. Given the similarity of this study conditions to the ones of this doctoral thesis (bright objects perceived in landscapes), it is assumed as the psychophysical reference for the methodology development.
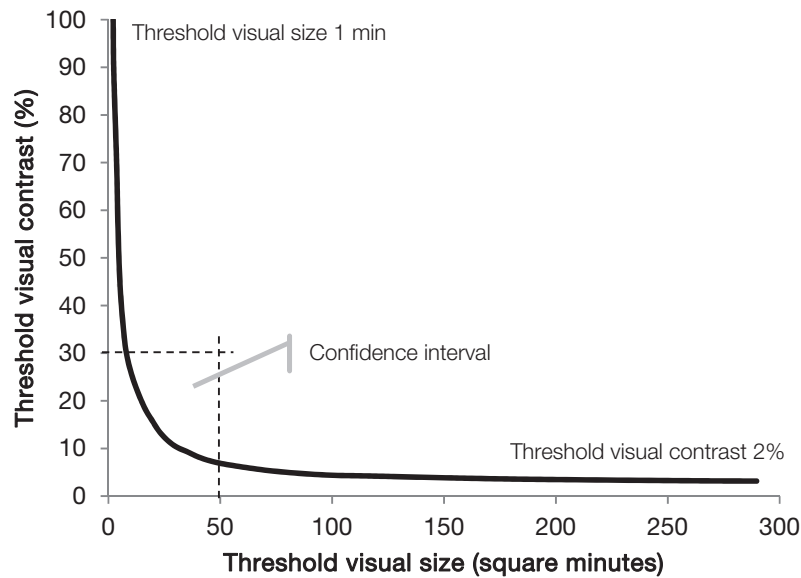
Figure 2.12 Uninformed detection threshold as a function of visual size and contrast.

(Author's re-elaboration from [66, Fig. 10])

2.5   From detection to recognition

Knowledge and experience are important in the perceptual process: when stimuli are processed by the brain, they are mediated by memories and learning, which produce sensations and psychological effects. An object that has been detected in the physical world is then properly recognized since it is categorized in accordance to previous experience. For example, a chair will always be recognized as a chair despite the different viewpoints from which it can be perceived and the different visual stimuli or retinal images it creates. First, the object is isolated from the background and then its elements are grouped into a meaningful whole through a psychological logic (Figure 2.13a): these operations are called perceptual segregation and perceptual organization by the Gestalt scientists (Ernst Mach, Edmund Husserl, Christian von Ehrenfels [67]), who provide heuristic laws at the base of perception. According to the recognition by components theory [68], essential volumes composing the object, like spheres,

cubes or cylinders, are analyzed separately and recombined together. This analytical process makes the object recognizable from most viewpoints.

(a) photovoltaic module as an iso-
lated object. Credits: Javed Raja

(b) roof BIPV system in Nieuwland, Amersfoort (Netherlands). Credits: Frank Van Der Vleuten, Flickr

Figure 2.13 A solar panel as an isolated object (a) and in a scene (b). rooftop PV are in a tilted and elevated position, making it difficult to recognize them. In this case PV mimics roof cladding, and it is necessary to focus attention on usual PV features, like color and re-flectivity, to recognize the modules.

Nevertheless, the presence of obstacles may obstruct the vision of essential components, compromising the discriminability of the object from certain viewpoints. In fact, the perception of an object in the real world is rarely isolated from a set of many other interacting objects (Figure 2.13b).

The arrangement of target objects and obstacles visible from a given viewpoint is denominated "scene": a *scene is a view of a real-world environment that contains background elements and multiple objects organized in a meaningful way relative to each other and the background* [49, p. 114]. By extending the perceptual limits between the target object and the surrounding context, much of the information regarding the object itself can be retrieved by the observer. Regularities are remarked in the physical environment, such as geometric shapes and contour morphologies or lighting and shading patterns. A semantic scanning of the context is also performed, collecting stimuli from the various senses that contribute to identify the environment and the objects it could most probably contain. The image issued from the visual system is

reconnected to similar occurrences from previous experience and the target object acquires a meaning relative to its context (Figure 2.13b).

The position of items in a scene is also essential to determine the size of a target object. In fact, objects subtending the same visual angle (see definition in Section 2.4.1 and Figure 2.9) may have different sizes, depending on their distance from the observer. The determinant variable in this case is depth, as the ability to attribute the object to a visual plane comprised between the observer and the horizon (Figure 2.14). Depth can be assessed through comparison of recognized objects in a scene characterized by a given perspective: for example, lamps having the same size on the side of a street give the impression of a depth gradient and are a reference measure for objects in the street. Depth can be inferred through other pictorial cues in the scene, like light and texture patterns, or through detection of moving features, like a train whose apparent size increases by approaching. The contraction of ocular muscles and the overlap of the two images issued from each eye in binocular vision are other means of depth deduction. The relationship between the perceived size of an object S, its perceived distance D and the size of its retinal image R is expressed by Equation 2.11 according to Emmert's law, where K is a constant [69] (Figure 2.15).

$$S_P = K(R \cdot D_P)$$

Equation 2.11 – perceived size as function of retinal image and perceived distance (Emmert's law)

(a) solar façade of the ELL building at EPFL campus. (b) Depth map of the scene. Used tool: Rafal Lindemann, Depthy
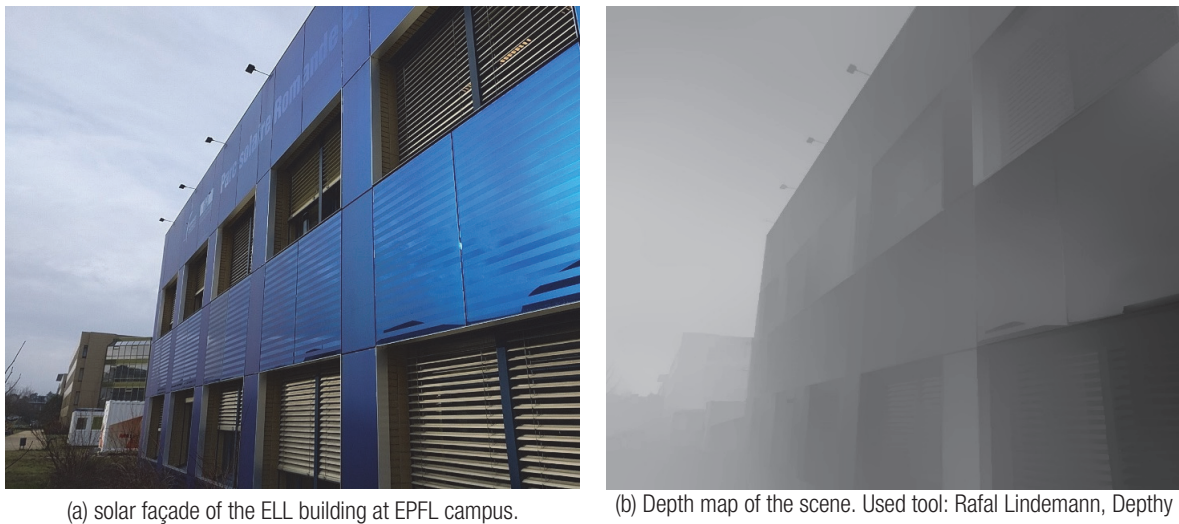
Figure 2.14 An example of depth map. Pixel color in the grayscale image goes from black (closer) to white (farther). Some smartphones equipped with double camera can compute depth by imitation of binocular vision.

Figure 2.15 Emmert's law demonstration (Equation 2.11) alias Ponzo's illusion. A dismissed railway has been transformed into a wind farm. The perceived size of the upper wind turbine is bigger because the perceived distance is higher, despite the same size and same retinal image it forms compared to the lower turbine.

2.6   Attention and motion

Given that many different objects lie in a scene engendering many different potential stimuli, selective attention is necessary to focus on a single item to be processed by the brain. Physiologically, stimuli falling in the foveal area and allowing an acute vision, benefit from more neural responses from the cortex (Section 2.2): moving the eyes, the head or the whole body to stare at a particular object and let its visual stimulus fall in the foveal area is the main way to focus attention on it Figure 2.4). By considering view direction as a reliable indicator of selective attention, eye pointing devices, like camera synced eye-trackers, provide a precious information on what captures generic observers' attention in a scene. Factors influencing attention usually depend on the knowledge and the observer's task, being therefore subjective and cognitive related. Nevertheless, some objective characteristics like brightness, contrast, color and orientation of stimuli, determine what "stands out" in the scene and has a higher probability to be attended by most observers. With this regard, saliency models have been developed taking into account these properties in a set of images and a thorough application of these methodologies to the building integrated photovoltaics is available [70], [71] (Figure 2.16).

(a) view of the ELL building at EPFL: salient zones on the image. Used tool: SaliencyToolbox [72]
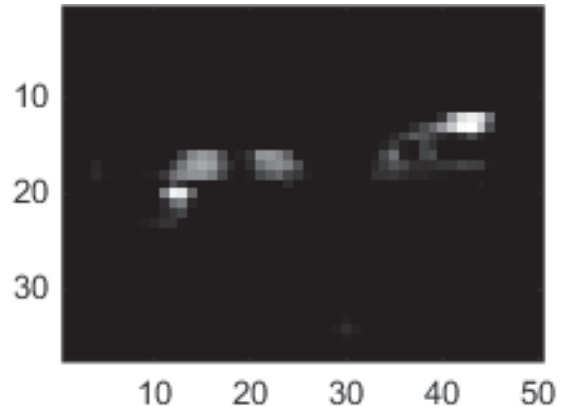
(b) Saliency map of the scene. Used tool: SaliencyToolbox [72]

Figure 2.16 An example of saliency map. Pixel color in the grayscale image goes from black (less salient) to white (more salient).

Attention allows binding of the different features perceived simultaneously by different areas of the brain, like shape, color, movement, etc., into a single meaningful object characterized by many properties [73]: for example, information about a yellow object, with spherical shape moving in the middle of a court is recombined into a tennis ball. Similarly, focusing attention on the conjunction of different characteristics is necessary to search an item among a multitude of objects in a scene (Figure 2.13b). In fact, an item is noticed only after being focused by attention and recognized as the expected combination of features. People with autism and other attention peculiarities may experience differences in focusing their attention to objects.

Until this point, perception has been considered with regard to a single isolated object and to a set of objects, viz. the scene, in which a target item like a solar panel can be detected and recognized. Another level of complexity arises because scenes are not static but can change with the observer's motion: this is particularly relevant when considering the observer in an urban environment, as for this thesis work. Perception is then analyzed under a so-called "ecological approach" and the succession of scenes presented to the observer is translated into an optic flow [74]. An optic flow generates a complex perception that can be used to drive further motion towards a target: perception and motion influence each other, since an observer needs to move in order to perceive a complex environment and needs to perceive in order to move coherently. The center of the flow, pointed by the vector in the direction the observer is heading to, is called focus of expansion and increases in visual size without changing its position in the visual field: on the contrary, stimuli far from the focus of expansion move out faster from the visual field (Figure 2.17).

Figure 2.17 A simulation of the motion effect in proximity of the ELL building on the EPFL campus. The "optic flow" effect is obtained by radial blur in a photo editing software tool. The focus of expansion is the vanishing point on the horizon, in the direction the observer is heading to.

With the Gibsonian "ecological approach", the problem of vision and perception is extended to the scale of the city. In the next chapter, the principles explained here are examined in the urban context. Visibility assessment practices are analyzed with a special focus on renewable energy and solar energy technologies.

Chapter 3   State of the art on visibility assessment

Physiological aspects of vision and psychological processing of external stimuli have been considered in the previous chapter. Perception has been examined according to its main stages, from the most unconscious to the most rational ones, involving experience and memory. This breakdown shifts from the observer's receptors (the eye), through the observer's mind, towards the external environment, leading to a path from the anatomic objectivity to more subjective and abstract phenomena. By moving towards an "ecologic approach" of perception, defined as the simultaneous accounting for the multitude of stimuli in an urban landscape, this chapter focuses on visual environments subtending more complex psychological processes. An investigation regarding the quantity and quality of stimuli reaching an observer in an urban context is essential to understand the perception and the sensation they produce, determining whether he/she will appreciate (or not) the scene. Furthermore, the physical world is mediated by biological, cultural and individual factors characterizing the observer's experience [75, Ch. 2]: research on subjective interpretation of reality shifts towards phenomenology, which also deals with psycho-social affection. Using the categorization proposed in [75, Ch. 1.3], current studies can be classified following their assessment base:

- *Expert based*: issued by experienced observers, researchers, trained specialists developing heuristic methods to categorize different perceptual scenarios and situations into systematic inventories.

- *Spatial description models*: aiming at the quantification, geometric description and geographic referencing of visual perception, in relation to the morphology of the territory. This is the core interest of this thesis.

- *Population based*: studies involving general public or a selected population, assessing reactions to a set of physical features in the real world (psychophysical), examining hu-

man cognitive processing of landscape characteristics (psychological), or their subjective interpretation (phenomenological). This domain is partially addressed in this thesis, when related with the perceptual characterization of the territory.

A panorama on the most well-known studies concerning visibility assessment is given here, with a special focus on applications for renewable energy planning.

3.1 Expert-based visibility assessment in urban contexts

At the end of the previous chapter, the optic flow constituted by moving through a sequence of scenes was mentioned: extensive research on the subject was performed by the psychologist James Gibson. He examined the geometric, anatomic and mechanic aspects of vision and defined perception as a function of possible interactions with the environment through the theory of "affordances" [74]. Gibson coined the term "ecology of vision", stating that the perception of multiple stimuli in the surrounding context mostly occurs in movement and free body articulation, in a sort of "education of attention". Among the first enquiries on the perception of complex urban environments, research carried-out by the urbanist Kevin Lynch is particularly relevant. In his book "The Image of the city" [76], he defined *imageability* as *that quality in a physical object which gives it high probability of evoking a strong image in any given observer. It is that shape, color or arrangement which facilitates the making of vividly identified, powerfully structured, highly useful mental images of the environment* [76, p. 9]. This feature of the urban landscape could also be intended as *visibility in a heightened sense, where objects are not only able to be seen, but are presented sharply and intensely to the senses* [76, p. 10].

Mental maps theorized by Lynch and experimented by himself and a set of individuals in few American cities acquire a social dimension by aggregating the impressions from a sample of citizens, to form a sort of "public image" (Figure 3.1). Essential components of this image are: (i) *paths* as infrastructural elements arranging space and movement within space; (ii) *edges* as physical or imaginary boundaries enclosing space, like walls, buildings, shorelines, etc.; (iii) *districts* as relatively large sections of the city characterized by a unique specific identity; (iv) *nodes* as focal points, intersections in the spatial network of the city and (v) *landmarks* as emerging landscape elements constituting reference points.
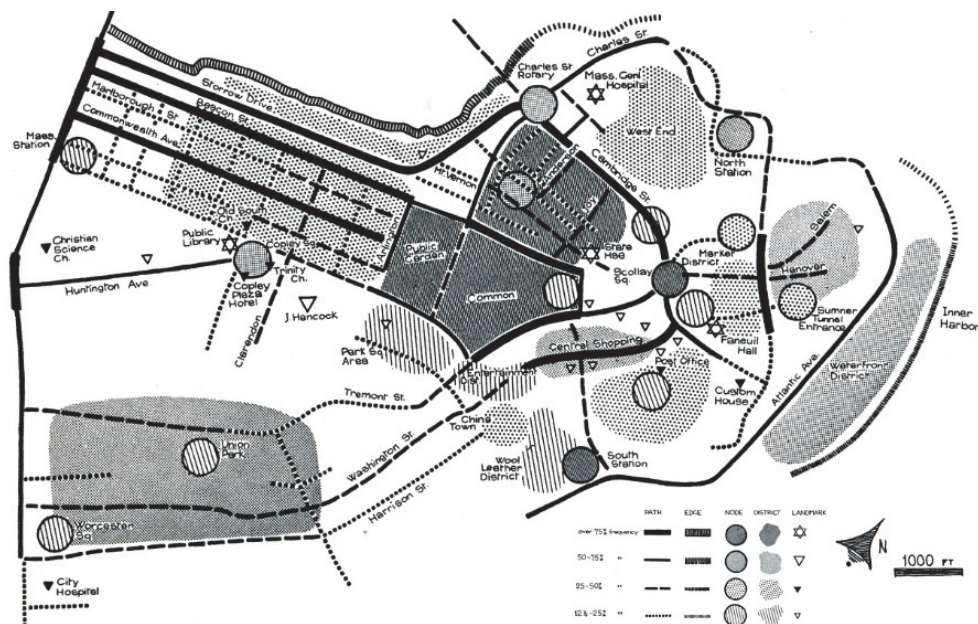
Figure 3.1 Lynch's public image of Boston [76, Fig. 35]. Lines represent paths and thick dashed traits stand for edges; circles and hatches represent nodes and districts respectively; landmarks are shown as triangular icons. The elements hierarchy is in grayscale.

(Credits josh s Jackson, got from https://www.flickr.com/)

With these components as lexical elements, plenty of semantics arise from their combination. The work of Gordon Cullen explored this concept in cities under the name of *serial vision*, as the visual experience accompanying an urban walk and shaping the sensory mix that leaves a mental trace (Figure 3.2).

The human mind reacts to a contrast, to the difference between things, and when two pictures are in the mind at the same time, a vivid contrast is felt and the town becomes visible in a deeper sense. It comes alive through the drama of juxtaposition. Unless this happens will slip past us featureless and inert . [77, p. 9].

De Wolfe and Panerai embraced this "dramatic" representation of space in a catalog of "visual effects" (Figure 3.2) [78], while Edmund Bacon collected a set of eight "elements of involvement" as perceptual impressions that should be used to design urban spaces [79]. Philip Thiel elaborated a method to annotate the pedestrian visual perception in an urban walk, a *space sequence notation*, which investigates part of the suggestions from Lynch and Gibson. He also formulated a distinction between O-type and X-type spaces: the former are *characterized by a feeling of completeness, cohesion, symmetry and balance* and the latter by a *tendency towards mobility, expansion and change* [80, p. 41] (Figure 3.3).

The question underlying all this research is how the urban space communicates with the perceptual system and how the image of the city is formed in our mind. The hypothesis is that part of the visual experience relies not only on the observer but on features of the space, which can be objectively described and assessed. In other words, to reuse an expression that will be specified further, there is a quest for a *space syntax* to decrypt the perceptual process triggered by the urban space.
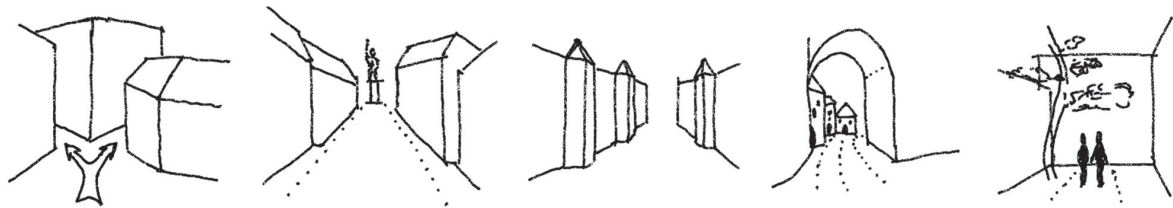
Figure 3.2 Some of Cullen's and De Wolfe's "visual effects". From left to right: choice, focus, punctuation, enclave, enclosure.

(redrawn by the author after [77] and [78])

(a) Place des Vosges, Paris, France. Credits : MaxPixel, CC
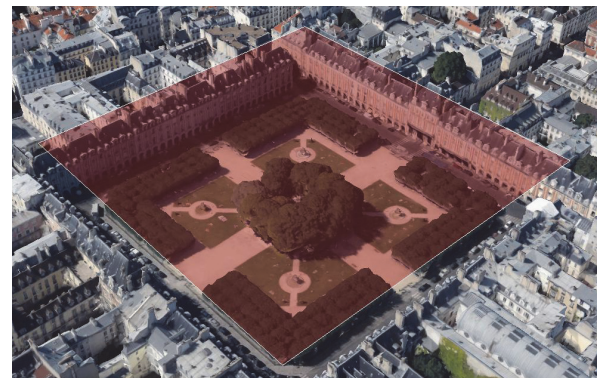
(b) Aerial view of Place des Vosges and its footprint. Credits : Google Earth © Landsat Copernicus

(c) Times Square, New York City, USA. Credits : BobbyMikul, CC
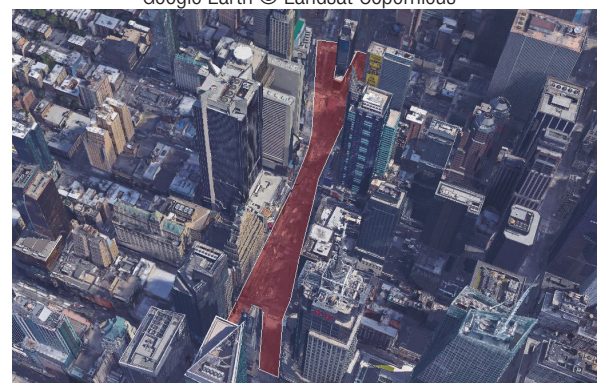
(b) Aerial view of Times Square and its footprint. Credits : Google Earth © Landsat Copernicus

Figure 3.3 Philip Thiel's conception of space. Place des Vosges as an O-space and Times Square as an X-space.

3.2 Visibility assessment by spatial description

In this gradual shift from the observer to the physical world, there is a need for significant descriptors that characterize space perception. The description of space passes through its geometric analysis, which even involves geomatics when dealing with a reasonably large region of interest. In fact, visual analysis develops from the broad landscape scale, starting from a simple orographic approximation of the territory. Often, studies refer to this domain as "visual impact assessment", as it is usually employed to evaluate the acceptability of new infrastructures in the landscape. The expression "visibility assessment" is preferred here for its more neutral connotation that transcends the positive or negative impact on the observers, related with phenomenological and psycho-sociological factors.

3.2.1 Viewsheds and landscape scale analysis of raster grids

Among the first quantitative attempts to assess visibility, Tandy conceived the so called "viewshed" [81]: just like water flows from a corrugated territory to streams, visual rays are conveyed to the observer in a sort of visual basin, from the boundaries of a "visual watershed" or viewshed. In other words, a viewshed is the set of visible locations from a given observer's position: by visible, it is meant here unobstructed, as locations that are reached by an uninterrupted line of sight from the observer to the target, up to a certain distance limit. A viewshed could be imagined as the portions of territory that can be enlightened by a laser beam held by the observer pointing in all directions (Figure 3.4). The main limitation of this model is that all the visible points are equally weighted, independently from the distance, the angle of vision, the contrast produced from meteorological conditions, etc. Nevertheless, the original purpose of viewshed is the identification of the geographic boundaries of possible view, rather than characterizing the visual experience of the observer. In this prospect, viewshed is a valuable index for urban design and has an interesting aspect: areas that are not comprised in the visual basin, are completely invisible from the originating viewpoint and might be relieved from most severe architectural constraints, including a possible prohibition of solar panels installation. Higuchi and Lynch explored the possibilities of viewshed analysis for landscape planning purposes, in particular forestry management in parks and sightseeing preservation [82], [83]. To extend the interest of viewshed though, it is necessary to compute it from many different viewpoints, in accordance with Gibson's "ecologic" approach and the freedom of the observer's movement as "optic flow". When the most probable observation points are identified in a landscape, the output of viewshed is much more meaningful.
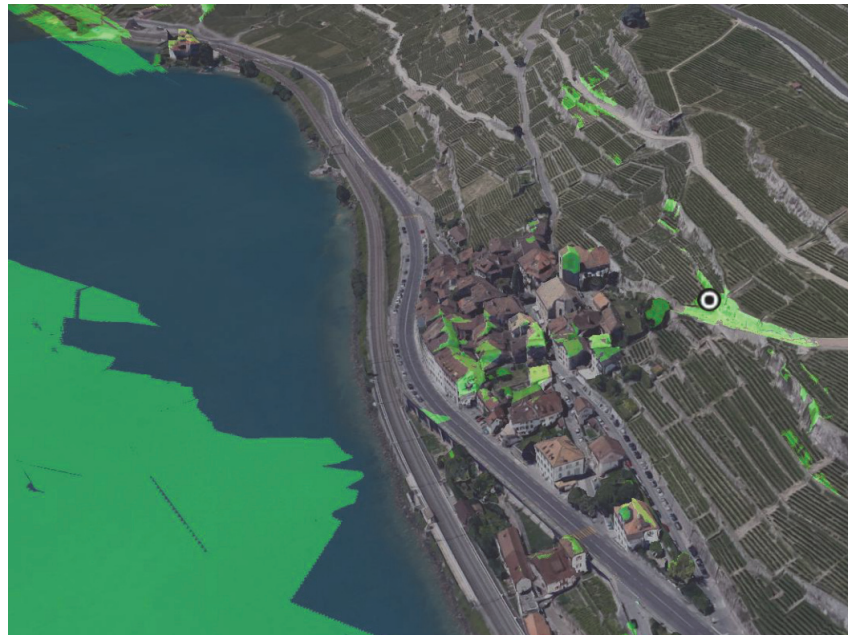
Figure 3.4 Three-dimensional image of the Viewshed from a viewpoint in St-Saphorin (indicated by the marker), Vaud, Switzerland.

(Used tool: Google Earth ©, Credits: Landsat Copernicus)

This extension to multiple viewpoints requires a sequence of calculations that becomes more efficient with automatic processing: this has been experimented in early stages with the software tool VIEWIT [84] and made comprehensively possible through Geographic Information System. Viewshed analyses are widely used and have become increasingly popular since their implementation in GIS: one could say that viewshed constitutes the visual impact analysis par excellence, at the point that they are commonly used as synonyms. The viewshed algorithm in GIS returns two values for an examined location: either "visible" or "invisible" from the observer's position. In this sense, the result is a "Boolean" variable, embedding the logic opposition "true" or "false" to the question: is location A visible from observer positioned in B?

Llobera investigated the opportunity offered by a viewshed analysis in GIS from multiple viewpoints, writing a comprehensive state of the art of the subject [85]. He introduced the concept of "visualscape", as the spatial representation of visibility indicators, such as viewshed, generated from many different observation configurations. One of the immediate outcomes of multiple viewshed calculations is the frequency of visibility occurrences for a given location, i.e. the number of times that a location is marked as "visible" by any viewshed. Such an indicator appears to be useful for archeologists to examine human engagement and socialization in historic and pre-historic natural and built settlements [86]. This sum is called *cumulative viewshed*,

or *times seen* indicator, following the denomination proposed by research focused on the subject, performed in the 90s by Fisher and others [85, Para. 3.2].

In the same time, researchers pursued the refinement of viewshed accuracy by tackling the aforementioned limitations and making it "fuzzy": Gross provided a mixed psycho-physical approach, introducing both distance and visual angle attenuation with the adoption of an indicator based on solid angle, corrected with a color difference factor and integrating visual acuity considerations [87]. Llobera suggested an index named *visual exposure*, taking into account the visual angle subtended by a target [85, Para. 3.4]: variants to this model follow [88], sometimes referring to the different designation of *visual magnitude* [63], [89]–[91]. Some of these assessment techniques are very thorough and complex but face the same trial: the spatial configuration as a *raster*, with the consequent resolution limitation.

Spatial configuration is the way physical space is sampled and stored in a virtual memory: most of the studies cited in this section are raster-based, meaning that the geographic space is subdivided into a grid composed of a discrete number of raster cells. The terminology comes from the Latin *rastrum* (rake) and the German *raster* (screen), evoking the idea of a grid made of parallel lines: a digital image is also a raster, formed by a set of picture cells (pixels). The number of cells per surface unit is commonly referred as raster resolution. Raster sampling is not the only possible spatial configuration, but it is particularly versatile when dealing with smooth slope variations in regards to cells resolution, as for orography and landscape morphology. In fact, most of the times Digital Elevation Models (DEM) of a territory are distributed in raster format, i.e. a color scale image where the pixel color corresponds to its elevation (Figure 3.5a). DEMs are obtained by the way of interpolation of topographic measures, currently performed in most cases via airborne laser-scanning (LiDAR): their accuracy depends on terrain roughness, elevation, data sampling density and interpolation algorithm. Based on these factors a finer or coarser raster resolution is determined as outcome. Hence, raster DEMs constitute reliable representations of a corrugated surface such as a terrain (Digital Terrain Models, DTM), eventually including anthropic modifications of land such as buildings (Digital Surface Models, DSM); on the other hand, they are not suitable to effectively describe vertical planes and complex surface interactions, occurring in roof covered spaces, porches, cantilevers, holes, tunnels, etc. In other words, DEMs are 2.5 dimensions models, since a single elevation coordinate can be associated to a raster cell: such a characteristic is exhaustive for broad

landscape description but becomes less adapted for dense and multi-faceted urban environments, especially when façades have to be taken into account. As a consequence of all said, viewshed, since mostly applied to raster datasets, incorporates the same limitations of this scalar discretization of space.

(a) DEM as raster   (b) DEM as TIN
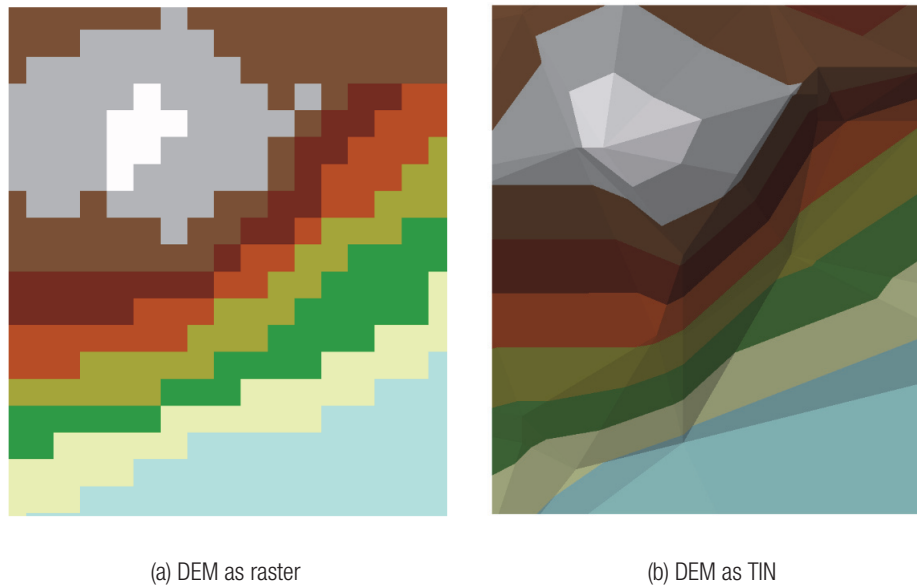
Figure 3.5 Hill of Signal, Bernex, GE, Switzerland. Different representations of a DEM from the same set of LiDAR points: Color gradient represents the altitude in steps of 10 m.

(Used tool: ArcGIS ArcMap © elaboration on CC data from Système d'information du territoire à Genève - SITG)

3.2.2   Isovists and urban scale analysis

Together with the viewshed, Tandy defined another representation of visible space under the name of *isovist*, which would mean *line of equal vision, from the precedent of isobar, isotherm, etc.* [81, p. 9]. In fact, an isovist is the locus of all visible points from the generating viewpoint, namely the vantage point; as already discussed, visible points are not equally perceived but can be all visually attained by an observer at the vantage point. Strictly speaking, this statement outlines the same definition of the viewshed but isovist, for its geometric genesis, history and usage practice, is more adapted to urban environment. A formal definition of the concept can be found in an article written by Benedikt [92]. In his demonstration, isovist appears as a concave polygon, whose area, perimeter and generating rays can be clearly identified and calculated with a dedicated function. By comparing viewshed with isovist (Figure 3.6), it is evident that a shape simplification has been operated: the dispersion of the visibility information in a myriad of pixels is condensed here into a single surface, which is proper of the vantage point

and characterized by geometric properties with a specific meaning for urban perception. At this stage, the polygonal form of the isovist is planar; at the same time, its sides are determined by obstacles and obstructions delimiting the visible space and generating a closed profile. *Isovist analysis requires well-defined borders in order to be realistic* [93]. These features make isovist particularly adapted for a relatively flat and limited space like an urban district with several buildings. Moreover, its polar construction around a source vantage point qualifies isovist as a parametric geometry, which is suitable for a vectorial spatial configuration.
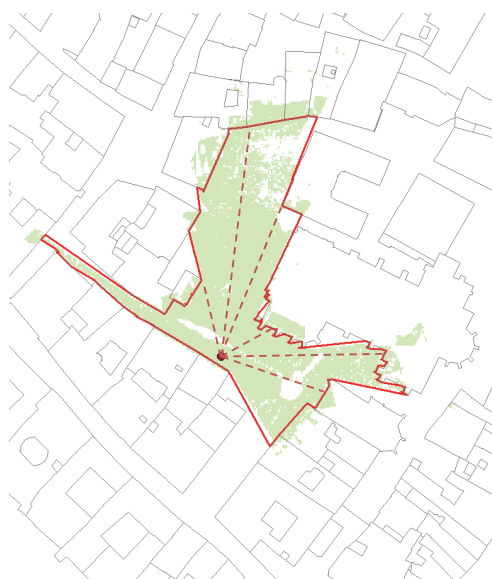
Isovist indicators	
Drift: distance from the generating viewpoint to the center of gravity of the isovist	27 [m]
Occlusivity: cumulative length of the occlusive segments of the isovist, separating visible from invisible open space	216 [m]
Entropy: Shannon's entropy calculated on the length of the generating lines of sight	3.46 [-]

Figure 3.6 Place du Bourg-de-la-Four, Geneva, Switzerland. Viewshed (green fill) vs Isovist (red edge) from the same viewpoint (red dot): some generating lines of sight, used for the construction of the isovist, are highlighted (dashed line). Note that the isovist does not take into account visible points on roofs. Some isovist indicators are listed in the table (see [94] for more specifications).

(Used tool: ArcGIS ArcMap © and Isovist program by Suleimann W © elaboration on CC data from Système d'information du territoire à Genève - SITG)

In a vectorial space, geometric primitives are conceptualized with a series of attributes. For example a line, which in a raster space is represented as a sequence of grid cells: in a vectorial space it is stored as the conjunction of two triplets of coordinates. This conjunction is coded as a rectilinear path from point A to point B that univocally qualifies the resulting object as line. Other geometric primitives such as arcs, curves, closed surfaces and meshes are parametrized in a vectorial space. Without going into detail, a vectorial space configuration has the advantage of not being dependent on resolution, compared to a raster; on the other hand, it relies on a topologic description of elements and their interactions, with an increased complexity in the stored information. Vectors are not adapted for continuous data with a homogeneous space

distribution, since they require substantial generalization into independent features; on the opposite, they are suitable to describe isolated edges, boundaries, polygons, and regions like isovists. Another drawback is that vector manipulation algorithms are complex and require high computational resources. In the previous paragraph, DEMs are illustrated as raster datasets but they can also be represented as triangulated irregular networks (TINs), a vector dataset similar to a points mesh (Figure 3.5b). The characteristics of a vector space configuration make it ideal for complex surface interactions in a discrete, delimited, hierarchized and feature-oriented geometric dataset: this is the case for buildings, which are independent objects scattered on the territory and subdivided into envelope surfaces often characterized by intricate intersections.

A vectorial characterization of isovists allows their manipulation as individual entities linked with the source vantage point; the computation of their geometric properties such as area, perimeter, etc. can be easily performed and memorized. Benedikt exploited this potential of vectorial isovists through the concept of *isovist fields* [92] (Figure 3.7a). The purpose was to explain Gibson's optic flow with an understandable and mathematically rigorous metric, by varying the position of the vantage point in a hypothetic urban walk. In an interesting experimental setting, Benedikt placed an omnidirectional light source in correspondence of many selected vantage points, into a physical model of a neighborhood. The resulting light pattern is the isovist field: this strengthens the analogy between light rays and visual rays that is the main hypothesis underlying this thesis work and the conception of *the visual world as a field of light-borne information in which the observer is immersed* [92, p. 48]. By overlapping the different isovists produced at each stage, it is possible to build a Minkowski model, viz. a solid representing the evolution of the visual boundaries (Figure 3.7b, see also another recent application in [75, Para. 5.4.2]).

After some years of skepticism, isovists reappeared with the advent of GIS and increased their success in vector environments thanks to the growing computational power. Batty pioneered the use of raster isovist fields to implement various assessment indexes both in a dense urban site and in an art gallery [95]: in fact, isovist employment reveals to be very fruitful for indoor applications and museums in particular, where the visual connection between artworks and visitors interacts with the architectural structure. Turner et al. generated a graph of mutual visibility between locations from a set of isovists and argued that these interactions have implica-

tions on way-finding, movement and space use [96]. The relationship between pedestrian motions and isovists expands the range of their application fields and continuously unveils new aspects of isovist analysis [97]. Currently, plenty of isovist-related indicators give clues on urban visual experience: worth to be cited are convexity, openness, entropy, and drift (Figure 3.6). An exhaustive catalog of these indicators and their meaning can be found in the literature ([94], [98], [99]). After all, it should be noted that, despite the thorough research on the topic, isovist is affected by the same limitations as viewshed in terms of attenuation along distance, visual angle, and atmospheric path.

(a) isovist field   (b) Minkowski model
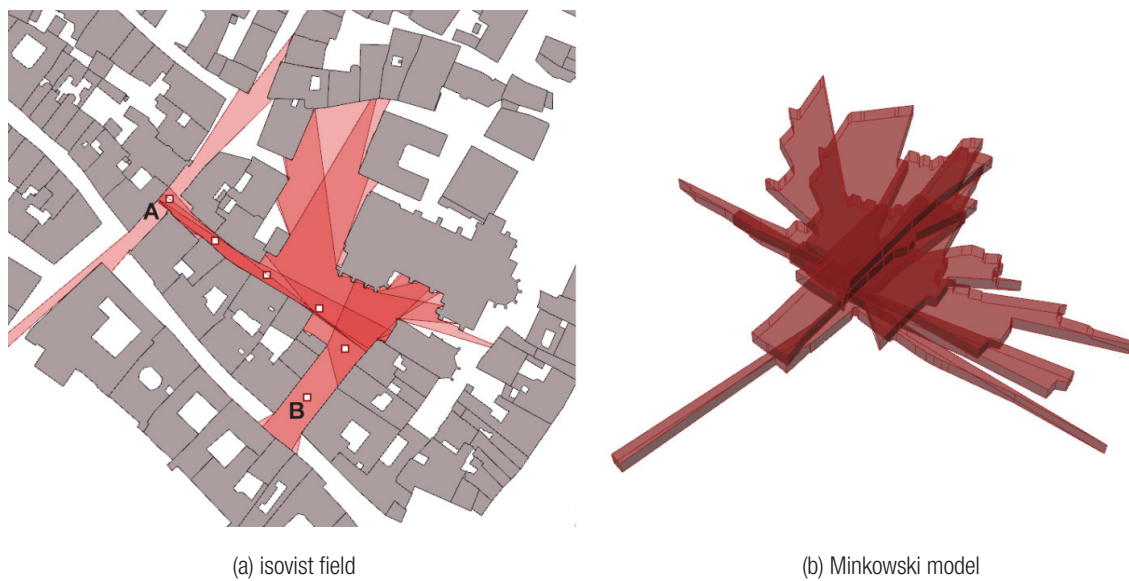
Figure 3.7 Place du Bourg-de-la-Four, Geneva, Switzerland. (Left) isovist field generated by the viewpoints in a path from A to B: color becomes darker when isovist polygons overlap. (Right) Minkowski model of the same isovist field, by overlapping the polygons in correspondence of their generating viewpoint

(Used tool: Grasshopper for Rhino © elaboration on CC data from Système d'information du territoire à Genève - SITG)

An important paradigm change in isovist analysis is the focus on target objects rather than on viewpoints (e.g. vantage points). Especially for urban planning purposes, it may be more convenient to quantify how much of a designated feature of interest (e.g. buildings, portion of buildings, streets, solar modules, advertisement panels) is visible from its surroundings: this translates into a spatial interrogation of an isovist field [100]. A possible application is the identification of the optimal video surveillance placement to guarantee the maximum visual coverage of an area [101].

In recent years, computational advancements permitted the extension of isovist in the third dimension. From a polygon delimited by visual obstructions on a plane, it evolves into a poly-hedron delineated by solid obstacles (Figure 3.10b). This is possible in *voxel* spaces, a sort of tridimensional raster grid, but also in 3D vectorial environments [102]–[104]. Possible representations of 3D isovists are a scheme based on contour lines sectioning the solid at different heights, a juxtaposition of horizontal and vertical sections of the solid, or a spiraled circumvolution of lines of sight from zenith to nadir [105]. Such a shift to the third dimension offers many possibilities and will be discussed further but before a list of alternatives to the isovist is addressed.

3.2.3   Space syntax and other bi-dimensional methods

Although isovists and viewsheds count the most disparate uses in the field of architecture, landscape planning, archaeology and security, they are not the only method to represent the visual environment. One of the critics to isovist fields and viewsheds is in relation to their need of a finite number of generating viewpoints among the infinite possible, which requires a sampling operation of space. On the opposite, space and its related features are always finite: hence, it could be possibly more accurate to explain visual perception by starting from the objects that populate the environment.

Hillier and Hanson developed a theory to link the social function and cultural meaning of buildings with their arrangement in space: they split the urban settlement plan into spaces delimiting socially meaningful groups of buildings, such as blocks or courtyard buildings and neighborhoods [106, p. 97]. Originally, these spaces were convex polygons. They drew the longest uninterrupted lines of sight connecting any pair of polygons and built an axial map (Figure 3.8). The number of axes connected to an axis, returns the *connectivity* of such axis; *depth distance* is the cumulative distance between the center point of an axis and all the others; *integration* measures how integrated, or central, an axis is with regards to the axial network; *choice* or *betweenness* measures the importance of an axis in joining portions of the network; many other indicators are available and are proven to be effectively employed for many purposes, i.e. from shelter finding to crime distribution analysis and best placement of commercial products. The resulting approach, commonly known as "Space syntax" is not exempt from criticism: limitations are relative to the selection of the longest lines of sight as privileged visual paths which is not consistent in all urban configurations, as well as the non-perfect association of visibility with

pedestrian movement. As for isovists, an extension of the space syntax methodology and indicators in the third dimension is possible thanks to the modern computation techniques: it might smooth some of its drawbacks or reveal new potentials [107].

Figure 3.8 Axial map of the zone surrounding the cathedral of Geneva. Connectivity increases from blue to red.

(Used tool: DepthmapX 0.30 © elaboration on CC data from Système d'information du territoire à Genève - SITG)
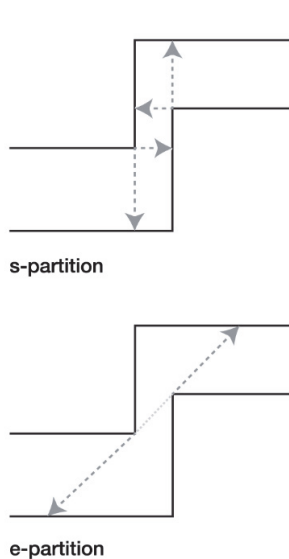
(a) Peponis' space partitions definition

(b) Peponis' space partitions in Place de Hollande, Geneva, Switzerland

Figure 3.9 Peponis' space partitions.

(Used tool: Isovists 2.0 CC elaboration on CC data from Système d'information du territoire à Genève - SITG)

The space partition into convex "patches" has been extended by Peponis [108], who aimed at subdividing urban settlements into visually uniform spatial units, probably inspired by Philip Thiel [80] (Figure 3.9). He defined s-spaces and e-spaces, where "s" stands for surface and "e"

stands for end points. The former are patches delimited by the extensions of building footprints' sides forming a reflex angle (between 180 and 360 degrees) in the open space; the latter are subdivisions of s-spaces with "diagonals", issued by connecting building footprints' corners with segments that can be extended in the open space. When crossing a line delimiting these spaces, a building footprint's side becomes either visible or invisible, marking an "event" in the visual experience. This approach was explored by Leduc et al. [94], [109] and can be combined with other isovist metrics.

3.2.4   Spherical indexes and the third dimension

Hillier and Hanson were convinced that three-dimensional analysis does not contribute significantly to the understanding of urban perception:

Human spatial organization is not three-dimensional in the same sense that it is two-dimensional – for the simple reason that human beings do not fly and buildings do not float in the air. Human space is in fact full of strategies – stairs, lifts, etc. – to reduce three-dimensional structures to the two dimensions in which human beings move and order space. This is not to say that the third dimension is unimportant: only that it is not comparable to the two-dimensional structure. [106, p. 272]

This conviction influenced research for some years: the two planar dimensions were the priority to address, in contradiction with Gibson's theory of ecologic perception that aims at the consideration of the extensive multitude of stimuli in the environment (Section 3.1). An increasingly widespread design of high-rise buildings though, characterized by a dense and compact appearance, strengthened the impression that height is essential to express urban sensations. As mentioned in Section 3.2.2 in regards to 3D isovists, lines of sight can be cast in all directions, not only on a plane. It is much more unlikely though, that a tridimensional space is bounded by obstacles in all directions to produce a meaningful isovist with well-defined borders. This is possible in an indoor location: Krukar et al. decomposed the 3D isovist into different pyramids facing top, bottom or side surfaces (i.e. ceilings, floors, walls) and treated these regions differently in accordance with the human visual field; horizontal information is privileged and top/down asymmetry is taken into account in their *embodied isovist* [110]. On the other hand, in a typical urban scenario, many lines of sight are not blocked by any building and escape to the sky, viz. towards the infinity. This issue can be overcome by conceiving lines of

sight as radii with equal length for an omnidirectional perception, in a spherical visual field (Figure 3.10b).

Inspiration comes from climatology: with the purpose of quantifying the urban heat island effect, the sky-view factor is defined as the fraction of radiant flux leaving a building surface which is intercepted by the sky vault [111]. In other words, it is the fraction of the overlying hemisphere occupied by the sky in a stereographic spherical projection, obtained through fish-eye lenses photographs or graphic reconstructions [112], [113]. In fact, when considering a hypothetic unitary subdivision of the sky projection on a sphere, sky view factor takes into account its position in the hemisphere and weights it in accordance with Lambert's cosine law, which is required for radiometric calculations. Nevertheless, in the view of a perception assessment, every "sky patch" impacts equally on an observer's feeling of confinement and should have the same weight. This is the hypothesis made by Teller, who proposed the use of an equal area spherical projection instead, to evaluate visual connection of people to the sky [114] (Figure 3.10a and Figure 3.11): the outcome is a *sky opening factor* (sometimes called sky exposure factor). The sensation of openness was deeply analyzed by Fisher-Gewirtzman et al., who defined the spatial openness index (SOI) as the unobstructed volume of the spherical visual field (Figure 3.10b), with a radius ranging *far enough behind the seen obstacles* [115, p. 579]: a questionnaire shows the consistence of the method with the openness feeling declared by sampled observers. Research on this topic leads to interesting applications on outdoor view appreciation from building users [116]. A kind of normalization of the spatial openness index is the *viewsphere index* from Yang et al. [117], which represents the total obstructed volume in proportion to the volume of the hemispheric visual field (Figure 3.10c). In terms of urban planning, such indicator can be combined with other metrics and easily used to compare different building design projects in terms of potential visual impact [118]. A remarkable synthesis of different spherical indexes as well as their implementation in urban design is available from Lin et al. [119].

All the spherical approaches are different, but most are affected by the common recourse to solid angle as a geometric indicator to approximate the size of an object in the spherical visual field. This solution is also the starting point of this thesis work and will be discussed thoroughly further. A spherical conception of space opens also possibilities to non-Euclidean assessment techniques that will not be investigated here [120].

(a) Shading mask obtained via projection of the buildings on a hemisphere

(b) Unobstructed volume of the spherical visual field (3D isovist), accounted for the Spatial Openness Index

(c) Obstructed volume of the spherical visual field, accounted for the Viewsphere index
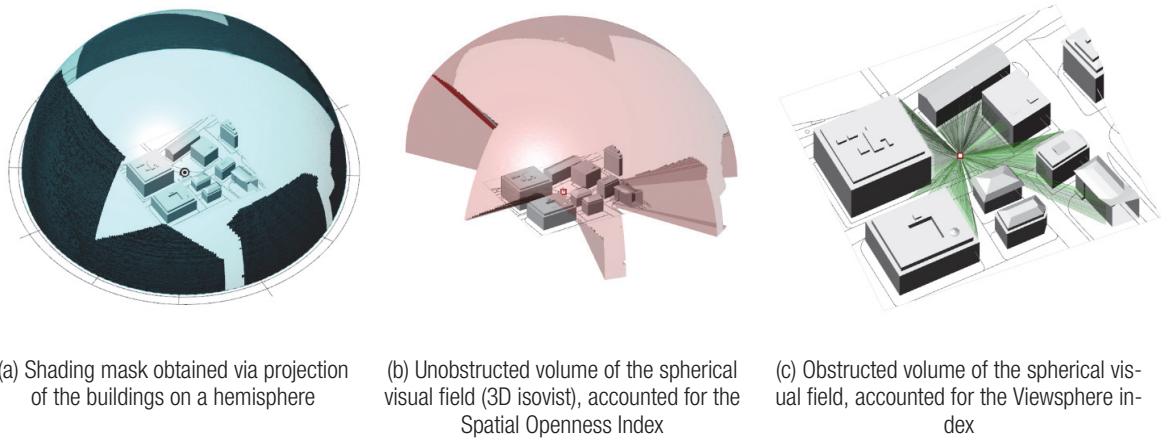
Figure 3.10 Place de Hollande, Geneva, Switzerland. Different portions of the spherical visual field used to calculate various indicators. Some works refer to the solid shown in (c) as a 3D isovist.

(Used tool: Grasshopper for Rhino © and Ladybug CC [121] on CC data from Système d'information du territoire à Genève - SITG)
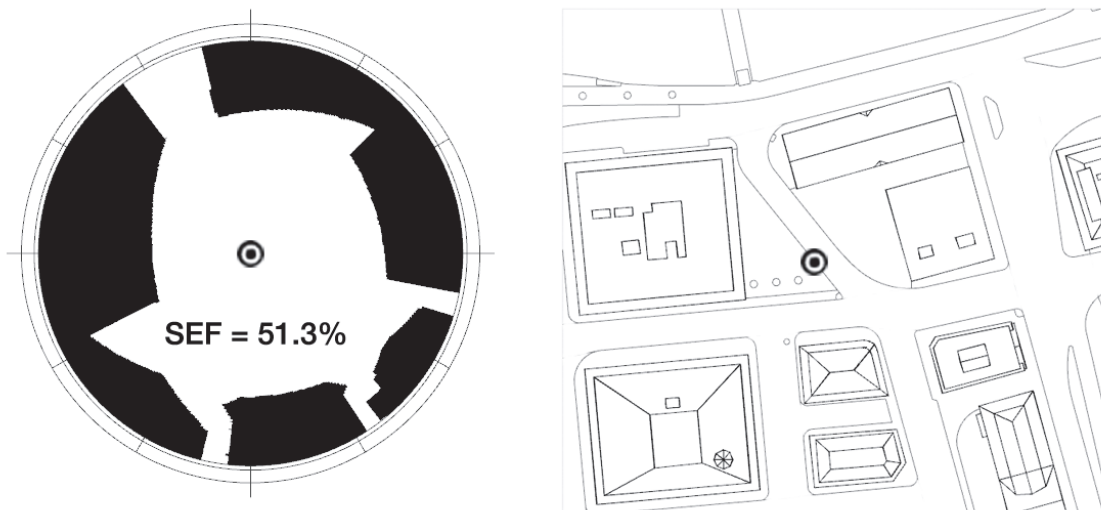
Figure 3.11 Place de Hollande, Geneva, Switzerland. Sky opening or sky exposure factor obtained from an equal area spherical projection; the viewpoint is highlighted in the plan on the right [114]

(Used tool: Grasshopper for Rhino © and Ladybug CC [121] on CC data from Système d'information du territoire à Genève - SITG)

3.2.5   Fuzzy visibility metrics

The majority of research reviewed to this point focuses on the definition of visual limits, the formulation of indicators that summarize the visual basin of an observer, the extension of these concepts to multiple viewpoints and the third dimension in space. Fewer works concentrate on the way vision attenuates in the visual basin, isovist, viewshed and viewsphere, etc.: ideally,

their boundaries should fade until visibility disappears. One of the first steps would be to consider the length of the line of sight from the observer to the target: the longer it is, the less impacting the vision in relation with depth. For instance, lines of sight can be represented with different colors proportional to their length (like in Dalton's *Isocam* [105], see also [116]) and eventually be ranked in a qualitative way [122]. When taking into account the targeted object's size as well, visual angle has to be introduced for line of sight weighting. Koltsova et al. proposed a 50%-50% weight of length and visual angle [123], Arabacioglu a fuzzy inference system [124]; cited works on visual exposure and visual magnitude (Section 3.2.1) compel with Beer-Bouguer-Lambert's law (Equation 2.8) and implement the cosine of the visual angle factored by the square of the distance. Spherical indicators, as already mentioned, are based on solid angles and mostly take into account object's size as projected on the spherical visual field: Teller produced hybrid indicators and mixed lines of sight to surface centroids with the relative solid angles [114]. With some remarkable exceptions though (e.g. [123] and [100]), these indicators often qualify the viewpoints: the information on visibility is stored and represented as a property of the viewpoint. Keeping systematically track of visibility on visual target rather than the observer's viewpoint is one of the objectives of this doctoral thesis.

3.2.6   Virtual geographic environments

A promising new platform to perform visibility assessment is virtual reality. One of the main advantages of such approach is the navigation through the virtual environment, which allows simulating a proper visual experience. By navigating, visibility indicators are recorded and a track of the interaction of the user with the surroundings constitutes the assessment method. Such interaction could also be simulated with virtual, computer-driven observers that move throughout the space, as for Batty's *agent-based* computation [95, Para. 3.1]. Much useful is the employment of known videogames interface, like *Second Life*, to explore the way people perceive space and assess visibility indicators [125]. In fact, videogames replicate a whole sensory experience nowadays, with visual and sound effects very close to reality; on the other hand, gaming devices are more portable and connected together via internet, offering new interactive platforms. The result is a tighter link between virtual and physical world. Virtual reality approaches real world scopes through the development of "serious games", which simulate military or fire-evacuation trainings, museum visits, or even reconstruct designed environments at the landscape, urban and architectural scale. In the domain of renewable energy planning, for example, a wind farm visualization in a virtual environment is employed as a complementary

resource to the traditional visual impact analysis [126]. Most of virtual models render the scene through radiosity algorithms which are not entrusted from the point of view of physics; in spite of this, it is possible to reliably imitate human experience of visual perception and visual comfort in a 3D simulation with more precise ray-tracing techniques [127]. At the present day, immersive virtual reality devices like VR glasses almost bring the observer into the scene; similarly, by framing real objects with a camera equipped device some relevant information appears on a screen in a sort of virtual elements overlap. This are the principles of *augmented reality* that complements virtual reality and has many applications in georeferenced data science. In terms of visibility analysis, for example, it is possible to extract the skyline of a live camera image and add 3D rendered objects (like PV solar modules) to assess the impact of new designs on the original situation [128]. The majority of these techniques are associated with a personalized experience since, just like in the physical world, each user interacts differently with the virtual interface. The advantage, in this case, is the digital trace that can be recorded by a computer appliance. In the following paragraph, the discussion on personalized approaches continues under the perspective of population based visibility assessment.

3.3   Interface with population based visibility assessment

Even if the subject of visibility assessment through the empirical observations made by a population sample is too broad and goes beyond the scope of this thesis, a non-exhaustive enumeration of relevant studies is presented: a complete review can be found in recent literature [75, Pt. 1]. Among the pioneers of psychological visibility studies, Kaplan and Kaplan collected the feedback on many different visual settings from a variety of observers [129]. They inspected the psychological effects produced by the natural environment, such as the feeling of wilderness, tranquility and well-being. Some of their conclusions can be useful in terms of landscape design and are worth mentioning. Already cited, population based psychophysical experiences by Shang and Bishop inspire the development of an indicator taking into account both visual acuity and lightness contrast [66]. An interesting combination of spatial description indexes (viewshed) and preferences expressed by students and local inhabitants is available for landscape showing that certain indicators based on spatial structure are correlated with the observer's preferences [130]. Surveys on visual preferences can be useful to weight lines of sights or fine-tune the outcomes of geometric indicators such as isovists (see [122]): they can also be used to argue the social predilection towards a place and tailor cultural heritage protection policies or to map the socio-economic segregation [131]. In conclusion, despite the inherent

subjectivity of population-based surveys, they can be valuable instruments to weight spatial descriptors, especially when the population sample is sufficiently large. Their use becomes even more interesting for renewable energy planning, when a target group of potential observers is concerned with the modification of a landscape in relation with a renewable energy facility (see for instance [132]). A closer look to this item is given in the following section.

3.4   Visibility assessment in renewable energy planning

Visibility assessment is often a major concern for large renewable energy facilities installed in open lands: in this case the setting-up of energy production plants is subject to an authorization from local authorities who manage the landscape and the cultural heritage. The process can be diverse since local authorities decide upon different legislative and operational frameworks; it becomes even more fragmented for small renewable power plants installed in urban sites, where municipal regulations come into force and opposition from neighboring ownerships can be raised. In this section, visibility analysis is considered in its main stages in order to identify at which moment of the planning process it is relevant and how it is usually performed based on the above listed methodologies.

Visual impact assessment is part of the environmental impact assessment, which is regulated by a dedicated Swiss act [133] and an European directive [134]. The methodology that is most commonly used to set-up renewable energy facilities includes the following tasks (see [135, Para. 4.8]).

1. *Definition of the extent of the study area*. This extent usually reflects the worst-case visibility scenario, i.e. in conditions of clear view without atmospheric attenuation and with no obstruction from vegetation (in case the study area is in open land, also buildings may be neglected). In practice, this operation can be performed by computing a viewshed on the appropriately selected Digital Elevation Models from the renewable installation site. The visibility distance limit should be accurately set according to the type of renewable energy production plant (land-based or offshore wind farm, concentration solar with or without receiver tower, tracking solar systems, steady solar modules) and the type of environment (land, offshore area, village, urban settlement). For wind farms, the threshold ranges between 30 and 50 km [135, Para. 2.6.1-2.6.2], mainly as a function of shape, size and motion of the turbines; for solar farms, rapid changes in color and reflectivity make them visible up to 35 km [135, Para. 2.6.3]. This threshold can be

reduced for small solar arrays in dense urban contexts, where the visual environment is characterized by more complexity in shapes, colors, skyline, and textures: no scientific source is available on this matter but urban planning practitioners assume 500 m for small scenic components [136, p. 36], with explicit reference to building integrated solar modules in a Swiss context [137, p. 9]. At the end of this phase, a Zone of Theoretical Visibility (ZTV) or Zone of Visual Influence (ZVI) is established.

2. *Description of the context and on-site visits*. In this phase all the relevant plans are collected, from landscape policies to municipal regulations. Land use has to be mapped and housing development too, to take into account any potential evolution of the observing population. Demographic surveys may also be pertinent in this phase. It is recommended to take photographs of the existing situation, especially from the selected viewpoints, as a base for eventual photomontages or diverse simulations.

3. *Identification of the territorial resources and their sensitivity (viz. sensitivity)*. A census of cultural heritage sites, conservation areas, designated landscapes, relevant landmarks and characterizing identity elements is carried-out. A sound analysis should embrace natural environment (orography, hydrography, wild flora and fauna), historic anthropic stratifications (parcels, canals, paths, agriculture and animal farming, villages, historic buildings), post-industrial infrastructures and settlements (roads, railways, buildings, industrial districts). The sensitivity of such a landscape can be assessed in terms of: (i) shared cultural value and social predilection attributed to each individual resource or to their combination as a whole; (ii) resilience to a specific type of change, in terms of interactions between the landscape itself, the way it is perceived and the specific nature of the type of modification or development in question and (iii) capacity to accumulate such changes.

4. *Identification of the visual resources and their sensitivity (viz. visual interest)*. As for physical resources in the environment, relevant viewpoints and sightseeing areas are collected. They are affected by a degree of sensitivity as well, which depends on: (i) the amount of landscape within the visual field; (ii) the number of people who can potentially see it (among local population, tourists and travelers on local infrastructures) and (iii) the nature and duration of the observer's experience (steady, dynamic, for touristic pur-

poses or not). In the literature, some studies considering the amount of permanent inhabitants in a zone [138], or the quantity of traffic along a road section [139] are available.

5. *Magnitude assessment of the territorial resources modification (viz. quality)*. The territorial resources are altered by the renewable energy facility: this alteration is usually negative but might also be beneficial. At this stage it should be determined whether the modification is dominant in affecting the site identity, highly incongruous and extended over a long time span, translating into a high magnitude. The difference with the global morphology, scale and pattern that could compromise the integrity of the site should also be considered. In practice, Sullivan suggests to check changes in forms, alignments, colors and texture [135, Ch. 6]. Form includes shape, geometry and size; alignment is the layout of the renewable generation units array in relation with the edges in the visual scene; color reflects hue, saturation and brightness (see Section 2.3); texture is the combination of color and light regularities that are perceived up to a certain distance. For wind farms, relevant variables are the height and color of the turbine, their position and alignment on the ground, the presence of aviation or navigation safety lighting. For landscape integrated systems, the enquiry considers: (i) the global shape and size of the land patch hosting the active surface; (ii) the pattern effect of the modules within the land patch, their porosity, distribution and unity [140] and (iii) the color, texture and reflectivity of the modules; the presence of concentration receptor towers and their shape, size and color has to be taken into account too. Ancillary devices like electricity conversion stations, cooling plants with their vapor emission plumes, transmission towers should be included in the analysis. For building integrated systems in an urban environment, Munari Probst et al. refer to "architectural integration quality" and recommend to consider the coherence of: (i) solar array size and position on the building envelope; (ii) visible materials, colors and surface textures and (iii) modules shape and size, connections and joints [28], [33], [34], [141]. Other references indicate rather criteria like co-planarity, alignment, shape, modules grouping, details accuracy [142], [143].

6. *Magnitude assessment of the influence on visual resources (viz. visibility or visual impact)*. As it has been explained in Chapter 2, observer's characteristics like visual acuity, experience and motion affect visibility. Following the lines of sight from the observer to the target, topography, vegetation or other elements may partially or totally obstruct the

vision. Over distance, earth curvature, atmospheric refraction, air pollution, dust and haze as well as meteorological conditions and artificial lighting have an influence. At the object level, its shape and size influence perception at visual acuity threshold (Section 2.4.1); object's color, texture and reflections mix with the background color, texture and skyline affecting visual contrast; light blinking, glare, moving elements capture selective attention. As such, each of these phenomena affects the magnitude of visual impact or visibility (Figure 3.12). In practice, some simplification can be adopted to estimate the resulting effect. The easiest method is to consider classes of distance from the renewable energy facility as an indicator of the visual magnitude. This can be done for large power plants in open lands, assuming high visibility within 5 km, a blend with the general landscape from 5 to 15 km and a fusion with the background beyond 15 km [135, Para. 4.8.4]. In urban areas, distinction of scenic components like solar modules and multi-sensory perception happens within 500 m, even if elements standing out of the background emerge until 1200 m; large volumes are detectable as texture, color and contrast patches within 2500 m; only profiles and skylines can be perceived beyond [75, Para. 1.3.1], [136, p. 33]. Apart from distance, another option is to compute the fraction of visible land area within the distance limit from the renewable facility [62] or vice-versa the fraction of visible facility area from the selected viewpoints, eventually cumulating their effect (cumulative viewshed [136]). To refine this basic assessment method with visual acuity-related factors of shape and size, it is possible to compute visual magnitude as mentioned in Section 3.2.1, taking into account the solid angle subtended by the renewable power plant [62]; spherical indicators can also be used [65]. Visual contrast considerations can be added too: in this case, meteorological conditions and the appearance of the renewable facility are compared with the background formed by other objects, the topography or the sky [59], [144]. Saliency methods are also suitable for this type of analysis, especially in urban settings that are richer in boundaries and skylines [71]. Finally, attention-capturing factors deserve to be addressed, in particular motion of elements such as wind turbine blades, solar tracking devices, mirrors; luminance distribution and glare risk are non-secondary indicators, especially in proximity of airports [145]–[147]. In case of multiple power plants, individual factors of each concur to a global visual magnitude index: objects falling simultaneously in the observer's visual field have a higher impact than those only detected when moving the head or displacing the whole body.
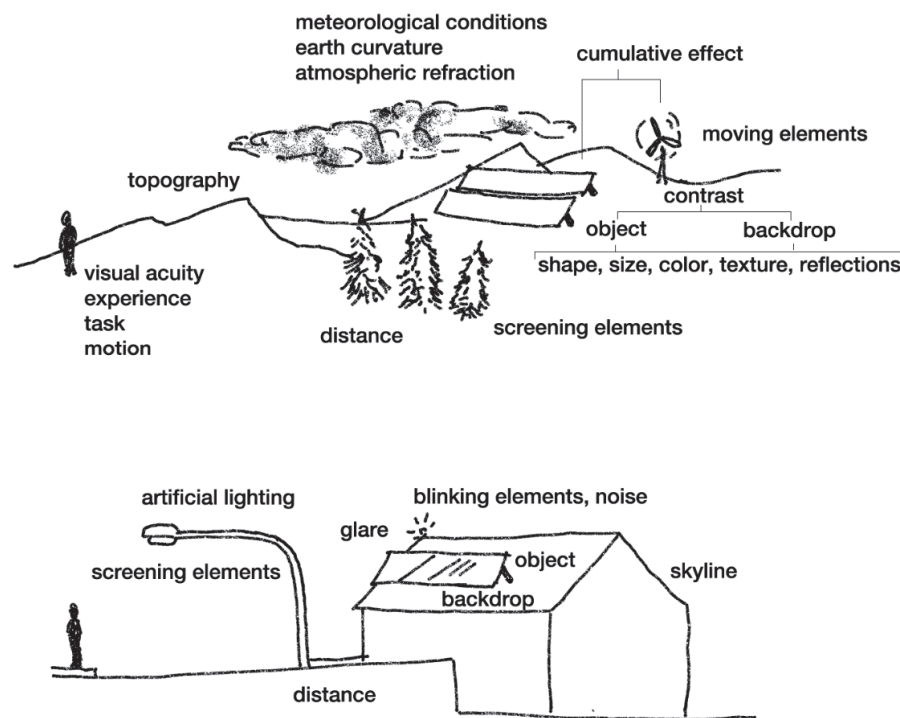
Figure 3.12 Factors influencing visibility of renewable energy production plants in open land and in urban contexts.

(Author's own elaboration)

7. *Social acceptance assessment*. Magnitude of visual impact is important since it is a dominating factor in public acceptability, but it is not the only one. In fact, as already highlighted, residents are objectively more visually exposed to a renewable energy facility and consequently in probable opposition to it: in spite of this, they can sometimes encourage it. On the other hand, visitors are generally less concerned if they have no particular predilection for the target territory [148]. Factors that play a role in this context are [135, Ch. 5]: (i) environmental factors (acoustics, glare, vapors, odors); (ii) contextual factors (traffic, infrastructural development, security of the site); (iii) policy and institutions (support, coherent energy strategy, proximity, equity of treatment); (iv) population involvement (information, consultation, participation, media communication); (v) ecology (land use and consumption, clean and local energy, greenhouse gas reduction, biodiversity and animal threats for birds) and (vi) economy (economic improvement, job creation, local tax revenue increase, secure energy supply, shareholding). It is important to state that the objective relevance of these variables is less impacting on social acceptance, rather than their social perception. Ideological processes influence the latter

and vary a lot from place to place, such as local identity, sense of community, sense of control, local pride, "Not In My Back Yard" effect. In this sense, demographic composition counts: younger residents and rural areas inhabitants are in general more favorable to renewables; once the installation is completed though, social acceptance may increase [135, Para. 5.3.2].

8. *Multi criteria decision making (MCDM)*. In most complicated scenarios, the diversity of variables determining the appraisal of a given project may lead to the use of multi-criteria decision methods, eventually corroborated with quantitative mathematical models (see Section 1.2). Mostly technical feasibility, grid compatibility, economic remuneration and environmental factors are considered, together with energy generation [27]. According to a recent census [149], 28% of multi-criteria studies in renewable energy investments across the last 20 years took "social acceptability" into consideration; only the exact half (14%) though, is concerned with the "visual impact" of the project. Sometimes the latter is only estimated in qualitative terms according to the distance from the nearest observer, the type and the size of plants [26] and is considered separately from social acceptability. In other occasions, visual impact is explicitly associated to social acceptability [150], especially in landscape or archaeological sites representing specific high sensitivity zones: an interesting study about the installation of photovoltaic power plants in Corsica Island takes into account the reciprocal position of the potential observers and the envisaged facilities (geometric factor). The relevance of viewpoints is sorted based on their location on significant roads, homes or villages, thus setting a sort of viewpoints hierarchy [151]. Moreover, land uses are assigned a score based on their touristic and cultural interest and on their agricultural exploitation, approaching the concept of sensitivity. Multi criteria methods are less employed, but also available for small renewables in urban contexts, in particular building integrated solar photovoltaics (BiPV). Apart from the already cited ones ([28], [143]), worth to mention is the technique by Di Giovanni et al. [152], for its comprehensive articulation of environmental, economic, social and technological criteria.

9. *Identification of mitigation procedures*. The renewable energy facility is not the only object that needs to be designed. The surrounding environment can mitigate the visual impact of the intervention and even modify the global perception of the scene by influencing the social acceptance. This operation deals with scenic design as if the whole

landscape was a sort of scenography. For instance, the panorama may expand in a wide, extensive view (such as for lakes or prairies); otherwise, it may be framed by enclosing natural elements (like cliffs or forest canopies) or architectural components (walls, terraces, cantilevers, fencing); it can also be physically dominated by a feature (like a mountain or a landmark). The scene is populated by objects that affect the visual rhythm, eventually stressing perspectives and depth (like trees on road sides or buildings). As such, visual axes, visual planes, focal points are defined. The relative position of the renewable facility in this setting is particularly relevant. Generally, the more "visual pollution" affects the scene, the easier it is to hide the renewables facility to an observer. In terms of mitigation strategies, vegetation and plants is a typical mean to screen or redirect the view. Color painting on the back side of solar panels or mirrors, fencing, enclosures and earthen berms can also be fruitful. For building integrated solar technologies, a valid solution is the use of non-active modules (viz. dummy modules) to give a uniform appearance to the hosting envelope surface.

10. *Participatory process*. In all project phases, especially at the last stages of the decision process, an implication of the concerned population is essential. Different steps in the public involvement can be identified ([135, Ch. 10]). In the first one, stakeholders are gathered, the main project issues are presented and the consultation method is designed. In the second stage, reciprocal listening and learning contributes to the optimal development of the project: this is the key moment for new ideas and solutions finding to emerge and awareness to rise. Stage 3 is for adjusting the project, monitoring, evaluating the results and keeping contact with the stakeholders. Participative tools entail different levels of involvement. Public hearings are more formal and addressed to representatives from local co-operatives, non-governmental organizations, producing official statements; personal surveys are useful instruments [153], but they do not allow public debate. Social media represent a valuable resource to share quick messages through images or videos, but lack mediation and moderation of public reaction. Exhibitions and informational meetings are often characterized by ex-cathedra presentations and should foresee questions-and-answers consultations; communication sessions and public debates can be more effective by adapting the message to specific target groups and valorizing their feedback. Participatory workshops, ideally accompanied by

a cultural mediator, are the ultimate level of involvement with renewable developers and local stakeholders sharing their expertise and working at a common task.

3.5   Discussion

Solar energy planning may vary a lot from large-size landscape power plants to small-scale building refurbishment. All the cited methods and the considerations made in this chapter should be fitted to the envisioned application. For instance, at the territorial planning level, it may be sufficient to establish a buffer distance from a bunch of significant, panoramic viewpoints, which delimits the solar systems-free zone. Only if the designed solar power plant falls in the buffer zone, a more detailed assessment is needed. The circular buffer may be restrained to particular "viewing corridors" subtending essential landscape elements (see Section 4.2.2); at this point, a viewshed analysis from the renewable facility design can reveal from which locations it would be visible. Depending on the significance of the viewpoints and the size of the solar modules, a magnitude estimation of visual impact may be performed at this stage: a rough measurement of the distance from the viewpoints to the installation site or more refined methods based on solid angles can be used accordingly. In wide landscapes, solar power plants can be immediately distinguished as intruder elements in a natural setting, this sensation being maintained even at long distances: only atmospheric and meteorological attenuation may intervene to limit the visual perception. In urban contexts, this magnitude depends more on the buildings skyline as well as on the objects and the materials characterizing the scene, rather than on atmospheric and meteorological components. Concurrently, potential observers and viewpoints are more evenly distributed in urban areas, where it might be more difficult to identify privileged viewpoints, in comparison with open land.

A sound visibility assessment helps in appraising social acceptance of a particular solar system project: a visible system may rise opposition from the neighbors and from the developers themselves, especially when visual comfort is involved. To that extent, it is relevant to estimate glare risks engendered by solar modules reflections. Opportune coordination with local communities and mitigation procedures should be set-up in most critical cases.

3.6   Conclusion

At the end of this chapter, the reader should be aware of the current advancements in visibility assessment and the way it is useful for renewable energy planning. A thorough list of available indicators has been presented and their practical relevance in the renewable design process

has been highlighted. It is obvious that not all visibility models available in scientific literature are employed as urbanistic tools, either in the pre-design phase or in a post realization assessment. This may be explained by their complexity, which is not sufficiently beneficial in terms of synthetic answer to the public perception of renewable facilities and does not justify their widespread implementation. On the other hand, urban contexts still lack reliable, experimented and extensive methodologies to include visibility assessment in building design and urban integrated solar technologies. At the boundary between urban design and perceptual research, there is space for new tools satisfying such a need, supporting the whole decision chain including administration, institutions, urban and building designers and stakeholders. In the next chapter, the framework for a development in this sense is set before describing into detail the proposed methodology.

Chapter 4   Research framework

4.1   Research question

The state of research presented in the previous chapter demonstrates the crucial need for Multi-Criteria Decision Making tools at the city scale to pursue an effective deployment of renewable energy plants, especially active solar technologies. Among different criteria, social acceptability is important and finding objective and systematic ways to assess it could improve the relevance of decision tools. Visibility is essentially linked to social acceptability: many interesting experiences conducted at the large geographic scale could inspire an implementation and an adaptation to the urban environment, specifically re-oriented to the purpose of solar energy refurbishment. Currently, though, a lack of reliable indicators for building integrated solar technologies in urban contexts comes as evidence. The scope of this work is to provide a scale-dependent methodology to assess visibility in urban areas, from the strategic broad territorial scale to the district level, even the neighborhood or the cluster of buildings. With the specific aim to include it as a variable in a multi criteria model, a scale-adaptive visibility index is determined. At the broader scale, visual interest and viewshed based indicators are proposed. At the district scale, photometric models and ray-tracing techniques are explored to mimic human vision and identify the perceived areas of building envelopes that can potentially host solar modules. Visual perception modeling based on a bundle of light rays (viz. a luminous flux) allows introducing illuminance attenuation as a function of human visual acuity: this constitutes a fuzzy visibility metric, which can be adapted to the complexity of urban morphology, featuring buildings with differently sized and oriented envelope surfaces (Figure 4.1). Under such approach, lines of sight are translated into light rays and viewsheds into illuminance levels: thus, the visibility model acquires a physical meaning that can be associated with psychophysical evidence. The development of this visibility metric called "Visual amplitude" will be detailed further in Chapter 7: it constitutes one of the main scientific outcomes of this thesis.
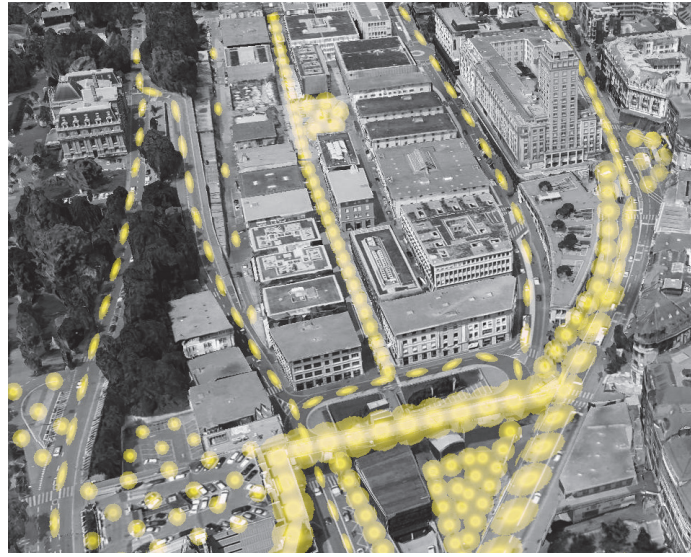
Figure 4.1 Flon district, Lausanne, Switzerland. Creative representation of the photometric model.

(Used tool: Google Earth ©, Credits: Landsat Copernicus)

The visibility indicator is combined with an solar radiation map at the various scales and with an estimate of the socio-cultural sensitivity to the implementation of solar technologies. This "criticity" designation is a key element for the implementation of the "Cross-mapping" tool suggested in the LESO-QSV method (see Section 1.4): superposing "Criticity" maps to solar radiation maps is intended to help planners and authorities to define appropriate solar promotion policies, by taking simultaneously into consideration solar radiation availability and architectural integration quality issues [28], [31].

4.2   Cross-mapping variables

The simultaneous representation of solar radiation, visibility and urban sensitivity on a map is not fully new in terms of urban planning of solar installations. It can be achieved with a very simple method. First, solar radiation can be estimated according to the orientation and tilt of the building envelope surfaces. The optimal orientation to maximize solar gains in an entire day is due south (in the northern hemisphere). East and West orientations are appropriate for morning and afternoon solar generation respectively. The optimal slanting angle depends on latitude. In general, peak irradiation is reached on horizontal surfaces, while the surface collecting the maximal radiation throughout the whole year ranges from horizontal (at the equator) to vertical (at the poles). As for visibility, it can be assessed by walking and eventually taking photographs at the locations offering the clearest view of the buildings in the public space. Sensitivity is

linked with the presence of listed buildings as well as the proximity of the site to monuments and landscapes.

LEGEND:

Visible and/or not sufficiently sun radiated roofs:

Invisible (within 500 m) and sufficiently sun radiated roofs:

Pitched roofs with favorable exposure

Pitched roofs with sufficient exposure

Flat roofs / terraces with favorable exposure

Gardens with favorable exposure
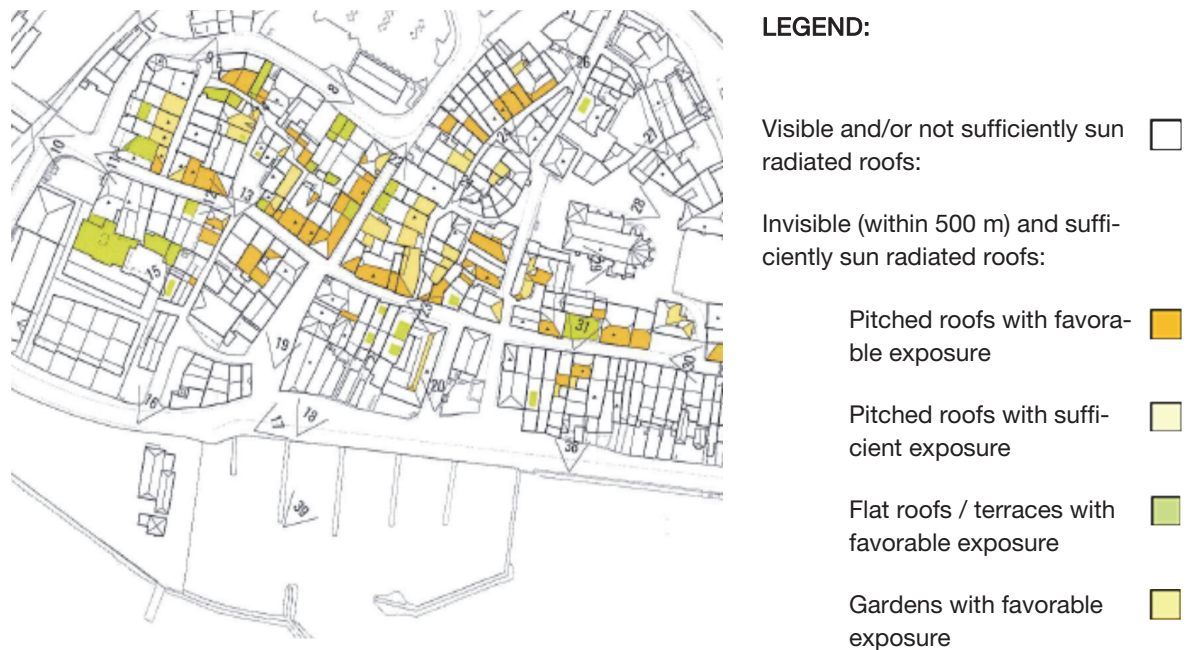
Figure 4.2 Extraction from the solar modules adaptability map of Lutry [137].

(Credits: Frei Rezakhanlou SA © [137] available online on the website of the municipality of Lutry: https://www.lutry.ch)

As such, a reasonably reliable set of criteria can be included in a cross-mapping decision tool: an interesting example of such an approach is the solar integration maps of the village of Lutry on the Swiss coast of the Leman Lake (Figure 4.2) [137]. It should be noted though, that a methodology involving on-site visits implies a lot of effort to be systematic. In fact, solar radiation may be affected by partial or total shading and reflections between building elements, showing a considerable local variability. Concerning visibility, it is time-consuming to check that all relevant viewpoints have been considered when taking the photographs: rules of thumb can considerably help the quick assessment of the envelope surfaces even without a full photographic coverage of the site (see visibility assessment in [28]). Regarding sensitivity, it should be extensively evaluated by considering morphology, materials, constructional techniques, historical and cultural relevance of buildings. In spite of this, the use of local cartography (e.g. land use plans, landscape and strategic plans, cultural heritage spatial surveys) can simplify the task. The use of a simplified methodology as the one described herewith is particularly effective

at the scale of the village and offers a general orientation for metropolitan areas too. The opportunity to develop a more accurate and robust method is discussed briefly in the following sections, analyzing each variable respectively.

4.2.1 Solar radiation vs. solar potential

Solar radiation (or simply insolation) is the integral sum of the incoming solar irradiance on a determinate surface with a certain orientation and slanting angle, across a given time. Hence, it is defined as an energy quantity (Wh or J) per unit of area (m^2), for a given period of time (day, month, year). It is possible to obtain typical irradiance data from meteorological Test Reference Years for a given site in order to estimate average solar radiation (daily, monthly or annual). Solar radiation is converted into useful energy by the way of an appropriate energy conversion system: the result of this process is often designated as *solar potential*, namely the potential useful energy that can be produced, if the conversion system is in place. Passive solar potential is the share of solar radiation that can be converted into useful heat without employing any mechanical or electrical device (such as fan, pump, damper, valve, photovoltaic cell) in order to trigger a mass or energy flow. Inversely, active solar potential implies the use of such devices: this is the case for solar thermal and solar photovoltaic systems.

The solar potential has not been univocally defined but is rather organized in a hierarchy according to the level of available details characterizing the site [154], [155] (Figure 4.3). *Physical potential* encompasses the total amount of solar energy reaching the considered area, in an ideal condition. It is equivalent to the annual global horizontal solar radiation (insolation), and usually obtained by the way of interpolations from the nearest meteorological station. It can be refined via GIS analysis, which is used to simulate accurately the shading effects due to orography (mountains) and territorial morphology. Such a variable is useful for the strategic international / national energy planning (such as renewable goals burden sharing). *Geographic potential* is derived from the physical one by successively excluding zones with incompatible land uses, typically roads, rivers, lakes, beaches and their influence areas or protected areas, such as national parks and cultural heritage sites. Such a variable is useful for renewable planning at the broad strategic level. *Location potential* depends on technically available areas, their orientation and tilt, and possible shading by neighbouring obstacles. Compatibility with agriculture and farming is taken into account for open land venues; in urban contexts, the effective sun exposed area of available building envelopes is computed. At this stage, the solar potential details are sufficiently refined to be used in urban contexts. For the purposes of this thesis

work, location potential will be used. It should be highlighted, though, that other factors intervene at the district scale: the efficiency of the energy conversion system and the optimization of the energy yield according to the grid capacity (*Energy generation potential*). Finally, economic parameters can be considered for local building design purposes, such as the energy customers' purchasing power, energy system prices, energy carriers' tariffs, financial incentives and expected system lifecycle.
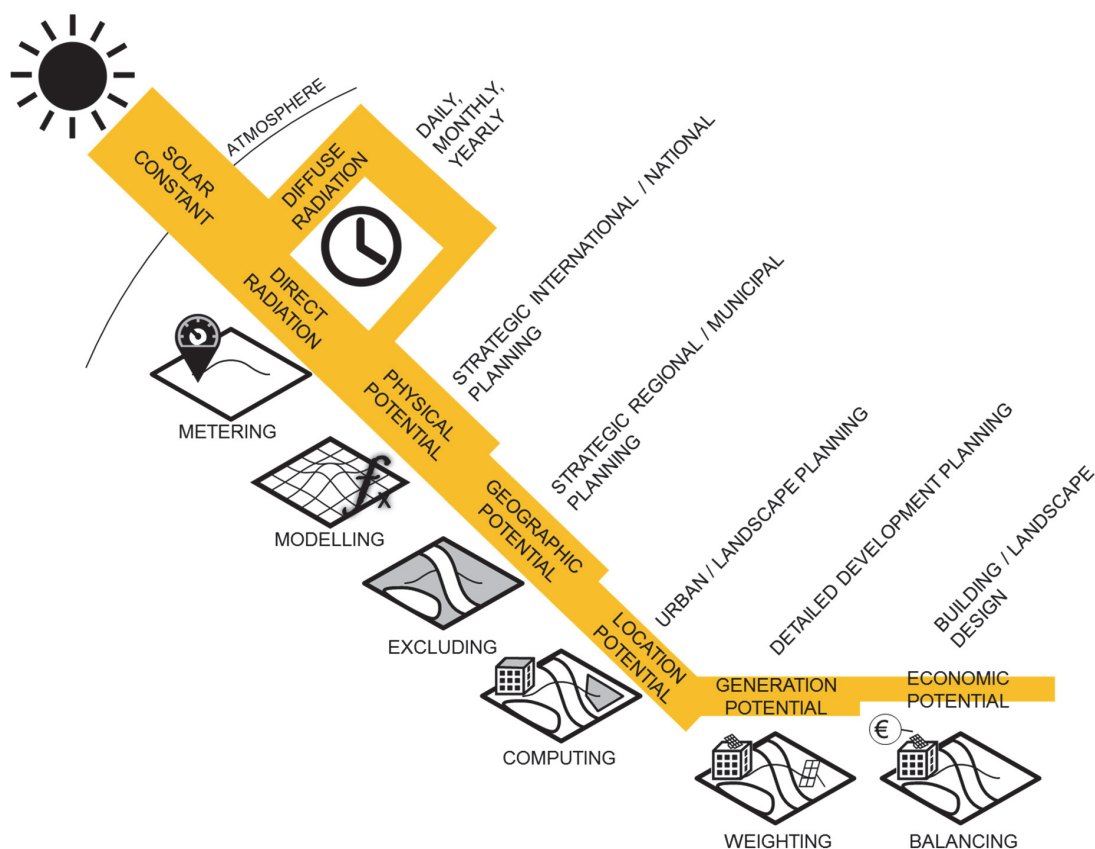
Figure 4.3 Representation of the different levels of solar potential.

(Author's own elaboration)
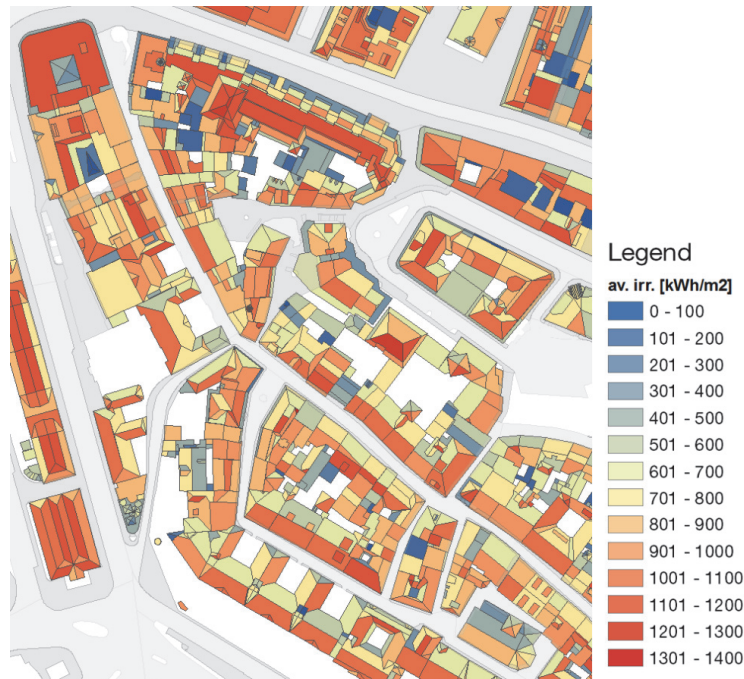
Figure 4.4 Grand Rue, Geneva, Switzerland. This solar cadaster shows average annual solar radiation per roof pitch, constituting the location solar potential.

(ArcGIS ArcMap © elaboration on CC data from Système d'information du territoire à Genève - SITG)

Many cities have recently proposed online solar cadasters, showing 2D or 3D maps of solar radiation values in urban sites. The aim is to provide information regarding solar availability not only to urban planners and stakeholders but also to architects, designers and private investors. Usually these maps include existing buildings but some foresee the possibility of importing new designs and projects, to estimate their solar collection potential and check the impact on other buildings' solar exposure. Most solar models are obtained through appropriate software applied to Digital Elevation Models or to 3D vectors of cities, including the open format CityGML. As a result, classes of annual solar radiation reaching building roofs are represented in a color scale (Figure 4.4); simulation tools based on 3D vectors propose also solar radiation on façades. Most advanced ones offer an estimation of the energy generation capabilities, the economic potential with payback time, as well as the solar saving fraction in regards of energy consumption [156].

An interesting design-oriented method to identify solar irradiated areas is, among others, the *solar envelope* method. A solar envelope is defined as *the volumetric limits of buildings that will not shadow surroundings* for a minimal number of hours [157]. Subsequently, Capeluto et al.

elaborated the concept of solar right envelope and solar collection envelope, the former corresponding to the original definition and the latter representing the volumetric limit outside which new building insertions would receive sun access, given an urban context [158] (Figure 4.5).
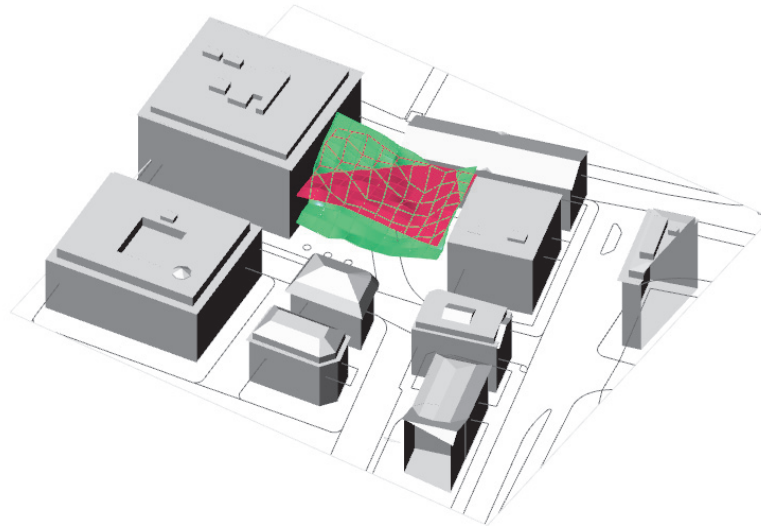
Figure 4.5 Place de Hollande, Geneva, Switzerland. Solar collection envelope (green) and solar right envelope (red), for solar exposure between 10 AM and 15 PM at the 15th of every month of the test reference year. Masses whose height is comprised between the green surface below and the red surface above are sun exposed and do not shade the surroundings in the given period.

(Used tool: Grasshopper for Rhino © and Ladybug CC elaboration on CC data from Système d'information du territoire à Genève - SITG)

Solar collection envelopes can also be characterized by particular thresholds of solar radiation [159] and applied to building blocks or units [160]. Concerning solar right, a new building design should avoid shading on surrounding buildings and/or open spaces to avoid unfavorable conditions into the buildings and in the public space (consider discussion on this matter in ref. [161]). One of the typical urbanistic measures that is historically adopted to ensure daylight and fresh air is the *setback*, representing the limit of façade planes that recedes with the height, sometimes behind an ideal *sky exposure plane,* a precursor of the solar envelope (see for example [162]).

4.2.2 Visibility

Visibility assessment has been thoroughly explored in the previous chapters. For the purposes of this work though, it is useful to specify some particular features of the analysis to be performed. Visibility is intended here as a property characterizing the surface of a building envelope component, before any eventual solar refurbishment. Since the aim is to respond to a planning need, the "objects of interest" included in the assessment are the building surfaces and not the

solar collectors themselves, which are unknown at this stage and will be designed in a later stage. A representative set of possible viewpoints located in the public space, both close and remote, is included in the analysis.

In the current urban planning practice, some examples of visibility assessment exist: they are carried-out in order to ensure the view of remarkable buildings within the urban landscape (Figure 4.6). This can be translated into a limitation of building heights in certain zones, often called "viewing corridors", which are offering views to a protected site. The cities of Paris and London feature a dedicated appendix in their urban regulation plans, highlighting the viewing corridors of many listed monuments (in French *fuseaux de vision*, visual spindles). Formally, they can be described as portions of 2D or 3D isovists subtending a landmark (see Chapter 3), in which the erection of new buildings is managed by stricter constraints.

Another interesting design-oriented method, in correlation with the one presented for solar radiation, is the *view envelope*. In fact, the intersection of different obstructed volumes generated by as many viewpoints as possible in a 3D visual field constitutes the space in which any structure can be built without being visible. A clarifying example of this concept is an outstanding building rooftop addition in New York City, whose roof has been shaped by projection of lines of sight from three different surrounding viewpoints (Figure 4.7).
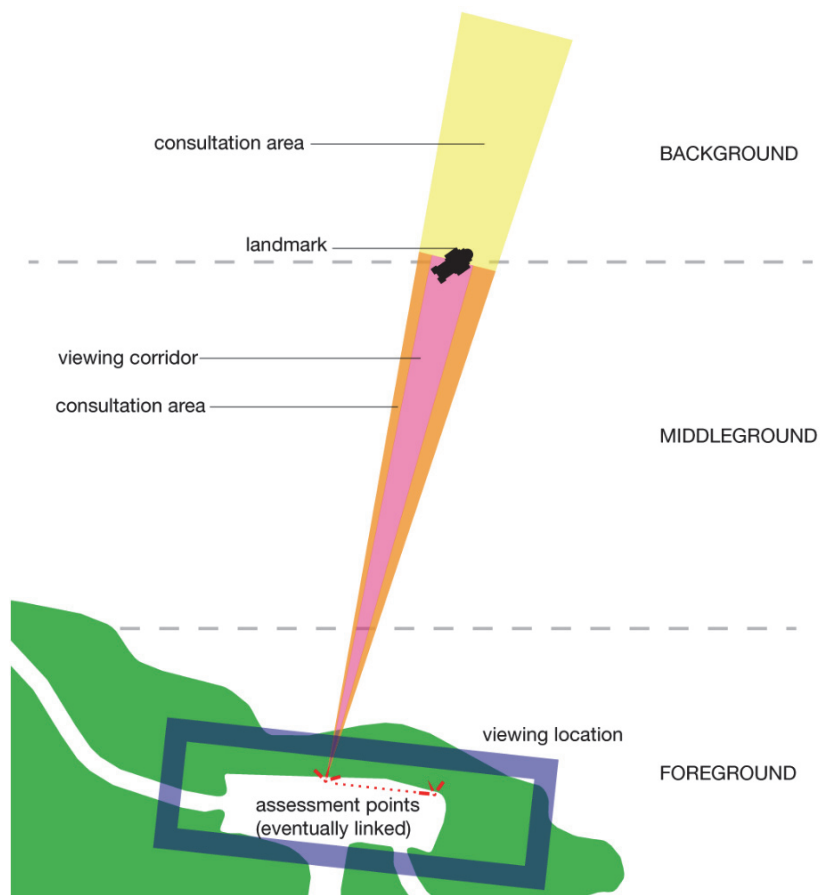
(a) London viewing corridor demonstration. Redrawn after: Greater London Authority [163]
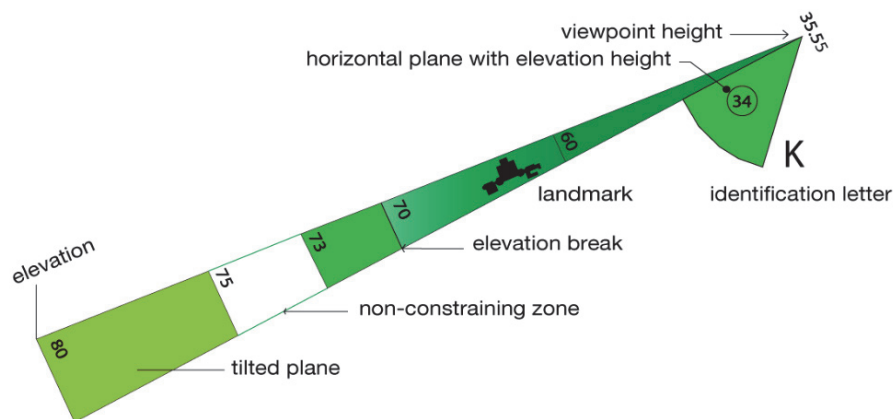
(b) Paris visual spindles demonstration. Redrawn after: Atelier Parisien d'Urbanisme [164]

Figure 4.6 Urban planning practice of view preservation. Approaches from London and Paris.
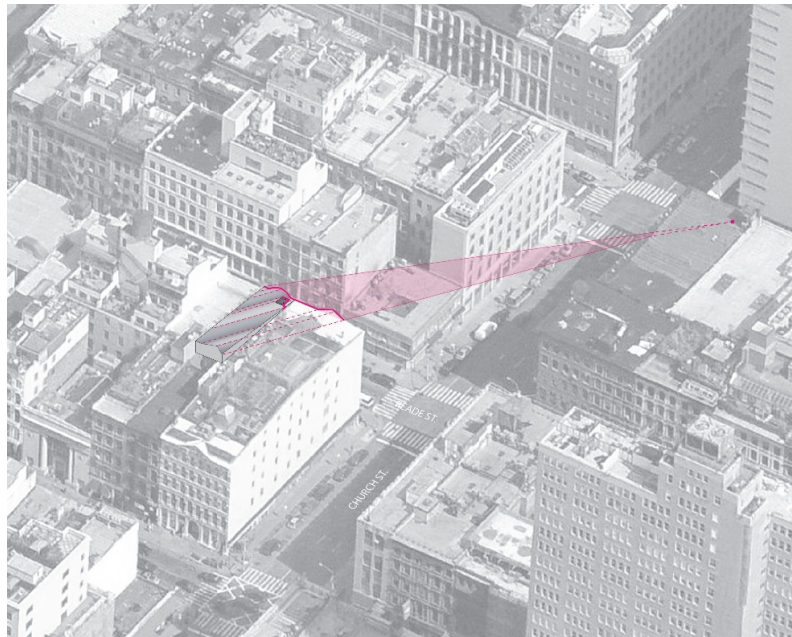
(a) Concept of the Stealth-building project, lines of sight generated by a viewpoint. Credits: WORKac ©

(b) View of the rooftop. Credits: Bruce Damonte ©

Figure 4.7 The Stealth building by WORKac, 2016, New York City, USA.

4.2.3   Urban sensitivity

Sensitivity or urban sensitivity is the socio-cultural value attributed to an urban zone. A rigorous definition of this "cultural significance" can be found in the UNESCO Recommendation on the Historic Urban Landscape [165, p. 6]:

Cultural significance means aesthetic, historic, scientific, social or spiritual value for past, present or future generations. Cultural significance is embodied in the place itself, its fabric, setting, use, associations, meanings, records, related places and related objects. Places may have a range of values for different individuals or groups.

In particular, sensitive zones include certainly historic urban areas as combination of natural and man-made environments embodying the traditional urban identity. Nevertheless, *the shift from an emphasis on architectural monuments primarily towards a broader recognition of the importance of social, cultural and economic processes in the conservation of urban values* [165, p. 2] imposes the consideration of a wider context, beyond the physical limits of the historic urban areas. Visual environment is recognized as a local resource to protect when appropriate (see visual corridors in the previous section). Urban heritage includes also non-exceptional elements that are presented in a coherent context with relative abundance, like open spaces and infrastructures [165, pp. 3, 6]. Hence, industrial and residential areas can be considered as urban heritage. *Research should target the complex layering of urban settlements, in order to identify values, understand their meaning for the communities, and present them to visitors in a comprehensive manner* [165, p. 5]. To what concerns renewable energy, it *should integrate natural and cultural heritage as resources for sustainable development* [165, p. 4]. In this sense, urban planning tools should *include documentation and mapping of cultural and natural characteristics. Heritage, social and environmental impact assessments should be used to support and facilitate decision-making processes within a framework of sustainable development* [165, p. 4].

Sensitivity assessment involves complex territorial aspects as well as their mutual interaction. In Switzerland, a specific documentation named "Federal Inventory of Swiss Heritage Sites of national importance" (ISOS), covering the entire national territory, provides a sound characterization of built clusters deserving preservation, beyond a mere list of individual listed objects, constituting a coherent and homogeneous system. *The ISOS assesses the sites in their entirety by considering the relationship of the buildings to each other as well as the quality of the open spaces between them and the relationship of the site to the immediate and more distant surrounding areas* [166]. In addition to ISOS, some cantons establish a comprehensive inventory of buildings within the historical center, complemented by some remarkable buildings outside the central perimeter (for example Neuchatel and Vaud [167]). In these cases, buildings are graded on a scale of "historical and architectural value", ranging from monuments of national,

regional and local importance to well-integrated objects, until neutral or even degrading accretions. This is also a precious resource to determine the sensitivity level.

For the purposes of this work, ISOS perimeters are assumed as high sensitive areas. Concerning other levels of sensitivity (medium and low), land uses issued from the land use plan are assumed as a possible indicator. This process constitutes an example: it could be complemented by deeper investigations and understanding of the territorial identity. Nevertheless, such analysis goes beyond the objectives of this thesis.

4.3   Thesis outline

This thesis is dedicated to the development of a scale-dependent methodology to assess visibility in urban areas, from the strategic broad territorial scale to the district level. The appendix describes research implications of this work as well as the experience of the author in the field of architectural integration of solar modules, relative to international and nation-wide collaborations with both academic and industrial partners.

4.3.1 Multi-scale visibility assessment methodology

Table 4.1 offers an overview of the methodology developed in the framework of this doctoral thesis. Three main urban planning scales are considered, in accordance with the international consensus that exists on this matter in the solar energy and urban planning domain ([35]). As already discussed, not all indicators are meaningful at all scales. For this reason, the information of the three main variables analyzed in this chapter (solar radiation, visibility, sensitivity) is represented by different indicators at the various scales.

1. At the *strategic planning level*, visions and strategies to reach certain goals in the political agenda are developed and connected to land use and zoning. Priorities regarding urban growth, mobility axes and development objectives of main areas are identified. At this scale, buildings and neighborhoods are dissolved into districts, which represent the data aggregation level of the map. Solar radiation can be roughly estimated in terms of geographic potential, based on the topography of the territory. Regarding sensitivity, particularly sensitive (or non-sensitive) districts are relevant as "emerging peaks" over a uniform medium-sensitive territory. Protected zones in land use plans represent a sound exemplification of highly sensitive areas, as well as commercial / industrial zones of low sensitive areas, even though not always exhaustive without a deep understanding of the
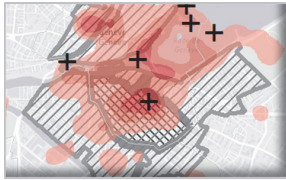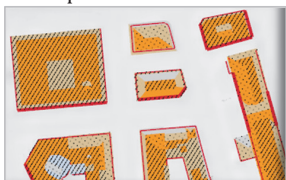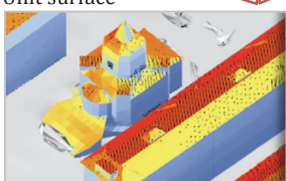
local specificity and a constructive discussion with the local site protection authorities. Visibility instead, can vary a lot from building to building and even from façade to façade, making it meaningless to estimate a "district average" visibility index. Nevertheless, it is obvious how some precincts are more prominent in public perception: they are simply more frequented or they benefit from a more focused interest by the visitors. At this stage of the planning process, this variable is less related to geometrical or physical phenomena, but rather to the general perception of a place, as its global visual interest within the "public".

2. At the scale of *development planning*, urban fabric becomes visible and division between public, semi-private and private space comes to evidence. A first estimate of *location potential* can be made in regards to buildings form and orientation within the urban pattern: blocks of buildings represent the data aggregation level of the map. In this case too, sensitivity level may be inferred by land use zones, by taking into account special clusters of buildings, such as particular squares or well-known settlements, ideally in agreement with the local authority for cultural heritage protection. Visibility is assessed per building: however, it still depends mainly on geometric factors and reciprocal obstructions. It means that, at this stage, it is more important to know whether a surface on the building envelope can eventually be visible or not, and from how many unobstructed locations, rather than trying to quantify the degree of perception from each viewpoint. This would require a more detailed form definition and a complete material mapping of the different surfaces, which is appropriate to the following stages in the planning process. Concerning urban design level, one possible geometric indicator for GIS applications is the cumulative viewshed (see Chapter 3).

3. *Detailed planning* level entails the resolution of building components. Differences among façades and roof pitches become relevant at this stage as well as urban furniture (lamps, benches, advertisement, car parking sites) and vegetation occlusion: envelope surfaces represent the data aggregation level of the map. Usually maps at this scale focus on one district with a constant level of sensitivity or across a couple of different sensitivity zones. Solar potential of façades becomes interesting in this phase, as it can be assessed with sufficient detail. Visibility is now dependent on physical and physiological factors such as visual acuity and contrast: it should be quantified for each envelope

surface beyond the simple distinction of "visible"/ "invisible" features made in the previous section. To do so, visibility rays are cast from a grid of possible viewpoints in the public space to building surfaces, representing potential solar installation spots: visual stimulus is quantified as the solid angle produced by a target surface on the spherical visual field of each viewpoint in relation to its perceptual threshold.

4. At the *Architectural planning* stage, differences between envelope fractions become relevant. The façade layout, including openings, terraces and decoration has an impact on available space for solar modules and on their shading. Roof solar potential is also influenced by the presence of technical equipment, such as chimneys and other fixtures. Location potential may be refined with the system efficiency and according to grid management issues, in order to estimate the available energy production. Solar modules are located in a way to match the buildings' energy loads with the optimal solar radiation profile, in accordance with the selected technology (solar thermal or photovoltaic). As for solar rays, lines of sight can be locally obstructed: the identification of most and least visible portions of the envelope influences the solar array design. At the observer level, attention distribution becomes relevant to determine most salient areas on the envelope. Surface resilience is affected by surface morphology and planarity, as well as by its materials composition and characterization: as such, it is easier to integrate the same product in some envelope fractions than others. Those featuring smooth and reflective finish, like metal cladding, are in general more adapted to host standard solar modules, even though tailored market products are available also for matte surfaces with complex textures and light regularities, such as tiles covering. Due to the variability of all the cited parameters, building envelope surfaces are not considered as a whole but decomposed into unitary subdivisions that represent the data aggregation level.

Table 4.1: Overview of the methodology

	Strategic planning ~ 1 : 100 000 – 1 : 30 000	Planner's goal	Visibility Index	Possible cross-mapping layers
Urban planning scales	Data aggregation level Districts In Switzerland: Plan directeur cantonal, Plan directeur communal	Understand which the most visual prominent areas are, and compare with sensitive areas (visual hierarchy vs sensitivity) to map the interest of public places for the community.	Important and historical views; visual interest	Protected zones (sensitivity) and ISOS perimeters Geographic potential: calculated solar radiation over terrain model
	Development planning ~ 1 : 10 000 – 1 : 5000 Data aggregation level Building (roofs) In Switzerland: Plan général d'affectation	Identify uniform urban zones in terms of: •Visibility •Production potential •Sensitivity to tailor solar energy development strategies at the city scale	Visible surface or Roof visibility ratio (visible roof area / total roof area) per building = VISRATIO	Land use (sensitivity); Location potential: calculated solar radiation on roof surfaces and relative ratio=RADRATIO CHECKMATRIX
	Detailed planning ~ 1 : 2000 – 1 : 500 Data aggregation level Envelope surfaces In Switzerland: Plan localisé de quartier	Identify coherent solar application strategies in relation with the characteristics of visibility/sensibility /solar radiation of the different building surfaces composing a specific city district	Visual amplitude per surface mesh	Land use (sensitivity); Location potential: calculated solar radiation over all building surfaces
Architectural scale	Architectural planning ~ 1 : 500 – 1 : 100 Data aggregation level Unit surface In Switzerland: Permis de construire	Target suitable portions of the building envelope in terms of visibility and solar radiation	Visual amplitude per surface mesh, weighted by visual attention	Characterization of materials (resilience) Location potential: calculated solar radiation over all building surfaces subdivisions or Generation potential: location potential weighted by energy system efficiency

(all images from the author, elaboration on CC data from Système d'information du territoire à Genève - SITG)

4.3.2 Considerations on the planning scales

The notion of scale is essential to the comprehension of this thesis work. A continuous scale is discretized here into different stages, which can slightly vary as a function of the target territory: they correspond roughly to the spatial units that can be appreciated at the relative level of detail. Districts are focused at the strategic planning stage, as territorial patches; buildings and their envelope surfaces, even fractions of them emerge by narrowing down to a more detailed scale. Maps and geo-data may differ a lot across the various steps cited above, as well as perceptual aspects.

Topographic plans are available at the geographic scale, usually as digital elevation raster data or as vectors with contour elevation lines. These are suitable for tracing buffer distances and visual corridors from panoramic viewpoints to designed renewable facilities (or reverse), in a landscape set-up. Eventually, Digital Elevation Models at this scale can be used for viewshed analyses of large solar power plants, being the resolution in the range of one or more meters. Visual perception magnitude can be hardly quantified in a meaningful way, since even a small-size array of solar modules can significantly alter the natural sightseeing from a remote view-point.

In the geographic milieu, cities arise as anthropic systems of artificial constructions. Visual observation in cities develops in a fragmented way, since space is segmented in roads, piazzas, squares; multiple and varied perceptual stimuli appear in the urban environment, in a process described as "serial vision" (see Section 3.1). Thus, it is obvious that perception is different in urban areas compared to open land. Cities are complex systems that can be hardly described by a comprehensive and synthetic perceptual indicator. As such, visibility indicators are relative to the different scales.

The expansion of cities is regulated by local authorities in strategic plans: the vision for the evolutionary scenario of the urban territory is stylized with symbols, arrows and lines showing the interactions between districts. Cities are densely populated, thus benefit from more diffused observers in comparison with other land portions. Within this strategic framework, it is important to know which areas are more visited: in this sense, visibility can be intended as public "appeal" or "interest" of given places. Districts characterized by higher appeal may deserve more attention for a solar deployment strategy compatible with the public image.

At the stage of development planning or master planning, building footprints are usually available as vector maps. This is the appropriate scale for an assessment involving planar isovist fields, enclosed by the buildings as obstructions and providing a first geometric characterization of the fields of view. Building vector maps may be bi-dimensional, neglecting elevations of buildings and viewpoints. In such condition, planar isovists should be complemented by a viewshed analysis on a high-resolution Digital Elevation Model (e.g. 50 centimeters).

At the detailed level focusing on a district, 3D vector models can be easily handled and visualized. As such, visual magnitude can be assessed with spherical indexes or solid angles, accounting for the fraction of the field of view occupied by building integrated solar modules. Three-dimensional vector models are often available in many cities, even if their level of detail may vary: an increasing level of detail that features complex objects can significantly improve the assessment quality (i.e. window modeling on façades, trees and vegetation inclusion). The completion of the tridimensional model with real colors, material characterization and textures provides useful details to determine the probability of capturing observers' attention. In fact, the presence of an object in someone's field of view does not mean he/she is looking at it. The cognitive aspects behind this statement will not be explored in this thesis but some hypotheses on pedestrian movement and view directions are employed to simulate attention distribution (see details in Chapter 8), even in absence of material characterization.

Unfortunately, textured models are seldom available due to the complexity and the data volume of the stored information. In case available, though, saliency models can be used to determine the attention distribution across the field of view [71]: they are best effective with known lighting environment issued from meteorological conditions and with few viewpoints. Virtual reality simulations addressed to a sample of observers may be considered at this stage, to integrate cognitive aspects from human interaction: nevertheless, this goes beyond the scope of this thesis.

4.3.3 Research implications into practice

The methodology presented in Section 4.3.1 is mainly addressed to urban designers and urban planning offices of local public authorities. When setting-up strategic plans of a city, they are normally aware of the cultural heritage asset and the potential sensitivity level of the different urban areas; in most favorable cases, a list of remarkable viewpoints is available and visual corridors incorporating construction constraints are established to protect main monuments.

A distributed index of visual interest on the urban territory helps to identify building clusters in a highly appealing area, which have an impact on visitors and local communities beyond the listed items. Such information may be used to restrict the solar energy renovation rate or to foresee special incentives for high-end installations. Politicians can draw conclusions on the main touristic paths and preserve their decorum.

In case of development of a new district or by setting-up sustainability goals for an existing one, building integrated solar technologies and renewable shares come into the debate. At this stage, a decision driver can be the economically viable surface for building integrated applications that would raise less opposition from the public once equipped with solar modules. Knowing that a solar design is less visible from the public space may be a good reason to compromise on its unaesthetic appearance for the sake of renewable energy generation. Energy efficiency brokers and Energy Service Companies may be interested in targeting the suitable buildings for standard, inexpensive installations as the most remunerative deals. Building ownerships as well, may select the buildings that deserve the most urgent investments within their stock.

Focusing on a single neighborhood with few building blocks, in detailed planning the number and layout of building integrated solar modules is determined. Most relevant building views and urban perspectives should be preserved by optimizing the modules arrangement to benefit from the highest solar radiation. A visual amplitude index quantifying visibility on a continuous scale constitutes a valuable pre-design information for solar products installers, who can profit of a range of values between the "non-visible" and the "fully visible". In fact, at the district scale it is easier to identify the locations from which the solar modules would be visible (e.g. a segment of road, a piazza, a sidewalk), but not at what extent. Advertisement companies and real estate promotion agencies may also take advantage of the "added value" of such a tool.

The author participated in a fruitful international, multi-disciplinary collaboration project within the expert group of the International Energy Agency, Solar Heating and Cooling program, Task 51 'Solar Energy and Urban Planning'. The most relevant activities within this framework are described in the appendix of this thesis, including architectural consultancy for an international design company and the update of a website collecting innovative products for architectural integration of solar modules. The final part presents the author's contribution to the architectural design and construction of the NEST SolAce unit, an example of sustainable construction

showcasing research and innovations in the purpose of fostering advancements in the domain of building energy efficiency, renewable energy and indoor comfort.

Chapter 5   Strategic planning

At the strategic planning, ranging from around 1:100 000 to 1: 25 000 scale, general indicators at the district level are offered to allow an improvement of the assessment in a further stage. Concerning visibility, a district-average visual magnitude estimated according to the geometric relation between observers and envelope targets would be ambiguous: due to the large variability of potential observers' positions, of building morphology and orientations, district aggregation would entail a scale error without being representative of all the possible viewpoint-building configurations within the district. At this stage the use of a visual sensitivity or visual interest indicator seems more appropriate, depending on the number of people who are potentially concerned among the local population, tourists and travellers by nearby infrastructures. Consequently, visibility is a result of public concentration and place attractiveness, determining the exposure of a set of buildings to the general perception. This section investigates the relation between the urban heritage and the most visually prominent areas in the public interest, in order to identify possible matches. Highly sensitive urban areas are usually denser in cultural heritage and / or in urban landscape features that emphasize the identity of a given place. In principle, these areas deserve more visual interests than others but they are not the only ones. The reliability of the proposed method is also discussed.

5.1   Public perception assessment through crowd-sourced data

Population sourced studies have been mentioned as methods to assess psychological reactions to territorial features. The idea of elaborating a public representation of a city that reveals the attractiveness of certain zones dates back to Lynch, with his "public image" maps [76]. More recently, the spread of web-connected devices such as smartphones and the evolution of Geographic Information Systems (GIS) makes data collection easier and more detailed. The "Place Pulse Project", for instance, tries to measure urban perception, by crowd-sourcing visual surveys to users around the globe. One of the outcomes is an index issued by a machine-learning algorithm that predicts six perceptual attributes of a place: safe, lively, boring, wealthy, depressing, and beautiful [168]. The training has been performed on a set of more than 100 000 images from 56 cities provided to a sample of circa 80 000 volunteers. It is also possible

to use dynamic data that visitors of an area generate: for example, Wi-Fi connections to track people's movement within a zone of interest [169]. Other useful data can be extracted from the density and the distribution of phone calls as well as the photographs taken over time [170]. The latter is better discussed in the following paragraph. In general, crowd-sourced databases provide useful distributed information, especially when the number of records is proportional to the analyzed area. Data cleaning, filtering and re-elaboration is often required in accordance with the prefigured level of detail. The scarce accuracy of the dataset is balanced by a massive number of entries, so called "Big Data", offering a bottom-up model of the urban scenario. Crowd sourcing is adapted to popular and spatially distributed investigations, as a complementary alternative to top-down urban planning made by expert designers and administrators. It should not replace the traditional expert-based approach though, which is generally enriched by a more comprehensive vision. In this section, the proposed methodology uses both approaches to compare urban sensitivity and visual interest.

5.1.1 Web-shared photographs databases

Among different available online data, public-accessible photo databases are particularly relevant for this work. Currently, almost any portable electronic device is equipped with one, two, even three cameras and sharing photographs on the web is a new form of social interaction. Pictures witness which places people visit the most and what they are interested in watching. A snapshot taken by an urban user in the public space marks his interest, his attention focused on something worthy to be stored in a digital memory, and either accidentally or intentionally a portion of the urban scenario is comprised. Together with the digital image, a set of attributes or metadata qualifies the shot, specifying for instance the location and the time at which the picture has been taken, the keywords or tags classifying the subject, the camera optics, the exposure time, the copyright notice, etc. Many online photographic repositories give also access to these metadata, sometimes provided by other sensors featuring the camera (such as a GPS tracker), sometimes inserted by the author directly, sometimes edited by automatic or manual post-processing.

An interesting application at the landscape scale is the use of geotagged photographs to identify popular locations in natural areas, e.g. natural parks [171]. The same principle is used to map the most photographed landmarks of a city, constituting the hotspots of an urban density "heat map" according to the number of snapshots. The more pictures are taken in a given location, the more interest the surrounding buildings attain. A world-wide visual interest "heat

map" is available online [172], based on the currently dismissed Panoramio photo repository and other web-services. It is interesting to observe how some unconventional places like grand hotels and commercial centers arise interest beyond the perimeter of the historic and cultural heritage core of many cities. Another relevant topic is the different spatial distribution between photographs taken by tourists and local residents. In a recent study [173], photographs taken by tourists and by local residents are differentiated based on the timestamp in the attributes: whenever a set of pictures is uploaded on the web by the same user in a timespan lower than one month, it is marked as taken by a tourist and vice versa. Results show tourists' photographs are more concentrated, taken in fewer places: some cities, like Rome and Barcelona, are characterized by localized peaks of pictures around monuments. On the other hand, Paris and London show a more even distribution on the urban territory. A worldwide, online available map of photographs taken by tourists and local residents is made using the same method by the digital artist and data visualizer Eric Fischer [174]. The cited studies demonstrate the possibilities offered by crowd-sourced photographic databases to find visual prominent areas of cities. A similar approach is described in the following paragraphs; its compliance with expert-based census of remarkable viewpoints and urban sensitivity maps is analyzed. The compatibility of this method with the objective of the thesis is discussed.

5.2   Visual interest

5.2.1 Census of remarkable viewpoints

The case study adopted for the current analysis is the metropolitan area of Geneva. As a first step, visual interest can be estimated by mapping the focal points of squares, the road perspectives, the sightseeing points that are (or have been) more significant in the cultural representation of the city. In a typical top-down approach, these viewpoints are collected based on experts' advice, touristic guides, pedestrian itineraries and observations. In this case, also amateur photography websites have been consulted. The viewpoints are identified to offer a global view on the city, rather than a selective view on a specific monument: they could be qualified as urban panoramas, since their aim is the contemplation of the city as a whole. The choice of the viewpoints is made to author's discretion; a more complete census can be complemented by local authorities and view corridors set-up as a protection countermeasure. The result is shown in Figure 5.1: most viewpoints are located on the lakeshore, on bridges, in gardens or along quays. One is on top of the cathedral's tower and the last one coincides with an observation point on the Salève hill, in the French territory to the south of the city.
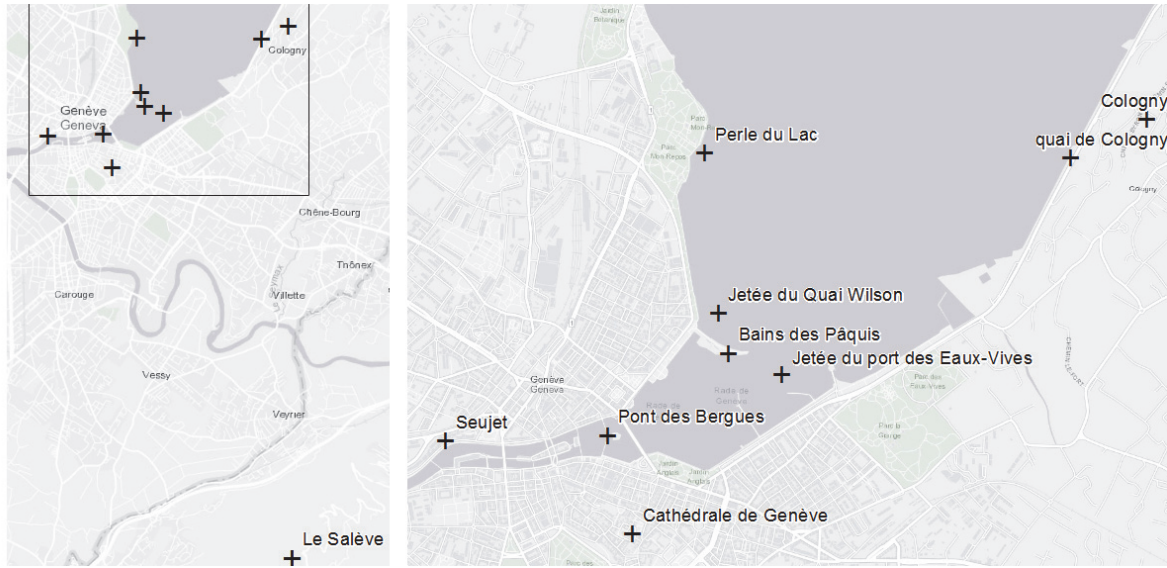
Figure 5.1 Geneva, Switzerland. Significant viewpoints identified by the author.

(Credits: Esri, HERE, DeLorme, MapmyIndia, © OpenStreetMap contributors, and the GIS user community)

5.2.2 Data extraction and geo-mapping

The crowd-sourced dataset for the analysis is extracted from a social network dedicated to photography and picture sharing, called Flickr (www.flickr.com). Flickr is a website hosting images and videos, featuring almost 90 million registered members and more than 3.5 million images uploaded every day [175]. A set of 97 521 public photographs self-loaded and geotagged by the website community is available for the Geneva metropolitan area. A specific metadata attribute qualifying the positioning accuracy is employed to filter the dataset: it ranges from 1, i.e. world-scale accuracy to 16, i.e. street-scale accuracy. Only locations with accuracy larger than 13, corresponding to street address, were kept for this analysis, with a loss of 16% from the base sample. Consequently, 81 570 points corresponding to the shooting position of photos are extracted from the Flickr public web repository through the Flickr API. The latter is a software library allowing the interrogation of the worldwide database to filter the pictures in a given territory of interest. After the extraction, latitude and longitude values incorporated in the attributes are used to map the points in a GIS environment (ArcMap ©). The outcome of this operation is shown in Figure 5.2: at a glance, it is evident that lakeshores, bridges and the lake itself, from the cruise boats, constitute privileged viewpoints on the urban landscape. As a consequence of the high concentration of points, it is difficult to read the map as is. Thus, a density algorithm is employed to split the territory in classes of points density and enhance readability.
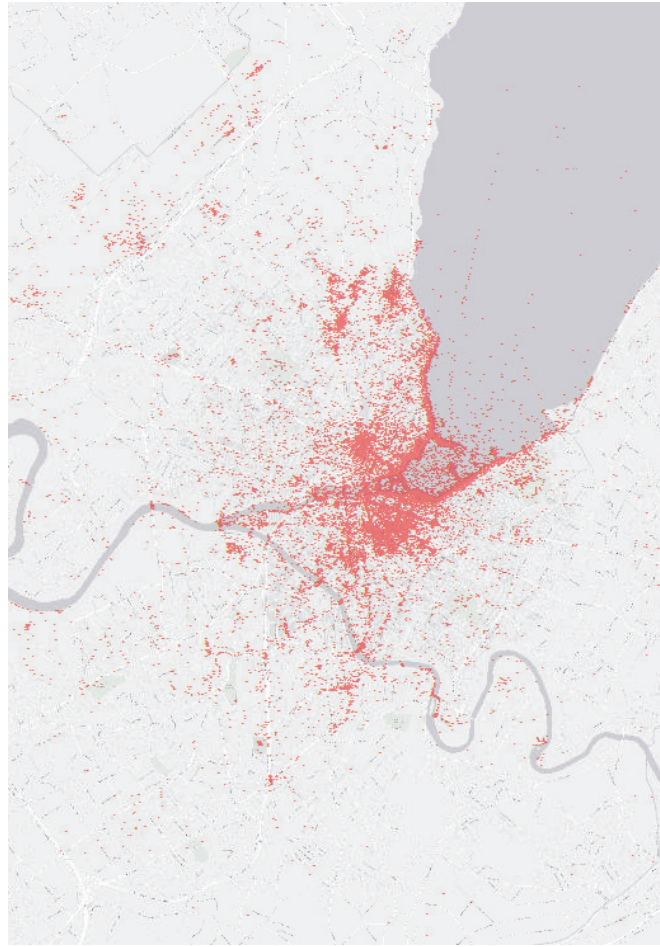
Figure 5.2 Geneva, Switzerland. Coordinate points of geographic locations of photos, crowd-sourced from the Flickr API.

5.2.3   Kernel density computation

Before computation, a raster layer is elaborated with a resolution of 10 m x 10 m, storing the density of shooting locations around each pixel. A kernel density algorithm is used, with a search radius based on the dispersion of shooting positions from the center of each pixel [176]. In practice, a circular neighborhood is drawn around a given point representing a photograph. Circle radius is determined via Equation 5.1, where r_k [m] is the radius, D_m [m] is the median distance from each point to the mean center and SD [m] is the standard distance calculated in Equation 5.2, with x_i, y_i, z_i coordinates of shooting point i and X, Y, Z coordinates of the mean center. At the center of the circle, kernel's value is equal to 1 and at the radius distance it is equal to 0; between the two extremes, the variation is disciplined by a kernel function [176, Para. 4.2.1], a type of Gaussian. The density value for each raster cell is calculated by adding

the values of all the shooting points' kernel surfaces where they overlay the cell center. Generated data are classified in three density classes, based on the Jenks' Natural Breaks algorithm, which is a common method to classify spatial data. It groups similar values and maximizes the differences between classes [177]. Results are shown in Figure 5.5.

$$r_k = 0.9 \cdot \min\left(SD, \sqrt{\frac{1}{\ln 2} \cdot D_m}\right) \cdot n^{-0.2}$$

Equation 5.1 – kernel's search radius

$$SD = \sqrt{\frac{\sum_{i=1}^{n}(x_i - X)^2}{n} + \frac{\sum_{i=1}^{n}(y_i - Y)^2}{n} + \frac{\sum_{i=1}^{n}(z_i - Z)^2}{n}}$$

Equation 5.2 – standard distance

5.3   Geographic solar potential

In compliance with the objectives stated in Chapter 4, the geographic solar potential available in the urban area of Geneva is estimated. In particular, the orography, the topography and the morphology of the territory are analyzed without considering the buildings, only the rough terrain and the overall land use. For this purpose, a raster of the Digital Terrain Model (DTM) with a resolution of 0.5 meters is used. The employed radiation algorithm is the Solar Analyst [178] of ArcGIS ArcMap ©. It estimates the direct component of solar radiation as a function of latitude, atmosphere transmittance and relative optical path length; sun positions are calculated for 30 minutes intervals through the day and biweekly intervals through the year. The direct solar radiation for a given sun position on a given pixel of the DTM is determined using the angle of incidence defined between the sun rays' direction and the axis normal to the pixel. Direct radiation values are opportunely weighted by shading factors as a function of pixel surrounding obstacles and cumulated over the entire year. Diffuse radiation accounts for 30% of the global normal radiation and is estimated for a uniform sky, subdivided in 8 sectors in the zenithal direction and 8 sectors in the azimuthal direction. Shading factors are also applied to diffuse solar radiation before computing it over the entire year, then direct and diffuse components are summed together to return the annual global solar radiation, expressed in kWh/m^2.

Figure 5.3 shows the annual global solar radiation averaged on a pixel neighborhood of 100 m, i.e. a distance that allows smoothing localized variations and point cloud errors by preserving a territorial overview. The terrain of Geneva receives an approximately uniform solar radiation

of 1000 kWh/m^2 year. The elevations of Saconnex, Lancy and Carouge feature positive deviations from this value to the southern slope and negative deviations to the northern slope. The Saconnex area in particular is among the most well irradiated, since the terrain leans slightly to the south. The course of the river Arve at the bottom of the image and the railway in the northern sector are characterized by lower than average solar radiation; non-negligible is also the effect of the Cathedral's hill in the city center with its shading on the side towards the lake.
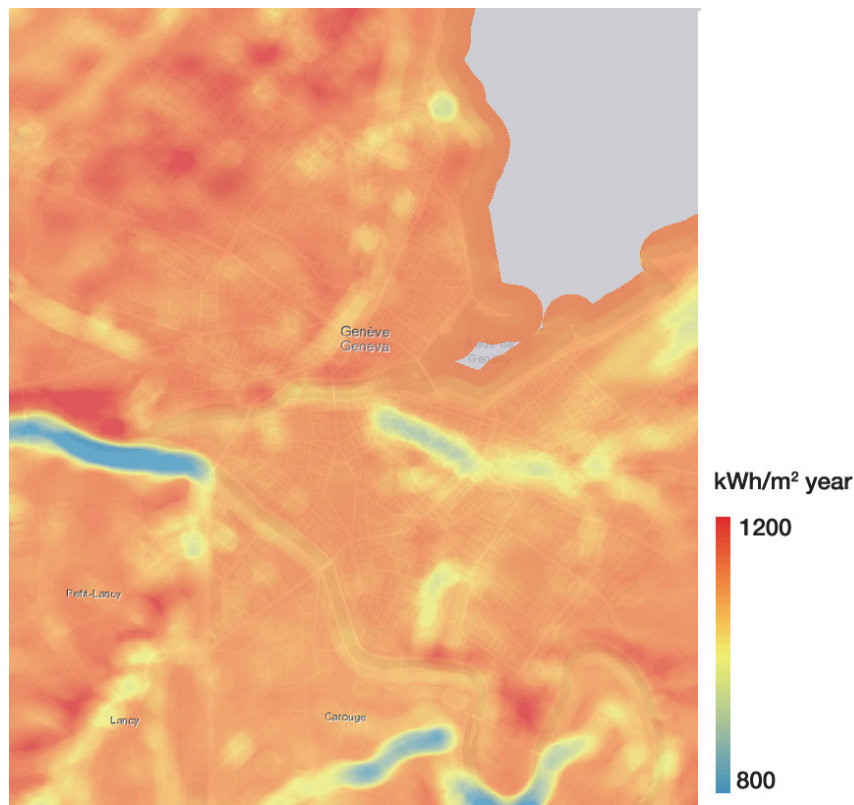
Figure 5.3 Geneva, Switzerland. Geographic solar potential (annual global solar radiation) issued from DTM, pixel neighbourhood 100 m.

(Used tool: Solar Analyst © elaboration on CC data from Système d'information du territoire à Genève – SITG. Credits: Esri, HERE, De-Lorme, MapmyIndia, © OpenStreetMap contributors, and the GIS user community.)

5.4   Sensitivity

Sensitivity to solar development projects is a spatial variable that relies much on the specificities of each territory; however, it has strong links with the land use and the cultural heritage density. A city center rich in listed buildings embodies a major part of the local cultural identity and attracts a high social predilection too, when this finds a clear expression in the architectural language: to preserve this, land use plans usually limit morphological alteration and new constructions.

In the case of Geneva, a sensitivity zoning is made by the author based on land use regulation: high sensitivity is attributed to Zone 1 and 2, corresponding to the city core within the ancient fortifications and the immediate surroundings. The zone composed of small residential buildings around the historical center, is also labeled as highly sensitive. Urban development areas with mixed uses constitute the medium sensitivity zone. Low sensitivity is respectively assigned to railway stations and airports, industrial and manufacturing zones and sport venues. Apart from land use attribution, ISOS perimeters are assumed as high sensitive areas, as discussed in Chapter 4. In most cases, they correspond to the zones issued from the land use plan. In ISOS maps, continuous line protected perimeters marked with numbers represent *built precincts which can be perceived as an entity via their historical-architectural and spatial characteristics or as for their regional specificity* [166]. These perimeters can include smaller "ensembles" clustering coherent buildings sets (e.g. the cathedral square), numbered after the reference perimeter (the format is [digit].[digit]). Dashed lines represent surrounding areas having a strong relationship with the previous ones, often parks, fields or landscape elements: they are marked with roman numbers. Remarkable buildings listed in the Federal Protection inventory in case of conflict [179] are represented in plain black hatch. Results of sensitivity allocation are shown on a dedicated map layer in Figure 5.4 and Figure 5.5.

5.5   Cross mapping results

As a first step, the three variables are plotted on a map of the administrative districts of the municipality of Geneva (GIREC). They cover a territorial unit at an intermediate scale between the parcel and the whole city: the entire municipality counts 128 districts among the 475 of the whole canton, which are differentiated based on the prevalent land use. In Figure 5.4, high sensitivity zone is highlighted as a relevant and homogeneous territorial entity. Low sensitivity zones appear like small isolated patches on a uniform medium sensitive background and they are not represented at this stage. Listed buildings represent punctual attention catalyzers.
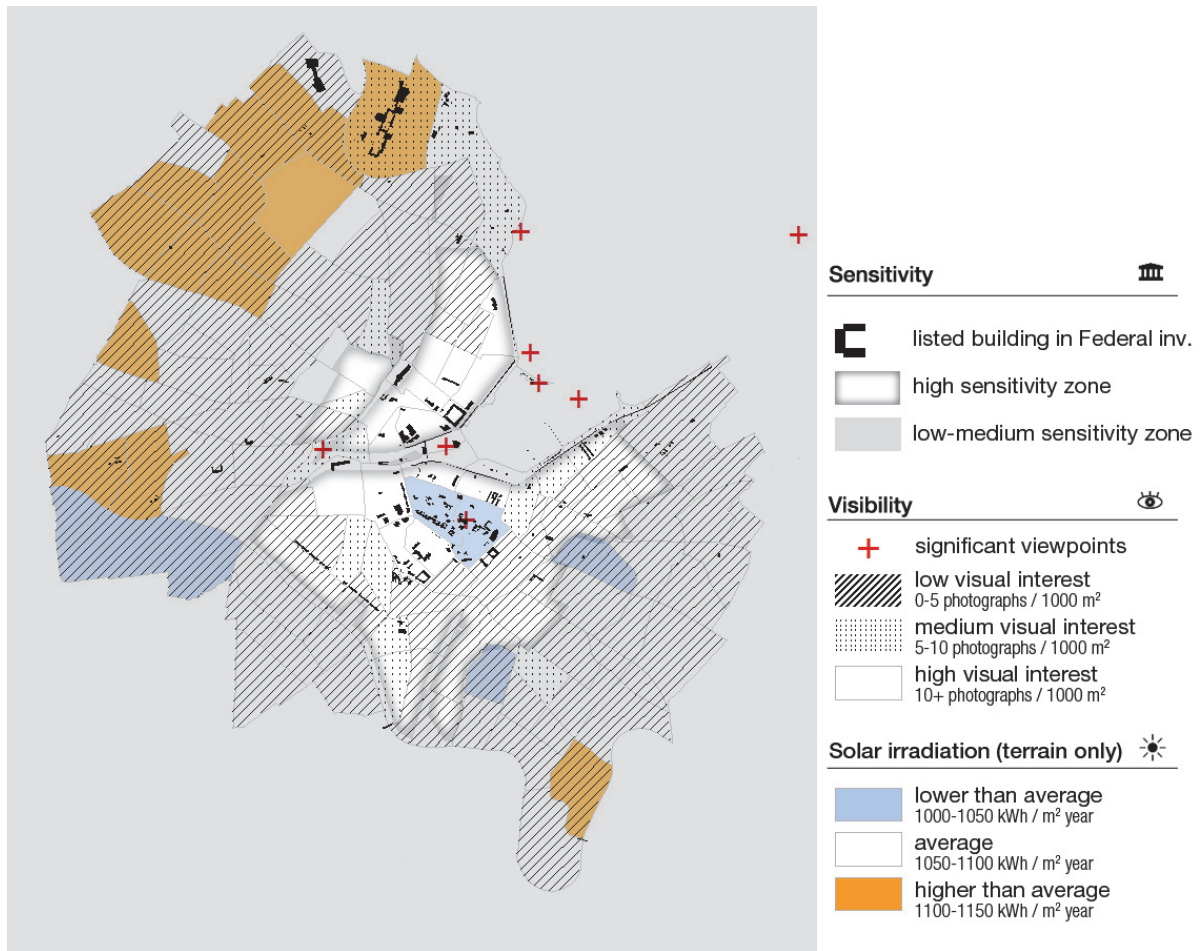
Figure 5.4 Geneva, Switzerland (original scale 1:30 000). Cross-mapping example for strategic planning on GIREC statistic sectors.

(Author's elaboration on CC data from Système d'information du territoire à Genève – SITG.)

Average solar radiation on ground is quite constant over the municipality of Geneva; small variations discussed in Section 5.3 are considered for a general strategic orientation. Visual interest is indicated here in relation to the number of photographs located in each district per 1000 m^2 unit area; remarkable viewpoints emerge as singularities. From this map, it is already obvious that lakeshores are privileged view areas, thus confirming the tendency from the census of remarkable viewpoints. The city center is dense in monuments and consequently more observed, as expected; the irregular topography makes it more unfavorable in terms of solar radiation, which complicates the task of a successful and non-impacting solar development. Another relevant area of high visual interest is the station area on the northern lakeside. This trend is even clearer when comparing sensitivity from ISOS maps and kernel density of photographs, as shown in Figure 5.5 and in Annex I.

Sensitivity (ISOS)

1	protected perimeters: built precincts which can be perceived as an entity
1.1	ensembles: coherent buildings clusters
XV	meaningful surrounding areas and environment

■ remarkable building

][relevant building or façade

▨ perturbing element

Visibility

● significant viewpoints

low density (0.0036 to 0.14)

medium density (0.15 to 0.32)

high density (0.33 to 0.8)

Figure 5.5 Geneva, Switzerland (original scale 1:20 000). Cross-mapping between ISOS sensitivity and kernel density of photographs.

(Author's elaboration on © data from Swiss Federal Office of Culture – OFC)

When observing the match with the ISOS perimeters, a partial overlap between high visual interest and high sensitivity to solar development can be identified, with a few exceptions: (i) leisure and landscape areas (rivers, parks, and lakeshore), where people spend their time relaxing, sightseeing and taking pictures. Particularly interesting is the high density marked on the lake, since many touristic cruises are proposed; (ii) Infrastructural nodes (railway station, airport), where the combination of travel excitement and people concentration increases the number of photographs. This can be explained by the high presence of travelers, having maybe a quick look at the surroundings before leaving, or taking photographs while waiting to leave, or witnessing their arrival in the city. Highest photo density spots fall mostly within ISOS perimeters or "ensembles": the cathedral and the "Grottes" district close to the station can be clearly identified. The Mont-Blanc Bridge and the surrounding shore are an exception: these are in fact very relevant environments, since they offer view on the historical center and on the famous "Jet d'eau". This separation between cultural heritage area and prominent visual access to it is even more evident for the United Nations Palace, at the northern boundary of the image: it lies in an almost completely fenced garden. In this case, the "Place des Nations" with artworks and a nice view on the palace is the most accessible public space chosen as privileged photographic location. Finally, the settlement of Carouge at the southern boundary of the image is particularly interesting. Despite the lower number of pictures in this area, the domain around the church is still clearly highlighted. Moreover, the zone around the library emerges, since it usually hosts some pieces of art and few panoramic views of the river "Arve", e.g. the Carouge Bridge, a shore in front of the Champel Tower and the Vessy Bridge.

5.6   Discussion

A cross mapping representation of solar radiation, visual interest and sensitivity to solar development is presented at the district level for the strategic planning. Annual solar radiation is determined through the validated Solar Analyst module for ArcGIS © at the stage of geographic potential, considering only the topography of the terrain. The impact of land uses and shading from buildings are neglected and will be considered in a more advanced phase. Current level of details is sufficient to estimate solar radiation singularities due to ground slope and orientation, compatible with a district aggregation. Sensitivity is deduced from the land use plan and the Federal Inventory of Swiss Heritage Sites (ISOS), the two layers having a reasonable correspondence: at this stage, only high sensitivity areas are identified as relevant and clearly delimited enclaves deserving a particular attention.

A method to assess visual interest of urban areas in a strategic planning process is presented. The kernel density indicator is appropriate to highlight the "mass effect" on the perception of large urban areas, which prevails at the strategic level and does not include geometric nor physical properties of vision. It is conceived for the large urban prospect (1:100 000 to 1: 30 000 scale), in the framework of the methodology presented in Chapter 4. Such an analysis provides a bottom-up estimation of visual interest, which should be coupled with a top-down punctual census of relevant viewpoints validated by experts or entitled local authorities (building heritage offices, land use planning services, historic archives, touristic promotion). Photo shooting location density is also affected by some limitations: in particular, inaccuracies in geo-referencing of pictures or insufficient number of photos can influence density computation, as well as the presence of irrelevant pictures. Well-documented cities with rich photo-databases undergoing a careful data filtering should be used only. On the other hand, different categories of photographers, such as tourists and local people, are mixed and could be separated to target their specific interest: even if they are both concerned by the presence of solar panels in the urban landscape, it is questionable whether they should be considered equally in an urban planning process. In spite of these shortcomings, kernel density of photographs seems a valuable method to map a continuous and distributed visual interest index beyond the discrete census of remarkable viewpoints in a city. It can be used to weight the viewpoints sample for more detailed assessments and to establish a "viewpoints hierarchy", as a first approach for a solar deployment strategy. For example, least sensitive / least visible areas can be considered for massive deployment thanks to their low architectural quality needs, most sensitive / most visible areas for demonstrative showcases of outstanding solar integration solutions.

5.7   Acknowledgements

Chapter 6   Development planning

At the level of development planning (about 1 : 10 000 to 1 : 5000 scale), urban fabric becomes visible and construction morphology is compliant with land use. Street widths define the infrastructural mesh and the magnitude of heights is becoming relevant when designing building volumes. The city model evolves from a corrugated terrain with local singularities to a systematic mix of the natural terrain and anthropic traces, including infrastructures and buildings. The level of details increases from land patches characterized by more or less uniform uses to independent building units. Some professionals refer to this as the scale of master planning, where a spatial connotation of urban territory begins to rise from parcels, relationships of buildings and circulation. Empty and filled spaces assume a functional identity that corresponds to their envisioned role within urban growth.

At this stage, solar radiation can be assessed in terms of location potential, refining the geographic potential to a narrower scale that includes only building envelope outdoor surfaces as the focus of this work. Solar radiation on rooftops can be estimated with sufficient accuracy, taking the slope and orientation of roof pitches into account. Façades are usually less sunlit and are likely more subject to shading by elements such as trees, urban furniture and architectural features like terraces, balconies, which are neglected in this phase: they will however be analyzed in a further stage.

Sensitivity is determined from land use as for strategic planning; differences between high, medium and low sensitivity areas become however relevant at this level. Minor singularities emerge, such as listed clusters of buildings in residential areas, erected using local materials and techniques, which may constitute a high sensitivity enclave in a medium sensitivity zone. Industrial precincts are usually scattered on the territory in relatively small and isolated compounds and are labeled low sensitive.

Visibility depends mainly on geometric factors and reciprocal obstructions: it is evaluated per building roof. It means that, at this stage, it is more important to know whether roof surfaces can be visible or not, and from how many unobstructed locations, rather than trying to quantify

the degree of physical perception from each viewpoint. This would require more details regarding the building envelope shape as well as a complete material mapping of the different surfaces, which is appropriate for the following stages in the planning process. A possible geometric indicator for GIS applications is the "Cumulative Viewshed" (also known as "Times seen"), which counts the number of times each building surface is intercepted by a visibility ray issued from several viewpoints disseminated in the public space. Beyond its established meaningfulness for landscape and geographic planning discussed in Chapter 3, an extensive application to the urban environment is here attempted with specific reference to solar energy deployment.
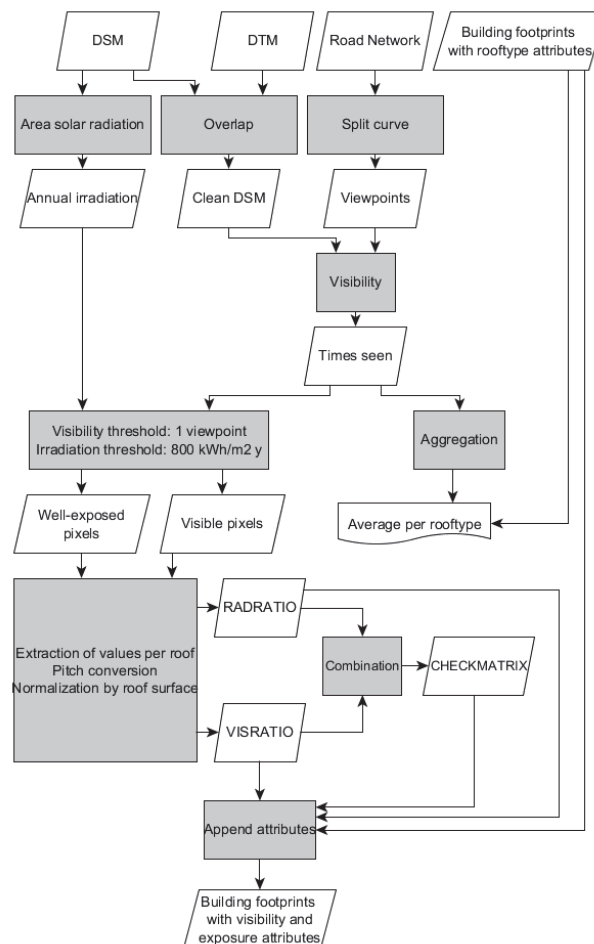
Figure 6.1 Workflow to issue the CHECKMATRIX in ESRI ArcGIS and ModelBuilder ©

(Author's own elaboration)

As for solar radiation, façades are subject to a high variability in visibility, depending on their exposure to the public space and on the occlusion from vegetation and urban furniture. Consequently, cross mapping is performed only on rooftops, while façades will be introduced in a more advanced phase. The aim is to make the workflow applicable in most situations (Figure 6.1), a minimum of geographic data and GIS software tools being the only requirements.

6.1   Visibility

6.1.1   Viewpoints sampling

The case study adopted for the current analysis is the municipality area of Geneva, which comprises 10886 buildings as solar deployment targets and 2254 road segments as public space subdivisions. Model inputs for viewpoints sampling are the DSM (Digital Surface Model) raster, the DTM (Digital Terrain Model) raster, the road network vector and the building footprint polygons. The two elevation raster datasets were merged to get a simplified DSM file including only the terrain and the pixels within the building shapes. In that way, trees and urban furniture that might partially block the view are discarded, providing a "most visible" case-scenario; they will be considered at the stage of detailed planning. This "clean DSM" can also be obtained by filtering raw LiDAR data from airborne laser scanning. Subsequently, the viewpoints are extracted from the road network, thanks to a dedicated script that creates point features at fixed distances on a line / curve (Figure 6.2).

Figure 6.2 Augustins district, Geneva, Switzerland. Viewpoint sampling on the road network (street axis) with a 10 m distance.

(Used tool: Create Points From Lines CC, ArcGIS ArcMap ©, elaboration on CC data from Système d'information du territoire à Genève – SITG. Credits: dwynne ArcGIS user, Esri, HERE, DeLorme, MapmyIndia, © OpenStreetMap contributors, and the GIS user community)

This distance is set to 10 meters, which is slightly smaller than any dimension of a generic building, to be sure to catch all its sides. Viewpoints are sampled on the street axis, and considered as standard observation positions: slight changes in visibility may occur across the road section, but are not relevant at this stage for development planning (see Section 6.5). Compared to strategic planning, viewpoints are evenly distributed on the road segments, which are making up the public space. In fact, public perception shifts from visual interest, linked with social relevance of a site, to visibility as a consequence of the geography and morphology of the territory: the latter is independent from the number of observers frequenting a place.

6.1.2 Threshold setting

Before running the viewshed analysis from the selected viewpoints, a maximal visibility distance limit has to be set: this constitutes the maximal length for the lines of sight, beyond which the viewshed is not considered. The corresponding distance assumed for calculations is 500 meters, imposed mainly by computational constraints: the outcome for a 3 km by 3 km area is returned in 26 hours with a standard desktop PC (3.4 GHz CPU frequency, 16 GB of RAM). A 3 km by 3 km tessellation of the municipality of Geneva is performed, by keeping a partial tile overlap corresponding to the visibility limit. Each tile features approximately 10 000 viewpoints x 36 000 raster cells, implying circa 360 million operations. Such a 500 meters "standard distance" is consistent with the established literature that adopts it as the limit to identify specific landscape components [182]. It is also compliant with pragmatic urban regulations that try to balance design freedom and visual constraints. Even if it can be extended up to 15 000 meters for panoramic viewpoints, a 500 m threshold is also considered as appropriate by urban designers and editors of urban planning guidelines in this context [136, p. 34], [137, p. 9] (cf. Section 3.4 paragraph 6). This limit corresponds to the perception threshold for a 0.5 m x 0.5 m object in front view (model resolution) or a 1.65 m x 1 m standard solar panel, installed on a 20 degrees tilted roof at 4 m height. In fact, as explained in [61, Para. 3.2], the maximal distance for a rectangular feature perception (detection) with given dimensions can be determined using Equation 6.1:

$$d_{lim} = \frac{180 \cdot 60}{\pi} \cdot \left(\frac{A_p}{S_0}\right)^{\frac{1}{2}}$$

Equation 6.1 – Maximal distance for visibility analysis [61, Para. 3.2]

A_p [m] is the feature's projected area on the visual plane and S_0 [arcmin^2] is the minimal perceptible visual size expressed in squared minutes of angle, assuming that the length of an arc can be approximated to its tangent when the radius is large enough. Shang & Bishop found a relationship between the minimal perceptible visual size S_0 [arcmin^2] and the lightness contrast between the object and its background, relative to the maximal pixel lightness in a picture: the value of lightness contrast goes up to 26% under normal meteorological and atmospheric conditions (see [66, p. 128] and Section 2.4.3). In these circumstances, S is approximately equal to 12 min^2, even though some reference studies consider 25 min^2 [62, p. 241], generically assuming the most recurrent lightness contrast measured by Shang & Bishop (13%).

6.1.3 Viewshed analysis

A viewshed analysis is performed from the considered viewpoints with a z-offset of 1.5 m, corresponding to the eyes height of a standard observer, relative to the clean DSM raster cells: the higher the resolution, the finer the results, at the cost of a larger processing time. The configuration adopted features a 0.5 m resolution.
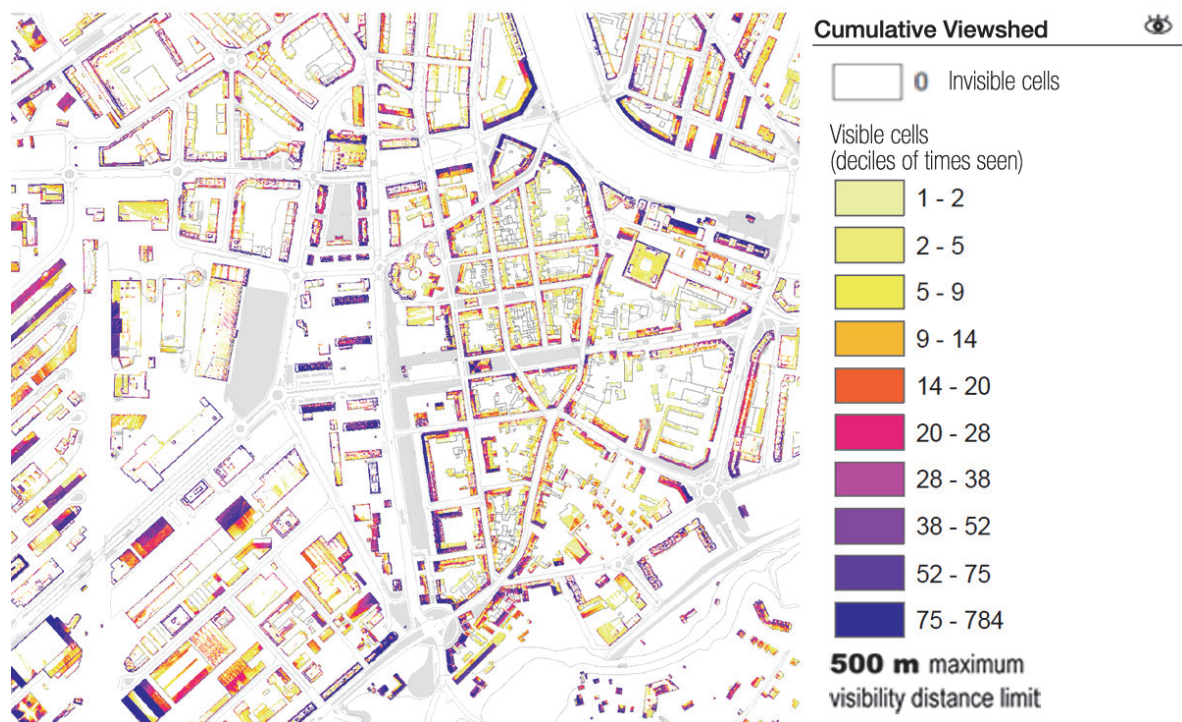
Figure 6.3 Carouge, Geneva, Switzerland. Cumulative viewshed per deciles of "times seen".

(Used tool: Viewshed, ArcGIS ArcMap © elaboration on CC data from Système d'information du territoire à Genève – SITG.)

According to the calculation procedure, each cell counts for the number of times it is visible from the set of viewpoints; as stated in the objectives though, there is no physical or physiological quantification of the cell visibility at this stage. This cumulated amount is known as "Cumulative Viewshed": invisible cells are characterized by a value equal to nil and visible cells by a value larger than or equal to 1. By observing the map in Figure 6.3, it is already obvious that roofs of isolated buildings are usually perceived through more viewpoints than those of buildings located around a courtyard, being surrounded by less enclosed space that enhances the probability of unobstructed viewpoints.

6.2   Location solar potential

Concerning solar radiation, an official map issued from validated measures or simulations is often not available: the Area Solar Radiation tool can be used in GIS to assess it using the original DSM (trees have to be included this time). The analysis is carried-out for a whole year keeping the initial resolution: both direct and diffuse components of solar radiation are accounted for (Figure 6.4).

Figure 6.4 Carouge, Geneva, Switzerland. *Location solar potential* issued from DSM.

(Used tool: Solar Analyst © elaboration on CC data from Système d'information du territoire à Genève – SITG.)

Calculation assumptions and details have been highlighted in Section 5.3. Compared to the strategic planning, it is important to emphasize that the solar potential is assessed on roof surfaces only, discarding solar radiation on ground and beyond building footprints. Hence, the *location solar potential* can be considered as a refinement of the corresponding rough estimation based on the terrain topography only (Chapter 5), issued from DTM data sets.

6.3   Sensitivity

High sensitivity areas are issued from land use plan as for strategic planning. Apart from buildings listed in the Federal inventory [179], the amount of remarkable buildings is enriched with cantonal listed ones [183], to which items mentioned in academic surveys that include more contemporary cultural asset (e.g. Recenssement Addor, Honegger, Recenssement des immeubles genevois, du Patrimoine Industriel [184]) must be added. Residential areas are assigned a medium sensitivity level since they are characterized by lower constraints: these are usually relative to building height and floor area ratio, sometimes impeding roof shape modifications. In industrial areas, except for historical facilities, fewer protection measures are in effect: they constitute low sensitivity areas.
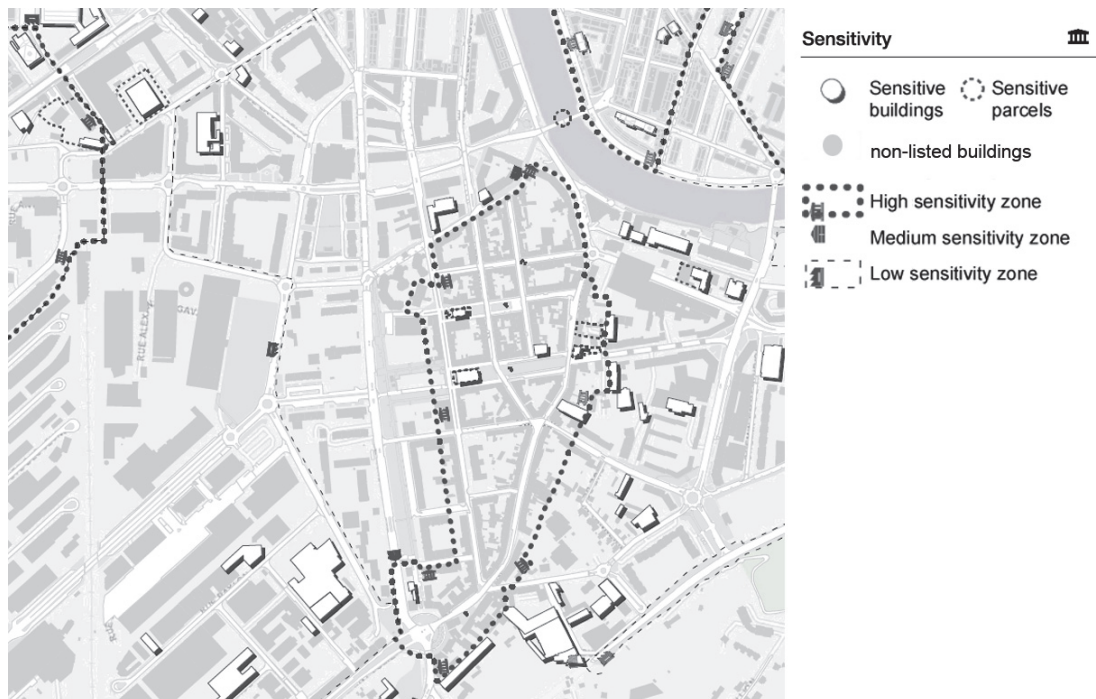
Figure 6.5 Carouge, Geneva, Switzerland. Sensitivity zones issued from land use plan and listed buildings.

(Used tool: ArcGIS ArcMap © elaboration on CC data from Système d'information du territoire à Genève – SITG.)

Land use maps are a good example of sensitivity mapping, even though not always exhaustive without a deep understanding of the local specificity as well as a constructive debate with the local site protection authorities. An extract of the sensitivity map is shown in Figure 6.5.

6.4 Cross mapping results

6.4.1 Binning, normalization and aggregation

To organize the results in a synthetic and comparable form, it is necessary to reduce the number of classes per information layer and to aggregate the indicators per unit of interest (i.e. each building roof).
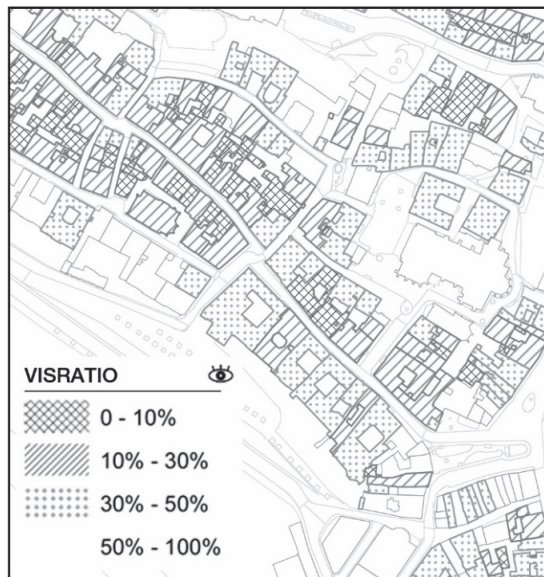
(a) VISRATIO
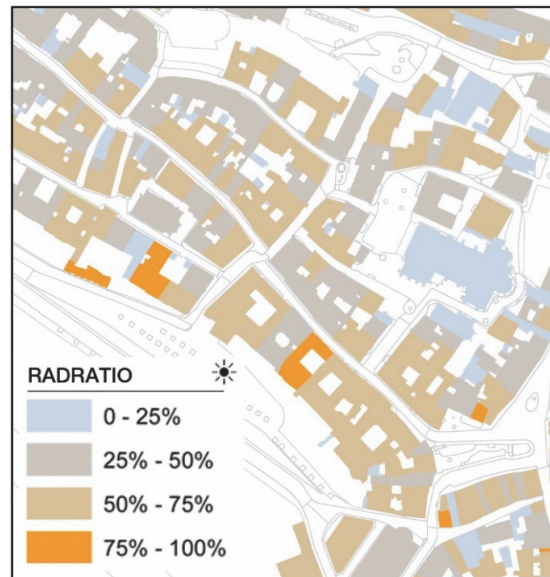
(b) RADRATIO
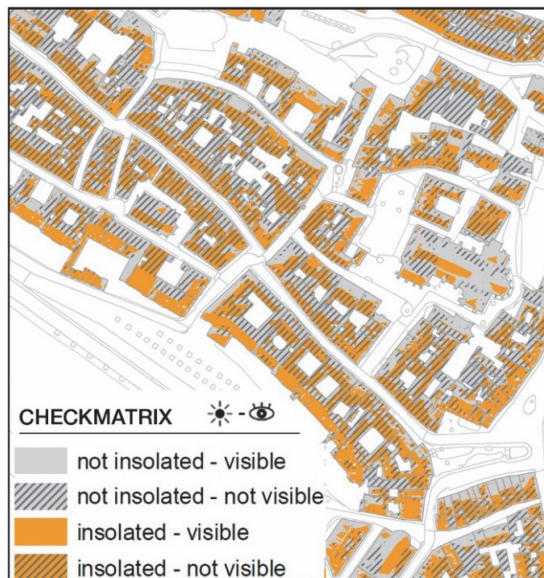
(c) CHECKMATRIX

Figure 6.6 Cité, Geneva, Switzerland. Indicators after binning, normalization and aggregation.

(Used tool: ArcGIS ArcMap © elaboration on CC data from Système d'information du territoire à Genève – SITG.)

As a first step, non-visible cells are flagged as "0" and cells that are viewed by a viewpoint at least as "1". The number of visible cells within each building footprint is computed by excluding cells located outside building boundaries, only considered as obstructions: then the ratio of visible cells over the total cells per building roof is determined, taking roof pitch into consideration through division of the cell area A [m^2] by the cosine of the sloping angle α [deg]. This ratio is called Visibility Ratio (VISRATIO) [-] (Equation 6.2) and represents the share of visible surface on a roof of a building perceived from the viewpoints in the public space (Figure 6.6a); as a consequence, (1-VISRATIO) [-] is the invisible roof portion. Such an index characterizes the visibility layer, aggregated per building, at the current analysis level: it has to be matched with sensitivity and solar radiation.

$$VISRATIO = \frac{\sum_{i=1}^{n} \frac{A_i}{\cos \alpha_i}}{\sum_{i=1}^{m} \frac{A_i}{\cos \alpha_i}} \text{ with } \begin{cases} n = \text{visible cells per building roof} \\ m = \text{total cells per building roof} \end{cases}$$

Equation 6.2 – Visibility Ratio (VISRATIO). Solar radiation Ratio (RADRATIO) is calculated similarly, with n being equal to the number of well-exposed cells per building roof.

Yearly solar radiation raster is filtered to keep only cells yielding more than 800 kWh/m^2 per year, as this is considered as the most credited threshold for the economic viability of a building integrated photovoltaic (BiPV) solar power plant in Switzerland [185]. This limit should be adapted according to specific market conditions as it is not constant in time nor in space: nevertheless, it is assumed as a standard reference value for comparison purposes. All cells below this threshold are flagged as "0" and all cells above as "1", characterizing another useful area ratio. This ratio is called Solar Radiation Ratio (RADRATIO): it represents the share of pixels benefitting from a sufficient solar radiation on a building roof, worth enough to consider installing a solar BiPV power plant (Figure 6.6b).

Finally, roof pixels are categorized into four situational groups:

-   (I) Those that are invisible (by any of the viewpoints) and well exposed to solar radiation (above the viability threshold);

-   (II) those that are visible (by at least a viewpoint) and well exposed;

-   (III) those that are neither visible nor well exposed

-   and (IV) the ones that are visible but not well exposed.

The share of pixels falling under each category over the total number of pixels on each roof is computed and stored in a dedicated (4 x 1) matrix called "CHECKMATRIX". A representation of such an indicator is illustrated in Figure 6.6c.

6.4.2 Results insights for Geneva

Results after the threshold filter and the normalization by roof surface are shown in Figure 6.7. Apart from the buildings that do not have a well sunlit roof area (e.g. not above the viability threshold), two main sets of interesting roofs can be identified (Figure 6.7a):

- (I) Those having a large fraction of well exposed areas which is also visible from the public space, subdivided in two clusters having around 50% (A) and 80% (B) of the total roof surface. These roofs can be selected for exemplary and highly qualitative solar deployment, since all the suitable area for solar power generation is visible;

- (II) On the other hand, a cluster representing about 10% of the buildings sample offers circa 45% of non-visible and well sun lit roof areas over the total roof surface, and contemporary 20% of visible well exposed ones (C). Such a subset could host a lower number of BiPV solar power plants.

Moreover, one third of all Geneva buildings have the largest fraction of roof surface falling in the non-visible and well-exposed category. By looking at the surface distribution in this category, it appears that the third quartile is approximately equal to 140 m^2, meaning that the remaining 25% of the sample benefits from equal or larger fractions of roof surface. A BiPV system of this size would roughly match the electricity demand of 6 Swiss households without having to worry about the visibility of the solar plant (Figure 6.7b): this is assuming a 15% PV solar cell energy conversion efficiency over the minimal solar radiation of 800 kWh/m^2 year and a 3000 kWh/year electricity consumption of a standard households of 3 persons. Another fourth of buildings shows most of the roof area is visible and well exposed, while the remaining 42% of the sample is less attractive, since most of the building surface has a low solar potential. Identified buildings can be marked down on the map and exported on a 3D visualization platform, to check the results and combine them with other useful information (Figure 6.8).
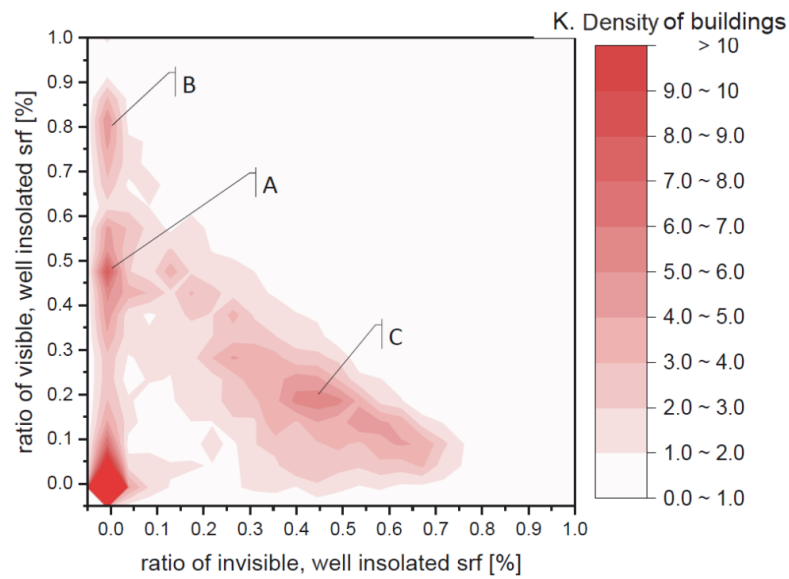
(a) Kernel density scatter plot of buildings as function of their useful, well insolated roof surface: ratio of invisible, well insolated roof surface over total vs visible, well insolated roof surface over total.
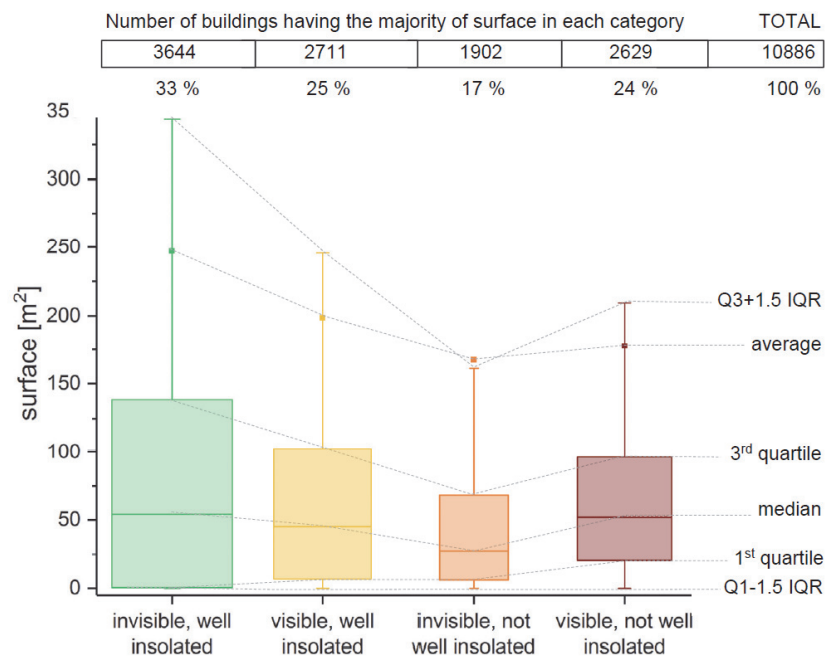
(b) Boxplots of the available roof surface under each category, per building. Boxplots width corresponds to the frequency of buildings having the majority of the surface in each category.

Figure 6.7 Geneva, Switzerland. Roof suitability analysis.

(Used tool: ArcGIS ArcMap © elaboration on CC data from Système d'information du territoire à Genève – SITG.)
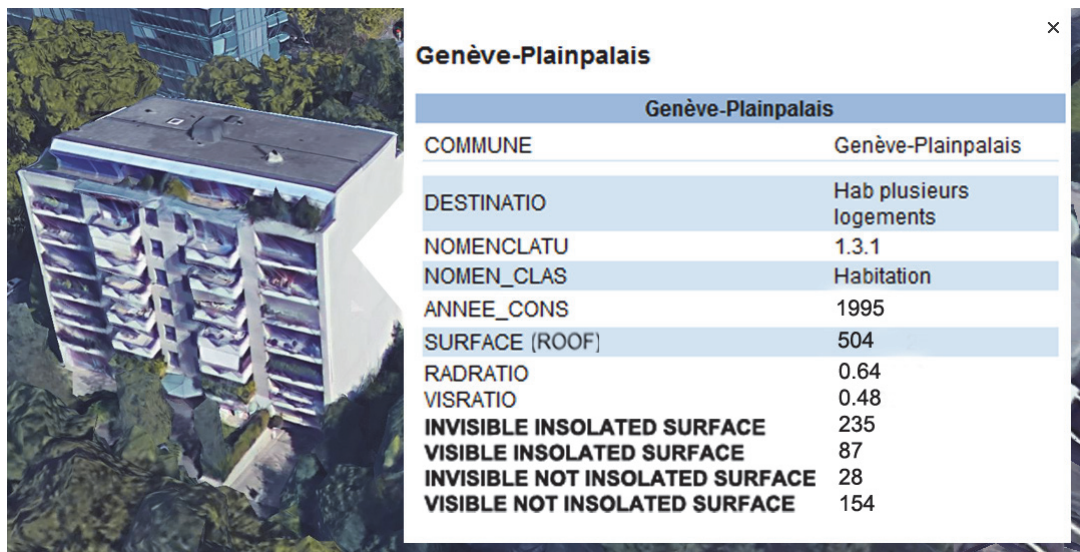
Figure 6.8 Geneva, Switzerland. Example of Google Earth © interrogation of the cross-mapping tool.

(Used tool: Google Earth ©, Credits: Landsat Copernicus)

Figure 6.9 Carouge, Geneva, Switzerland. Roof suitability analysis. Roof surfaces are classified by combination of insolation and visibility thresholds (CHECKMATRIX).

(Used tool: ArcGIS ArcMap © elaboration on CC data from Système d'information du territoire à Genève – SITG.)

In order to match visibility, sensitivity and solar radiation values in the framework of a multi-criteria decision analysis, it is necessary to represent all these variables together on a map.

Figure 6.9 illustrates roof surfaces that are classified in solar radiation and visibility categories according to the CHECKMATRIX (Section 6.4.1), for the city of Carouge (Geneva metropolitan area). Despite the usually scattered spatial distribution, optimal solar radiation is achieved in the industrial area (down left on Figure 6.9) where streets are wider and buildings are large and not tall, leading to a limited cast shading. Being covered mostly with flat or shed roofs, many of them are characterized by invisible roof surfaces and a considerable solar yield. On the other hand, the sensitive zone around the center of the figure (i.e. the center of Carouge) is characterized by shorter, narrower and more tortuous streets as well as more complex roof shapes. Less visible buildings are located in inner courtyards or in a parcel far from the street. For a thorough observation of whole results, the entire map of Geneva can be found in Annex II.

6.4.3 Considerations on roof types

Roof type is certainly expected to have a large impact both on radiation and on visibility from the public space. A very interesting study explored the relation between useful roof areas and different types of roof shapes [186]: the authors concluded that for most roof shapes the ratio between the useful roof areas for solar power and building footprint area is close to one, suggesting that the footprint is a good measure of useful BiPV roof area. The only exception are gable roofs featuring a ratio of 1.18.

A similar approach was attempted for visibility in this study, with the use of the same roof categorization provided by the former authors. For each pixel on the roof surface in all buildings, the number of viewpoints in the public space being able to see it is accounted: this indicator, also known as "Cumulative Viewshed" or "Times-seen" can be averaged per each building; results are averaged again per roof type. Figure 6.10a indicates that low pitched roofs are visible on average from half of the locations viewing hipped roofs and two thirds of gabled roofs; complex roof shapes show a non-significant increase in the cumulative viewshed compared to low pitched roofs. Similarly, low-pitched roofs show on average less visible areas than the more complex ones (Figure 6.10b), even if the trend is smoother. Low-pitched roofs may even be totally invisible if the related buildings are tall enough. Despite the bias that may be introduced by towers, hills or other viewpoints located above the average ground altitude, a certain trend can be identified in a globally flat territory, such as the urban area of Geneva.
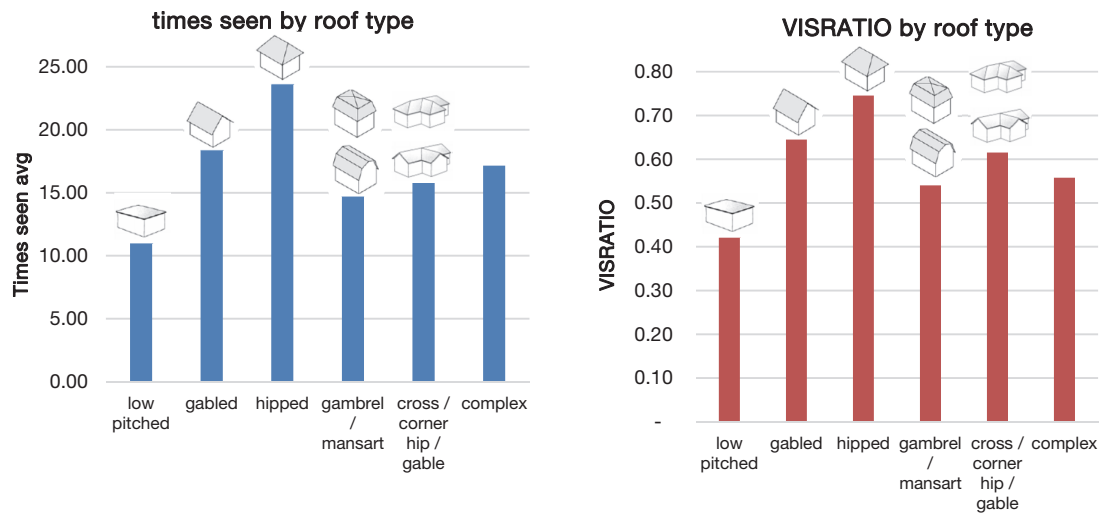
(a) times seen as a function of roof type

(a) VISRATIO as a function of roof type

Figure 6.10 Geneva, Switzerland. Times seen, and VISRATIO as a function of roof type, according to the categorization proposed by [186]. Times seen from each viewpoint are averaged per roof and per building type; VISRATIO is averaged per building type.

(Used tool: ArcGIS ArcMap © elaboration on CC data from Système d'information du territoire à Genève – SITG. Credits for roof categorization : Mohajeri, N. and Assouline, D.)

6.5   Model uncertainty and limitations

Model uncertainty is mainly linked to the chosen visibility threshold, the maximal distance adopted to perform the visibility calculation and the viewpoints sampling operation; moreover, some computational limitations are related to raster resolution. In Section 6.4.1 an absolute visibility threshold for a given viewpoint is set: features that can be viewed from one or more viewpoints are considered visible. In fact, cumulative viewshed follows a heavy-tailed distribution (Figure 6.11), 53% of the total roof surface in Geneva being visible and 47% being invisible: a value close to 50% is considered acceptable. Concerning the maximal distance to use when tracing the visibility rays, a sensitivity analysis has been conducted on the Hollande district in Geneva (250 m x 250 m, 52 buildings) for three different viewing distances, e.g. 100 m, 500 m and 1000 m. The sensitivity of VISRATIO to the maximal distance variation has been analyzed. Since there is no physical attenuation of visibility due to the atmosphere limited transmission over the considered distances, visible pixels only increase across the three scenarios. This is a consequence of the growing number of viewpoints included in the analysis, by effect of a distance limit increase. As it can be observed in Figure 6.12a, there is a large variation in number of visible pixels between 100 m and 500 m, affecting VISRATIO for more than 10% in two thirds of buildings. On the opposite, 90% of buildings show less than 10% VISRATIO variation between 500 m and 1000 m, leading to a certain stability of this indicator in absence of towers,

hills or other viewpoints above the ground. For this reason and in accordance with the psycho-physical considerations presented in Section 6.1.2, 500 m was adopted as standard visibility limit. Nevertheless, it must be noted that psychophysical perception varies as a function of the solar modules size, in this case assumed equal to the DSM resolution. In case of particular needs, such as a specific viewpoints analysis or particular solar power plant dimensions, the visibility limit can be adjusted. Viewpoint sampling represents also a possible source of uncertainty: in particular, distance between viewpoints and their position along the street section have an impact on the results. With regard to the former, a few simulations were carried-out on the reference district Hollande, with respectively 1 m, 2.5 m, 5 m, 10 m, 100 m spacing. Concerning the latter, viewpoints were placed at the boundary between the roads and the sidewalks with a 10 m spacing, this scenario being compared to the adopted road axis con-figuration.
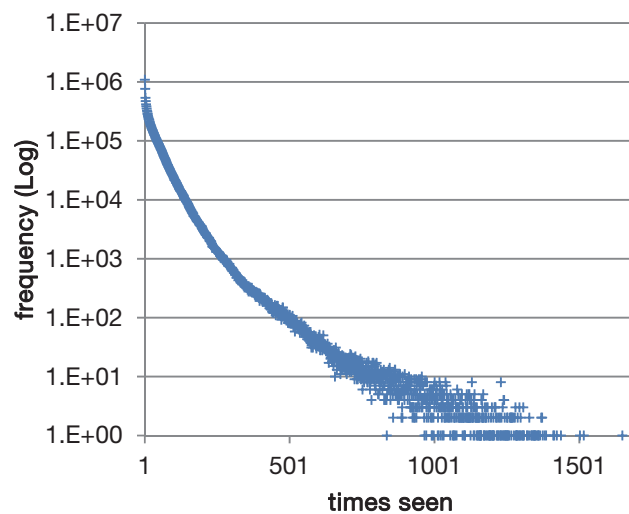
Figure 6.11 Geneva, Switzerland. Heavy-tailed power law distribution of occurring frequencies of the times seen indicator for roof pixels, in logarithmic scale.

(Used tool: ArcGIS ArcMap © elaboration on CC data from Système d'information du territoire à Genève – SITG.)

Legend:
- visible from 100 m
- visible from 500 m
- visible from 1000 m
- invisible

Maximum visibility distance

(a)   variation in visibility state according to maximum visibility distance change

Legend:
- viewpoints spacing (1-10m)
- viewpoints positioning (road axis - sidewalk boundary)

Spacing

Positioning

(b) variation in visibility state according to spacing and positioning on road axis or on sidewalk boundaries
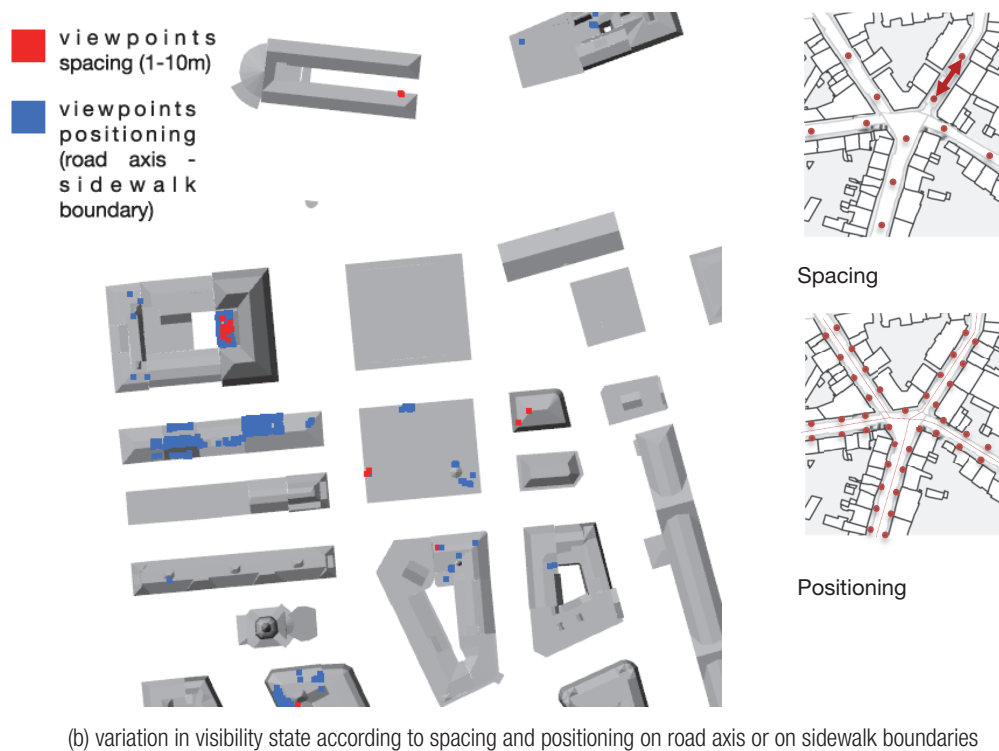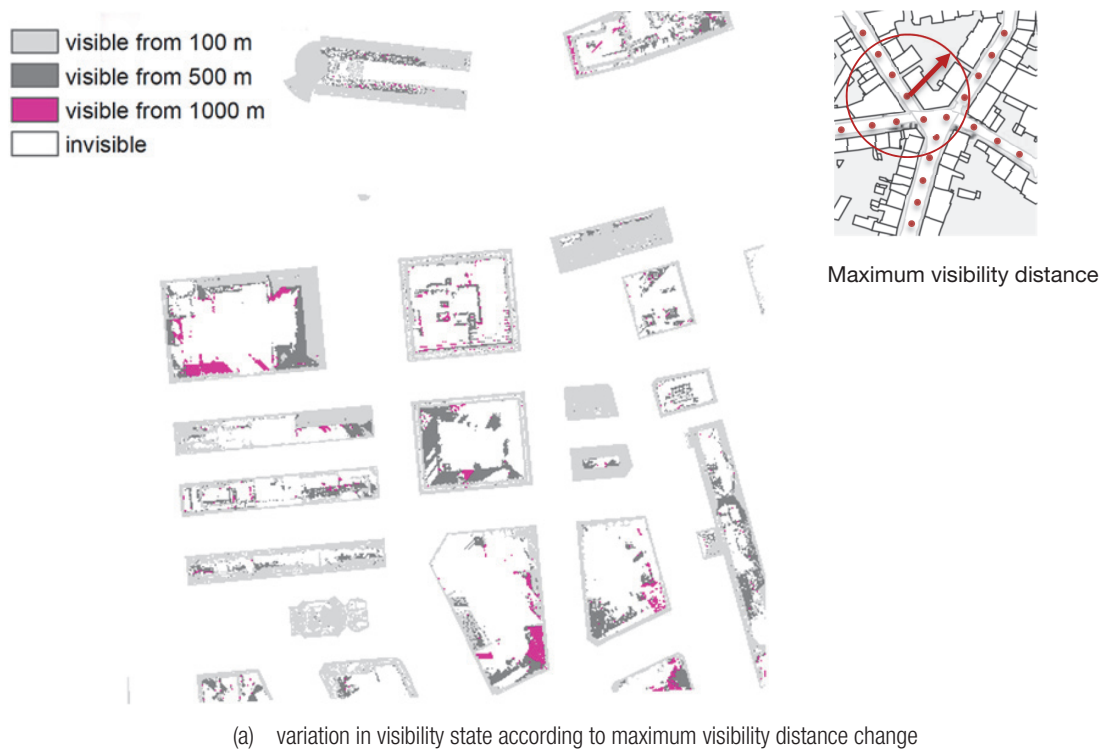
Figure 6.12 Geneva, Switzerland. Sensitivity of the visibility model to viewpoints sampling.

(Used tool: ArcGIS ArcMap © elaboration on CC data from Système d'information du territoire à Genève – SITG.)

Figure 6.12b shows that there is almost no variation between 1 m and 10 m spacing (except for 0.13% of target cells). However, there is a significant difference due to geometrical reasons of the road section (i.e. relation between roof pitch angle and road width), between positioning on the road axis and on the sidewalk edges. The entailed visibility state change for 2% of target pixels generates a substantial VISRATIO variation for almost 10% of sampled buildings by effect of pixel aggregation. This can be considered as acceptable at this stage of the planning process, which is focusing rather on differences between districts and clusters of buildings. Road axis is used as a standard position to sample a sufficient number of viewpoints without reaching heavy computational loads. In fact, one of the limitations of the method is the considerable use of CPU resources to analyze massive raster data, which requires splitting the input data into tiles.

Worth to mention in this section is the uncertainty of the solar radiation model. The Area Solar Radiation tool in ArcGIS © relies on a direct solar radiation model based on the sun position; the diffuse solar radiation is a fraction of the global normal radiation. This method is considered to be sufficient at the current stage of the planning process; more detailed models implying the generation of climate-based skies are needed to achieve more accurate results at a finer scale [187].

6.6   Discussion and conclusion

At the development planning level (1 : 10 000 to 1 : 5000 scale), a ratio representing the visible share of roof pitches is introduced and matched with the useful area for solar power production above the viability threshold. A handy "cross-mapping" representation is also shown in this section, in order to synthetize the information in a graphic way and provide a classification that might be used for multi criteria decision making. The combination of solar radiation, sensitivity and visibility is the core of the LESO-QSV method developed at EPFL [28], which is an efficient driver for solar energy planning. The main advantage of this method is that very few and widely available input is required to perform the analysis, such as an elevation model, road network and building footprint vectors. A large fraction of buildings in Geneva is both well sun lit and non-visible from the viewpoints in the public space: they can be refurbished without targeting a high architectural quality, using standard solar products available on the market (such as building added PV panels). Buildings within this subset are probably the most urgent to treat in a massive solar deployment scenario. More complex roof shapes can be less visible but are

less adapted to the installation of standard solar products due to their sharp angles and polygonal multi-faceted surface. At this stage, the "Viewshed" indicator is suitable to describe the portion of building envelope that is visible, based on the reciprocal position of viewpoints and target surfaces. Except from the "mass effect" highlighted by the "Times-seen" indicator, which counts the number of possible viewpoints, there is no precise quantification or differentiation of the visual perception. It means that a viewpoint very close to the visual target is affected in the same way than a viewpoint located far away from the target within the maximal distance limit, if there is no obstacle on the line of sight. Neglecting the trees in the current method leads certainly to an overestimation of visibility in some cases; however, it corresponds to the worst-case scenario in terms of design effort of solar modules integration.

Hence, this method is valuable for large districts or cities to spot more / less visible building sets and to identify adapted precinct solar deployment strategies; it is not accurate enough to reveal the parts of building envelope that are more suitable or technically adapted to host solar modules integrated in the envelope. On the other hand, it is useful to compare buildings on a common conventional basis and to detect zones deserving further investigations. To fill the gap, a geometrically reliable "Visual Amplitude" index is needed at the detailed planning level (1 : 2000 to 1 : 500 scale): it should take into account physical and physiological factors (see Chapter 7).

A model implementation in an existing case study of a multi-criteria decision method (MCDM) is expected: the contact with stakeholders will however be necessary to assign appropriate weights to the visibility classes as identified by this method. In this way, visibility becomes an established parameter for MCDM beyond "Visual impact" in its negative meaning.

6.7   Acknowledgements

Chapter 7   Detailed planning

At the detailed planning level, the scale of the analysis narrows down to districts, i.e. sets of buildings sharing a common base: this can be their uniform architectural character within the development of the city, a similar historical context or the uniformity of construction materials and techniques. There might be a common denominator determining the district boundaries or the infrastructural distribution, e.g. the proximity to a railway, a harbour, etc. In some cases, villages can be considered as made of a single district.

At this stage, buildings acquire a morphological character that goes beyond the simple shaping and space enclosure into a functional volume. In particular, exterior surfaces become part of a function expression as, for instance, the façade of an office building differs from a residential façade and the main façade differs from the one facing the backyard. Different slating angles and orientations of roof pitches influence significantly the appearance of buildings. Alignments of façades and setbacks are responsible for the interaction of buildings with the public space. In open space too, available areas are allocated to more specific uses, such as gardens, flowerbeds, tree lines for greenery and roadways, parking lines, sidewalks, pedestrian crossing, public transports as well as bike lanes for mobility. Even small elements of urban furniture, like street light, vegetation, fencing, road signs and advertisement, interact with vision and sun rays on building envelopes at this stage. The experience of perception in a district is affordable through an "urban walk" and occurs at the pedestrian level. Pedestrians are the real protagonists of perception and, at the scale of the district, stimuli are confined in a space small enough to return a vivid virtual image of the built environment. Hence, it is obvious that the public space where pedestrians walk becomes increasingly important as well as the rational assessment of their visual experience.

Visibility has been considered as an extensive variable in the strategic planning, depending on the number of observers frequenting a place. In the development planning, it evolves from the extensive concept of cumulative viewshed to a binary intensive feature of the envelope components, qualifying them as visible or not. In the detailed planning, visibility acquires a proper quantification on a magnitude scale, an intensity level determined from geometric relations that

are less dependent from the position of the viewpoints. The current chapter offers an overview of the method to determine this scale (Figure 7.1).
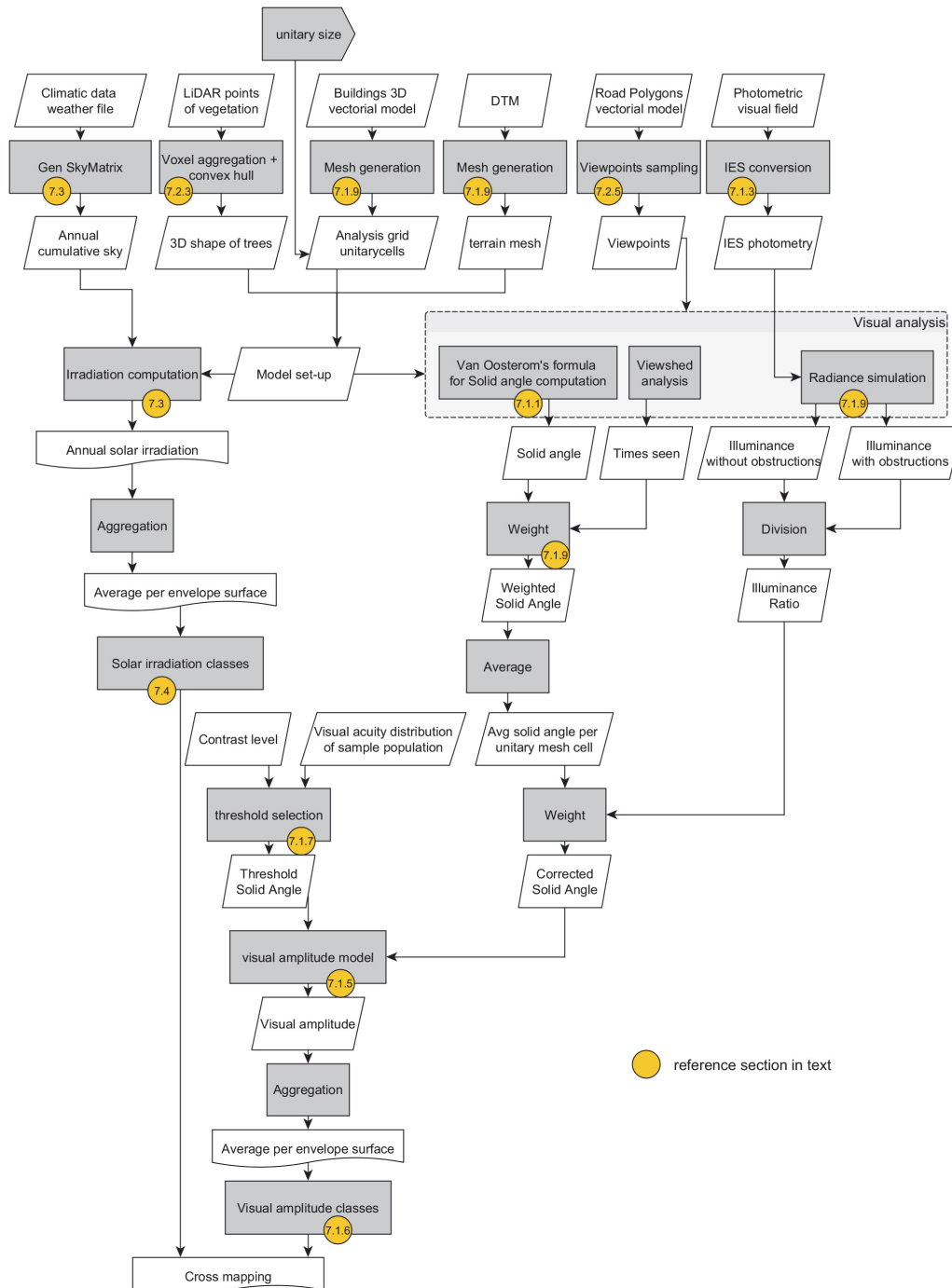
Figure 7.1 Methodology workflow in Mc Neel's Rhinoceros 5.0 and Grasshopper ©

(Author's own elaboration)

Required inputs are buildings tridimensional (3D) vector layer, Digital Terrain Model (DTM), vector polygons of the streets to be sampled with viewpoints, point clouds of vegetation issued from airborne LiDAR scanning. For solar potential assessment, meteorological data in form of a weather file is required, including direct normal and diffuse horizontal solar irradiance.

7.1   Visual amplitude assessment methodology

Visibility assessment ranges from the quantification of possible viewpoints offering a view to a given building envelope fraction to the impact evaluation of such a portion on the field of view of a set of observers. As such, visibility is independent from the number of viewpoints and is characterized by an intermediate degree between "visible" and "invisible". Replicating visual perception using a bundle of light rays that encompasses a given solid angle and distance decay is mimicking the attenuation of visual perception close to the visual acuity threshold. In other words: "what is far and viewed on its edge is less visible than what is close and in front of the view axis". A visibility metric which is appropriate to a complex urban context, featuring buildings with differently sized and oriented envelope surfaces is required. This is expressed in the current literature by using light ray bundles (i.e. light rays within horizontal and vertical angular domains angles specified by the user): such angular ranges, corresponding to the human visual field, can be incorporated in the visibility analysis [188, p. 382]. Benedikt, in the course of his investigations with the use of isovist fields, employs a wooden-made model for instance, in which he inserts light bulbs at the observers' location [92, Fig. 9]. A more rigorous approach implies the use of solid angles and spherical indicators (see Section 3.2.4). In fact, the relative size of an object in an observer's view field is proportional to the subtended solid angle. Similarly, the luminous intensity in a given direction is equal to the luminous flux per unit solid angle emitted in this direction by the light source. By reproducing the photometric features of the light source, it is possible to weight visual perception in a given direction accordingly.

7.1.1 Solid angle

The solid angle Ω [sr] subtended by surface A [m^2] from a point P is formally defined as the ratio between the surface projection on a sphere centered in P [m^2] and the square of its radius r [m] (Equation 7.1).

$$\Omega(A) = \frac{A_p}{r^2}$$

Equation 7.1 – Solid angle definition

For any given sphere radius, the solid angle will be constant. This is an extension of the concept of planar angle in Euclidean geometry, equal to the ratio of an arc length with the circle radius. A planar angle ranges from 0 to 2π radians corresponding to the whole circumference (360 degrees); a solid angle is comprised between 0 and 4π steradians corresponding to the whole sphere; one steradian is equal to $(180/\pi)^2$ square degrees.
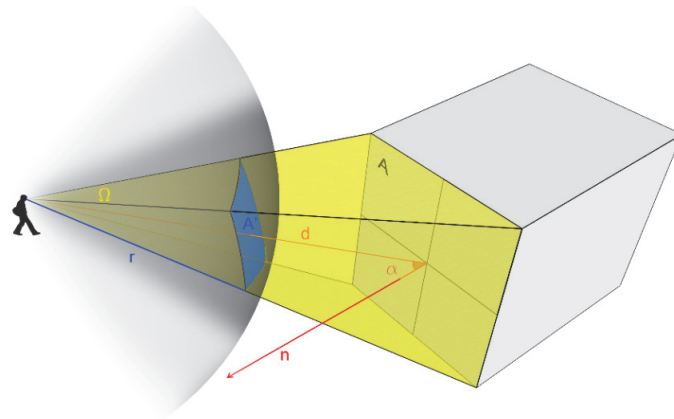
Figure 7.2 Solid angle subtended by a planar surface (comparable to a façade) within an observer's spherical gazing field

(Author's own elaboration)

When considering the human gazing field as spherical (see Section 3.2.4), the solid angle sub-tended by an object of interest corresponds to the fraction it occupies in the view field of an observer located in the center of the generating sphere (Figure 7.2). For the purposes of the current work, objects of interests are restrained to planar features (viz. surfaces), such as a façade or a slanted roof and their subdivisions. In this case, solid angles range from a minimum of 0 to a maximum of 2π steradians: the latter occurring when the observation point is located on the surface plan, which produces a hemispherical projection. With the reduction of the dis-tance between the observer and the object and the decrease of the angle defined by the line of sight and the surface normal, the solid angle increases from its minimum to its maximum: thus, it constitutes a magnitude estimation of the surface's visibility. Solid angles are additive, meaning that the solid angle of two or more adjacent, non-overlapping surfaces subtended from the same point is equal to the sum of each of the solid angles subtended separately by both surfaces (such as for surfaces A and B in Equation 7.2):

$$\Omega(A \cup B) = \Omega(A) + \Omega(B)$$

Equation 7.2 – Solid angle additivity

This property allows the decomposition of complex surfaces into more elementary forms, such as a mesh of triangles for instance. Meshing algorithms are commonly used in 3D modelling to subdivide complex geometries [189]. A handy equation for the calculation of the solid angle subtended by a triangle, based on vector algebra [190], is available in the literature (Equation 7.3 and Figure 7.3). In Equation 7.3, a, b and c are Euclidean vectors connecting the viewpoint to the vertices of a triangle; the absence of an arrow apex indicates the scalar magnitude of the vector [m]. Ordinary, dot and cross products are applied to return the solid angle subtended by the triangle.

$$\Omega\left(\hat{A}\right) = 2 \cdot \operatorname{atan}\left(\frac{\vec{a} \cdot \left(\vec{b} \times \vec{c}\right)}{abc + \left(\vec{a} \cdot \vec{b}\right) \cdot c + \left(\vec{a} \cdot \vec{c}\right) \cdot b + \left(\vec{b} \cdot \vec{c}\right) \cdot a}\right)$$

Equation 7.3 – Van Oosterom's equation for the solid angle of a planar triangle [190]
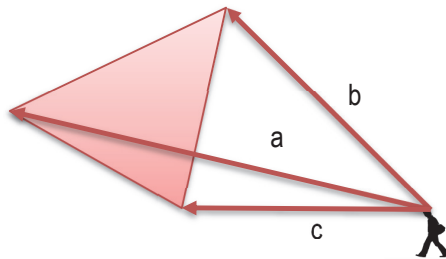
Figure 7.3 Illustration of Van Oosterom's equation

(Author's own elaboration)

Solid angles can also be computed by integral calculus, by means of the calculation of the projected surface on a unit sphere. The latter is found by computing a double integral that iterates a unit surface element in spherical coordinates. Within this PhD thesis work, Van Oosterom's equation is applied on triangular meshing of building surfaces.

7.1.2 Photometric variables

From basic physics, it is well known that light rays issued from a point source follow the inverse square law stated in Equation 7.4, where E [lx] is the illuminance on a surface subtending a solid angle Ω on a sphere with radius d, centered at the point light source characterized by a luminous intensity I. Illuminance is, by definition, the luminous flux emitted by the source per unit of illuminated surface; it is expressed in lux, namely lumens per square meter (Equation 7.5). Luminous intensity is, by definition, the luminous flux emitted by the source per unit solid angle; it is expressed in candelas, namely lumens per steradian (Equation 7.6). By combining

the inverse square law (Equation 7.4) with the definition of the solid angle (Equation 7.1), a relationship between the solid angle subtended by a surface, the illuminance impinging on the latter and the luminous intensity of the source can be drawn (Equation 7.8). As a result, the illuminance is proportional to the solid angle subtended by a given surface for a constant luminous intensity. By inversing the path of light rays, the luminous flux impinging on human eyes is redirected to target objects of the scene: this provides a physical interpretation of human vision, which leaves a trace on target objects.

$$E = \frac{I}{d_A{}^2}$$

Equation 7.4 – Inverse square law of light propagation

$$E = \frac{\phi}{A}$$

Equation 7.5 – Illuminance definition

$$I = \frac{\phi}{\Omega}$$

Equation 7.6 – Luminous intensity definition

$$L = \frac{I}{A_s}$$

Equation 7.7 – Luminance definition

$$\Omega = E \cdot \frac{A_p}{I}$$

Equation 7.8 – Solid angle as a function of the illuminance reaching a surface, its projected area and the luminous intensity of the source

7.1.3 Photometric model of human vision

The assertion that the human vision can be replicated by a backward light flux emission issued from the eyes implies modelling the visual field by considering the eyes as a point light source and the target objects as light receivers (Figure 7.4). A static observer staring at a target point can perform difficult tasks, such as word recognition within a range of 10 - 20 degrees from the line of sight. The visual performance is significantly degraded when passing this limit: colors can be discriminated up to 30 degrees, binocular vision is limited to 60 degrees from the line of sight (see Section 2.1). For this reason, vision is not equal within the whole visual field. A hypothetic light source, which is intended to replicate the visual perception of a static observer,

can be modelled as a spotlight centered at the observation point. It should illuminate intensively the objects placed within the foveal zone (see Section 2.1 and 2.2) close to the line of sight, then decrease its brightness towards the limits of the visual field. In a more rigorous formulation, luminous intensity is the largest at the line of sight with the densest luminous flux per unit solid angle. Luminous intensity is intended here as a "Visual Intensity", since it models observer's ability to resolve details in a given part of the visual field.
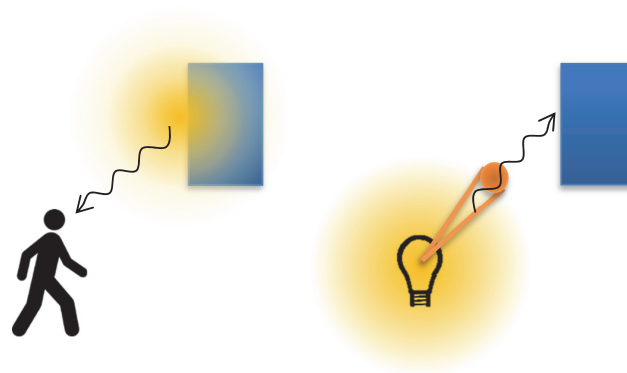
(a) Human vision schema   (b) Backwards raytracing representation of human vision

Figure 7.4 Backwards raytracing to track the effect of human vision on target surfaces. On the left (a) a schematic representation of human vision from visible light; on the right (b) the backwards inversion of the light path, which interprets the observer as a light source with a given "visual intensity" per solid angle.

(Author's own elaboration)

This "Visual Intensity" can be quantified in clinical ophthalmology by means of a differential sensitivity assessment to various visual stimuli, constituted by luminous sources with a given luminance level. Luminance is defined as the luminous intensity of a source divided by its emitting surface and is expressed in candelas per square meter (Equation 7.7). A luminance threshold is determined by the patient's response to stimuli (see threshold setting in Section 2.3) in an experimental setting known as *perimeter* [191]. In kinetic perimetry, a constant luminance stimulus is stirred from outside the visual field towards the foveal zone, the patient announcing when he begins to perceive it (light detection).
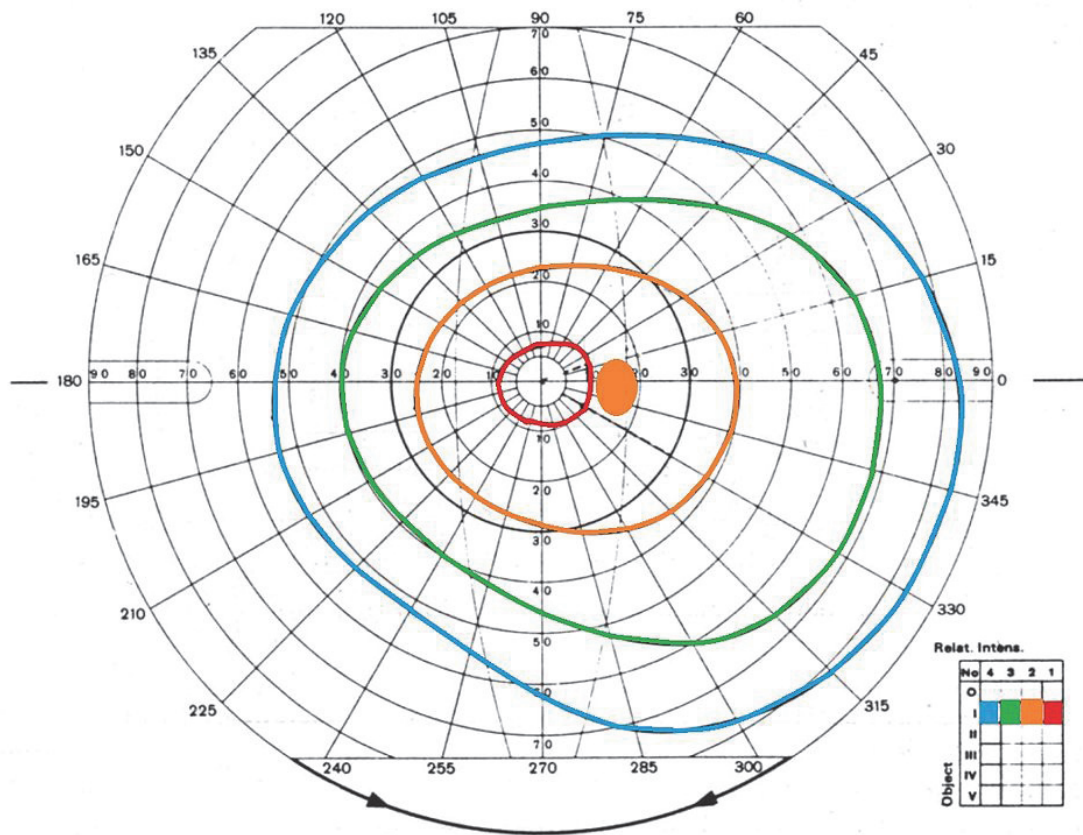
Figure 7.5 A perimetry showing isopters. Each color corresponds to a different luminance stimulus.

(Credits: Pignol23, got from https://commons.wikimedia.org/)

This is repeated for many directions, connecting the boundaries of the visual field to the fovea in order to identify the loci of points in the visual field with an equal response. These loci are named *isopters* and plotted as contours in a polar graph centered on the fovea (Figure 7.5). In static perimetry, a variable luminance stimulus at a given point located in the visual field is dimmed up, the patient announcing when he begins to perceive it (light detection). This is used to refine the sensitivity measure between the isopters. In most cases, a visual field test is performed by means of an automated ophthalmologic equipment.

Clinical studies on groups of healthy subjects are used to determine normal luminance sensitivity values. Luminance can be converted in luminous intensity via multiplication by the stimulus size. Normal isopters for a group of 40 subjects aged between 40 and 70 were employed as reference visual field, according to a study by Grobbel et al. [192, Fig. 4]. In particular, the visual intensity in a given direction of the visual field is determined as follows:

i.   The polar coordinates of the angle formed by the direction vector with the line of sight are intercepted in a polar diagram, like the one in Figure 7.5:

ii.   If the interception point falls on an isopter, the luminous intensity of the associated visual stimulus is annotated;

iii.   If the interception point falls between two isopters, the luminous intensity of the stimulus is interpolated and

iv.   Its reciprocal is assumed to be equal to the visual intensity 'emitted' by the eyes.

The results of the same procedure applied to the binocular visual field are shown on Figure 7.6a. As expected, objects located at a wide angle from the line of sight are illuminated, namely perceived, only if they are very close to the observer. On the other hand, objects falling within the foveal zone, e.g. at a maximum of 5 degrees form the line of sight, are perceived even at a long distance. Unfortunately, this model underestimates the visual intensity in the narrow foveal zone since detailed measurements for this small region are unavailable [192]. The location and size of the blind spot are also neglected as in this case, the needed level of detail goes beyond the scope of this thesis.

Another possible model of visual perception is based on the Guth position index [193]. The Guth position factor is widely recognized and used in visual comfort assessments to determine whether a light source may induce discomfort for a room occupant, when located in its visual field, engendering glare risks. Values of the Guth position factor can be extracted from the literature [194, Fig. 2.3], a similar procedure to the one described above being employed: Guth's factor is reported in a polar diagram, its reciprocal being used to define the backward emitted visual intensity (see diagram in Figure 8.4b). Figure 7.6b is characterized by a wider visual field since the visual task is not the luminous stimuli detection in this case, but the sensitivity to luminous inhomogeneity. The visual field extends also laterally. Given the recognized and well known use of the Guth factor, it is worthy citing it here and use it within another possible model.

Once the photometric model assumed, a conversion into a format compatible with ray-tracing simulations is necessary: for that purpose, the IES 2002 standard is used [195] (Figure 7.7).
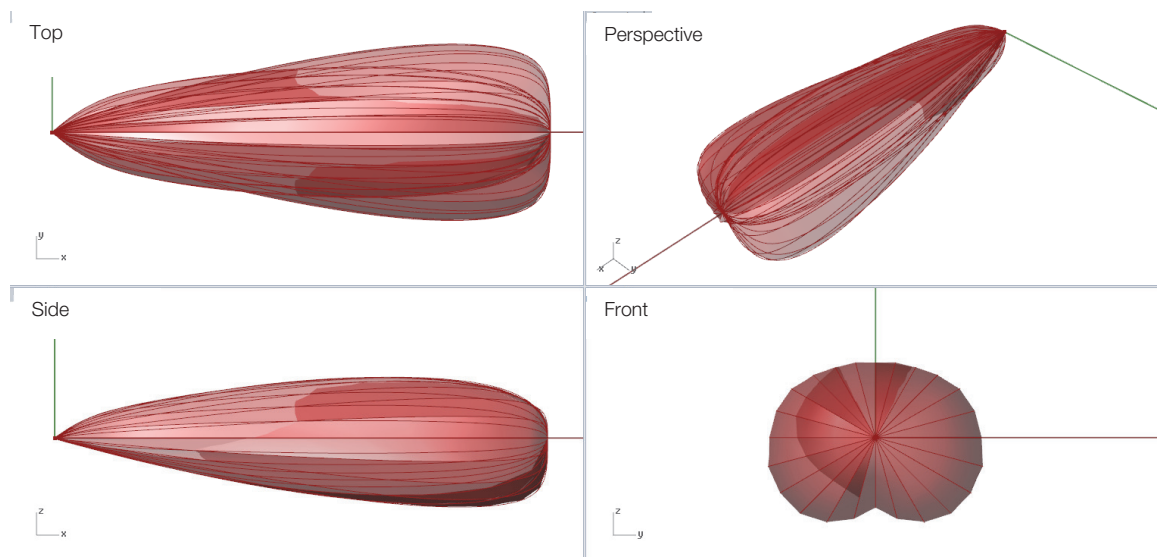
(a) Grobbel et al. visual field (values from [192, Fig. 4])
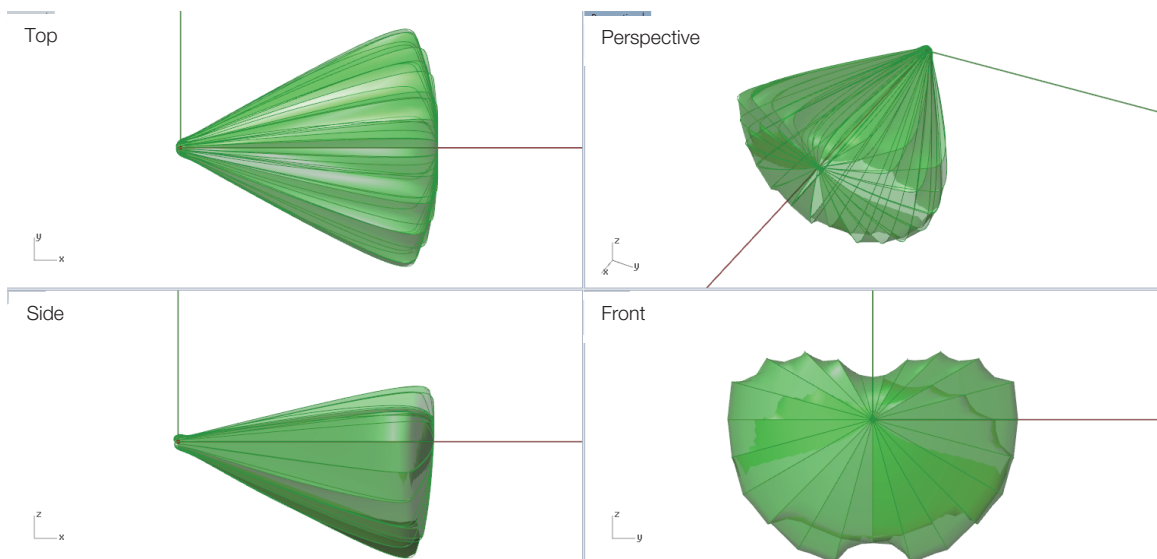
(b) Guth visual field (values from [194, Fig. 2.3])

Figure 7.6 Photometric solids of the visual field

(Used tool: Grasshopper for Rhino ©)

(a) Grobbel et al. visual field (values from [192, Fig. 4])
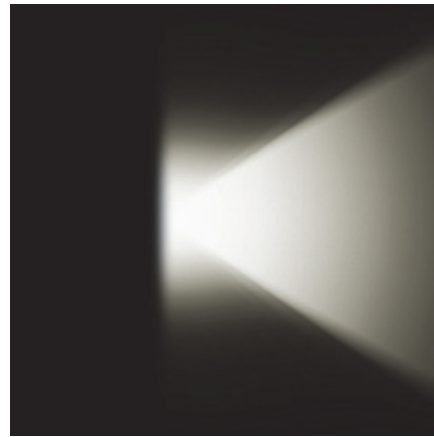
(b) Guth visual field (values from [194, Fig. 2.3])

Figure 7.7 IES render of the photometric visual fields (plan view)

(Used tool: Grasshopper for Rhino ©)

7.1.4 Dynamic gazing fields

All the above-mentioned models are valid for a steady observer. In case observer's head or body movement are allowed, the line of sight does not aim in a single direction. The resulting dynamic gazing field is a combination of static visual fields, one for each direction to which the observer is aiming at. If the observer is looking at a constant height on the horizon by holding his eyes and head position, and rotating on his vertical axis, the resulting gazing field is a kind of cylinder (Figure 7.8a). If the observer is looking in all possible directions around, the resulting gazing field is a sphere (Figure 7.8b). In fact, any object in any direction must fall in the foveal zone of one static visual field (e.g. the line of sight) pointing in the direction of the object. The integration of the foveal visual intensity emitted by a visual source in all directions represents a spherical photometric solid of a point isotropic light source. A spherical gazing field means that the observer perceives evenly in all directions, thus the attention is constant in all directions and there is no privileged focus.

At the detailed planning scale, this simplified hypothesis is assumed as satisfactory. At this stage, the view direction (viz. line of sight) constituting the focus of the observer's attention is undetermined. The objective here is rather the magnitude assessment of the building envelope components in a uniform and average view field of possible observers located in the public space. The implementation of a non-uniform gazing field through an observer's attention model is discussed in the next chapter.

(a) cylindrical dynamic gazing field　　　　　　　　　　(b) spherical dynamic gazing field
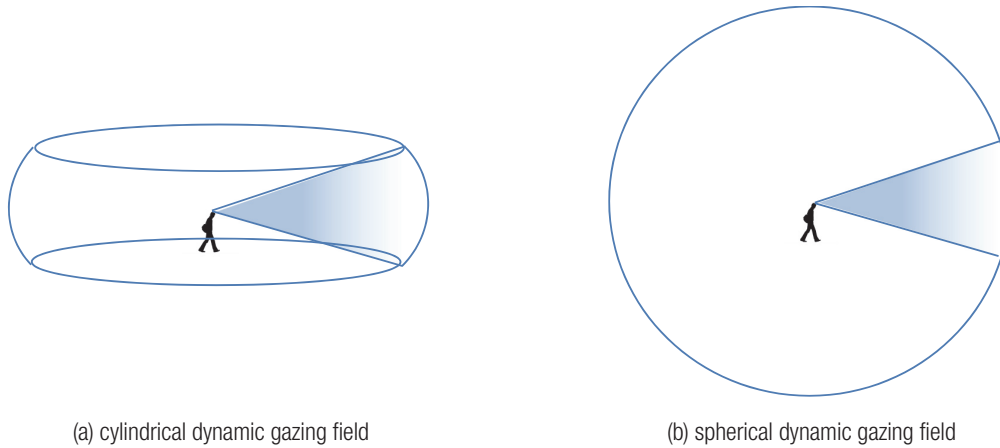
Figure 7.8 Types of dynamic gazing field

(Author's own elaboration)

7.1.5　Visual amplitude

Fechner's law, presented in Equation 2.2, illustrates the relationship between perception and stimuli by introducing the concept of threshold. A threshold is the minimal stimulus needed to complete successfully a visual task, in this case an uninformed detection of solar modules on a building envelope. Visual acuity threshold is usually expressed as the minimal angle subtended by an object to be perceived: this is called Minimum Angle of Resolution (MAR). Many references indicate that the visual acuity threshold of a standard observer is equal to 1 minute of arc in conditions of infinite luminance contrast [49], [66], [196], [197]. Hence, a surface subtending 1 square minute of arc is barely visible in conditions of infinite luminance contrast and represents the visual threshold. This critical dimension can be converted in steradians, to comply with the quantification of the stimuli using solid angles, suggested in Section 7.1.1. Knowing that the whole sphere subtends a solid angle of $360^2/\pi$ square degrees and/or 4π steradians, this conversion is operated in Equation 7.9, where Ω_0 is the threshold solid angle expressed in steradians, and 1/60 is the same solid angle expressed in degrees (1/60 degrees = 1 minute). The result is used as denominator in Fechner's law, while the numerator is the solid angle subtended by the considered target surface, occupying a certain position in the observer's visual field. By definition of solid angle (Equation 7.1), the Fechner formula becomes as in Equation 7.10, A_p [m^2] being the projected area of the considered target surface on a sphere of radius r and $A_{p,0}$ being the projected area of the threshold surface (1 square minute) on a sphere of radius r_0. Among the infinite number of spheres couples generating respectively the two solid angles, it is reasonable to choose those characterized by the same projected areas (Figure 7.9). In this case, the two stimuli are normalized with respect to their size and visual angle. As

a result, the Fechner formula is simply equal to the ratio of the two squared radii. In fact, to reproduce the same projected area on a sphere, a larger surface corresponds to a shorter radius. The square root of Fechner formula returns a ratio between two distances, namely the radii of two spheres hosting equal normalized visual stimuli (Equation 7.11). Such a ratio is at the basis of visual acuity definition, expressed in Chapter 2, Equation 2.5: $d_{1'}$ [m] is the standard threshold distance to a surface subtending 1 minute square angle and d [m] is the observer distance to the same surface corresponding to his/her personal threshold. In the case considered hereby though, the observer's visual acuity is not the objective of the assessment. The latter is rather the magnitude of a given surface with respect to the visual threshold, corresponding to the smallest surface that can be perceived by a standard observer. Thus, the wording of visual acuity can be reformulated, in favor of the expression "visual magnitude" or "visual amplitude": since the metric is the same in both cases, it is possible to keep the same notation, "VA" for both (Equation 7.12, Figure 7.9). In fact, both visual acuity and visual amplitude are quantified using the base 10 logarithm of the Minimum Angle of Resolution (MAR), designated by LogMAR.

$$p = k \, \log \frac{S}{S_0}$$

Equation 2.2 – Fechner's law

$$\frac{1}{60} \cdot \frac{1}{60} : \frac{360 \cdot 360}{\pi} = \Omega_0 : 4\pi \;\Rightarrow\; \Omega_0 = \frac{4\pi^2}{60 \cdot 60 \cdot 360 \cdot 360} \;\Rightarrow\; \Omega_0 = 8.46 \cdot 10^{-8} \, [\text{sr}]$$

Equation 7.9 – Solid angle conversion of visual acuity threshold in conditions of infinite luminance contrast

$$\frac{\Omega}{\Omega_0} = \frac{\frac{A_p}{r^2}}{\frac{A_{p,0}}{r_0^2}} = \frac{A_p}{A_{p,0}} \cdot \frac{r_0^2}{r^2} \;\Rightarrow\; \frac{\Omega}{\Omega_0} = \frac{r_0^2}{r^2} \;\; \text{with } A_p = A_{p,0}$$

Equation 7.10 – Fechner's fraction of visual stimuli expressed as solid angles

$$\sqrt{\frac{\Omega}{\Omega_0}} = \frac{r_0}{r} \;\; \text{with } A_p = A_{p,0}$$

Equation 7.11 – Square root of Fechner's fraction with normalized visual stimuli

$$VA_{(2)} = \text{Log}_{10} \, MAR = \text{Log}_{10} \frac{d_{1'}}{d}$$

Equation 2.5 – Visual acuity definition in relation to the logarithm of the minimum angle of resolution (LogMAR)

$$VA = \text{Log}_{10} \sqrt{\frac{\Omega}{\Omega_0}}$$

Equation 7.12 – Visual amplitude definition

(a) assessed surface   (b) threshold surface
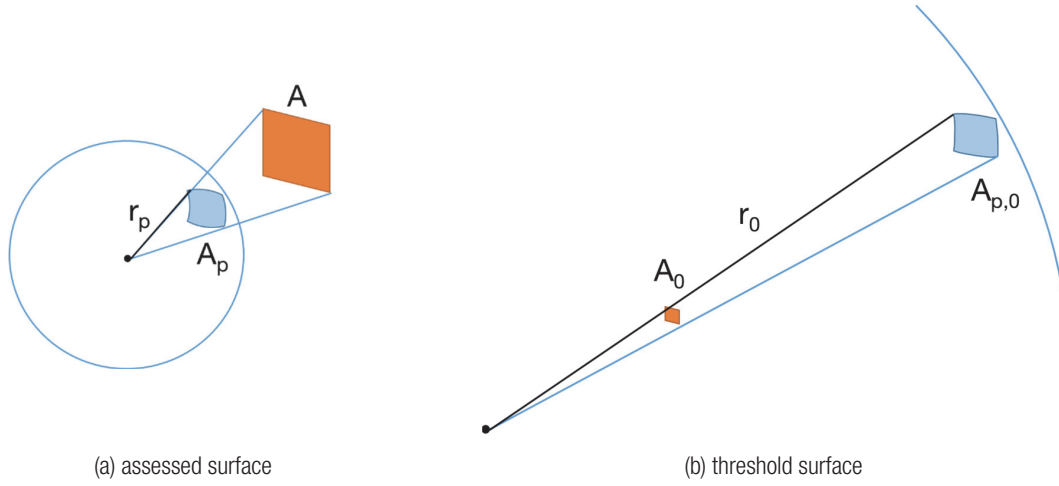
Figure 7.9 Visual amplitude geometric construction

(Author's own elaboration)

7.1.6   Visual amplitude metric and scale

Both visual acuity and visual amplitude are expressed in LogMAR; in practice, the difference between the two variables can be explained with an example. For the visual acuity assessment, if an observer barely perceives an object subtending 2 minutes of arc, he or she can distinguish a stimulus only twice as big as the standard observer can (e.g. according to its 'definition' the standard observer can perceive an object subtending 1 minutes of arc): this corresponds to 0.3 LogMAR on a perceptual scale. For the visual amplitude assessment, if a given object subtends 2 minutes of arc, it induces a stimulus which is two times larger than the threshold stimulus for the standard observer: this corresponds as well to 0.3 LogMAR on a perceptual scale. Such value represents the magnitude of visual perception, useful to compare different objects on a common scale. For planar surfaces, the visual amplitude domain at 1 minute threshold ranges from minus infinity, in case of an infinitesimal surface, to 3.94 LogMAR, in case the observer lies on the surface plane subtending a solid angle of 2π steradians. If the surface subtends a solid angle equal to the threshold of 1 minute squared, visual amplitude returns 0 LogMAR. Reference values of the minimal detectable visual amplitude, linked to a category of visual acuity on a LogMAR scale, can be found in the literature [49, p. 120], [198, Para. H54]; they are reported in Table 7.1.

Table 7.1 Observers' visual acuity or surfaces' visual amplitude threshold for certain categories of observers [49, p. 120].

Visual acuity category	Threshold (LogMAR)
Normal adult	-0.09
Standard observer	0.00
Unrestricted driving	0.30
Moderate impairment	0.54
Legal blindness	1.00
Profound impairment	1.40
Maximum for planar surface (hemisphere)	3.94

Although a visual acuity of 1 minute of arc is assumed for the standard observer, clinical studies demonstrated that most people can resolve finer details, up to the theoretical limit of 0.4 minutes of arc due to the retinal resolution [49, p. 118]. The normal distribution shown in Figure 7.10 is characterized by a mean close to -0.1 and a probability of a visual acuity larger than zero equal only to 18%. By extending the sample from healthy adults between 40 and 49 years of age to elderly people and children, the average shifts towards the standard observer value. For this reason, 1 minute of arc has been adopted at the international level as the standard visual acuity threshold [196], [197]. It should be noted that, assuming a threshold lower than 1 minute of arc would affect the absolute values of visual amplitude, but would not change the proportionality of two compared stimuli.

Within this thesis work, three visibility classes were identified. A surface with a visual amplitude lower than zero (less than standard) is labeled 'With low visibility'. Most healthy people can barely detect it since their visual acuity threshold is in this range but some of them are unable. A surface with visual amplitude comprised between 0 and 1.4 LogMAR is considered to be in 'Medium visibility' conditions. Most people are able to perceive it, with the exception of impaired subjects. Surfaces with larger visual amplitude values are marked as 'Highly visible'; only blind people are unable to perceive them.
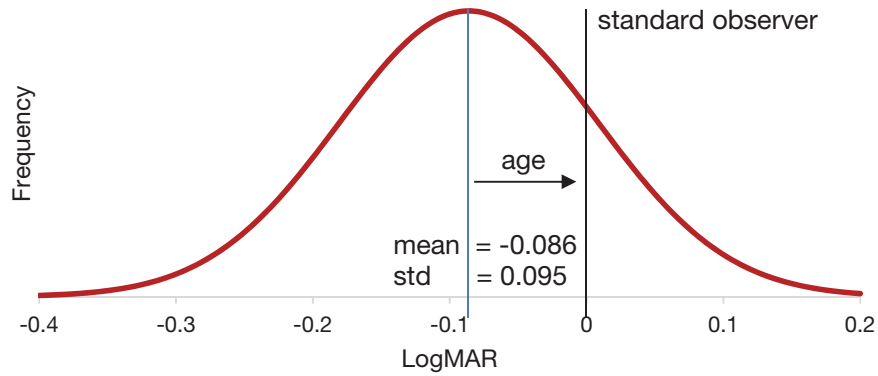
Figure 7.10 Normal distribution of visual acuity of 400 healthy adults between 40 and 49 years of age [49].

(retraced by the author after [49, Fig. 5.10])

7.1.7 Contrast modification

All the previous considerations are only valid in conditions of infinite luminance contrast according to Weber's formula (Equation 2.6). These conditions correspond to a value of 100% lightness contrast issued from luminance discretization into 256 gray levels (see [66], Section 2.4.3, Equation 7.13). This value can be used as reference but will never occur in a real context. In usual environmental conditions, the object-background lightness contrast ranges from 8% to 26%, the most frequent value being around 13% [66, p. 128]. Contrast varies as a function of meteorological conditions and luminous reflection properties of objects in the scene. Solar modules with their glass finish surfaces are usually more reflective than the building envelope surface hosting them. The position of the solar module relative to the observer as well as the daylighting conditions in the environment play also a role. In fact, sun rays characterized by an incidence angle on the glazing of a solar module larger than 56°, corresponding to the Brewster's angle between air and glass, are almost entirely reflected and eventually redirected to the observer's eyes, who perceives the surface with a high luminance. This phenomenon is inherent to Snell's law (Equation 7.14), n_1 [-] and n_2 [-] being the refractive indexes of the two optical media, in this case respectively, air and glass. An example of luminance contrast, generated on a roof pitch with different tilt angles by the equinox sun in Geneva, is illustrated on Figure 7.11.

$$C_l = \frac{\Delta l_{o-b}}{l_{max}} \quad with\ l_o > l_b$$

Equation 7.13 – Lightness contrast ratio from [66]

$$\theta_{crit} = \arcsin\left(\frac{n_1}{n_2}\right)$$

Equation 7.14 – Snell's law
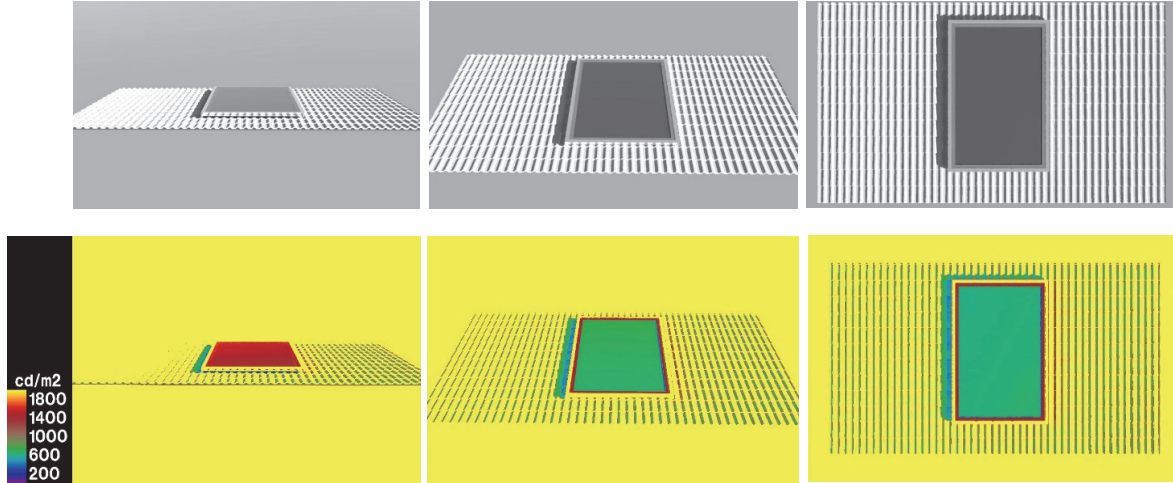
Figure 7.11 Geneva, Switzerland. Luminance contrast issued by a glazed solar module and a tiled roof pitch, tilted respectively 10, 45 and 90 degrees towards the south. The light source is the equinox sun on 23rd September at 12.00.

(Used tool: DIVA for Rhino © Solemma LLC)

According to this, it is obvious that the luminance of each solar module is very much impacted by the surrounding luminous environment. Thus, the threshold solid angle of 1 minute squared used in conditions of infinite contrast should be adjusted according to current contrast. Shang & Bishop identified a relationship between the visual acuity threshold and the lightness contrast, which can be used in this case [66, Fig. 10] (Section 2.4.3). In their open land experimental setting, they found lightness contrasts ranging from 8% to 27% with the most frequent value around 13% [66, p. 128]; these conditions correspond to an adjusted visual acuity threshold of 48, 12 and 25 minutes squared respectively. At this stage, considering a standard and uniform visual environment in order to be able to compare different surfaces is recommended: this implies the use of a unique and commonly agreed threshold. In case this is not explicitly mentioned, maximal lightness contrast conditions are assumed and 1 minute squared threshold is adopted.

7.1.8 Visual amplitude benchmark

In order to express the variation of the visual amplitude in conditions of maximal lightness contrast, a reference test has been set-up for a very simple configuration. In this test, a circle with a 30 m radius is used as the target surface and viewed by a single observer with variable

positions (Figure 7.12a). The location of the observer in relation with the target is determined through two parameters: (i) The distance [m] of the observer's viewpoint from the center of the circle and (ii) The view angle ω [deg], between the plane containing the circle and the line of sight to its center. Results shown in Figure 7.12b indicate that the solid angle attains its maximum of 2π radians when the viewpoint is located on the plane of the circle (zero distance) and decreases smoothly with the increase of the view angle. For a view angle of 0 degrees, solid angle is maximal as long as the viewpoint is comprised in the circle (e.g. distance lower than 15 meters), it jumps to 0 once outside the perimeter boundary. The logarithmic weight introduced in the visual amplitude index (Figure 7.12c) allows to discriminate small differences of the solid angle at low steradian values and to smooth large differences at high steradian values. A significant decrease of the visual amplitude can be observed accordingly, for 0 degrees of view angle, when the projected surface is close to a single line after the circle radius distance of 15 meters is passed. On the other hand, a gentler sloping curve can be observed for front views at a 90° normal incidence angle.
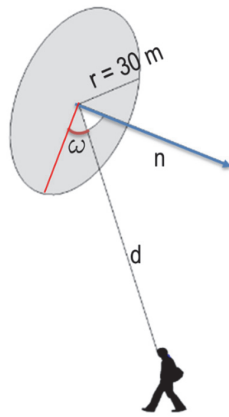
(a) test configuration
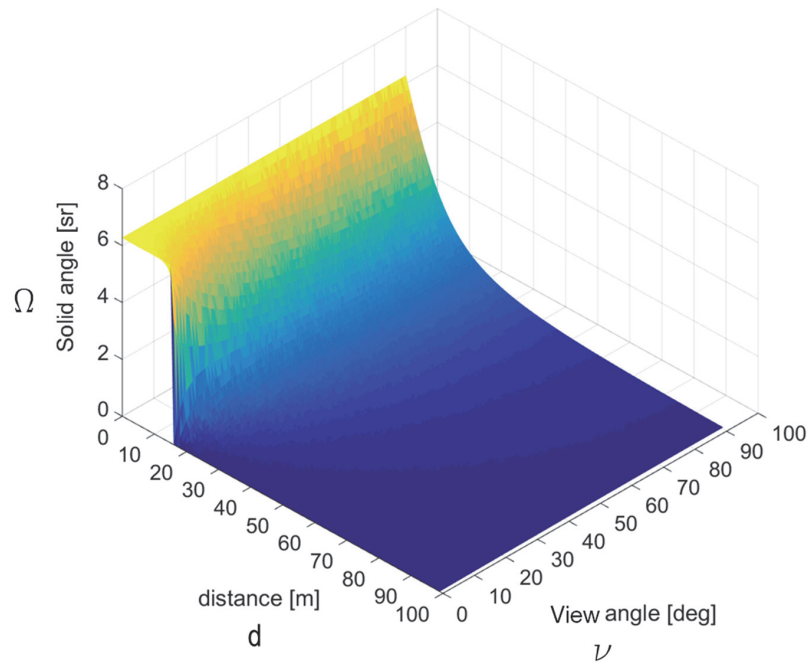
(b) solid angle as a function of distance and view angle from the plane of the circle
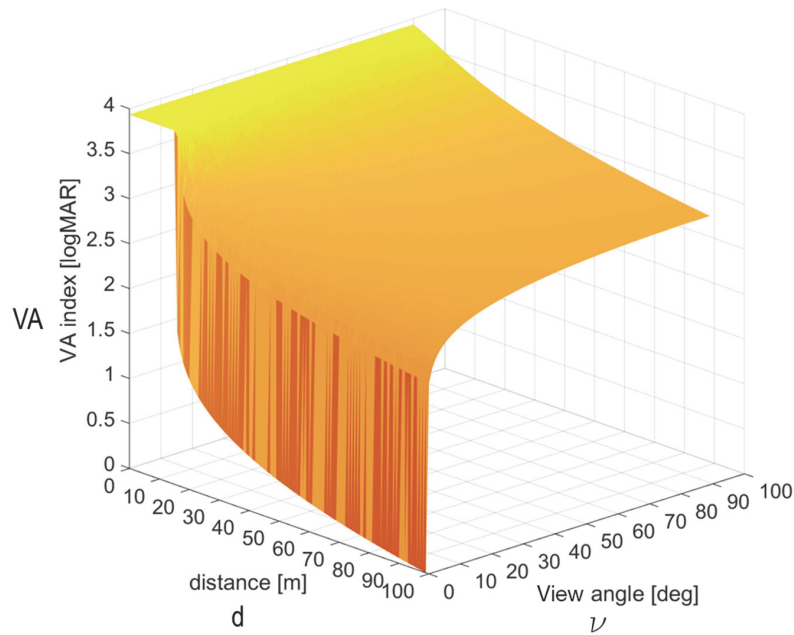
(c) visual amplitude as a function of distance and view angle from the plane of the circle

Figure 7.12 Solid angle vs visual amplitude

(Used tool: Matlab ®)

7.1.9 Complexification

In complex cases, which include urban contexts, several surfaces are assessed simultaneously from many different viewpoints. In particular, envelope surfaces can be accounted as a whole or divided into unitary subdivisions corresponding to the reference solar modules' grid size. For example, if the visibility of a group of solar modules integrated in an envelope surface must be analyzed, the unitary subdivisions of the envelope will match the area of such a group. As a result, the patches in which the envelope is decomposed reflect possible arrangements of these solar modules set. Subdivisions of envelope surfaces are operated through meshing algorithms [189]: among different possible options, planar face-vertex meshes were used. Each input planar surface is subdivided in quadrangular cells with unitary dimensions and parallel normal vectors, so that resulting cells are co-planar. Solid angles are determined for the two triangular sections on one of the diagonals of the quadrangular cell through Equation 7.3, then summed together. During meshing operation, triangular cells are produced at the boundaries of non-rectangular surfaces to match the polygon shape, when the use of regular quadrangular cells is impossible. In this particular case, twice the solid angle of the triangular cell is used as an approximation. An example of mesh subdivision of a building is shown in Figure 7.13.
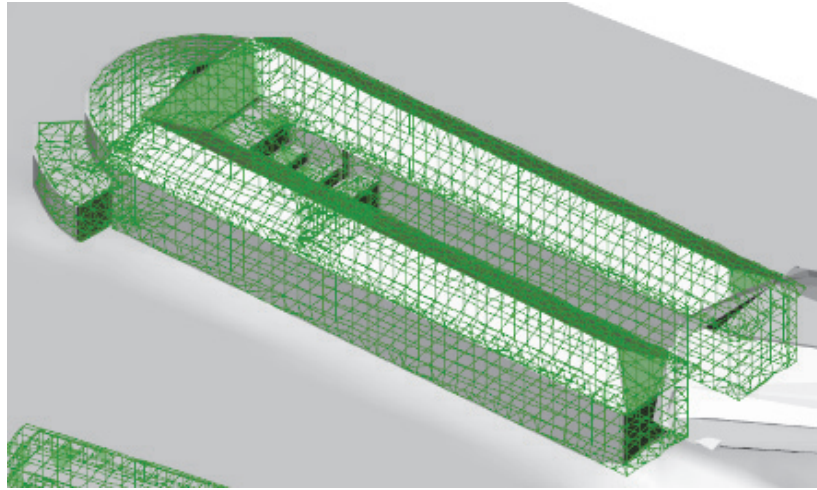
Figure 7.13 Hollande district, Geneva, Switzerland. Mesh subdivisions of a sample building.

(Used tool: Grasshopper for Rhino © elaboration on CC data from Système d'information du territoire à Genève – SITG.)

For each mesh cells used as target surfaces, it is necessary to compute the visual amplitude index from the different viewpoints, which are distributed in the public space according to the model configuration (see next section). Instead of considering the solid angle from a single viewpoint located on each surface, an average solid angle resulting from all non-obstructed viewpoints is calculated. The visual amplitude is thus determined according to Equation 7.15. As it can be observed in Equation 7.16 and Figure 7.14, the average solid angle is a weighted average of solid angles issued from x viewpoints on y target surfaces; the weight is represented by partial or full visual obstructions, namely obstacles blocking the view of the target from the viewpoint. A first method to estimate them is to run a viewshed algorithm before the computation of the solid angles. As such, rays corresponding to the lines of sight are traced between the observer and the target surfaces: the value 1 is returned if the target surface is hit by the ray (meaning it is visible from the viewpoint) and the value 0 otherwise (meaning it is invisible). The weighting coefficient b_p [-] is accordingly either 1 for visible targets or nil for invisible ones. Another possibility is to assume all coefficients b_p as equal to 1. In this case, the resulting solid angle is weighted by an illuminance ratio. The numerator of the fraction is the illuminance E_w [lx] observed on a surface n when all x light sources, modeled according to sections 7.1.3 and 7.1.4, are included simultaneously, together with the obstructions. The denominator is the illuminance E_s [lx] observed on the same surface n: all x light sources are included as well but obstructions are neglected. This second method is useful to evaluate the impact of partial obstructions, made of materials with different degrees of transparency.

y target surfaces
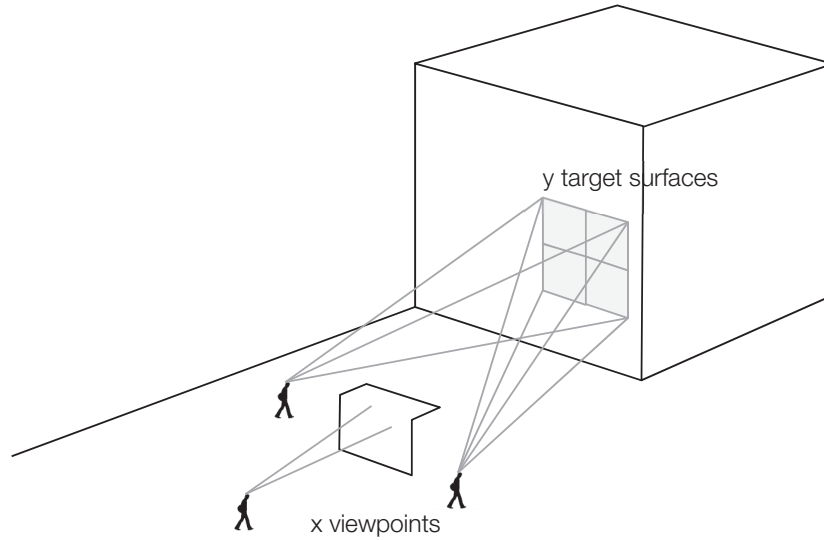
x viewpoints

Figure 7.14 Schema of visual amplitude assessment with multiple viewpoints and multiple target surfaces

(Author's own elaboration)

$$VA = \text{Log}_{10}\sqrt{\frac{\overline{\Omega}_{av}}{\Omega_0}}$$

Equation 7.15 – Visual amplitude from multiple viewpoints

$$\overline{\Omega}_{av} = \frac{\sum_{n=1}^{y}\frac{\sum_{p=1}^{x}(\Omega_p \cdot b_p)}{\sum_{p=1}^{x} b_p}\cdot\frac{E_w}{E_s}}{y} \text{ with } b_p = 0 \ \vee \ b_p = 1$$

Equation 7.16 – Average solid angle from multiple viewpoints

7.2   Practical implementation

7.2.1 Working environment

All the following calculations were carried-out in a tridimensional vector environment based on Rhinoceros ©. The latter is a 3D computer graphics and computer-aided design (CAD) application developed by Robert Mc Neel & Associates, which manipulates freeform surfaces, mathematically modeled surfaces (NURBS) and meshes. Grasshopper © is a module developed by David Rutten that permits the interaction with objects modeled in Rhinoceros as well as their modification through visual programming. The tool can be used for parametric analysis and geometric design. In this case, it is particularly useful for the computation of solid angles. Some Grasshopper plug-ins, like Ladybug tools developed by Mostapha Sadeghipour Roudsari

[121], allow the model implementation with ray-tracing algorithms used in lighting simulation. Backwards ray tracing is performed through a Radiance engine [199], a physically reliable lighting simulation software.

7.2.2 Building typologies analysis

In order to carry out a first visual amplitude assessment in an urban context, an analysis was run on building typologies arranged in different block layouts.
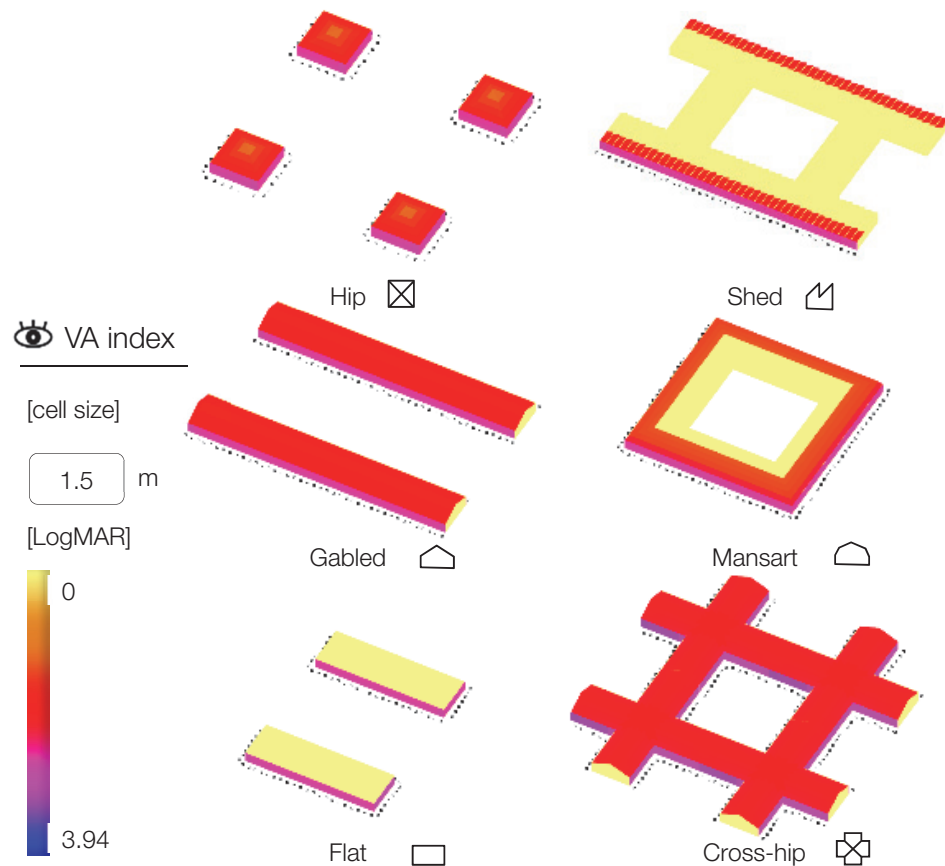
Figure 7.15 Visual amplitude index of possible building typologies.

(Used tool: Grasshopper for Rhino © on building typologies inspired from [200].)

These archetypes are extracted from the literature dedicated to environmental performance [200]. All footprints are raised 4 meters above ground and different roof types were arbitrarily placed on top of each, to appraise variations in visual amplitude. As an example, buildings are subdivided in rectangular meshes using cells of 1.5 m x 1.5 m, corresponding to a couple of standard solar modules. Viewpoints were sampled on the perimeter of buildings at 2 meters distance from the façade with 2.5 meters spacing between them: their elevation is set to 1.5

meters above ground. Results are shown in Figure 7.15: with the current configuration, gabled and cross-hip roofs are the most visible, while flat and shed roofs are the least ones. These outcomes cannot be extrapolated to other settings, because of the high variability in viewpoints sampling and possible building layouts. Nevertheless, they are useful for comparisons with other situations.

7.2.3   Trees modelling

As mentioned above, visual obstructions constituted by trees and vegetation are relevant at the level of detailed planning. Thus, trees must be modelled and inserted as context objects in the 3D model of the assessed district. Usually, a 3D model of trees is not available at the city scale. Nevertheless, LiDAR point clouds issued from airborne laser scanning are roughly classified based on the spectral radiation reflected to the monitoring device. For instance, vegetation reflects visible light in the green and radiation in the near infrared ranges: thus, it can be detected via appropriate indicators, such as the Normalized Difference Vegetation Index (NDVI) [201]. Water, soil, vegetation and buildings can be identified through spectrometry. Once points corresponding to vegetation have been selected, they are aggregated in tri-dimensional shapes, such as triangular meshes, to rebuild individual canopies. One possibility is to cluster them in point clouds using a voxel topology and produce a convex hull as result [202] (Figure 7.16). An opaque, light absorbing material can be attributed to the resulting shape. In this case, the luminous "visual" flux is entirely blocked by the canopy and will not illuminate the target surfaces. Another option is to assign a translucent material: this is useful to simulate different degrees of vegetation permeability to visual perception [203]. As a result, part of the luminous "visual" flux passes through the canopy and induces an illuminance on target surfaces, which is reduced compared to the unobstructed case. The ratio between the two illuminance levels – with and without translucent obstructions – can be used to weight the average solid angle calculated for the target surfaces, as explained in Section 7.1.9.

(a) picture of the tree (Credits: Google Street View ©)

(b) point cloud from LiDAR (elaboration on data from Système d'information du territoire à Genève – SITG)
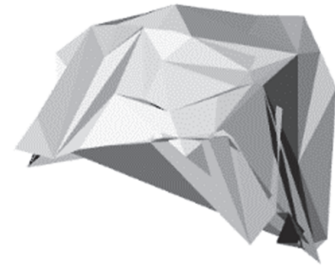
(c) resulting shape of the canopy

Figure 7.16 Tree 3D model from point cloud

(Used tool: 3D tree modeller from [202])

Table 7.2 Hollande district, Geneva, Switzerland. Principal demographic and building data inherent to the statistical district GIREC (CC data from Système d'information du territoire à Genève – SITG.).

Area of the statistical district GIREC	125 489 [m^2]
Number of resident inhabitants	475 [inhab.]
Population density	3785 [inhab. / km^2]
Fraction of buildings with residential / other uses	40% (0% single family house) / 60 %
Fraction of buildings with less / more than 3 floors	8% / 92% (80% between 4 - 6 floors)
Fraction of buildings constructed before / after 1960	90% (57% between 1919-1945) / 10%

7.2.4 Single viewpoint in an urban environment

To understand the meaning of visual amplitude in the day-to-day life, a preliminary computation was run in an existing square located in the center of Geneva. Square Hollande, in the core of Hollande district (see details in Table 7.2), has been selected for the simultaneous presence of building envelope surfaces with different slopes and orientations (e.g. flat, pitched, Mansard roofs and façades). These surfaces are split into unitary surfaces of 0.5 m x 0.5 m in order to account for the subtlest variations. A single viewpoint is placed in a favorable position to achieve a comprehensive view corresponding to the center of the square, at an elevation of 1.5 m

above ground. The outcome of the visual amplitude assessment (Figure 7.17a) is categorized in the three visibility classes (Figure 7.17b) and compared to the panoramic picture taken from the same viewpoint.

According to Figure 7.18, it is clear that most visible façades are estimated as being highly visible, except from the farthest and most tilted fractions relative to the viewpoint. The slanted roof of the post office in the north of the square is barely visible. Trees, which have been modelled with an opaque canopy, are completely masking the mesh cells behind them: the use of a transparent canopy would increase the permeability of the tree leaves and provide a smoother outcome (see Section 7.2.3). From this comparative analysis, a sound correspondence between the visibility conditions of the reality and the visual amplitude index assessed by simulation was found.

VA index

[cell size] [contrast]

0.5 m   100 %

[LogMAR]

0

3.94
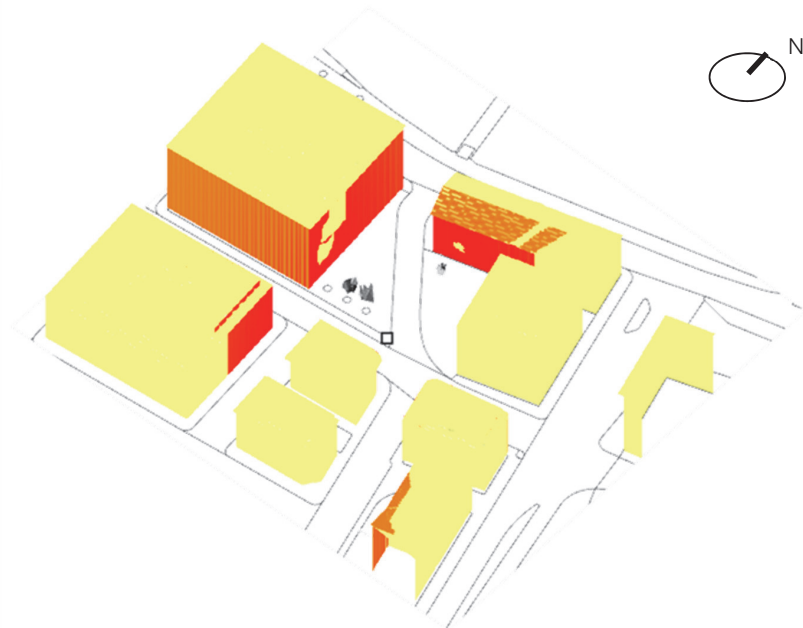
(a) Visual amplitude index issued from a single viewpoint on a mesh with 1.5 x 1.5 m cell size.

VA cat

[cell size] [contrast]
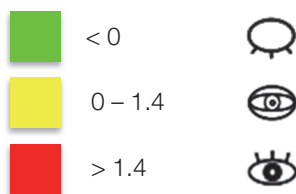
0.5 m   100 %

[LogMAR]

< 0

0 – 1.4

> 1.4

(b) Visual amplitude categories issued from a single viewpoint on a mesh with 1.5 x 1.5 m cell size.

Figure 7.17 Hollande square, Geneva, Switzerland. Visual amplitude and relative categories issued from a single viewpoint.
(Used tool: Grasshopper for Rhino © on CC data from Système d'information du territoire à Genève – SITG.)

(a) Overlap of visual amplitude categories on panoramic photograph. Northern side of the square.

(b) Overlap of visual amplitude categories on panoramic photograph. Southern side of the square.

Figure 7.18 Hollande square, Geneva, Switzerland. Visual amplitude categories issued from a single viewpoint, photographic overlap.

(Used tool: Grasshopper for Rhino © on CC data from Système d'information du territoire à Genève – SITG.)

7.2.5 Multiple viewpoints in an urban environment

After the focus on the eponymous square, the analysis has been extended to a consistent fraction of the Hollande district in Geneva (see details in Table 7.2). This sector of the city is particularly interesting for the heterogeneity of its buildings, in terms of form, category of use, construction date and typology. Squares, large avenues, local streets, pedestrian areas and bridges constitute the varied public space in which potential observers are located. Hollande district has also been adopted in another recent environmental study [204, p. 119]. For the purposes of this work, 52 buildings among the 111 of the whole district have been selected, covering roughly 250 m x 250 m of urban territory in Geneva. Their envelope consists in 2184 outdoor surfaces exposed to the sun (Figure 7.19). Buildings are decomposed in a 1.5 m x 1.5 m quadrangular mesh, representative of the dimensions a couple of solar modules, resulting in 98708 mesh faces. Viewpoints are sampled at the boundaries of sidewalks and walking areas,

with a spacing of 2.5 meters; within the walking areas, including internal courtyards, 5 meters spacing is adopted. All viewpoints have an elevation of 1.5 meters above ground level. As a whole 2483 viewpoints are located in this area. Trees are modelled with an opaque canopy.
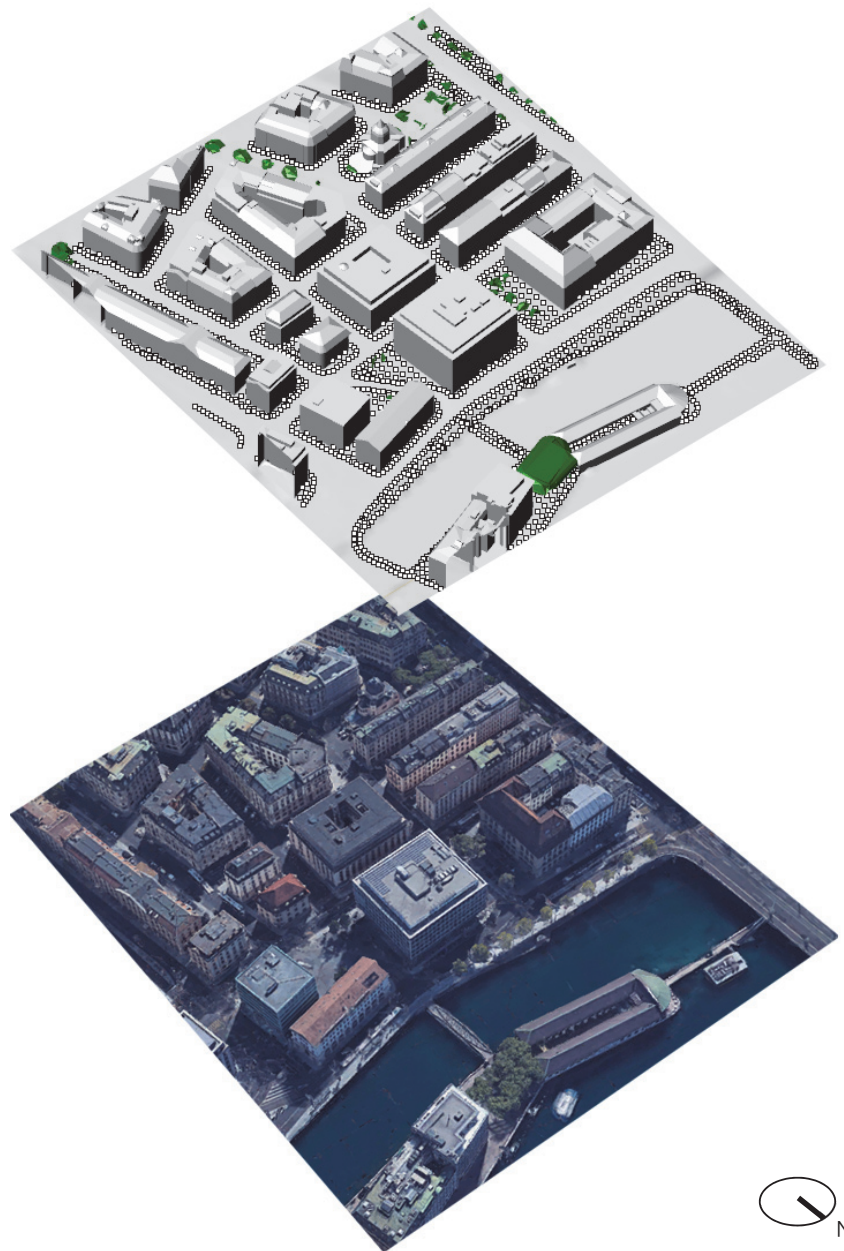
Figure 7.19 Hollande district, Geneva, Switzerland. 3D model and aerial photograph.

(Used tool: Grasshopper for Rhino © on CC data from Système d'information du territoire à Genève – SITG.

Credits for aerial photograph: Google Earth © Landsat Copernicus)

A cumulative viewshed analysis was carried-out in order to obtain a preview of the visible and invisible surfaces in the Hollande district. Results indicate that almost 60% of mesh faces constituting both roofs and façades are visible from at least one viewpoint. Surface visible by the largest number of viewpoints are facing the Leman lake, since a more open view, free of obstructions is accessible there (Figure 7.20).
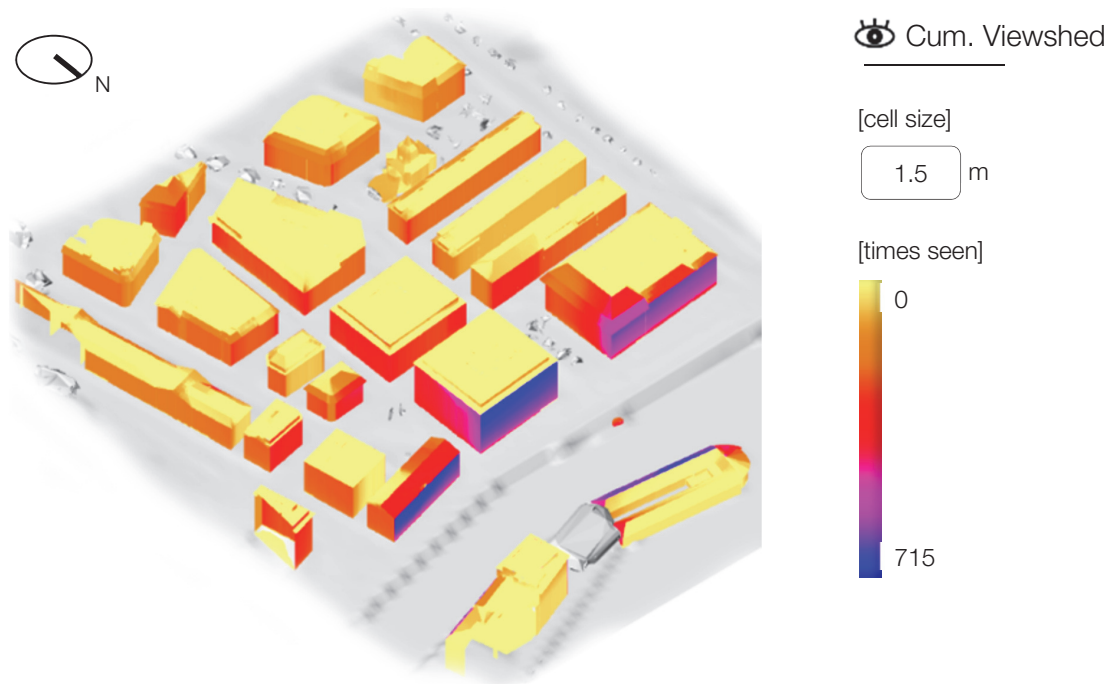
(a) Cumulative viewshed spatial representation
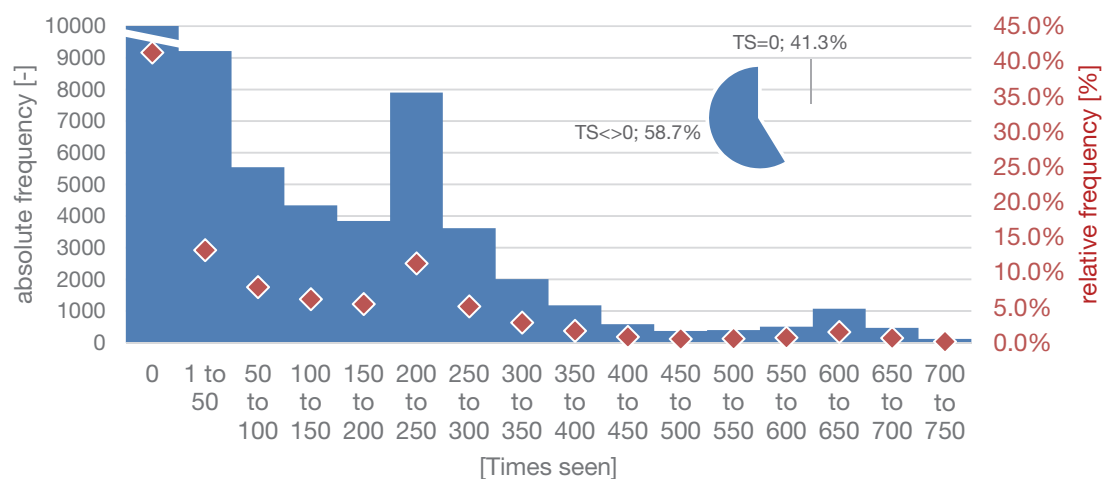
(b) Histogram of cumulative viewshed

Figure 7.20 Hollande district, Geneva, Switzerland. Cumulative viewshed analysis.

(Used tool: Grasshopper for Rhino © on CC data from Système d'information du territoire à Genève – SITG.)

a) Cumulative viewshed spatial representation

b) Koltsova's index spatial representation
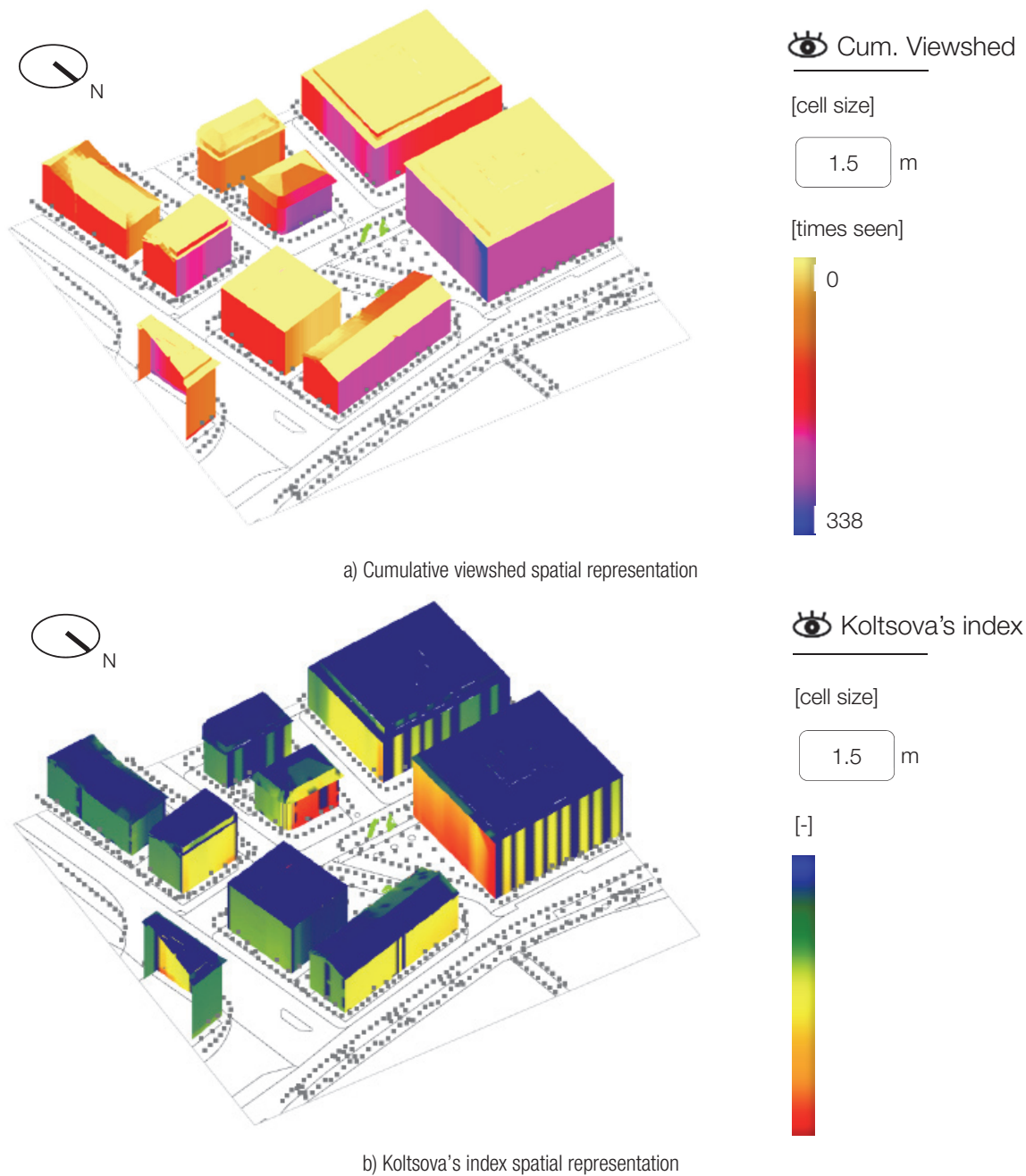
Figure 7.21 Hollande square, Geneva, Switzerland. Cumulative viewshed vs Koltsova's index issued from [123]

(Used tool: Grasshopper for Rhino © on CC data from Système d'information du territoire à Genève – SITG.)

The cumulative viewshed was compared to an existing qualitative indicator suggested by Koltsova et al. [123]. Such an index allows assessing the visual magnitude of target cells by considering both distance and visual angle with equal weighting in the cumulative viewshed

(50% respectively). Results, due to their dependency on the number of visible viewpoints, pro-
vide few additional information compared to the cumulative viewshed (Figure 7.21). Koltsova's
index is dimensionless: detailed values are unavailable due to access restrictions to the code.
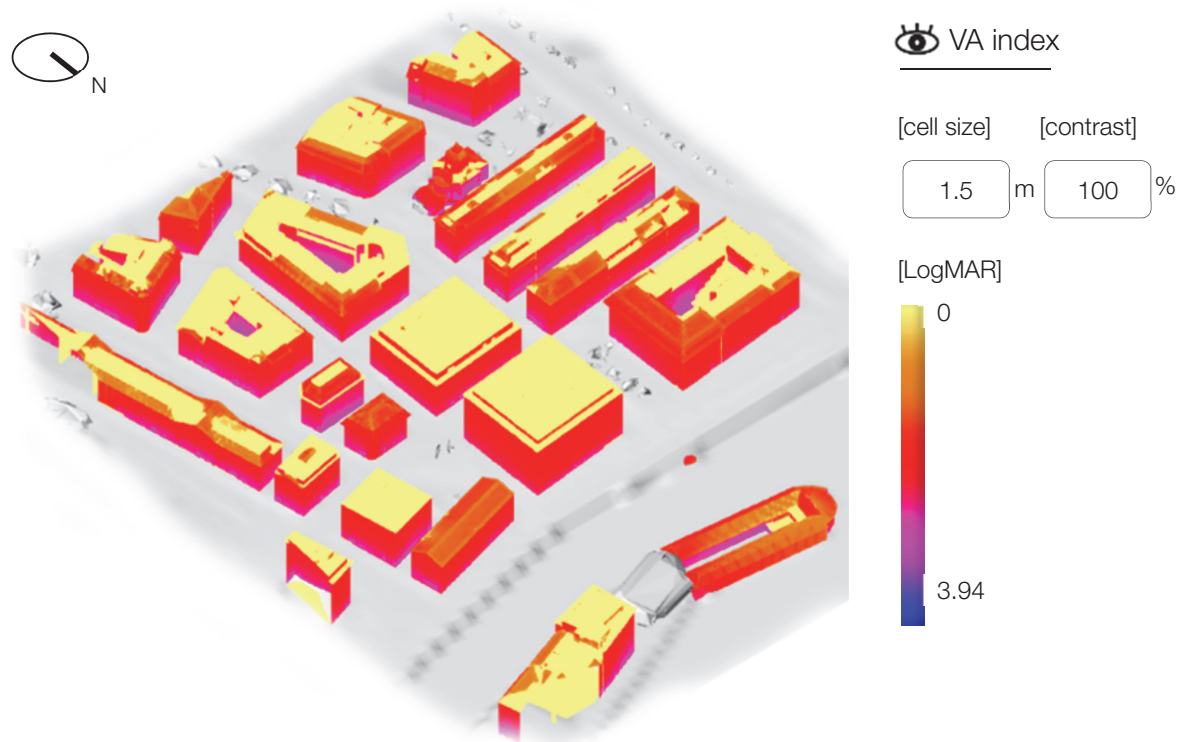
a) Visual amplitude index spatial representation
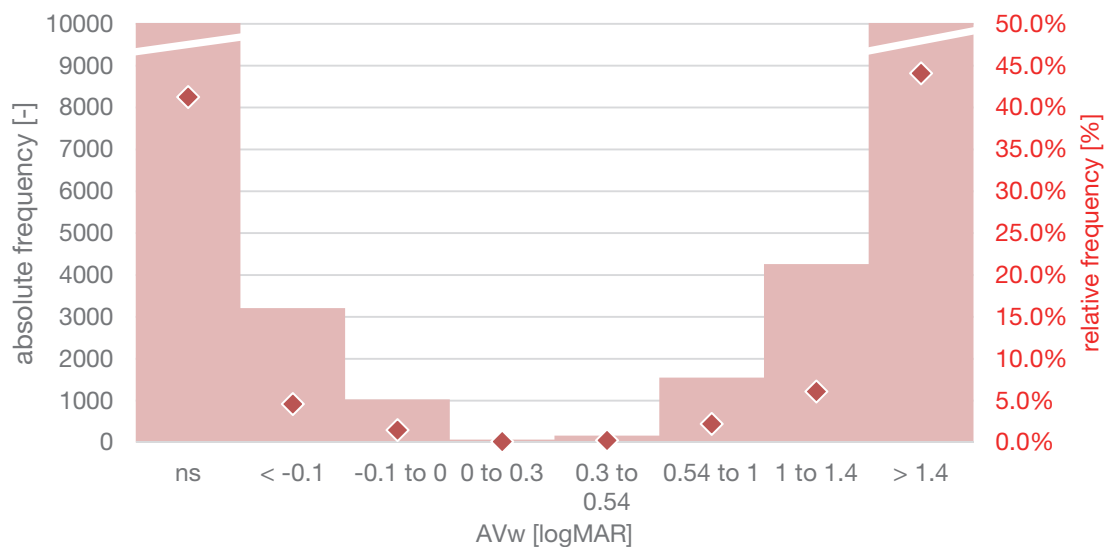
a) Histogram of visual amplitude index

Figure 7.22 Hollande district, Geneva, Switzerland. Visual amplitude analysis.

(Used tool: Grasshopper for Rhino © on CC data from Système d'information du territoire à Genève – SITG.)

Compared to the Koltsova indicator, the visual amplitude is more uniform across the various buildings (Figure 7.22a). This is due to the fact that the visual amplitude is averaged among all viewpoints able to see each target surface. Façades are characterized by a higher visibility than roofs, especially at viewpoints' level above ground and in narrow streets, where they are closer to target surfaces. Slanted roofs are slightly visible, while flat roofs are invisible. By classifying data as stated in Section 7.1.6, only 44% of mesh faces are highly visible (Figure 7.22b). Invisible surfaces, representing 41% of the whole surfaces, are grouped together with low visibility surfaces and reach a relative fraction of 46%. Circa 10% of the surfaces remain in the fuzzy zone, characterized by a medium visibility.

7.3   Location solar potential

The annual solar radiation is assessed on all mesh faces of the district. At this stage, a cumulative sky issued from climatic data is used for the computation of direct and diffuse radiation contributions. An annual Perez sky matrix is generated from direct normal and diffuse horizontal irradiance [205] according to the time step of the weather file [206], [207]. The International Weather File for Energy Calculations of Geneva (IWEC) [208], [209] provides hourly solar irradiance values and was adopted for the current analysis. Sky has been discretized by subdividing the hemisphere in 145 patches [210]. Once the model is set-up, a lighting simulation based on, a backwards ray-tracing technique is carried-out using the Radiance software embedded in the Ladybug plugin. Solar radiation are shown and commented in the following section.

7.4   Cross mapping results

All buildings considered in the Hollande district belong to the same 'High sensitivity' area, located in the city center of Geneva and determined according to the methodology explained in Section 6.3. Both the solar potential and the visibility values have been aggregated for each envelope surface, namely façades and roof pitches, in the plan illustrated in Figure 7.23. The average annual irradiation per square meter and average visual amplitude on 1.5 m x 1.5 m patches are shown. The solar radiation on the roof surfaces is represented using four bins on a color scale: values are considered as negligible below 350 kWh/m^2 year, unfavorable between 350 and 700 kWh/m^2 year, economically viable between 700 and 1050 kWh/m^2 year, very favorable above 1050 kWh/m^2 year. Façades collecting more than 400 kWh/m^2 year of solar radiation are marked with a thick red line. Three classes of visual amplitude are represented using different hatches: low visibility (e.g. VA < 0 LogMAR) with a line hatch, medium visibility

(0 < VA > 1.4 LogMAR) with a dotted hatch and high visibility (VA > 1.4 LogMAR) remains blank. Results, as expected, reveal a larger solar radiation on the South exposed envelope surfaces. Globally, tilted roofs are slightly visible and flat roofs are not visible. Most façades are on average highly visible; thus, their visibility does not justify a representation at this stage of the planning process. Such outcome is consistent with the consideration expressed in Chapter 6.
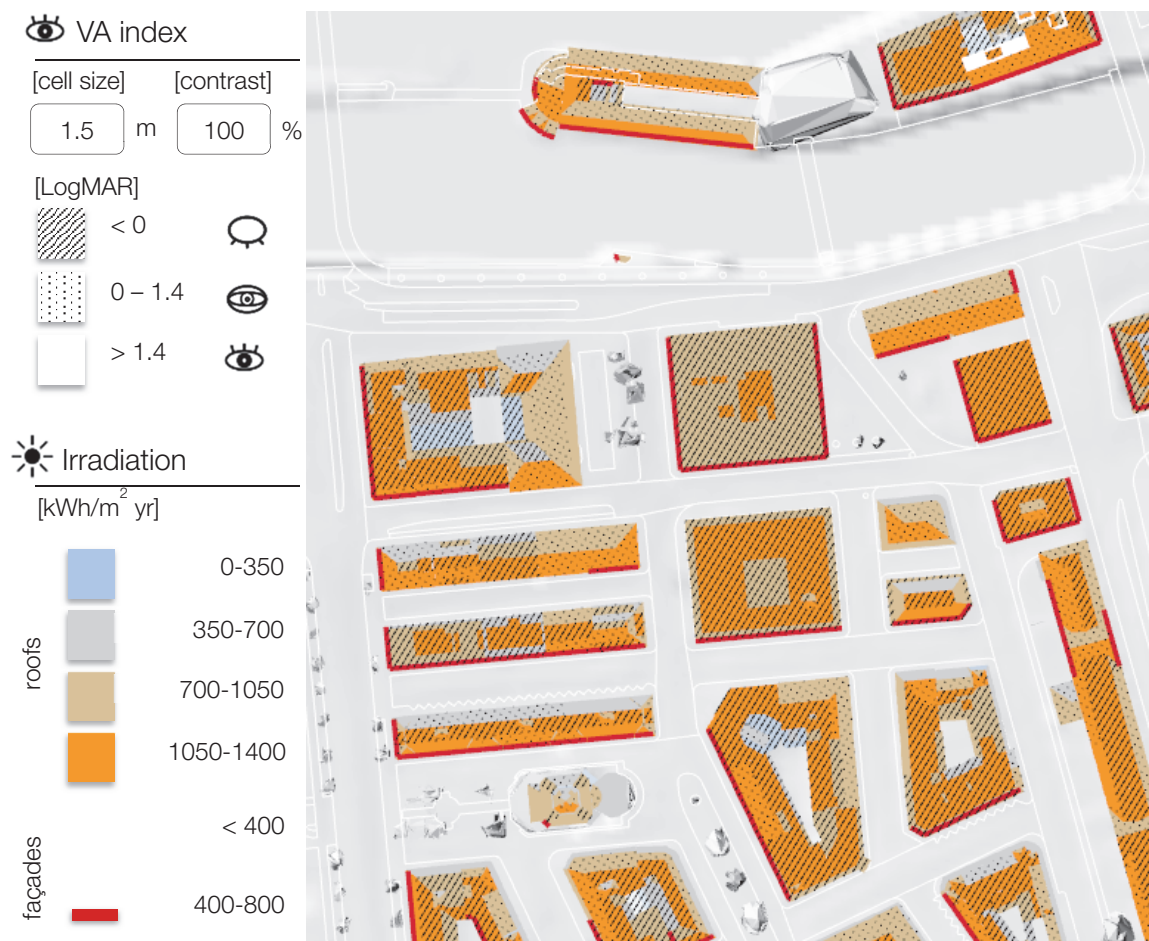
Figure 7.23 Hollande district, Geneva, Switzerland. Cross mapping of visibility and solar radiation, per envelope surface.

(Used tool: Grasshopper for Rhino © on CC data from Système d'information du territoire à Genève – SITG.)

7.5 Model sensitivity and uncertainty

The present model is sensitive to the selected solid angle threshold, the chosen size of mesh subdivisions as unitary surfaces, and the presence of obstructions, such as trees. Main uncertainties are due to the viewpoints sampling operation. The selected solid angle threshold of 1

minute squared is justified in Section 7.1.6 in relation with the assumed standard visual acuity. In case this threshold is modified according to the contrast or to different visual acuity in the observers' population, the outcome of the computation is simply shifted by a constant value. This constant, determined by logarithm product, is expressed in Equation 7.17 using as argument the square root of the ratio between the standard threshold Ω_0 (1' squared) and the adjusted threshold Ω'_0. If the latter is larger than the former, implying a visual performance lower than the average observer, the visual amplitude is shifted towards lower values and vice-versa. As an example, if the threshold is adjusted to 12 minutes of arc squared, the maximal, visual amplitude reaches 2.86 LogMAR instead of 3.94.

$$
\begin{cases}
VA' = \mathrm{Log}_{10}\sqrt{\dfrac{\Omega}{\Omega_0}} + c \\[2em]
c = \mathrm{Log}_{10}\sqrt{\dfrac{\Omega_0}{\Omega'_0}}
\end{cases}
$$

Equation 7.17 – Visual amplitude variation as a function of threshold variation

The dimension of the unitary surfaces is another sensible parameter. If the size of a given surface is modified, its spherical projection changes according to the transformation axes, the resulting solid angle being different. Due to the logarithm, the visual amplitude is not an additive function, as the solid angle is. Consequently, a modification of the mesh tiles dimensions does not induce a linear variation of the visual amplitude. A sensitivity analysis of the visual amplitude to the size of the unitary surfaces has been conducted based on the configuration described in Section 7.2.4 (e.g. featuring a single viewpoint in an urban environment). Starting from reference size of 150 cm used in most case studies, dimensions are reduced using 50 cm steps until the lower limit of 50 centimeters and the upper limit of 500 centimeters is reached. As the number of tiles decreases with the size increase, results are expressed according to the surface relative fractions. Against size augmentation, the incidence of invisible mesh tiles on the total is non-significantly raised, since the viewshed obstruction is calculated on the centroid of each tile (see Section 7.1.9). Figure 7.24, focusing on the visible sub-set is characterized by a peak (on the left) indicating that there is an isolated low visibility zone, without a significant amplitude variation, which has a larger impact when the tile size is growing. The right peak shifts to larger LogMAR values, as highly visible surfaces get bigger, characterized by a larger visual amplitude: the relative frequency of these tiles decreases with the growing size, compensating in

this way the relative impact increase of low visibility tiles. Between the lowest mesh tile size of 50 cm and the largest one, e.g. 500 cm, there is a LogMAR span of circa 0.7.
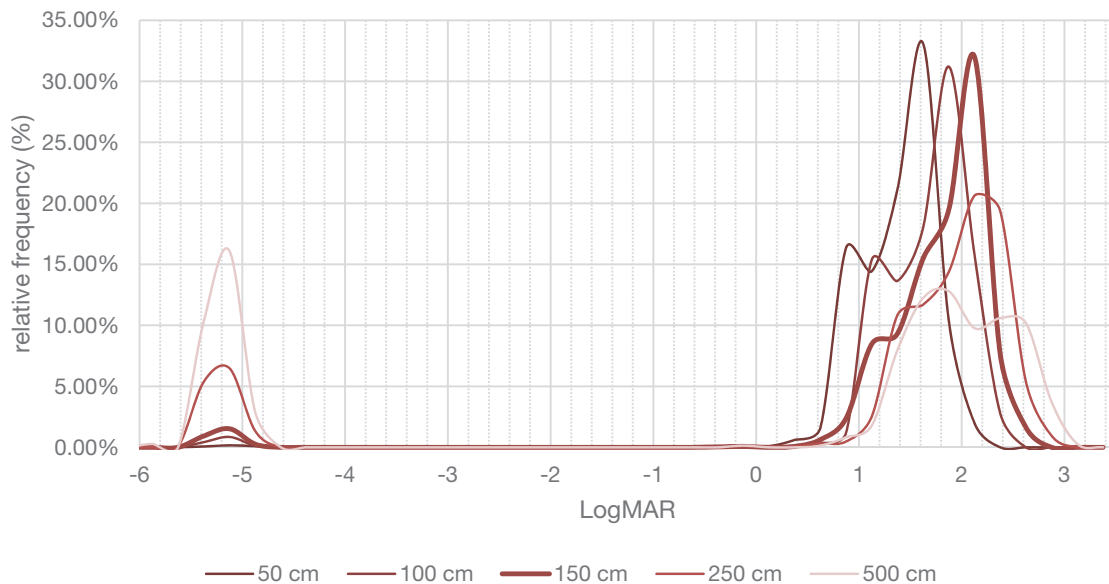
Figure 7.24 Hollande square, Geneva, Switzerland. Variation in visual amplitude of visible mesh tiles from a single viewpoint as a function of tiles size.

(Author's own elaboration on data from Système d'information du territoire à Genève – SITG)

A sensitivity analysis of the visual amplitude, regarding the visual obstruction due to the presence of vegetation, has been assessed in the whole Hollande district. The latter considers all sampled viewpoints defined by the usual 1.5 m x 1.5 m mesh subdivision. Figure 7.25 shows the results accounting for the impact of opaque tree canopies (see Sections 7.1.9 and 7.2.3). Even though it depends on the particular location of the trees, the majority of mesh subdivisions is not affected by them in this case (e.g. more than 65%): almost one third of mesh tiles differs from the unobstructed condition within a 10% range. The remaining 5% envelope cells is influenced by more than 10%. In general, upper portions of façades and visible roof pitches are obstructed by tree canopies. Surfaces towards narrow streets show the largest impact as they are exposed to fewer viewpoints that can be eventually blocked by trees.
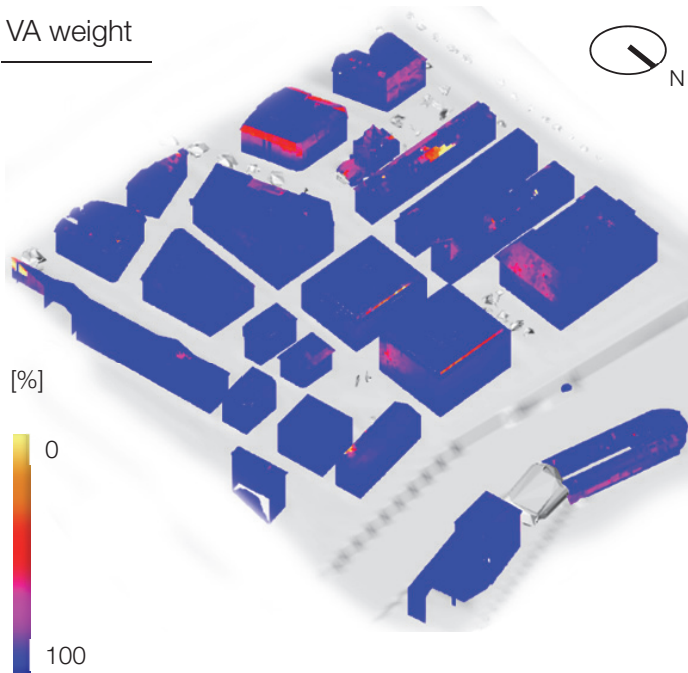
(a) spatial representation of visual amplitude weight (b) spatial representation of relative difference
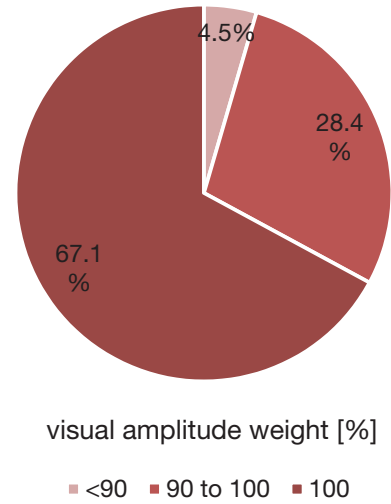
Figure 7.25 Hollande district, Geneva, Switzerland. Visual amplitude weight due to visual obstruction from vegetation.

(Used tool: Grasshopper for Rhino © on CC data from Système d'information du territoire à Genève – SITG.)

Sampling coarseness constitutes a source of uncertainty for urban contexts featuring multiple viewpoints. Hollande square in Geneva was analyzed with three different spacing configurations of the viewpoints grid in order to assess their impact on the visual amplitude: (i) 1 m at the boundaries and 1 m within the walking areas, (ii) 2.5 and 5 m and (iii) 5 and 7.5 m were respectively selected (Figure 7.26). Figure 7.27 shows that there is a limited variation of the visual amplitude from the finest to the medium grid size, which has been adopted for larger case studies in order to optimize the CPU load. A variation between 5% and 10% affects 11% of the mesh subdivisions and shows an influence on 14% of the envelope surfaces. A larger deviation is observed on 2% of mesh subdivisions, affecting 3% of envelope surfaces. Façades on narrow streets, being visible from a smaller fraction of the public space, are more concerned by a coarser sampling.

Figure 7.26 Hollande square, Geneva, Switzerland. Different spacing configurations of the viewpoints grid (fine, medium and coarse).

(Used tool: Grasshopper for Rhino © on CC data from Système d'information du territoire à Genève – SITG.)

(a) spatial representation of relative difference   (b) plot of relative difference
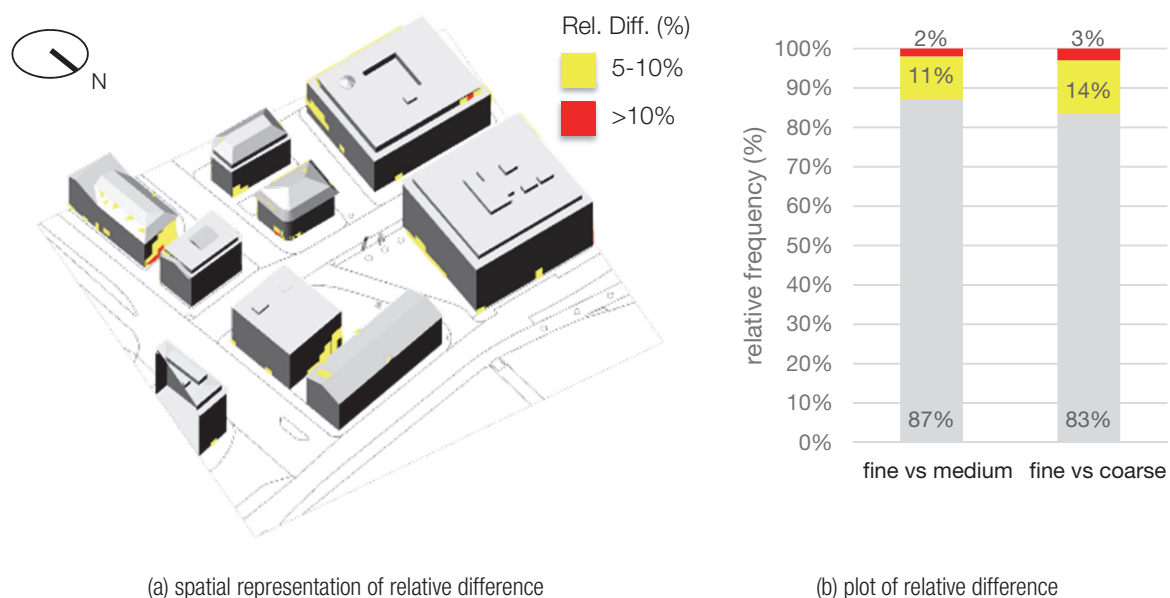
Figure 7.27 Hollande square, Geneva, Switzerland. Relative difference between fine (1m – 1m), medium (2.5m – 5m) and coarse (5m – 7.5m) viewpoints sampling

(Used tool: Grasshopper for Rhino © on CC data from Système d'information du territoire à Genève – SITG.)

7.6   Discussion

The methodology presented in this chapter is proposing a reliable physiology-based visibility index, which is used to assess the adequacy of building envelope surfaces to host solar modules at the detailed planning stage. This is a challenging objective many unknown variables being linked to the pre-design phase. Among them, one could mention: (i) The position and number of viewpoints, which are confined in the public space, (ii) The visual acuity of the potential population of observers and their viewing conditions, which are changing as a function

of day time as well as the weather, (iii) The activity and level of attention characterizing the observers, (iv) The positioning, size, layout and materials composing the solar modules and (v) The characteristics of the background surface on the building envelope. Within such a fuzzy framework, purely geometrical aspects can be analyzed, corroborated with some physical and physiology-based considerations. Many input variables are parametrized, inferred from well-known references and/or chosen by the users. This is the case for the average visual acuity of the observers as well as their dynamic gazing field model, in regards to the lightness contrast ratio between the target surfaces and the environment and to the dimensions of the solar modules: known values can be fed in the model, otherwise standard conditions are assumed. However, options for the installation of solar modules on different building envelope surfaces can be compared on a relative scale in standard conditions. In this sense, the current methodology is intended to offer a comparative basis for building envelope surfaces, which can be useful in a pre-design phase, to select the optimal solar refurbishment strategy in accordance with solar potential, visibility and sensitivity criteria. The confidence interval of the results seems reasonable. In spite of this, the latter are not accurate enough to draw a rigorous visual perception evidence that may vary a lot even for a single viewpoint, as shown in the sensitivity and uncertainty analyses (Section 7.5). Moreover, the spatial distribution of multiple viewpoints has a non-negligible impact on the visual amplitude, which should be addressed with deeper investigations of the pedestrians' and public's habits within the study area. An insightful and documented placement of viewpoints should be discussed with the local planner. A strong hypothesis is constituted by the selective attention of the observers: it is here assumed to be constant in all directions, even if attention models associated with photometry can possibly be introduced (see Section 7.1.3). Suggestions regarding this topic are presented in the next chapter and constitute a preliminary investigation which goes beyond the scope of this thesis.

Chapter 8   Architectural planning

A visibility assessment tool adapted to architectural planning is mainly addressed to building designers and stakeholders. In fact, the choice of a suitable sun exposed area to install solar modules narrows down to the level of building envelope parts. In this context, differences between diverse areas located on the same façade or roof pitch become increasingly relevant. The solar radiation assessment is not only affected by the configuration of the surrounding built environment modelled at the finest detail, but also by elements being part of the building structure and morphology, e.g. roof adjunctions such as chimneys, skylights, ventilation and air conditioning components. The same importance must be attributed to façades layout, which includes the setting of windows, balconies, recesses and ledges. Juxtaposition of surface materials and their joints are responsible for different luminous and short wavelengths reflection. All of these factors affect the solar energy generation, which varies dynamically over time throughout days and seasons.

A comprehensive perceptual model at the architectural scale implies considering the size and the setting of solar modules, as well as the materials involved, the artificial and natural environment, the weather conditions and fine visual obstructions; all of them can drastically modify the visual prominence and contrast across both the spatial and the temporal dimensions. In this sense, a remarkable work based on saliency models has been performed by Xu Ran, who employs high definition image renderings to analyze the visual impact of planned solar modules configurations, from a limited set of selected viewpoints [70].

The purpose of this chapter is not to accurately assess the visual impact of a set of solar modules on a given building from a single viewpoint or a bunch of viewpoints. In a pre-design stage, the aim is rather to build a bridge between the architectural practice and the neighborhood planning. Hence, improved viewpoints spatial distribution and few selective attention models are implemented, as a proof of concept, in the visual amplitude computation algorithm, presented in the previous chapter.

The author is convinced that it is possible to orient the designers' planning toward the most adapted building envelope parts by means of an interactive 3D interface, illustrating the solar

potential and visibility indexes simultaneously. A 3D visualization and interaction platform is suggested in a preliminary phase; a further development of the latter for practitioners was out of the scope of this PhD thesis and may be pursued immediately after it. 3D vector models are spread in many urban sites and are continuously enriched by the topographic services of cities and countries. The new industry standard CityGML allows to attach a large variety of attributes to the tridimensional geometry, with support applications from real estate to energy calculations: the Level Of Detail (LOD) increases regularly from simple building footprints (LOD 0), to full-detailed models featuring roof shape, windows location and even interior partitions (LOD 4) [211], [212]. The approach suggested hereby is applied on a 3D model with Level Of Detail 2, corresponding to the height extrusion of building footprints that include roof shapes. Nevertheless, it paves the way towards the use of more accurate 3D vector models.

8.1 Selective attention

A dynamic gazing field characterized by an evenly distributed attention was adopted for our procedure in Chapter 7: the photometric solid of a point isotropic source was adopted to model the visual intensity of a standard observer. As described in Section 7.1.4, this is a simplified hypothesis, which considers the case of a single observer staring indistinctly in all directions, without any specific focus. The distribution of an observer's attention depends on the visual task he/she is performing (see Section 2.6). A tourist visiting a square for the first time will more likely glance at the whole space, directing his gaze in all directions in a sort of dynamic observation: in this case, it can be admitted modelling his/her gazing field by means of a spherical isotropic 'candlepower' distribution (Figure 8.1a). On the other hand, if the square includes an outstanding monument or landmark, most of the observer's attention will be attracted by the latter (Figure 8.1b). Visitors of commercial streets look mainly at the shop windows and seldom notice the upper portions of buildings (Figure 8.1c). Busy people who are accustomed to a site, heading to a metro stop or to a particular location will focus their attention on their way finding: they aim at a target and the shortest path to attain it, without caring about the panorama (Figure 8.1d). Moreover, attention can be modified by external stimuli, such as advertisements and other sort of mental load, such as, a siren noise, a notification on the smartphone, etc. Even meteorological conditions can influence the way a pedestrian moves and gazes, in order to avoid glare sensations, rain, sun heat, etc. Finally, some researchers have found a positive increase of concentration after spending time in nature: vegetation stimulates contemplation and psychological relief, according to the Attention Restoration Theory [129].

(a) Potsdamer Platz, Berlin, Germany. Credits: Ansgar Koreng, Wikimedia Commons

(b) Piazza San Pietro, Vatican City. Credits: Carlo Pelagalli, Wikimedia Commons

(c) Ginza district, Tokyo, Japan. Credits: Daniel Ramirez, Flickr

(c) Main station, Helsinki, Finland. Credits: Diego Delso, Wikimedia Commons

Figure 8.1 Well-known places stimulating different selective attention distributions. A more evenly distributed one is expected in case (a), which features a higher isovist entropy (see text for explanations). A more focused attention is foreseen in case (b), driven by the architectural concept and a lower isovist entropy. Case (c) is affected by a high visual pollution, which deviates observers' attention from buildings. Case (d) is an example of visual target attracting pedestrians and their attention.

All these considerations affect the "townscape" perceived by a person moving in a urban environment (e.g. the 'urban space' expressed by Cullen [77]). Consequently, the attention of an observer can be very difficult to define and to model by the way of a photometric solid representing his/her gaze. This task can be simplified by considering the following different stages: (i) the identification of the attractor of the observer's attention that determines the main direction of the line of sight; (ii) the estimation of the probability distribution for the observer to identify an object in all the possible gazing directions, reaching a maximum in the attractor's direction. This distribution ranges from the perfect sphere reflecting equal chances to gaze in all directions to the pronounced peak reflecting the steady observation of a specific point of interest. In this second case, the probability distribution should be compliant with visual field models issued from credited psychophysical studies on humans (like the ones from Grobbel and Guth, cited in Section 7.1.3).
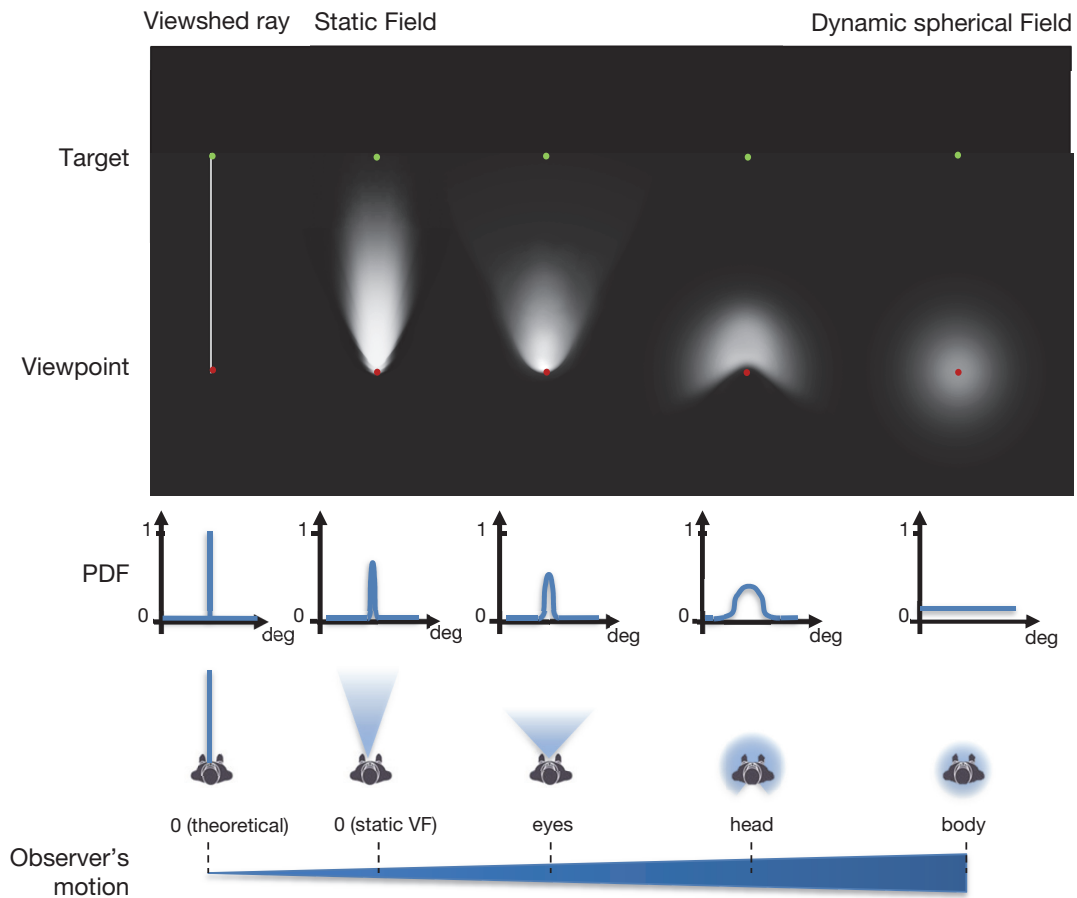
Figure 8.2 Concept of qualitative gazing field models with decreasing attention focus as a function of observer's motion (plan view).

(Author's own elaboration)

For the purposes of this thesis, the overall attention of an observer is supposed to be constant for all the different gazing models. An observer characterized by a spherical view range would have accordingly the same cumulative probability to look in all directions than a steady observer to aim exclusively at the gazing direction: namely, the integration of a Probability Density Function (PDF) over the view range would always return the unit (Figure 8.2). The translation of this hypothesis in terms of photometry is the conservation of the luminous flux supposing emitted by the light sources corresponding to the different gazing models. The psychophysical meaning of this assertion is an equal attention attributed to each gazing model: in other words, if an observer focuses his gazing on a small detail, he/she will lose the overview of the scene. Vice versa, if the observer is characterized by a global and panoptic gazing of the scene, he/she cannot contemporarily concentrate his/her attention on specific details.

8.1.1 Attention attractor

Any gazing model differing from the spherical one requires the identification of a main viewing direction that concentrates most of the lines of sight. As mentioned, the attractor catalyzing most of the observer's attention is subjective and varies in time and space. For moving subjects, this attractor coincides with the "focus of expansion", i.e. the steadiest point of the optic flow (see Section 2.6). Such a focus can be experimentally determined with an eye-tracker, namely a camera aiming at the subject's eyes and tracing the observed points back on the visual field. Few experiences are available on this matter in an open urban environment (see for instance [213]). In spite of this, simplified methods based on the tendency of pedestrians to aim at more open spaces are available. In particular, a correlation between a low isovist drift and pedestrian movement attractors were highlighted by Leduc et al. [97]. The isovist drift is the Euclidean vector connecting the generating viewpoint of the isovist to its center of gravity (Figure 8.3). Following this purely spatial logic, pedestrians are expected to move towards locations with lower isovist drift magnitude, i.e. characterized by a larger sense of openness. This behavior may be attributed to people experiencing emergencies, such as earthquakes, where staying away from objects drives a survival instinct. In this case, the main viewing direction most probably coincides with the direction of movement, even though this constitutes a strong hypothesis. The latter is assumed for demonstration purposes in the framework of this chapter, even if a validation of this hypothesis is necessary to lead to any conclusion on perception.

Figure 8.3 Place du Bourg-de-la-Four, Geneva, Switzerland. Drift magnitude of an isovist, from the generating viewpoint (red) to the center of gravity of the isovist (green).

(Used tool: Grasshopper for Rhino © elaboration on CC data from Système d'information du territoire à Genève - SITG)

8.1.2 Gazing intensity distribution

The peak gazing intensity is reached for the main viewing direction, i.e. the direction focusing the attention determined in the previous step. According to the chosen gazing model, this intensity decreases with the deviation angle from the main direction. Concerning the two steady gazing models adopted here, these decreasing function is illustrated on Figure 8.4 (right): the first one is issued from a clinical study assessing patients' sensitivity to different luminous stimuli [192] (Section 7.1.3). The second one is more extended laterally: it concerns human visual sensitivity to high luminance stimuli compared to their background in glaring situations [193]. The gazing model becomes dynamic with the observer's motion (Section 7.1.4), engendering a displacement of the line of sight. If the observer gazes in all directions as described above, the assumed gazing model is a sphere. By the effect of observer's movement, the attention is shifted along the moving direction and the sphere is stretched into an elongated shape, e.g. a droplet shape or an ellipsoid. The latter must have the same volume than the sphere, due to the conservation of the overall visual attention (see Section 8.1). The gazing light flux is arbitrarily set to 20 000 lumens, this choice having no impact the illuminance being only accounted in relative terms (see Section 8.1.3). For the purposes of this thesis, a prolate ellipsoid has been adopted, because of its modeling simplicity and well-known geometric description (Figure 8.4c). However, this is only an assumption that has no relation with any psychophysical or physiological consideration. More studies are needed in this sense to provide a validated perceptual model of a moving pedestrian. A possible theoretical justification of an ellipsoidal gazing field is the merging of both a centripetal and a centrifugal observer's motion: the center is the center of gravity of the isovist, as the pole of the highest perceived openness characterizing an observer at the isovist generating location. Such hypothesis constitutes a possible adaptation of Appleton's Prospect – Refuge Theory [214]. The prolate ellipsoid is a solid that can be generated through the rotation of an ellipse around one of its axes. In this case, the major axis is oriented in the main viewing direction: the eccentricity of the ellipse is driven either by the drift or the entropy of the isovist. The drift has been defined in the previous section: it quantifies the observer's impression of being located in the center of his viewing area. The drift vector direction is used to determine the main direction of view. The entropy expresses to what extent the visual environment expected by the observer is predictable or, on the opposite, raises a sense of surprise [94]. It is used to determine the gazing distribution around the main direction of view.
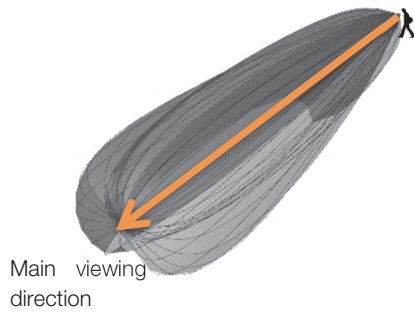
(a) Grobbel's steady gazing field [192]

(b) Guth's steady gazing field [193]

(c) Ellipsoidal dynamic gazing field, with entropy = 0.5
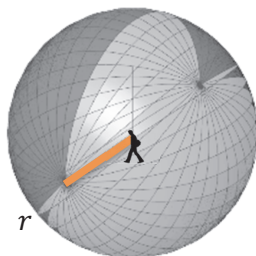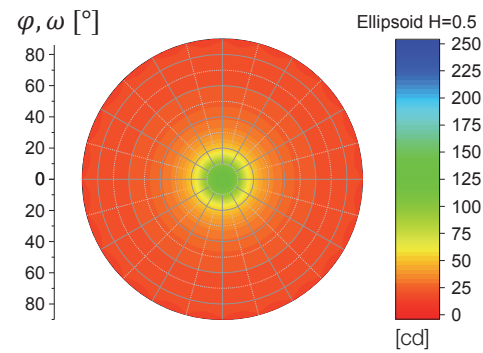
(d) Spherical dynamic gazing field
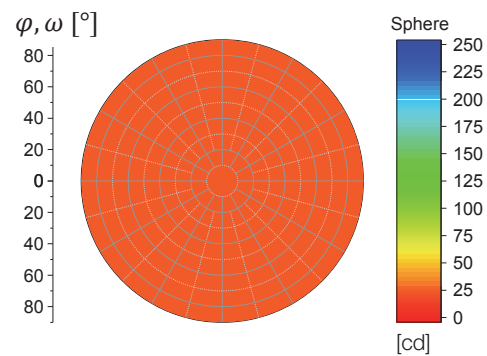
Figure 8.4 Spatial representation of gazing field models and polar diagram of their gazing intensity.

(Author's own elaboration)

(a) Spatial representation of the isovist and some of its generating
lines of sight

(b) Histogram of the length of the generating lines of sight
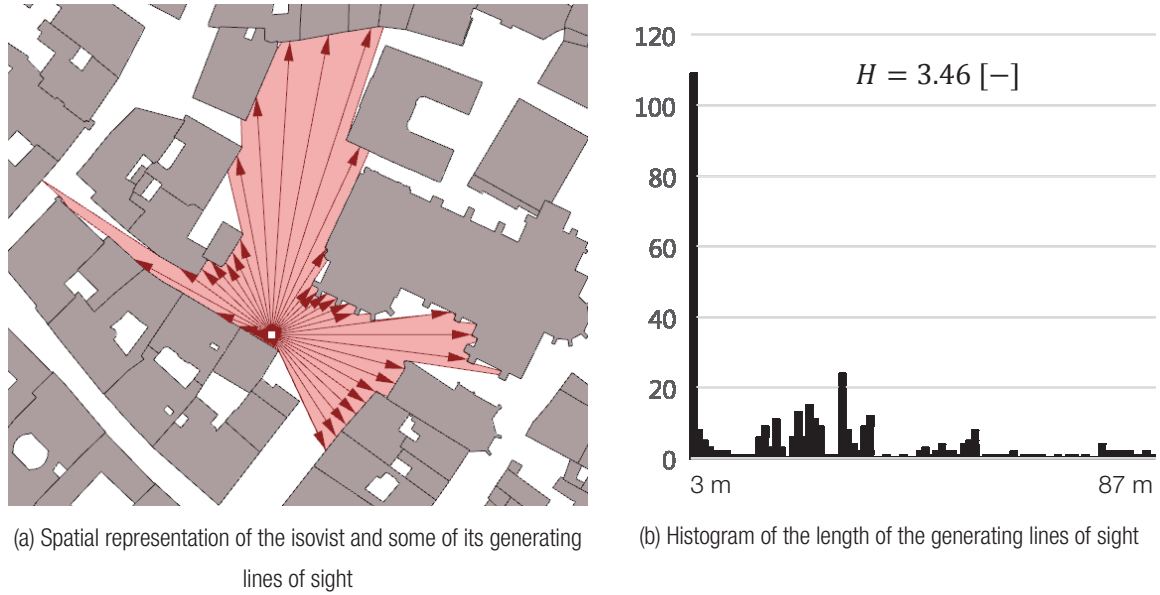
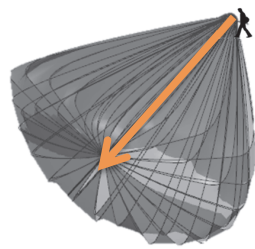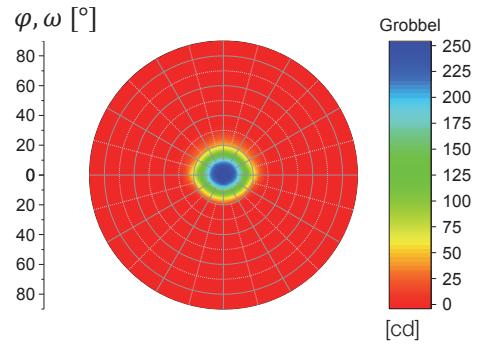Figure 8.5 Place du Bourg-de-la-Four, Geneva, Switzerland. Shannon's entropy of an isovist calculated on the length of the generating lines of sight.

(Used tool: Grasshopper for Rhino © elaboration on CC data from Système d'information du territoire à Genève - SITG)
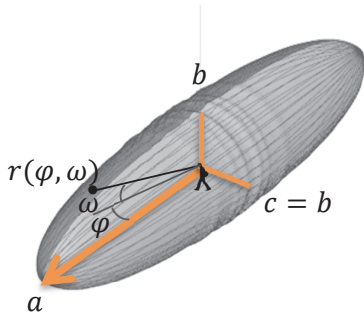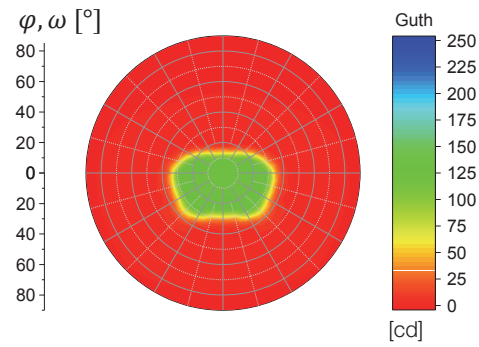
Shannon's entropy is determined using the distribution of a discrete random variable, i.e. the length of the lines of sight generating the isovist (Equation 8.1 and Figure 8.5). The lower the entropy, the more the space can be anticipately perceived by the observer: an observer situated in the center of a circular space, for instance, returns an entropy equal to 0. In Equation 8.1, H [-] is the Shannon's entropy of an isovist generated with n [-] lines of sight: in this case a line of sight is traced for each degree angle, with a total amount of 360. The lengths of these lines of sight are sampled using x [-] number of bins: in this case, the chosen bin interval is equal to 1 meter. P_i [-] is the probability of occurrence of the length corresponding to the "i" line of sight, within the total set of length bins.

$$H = -\sum_{i=1}^{n} P_i \cdot \ln P_i$$

Equation 8.1 – Shannon's Entropy of length of isovist lines of sight

The major axis of the ellipsoid is assumed to be equal to the radius of a spherical gazing distribution, divided by the square of the entropy (Equation 8.2). The minor axis is assumed to be equal to the same radius, multiplied by the entropy (Equation 8.3). Consequently, the volume of the ellipsoid is equal to the one of the corresponding sphere, as stated by an a priori hypothesis. The gazing intensity along a given direction issued from the center of the ellipsoid is equal

to its polar radius (Equation 8.4 and Figure 8.4c), which is a function of the azimuthal angle φ [deg], the zenithal angle v [deg] and the axes length a and b [meters].

$$a = r\frac{1}{H^2}$$

Equation 8.2 – Major axis of the ellipsoid representing a dynamic centrifugal-centripetal gazing field

$$b = rH$$

Equation 8.3 – Minor axis of the ellipsoid representing a dynamic centrifugal-centripetal gazing field

$$r(\varphi, v) = \sqrt{\frac{a^2 b^4}{b^4 \cos^2 \varphi \cos^2 v + a^2 b^2 \sin^2 \varphi \cos^2 v + a^2 b^2 \sin^2 v}}$$

Equation 8.4 – Gazing intensity as a function of azimuthal angle, zenithal angle and axes length of a prolate ellipsoid

8.1.3 Visual amplitude weight

Once the gazing intensity is determined and implemented in a backwards ray-tracing model (see Chapter 7), the photometric solid of each viewpoint is used to induce an illuminance on the target surfaces. Consequently, the visual amplitude can be weighted by an illuminance ratio as described in Section 7.1.9: in this case E_w [lx] is the illuminance assessed in the model accounting for a focused attention; E [lx] is the illuminance assessed in the model in the case of an evenly distributed attention, featuring a spherical gazing field (see Equation 7.15 and Equation 7.16). The arbitrary luminous flux of the sources (volume of the photometric solid) has no importance, since it is normalized by the ratio.

$$VA = \text{Log}_{10} \sqrt{\frac{\overline{\Omega}_{av}}{\Omega_0}}$$

Equation 7.15 – Visual amplitude from multiple viewpoints

$$\overline{\Omega}_{av} = \frac{\sum_{n=1}^{y} \frac{\sum_{p=1}^{x}(\Omega_p \cdot b_p)}{\sum_{p=1}^{x} b_p} \cdot \frac{E_w}{E_s}}{y} \text{ with } b_p = 0 \ \vee \ b_p = 1$$

Equation 7.16 – Average solid angle from multiple viewpoints

8.2 Practical implementation

8.2.1 Multiple viewpoints in an urban environment

Isovist drift

▲ Drift direction vector

(a) Drift direction

Isovist entropy

[-]

2.35

4.48

(b) Shannon's entropy of isovists' lines of sight

Figure 8.6 Place de Hollande, Geneva, Switzerland. Drift direction and Shannon's entropy of isovists' lines of sight.

(Used tool: Grasshopper for Rhino © elaboration on CC data from Système d'information du territoire à Genève - SITG)

The considered built environment is the one described in Section 7.2.1. In comparison with Chapter 7, the analysis area is restrained to Square Hollande, to allow in-depth calculations at a finer scale. Reference size for meshes subdivision is kept at 1.5 m x 1.5 m, while a more accurate viewpoints sampling is performed. In particular, viewpoints are placed at the boundaries of sidewalks and walking areas, with a spacing of 2.5 m; within the walking areas, a spacing of 2.5 m on offset curves is equally adopted, respecting a buffer zone of 1.5 m from building façades. Viewpoints' heights are equal to 1.5 m above ground. Globally, 15 242 mesh faces and 806 viewpoints are allocated in this area. Drift magnitude and entropy are calculated for the isovists generated at each viewpoint: results are shown in Figure 8.6. From that figure, viewpoints located in narrow streets are characterized by a lower entropy, in comparison with viewpoints located in the pedestrian area of the square or along the lake walk. In narrow streets, pedestrians' will more likely direct their view toward the more open space. At the road intersections, such direction is more uncertain, since the choice of possible paths and viewing corridors is larger.

The outcomes of the visual amplitude analysis for a 100% lightness contrast ratio are shown in Figure 8.7 and Figure 8.8: colors are rescaled to the upper limit of 2.94 LogMAR, in order to appreciate smaller differences in the results. In dynamic gazing models, the visual amplitude is more homogeneous on building surfaces. Façades are more prominently visible at the viewpoints' height, namely 1.5 m above ground. The upper façade parts are gradually less visible with a more focused attention, from the ellipsoidal to the steady gazing field models. In these latter cases, some façade corners stand out more, since observers are aiming at the open space that develops behind the corner. The more focused gazing intensity corresponding to the Grobbel's gazing field [192] produces more localized illuminance areas in comparison to the Guth's gazing field [193]. This trend is even more obvious for the relative difference of illuminance with the spherical model, represented in Figure 8.9. Compared to façades, roof surfaces show less significant variations in visual amplitude, across the different gazing field models. In particular, flat roofs are invisible in all models. In terms of relative difference in illuminance (Figure 8.9), some roof pitches are characterized by larger deviations. This is the cumulative effect engendered by the directionality of viewpoints located far away and focusing on the roof. As a general trend, a more focused attention shifts the peak of illuminance distribution to lower values with fewer envelope parts featuring larger isolated values (Figure 8.10).

Dynamic gazing field models

Spherical VF

Ellipsoidal VF

👁 VA index

[cell size]   [contrast]

1.5 m   100 %

[LogMAR]

0

2.94
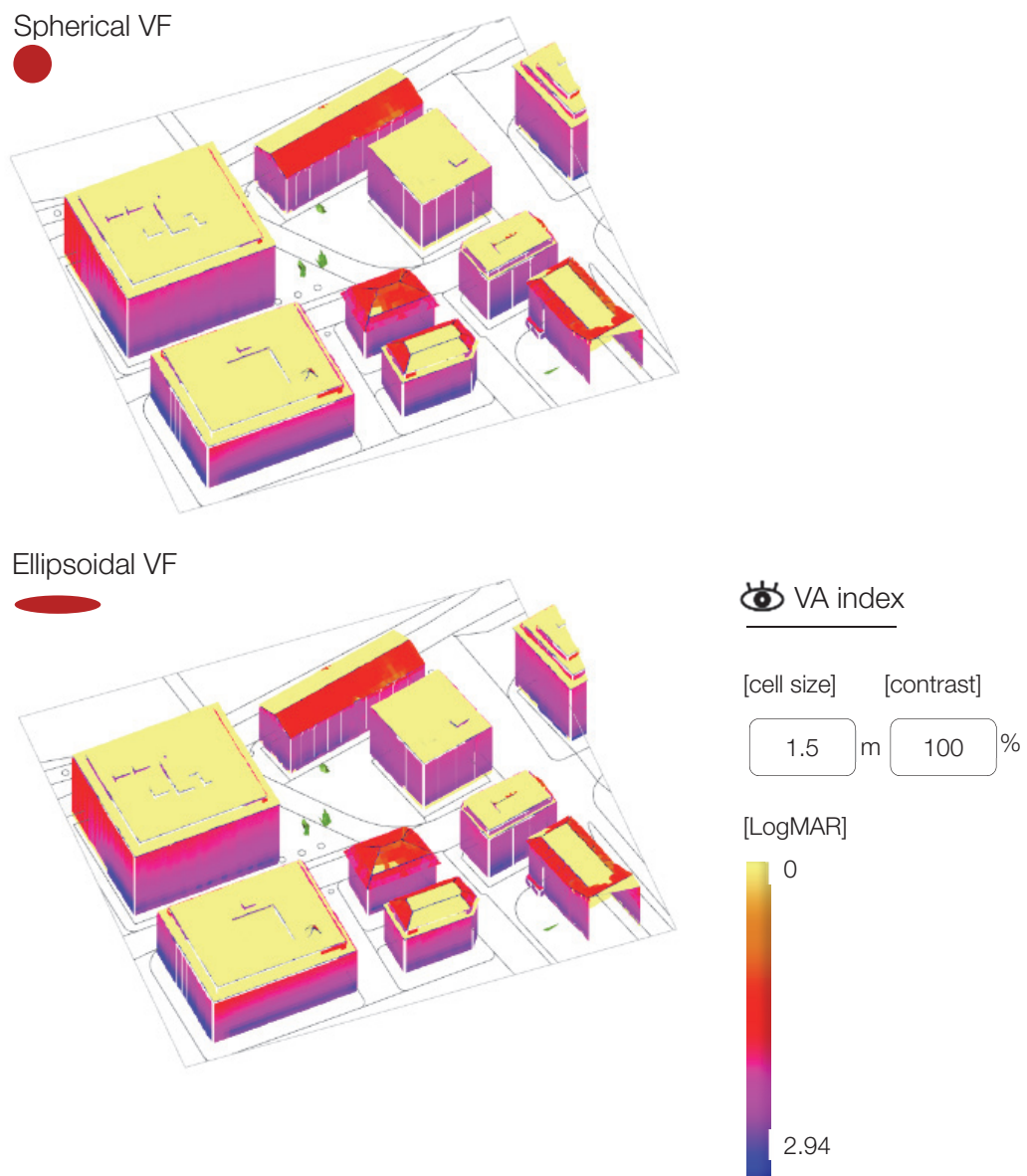
Figure 8.7 Place de Hollande, Geneva, Switzerland. Visual amplitude index for dynamic gazing field models.

(Used tool: Grasshopper for Rhino © elaboration on CC data from Système d'information du territoire à Genève - SITG)
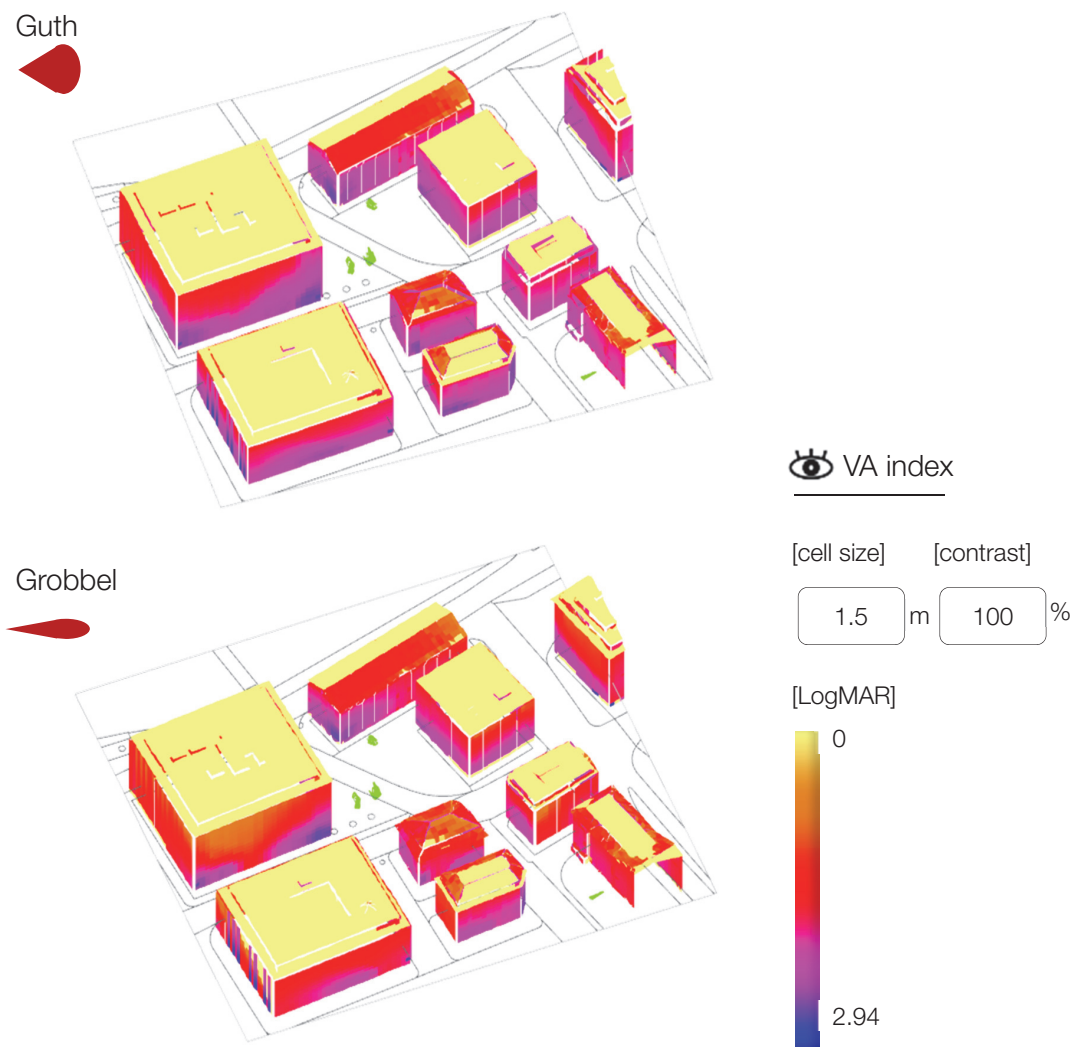
Figure 8.8 Place de Hollande, Geneva, Switzerland. Visual amplitude index for steady gazing field models.

(Used tool: Grasshopper for Rhino © elaboration on CC data from Système d'information du territoire à Genève - SITG)

Ellipsoidal VF
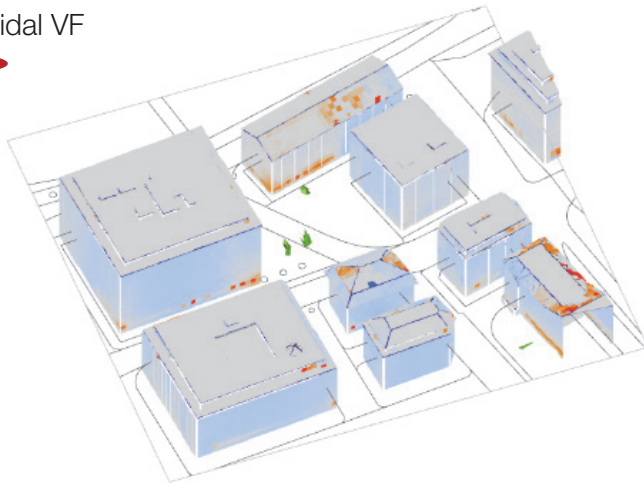
Guth
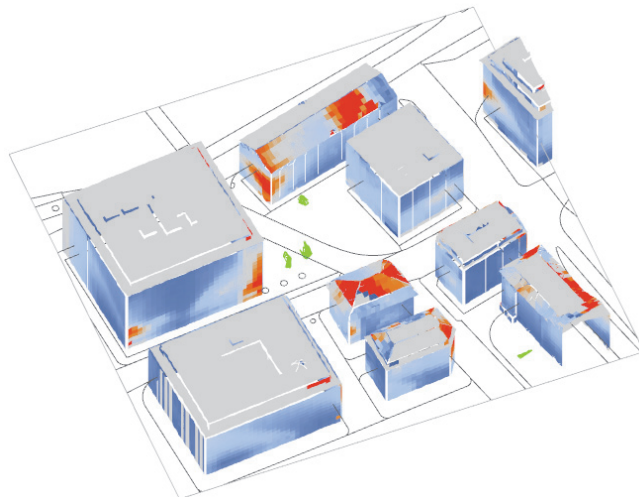
Grobbel
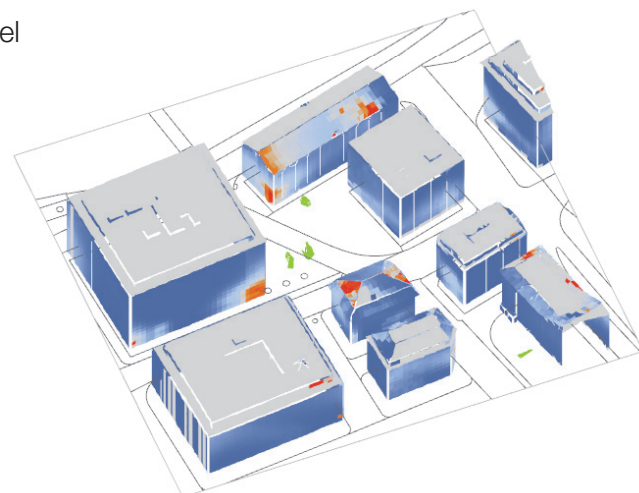
Illuminance rel. diff.

[%]

-100

0

+100

Figure 8.9 Place de Hollande, Geneva, Switzerland. "Visual" illuminance: spatial representation of relative difference with spherical gazing model.

(Used tool: Grasshopper for Rhino © elaboration on CC data from Système d'information du territoire à Genève - SITG)
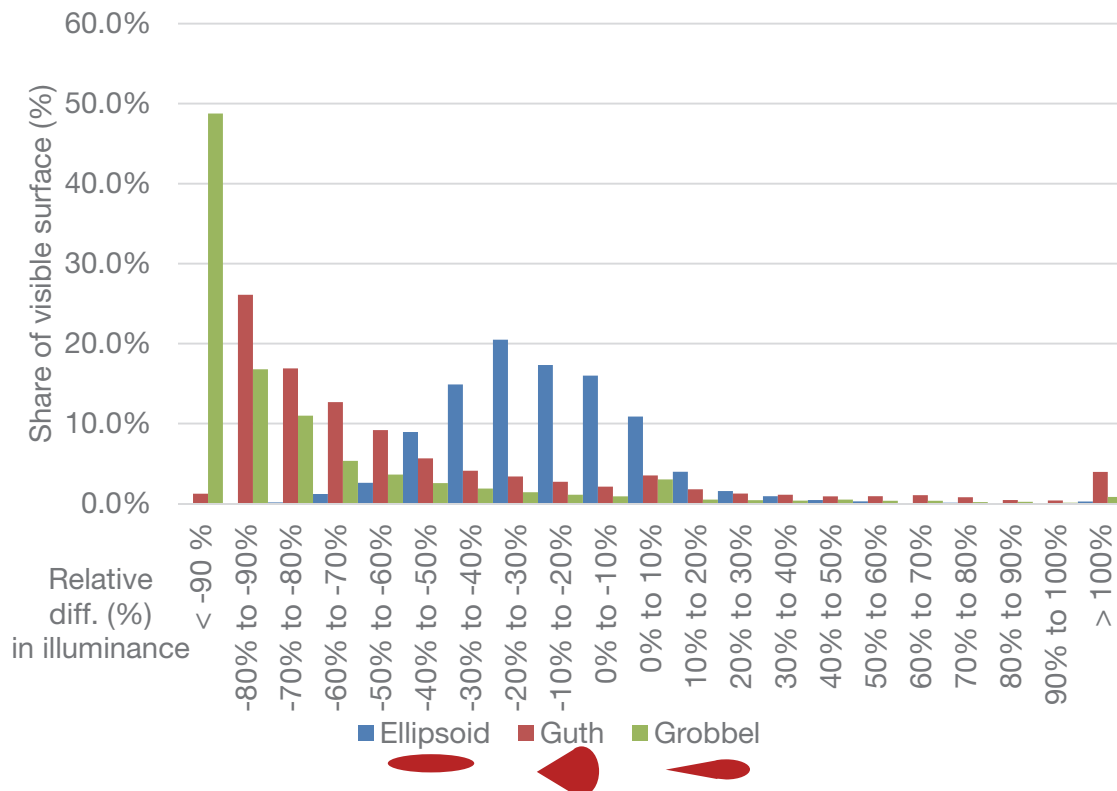
Figure 8.10 Place de Hollande, Geneva, Switzerland. "Visual" illuminance: histogram of relative difference with spherical gazing model.

(Used tool: Grasshopper for Rhino © elaboration on CC data from Système d'information du territoire à Genève - SITG)

8.3   Cross mapping

A cross mapping representation gathering both the solar radiation and the visual amplitude data is shown in Figure 8.11 for the whole Hollande district. The solar radiation is calculated as previously described in Section 7.3. It is eventually possible to multiply such outcome by the energy conversion efficiency of hypothetic solar modules (either solar thermal or photovoltaic): as such, the energy generation potential represents a more practical outcome, from an engineering perspective (see Section 4.2.1). Solar radiation is represented according to a gradient color scale.

Visual amplitude indexes are computed for maximal lightness contrast conditions in order to consider the most constraining scenario (e.g. the most visible one), even if the 100% lightness contrast ratio can be adjusted to match usual values in the outdoor environment (see Section 7.1.7, Section 2.4.3). The spherical gazing model is preferred herewith for simplicity, even though the observers' attention is available from the previous sections. Three visual amplitude classes are illustrated, in accordance with the assumptions of Section 7.1.6: (i) low visibility, in

line hatch, below 0 LogMAR; (ii) medium visibility, in dotted hatch, between 0 and 1.4 LogMAR and (iii) high visibility, left blank, above 1.4 LogMAR. Results indicate that the South exposed roof surfaces receive on average a large solar radiation of about 1200 kWh/m^2 year, while the North exposed ones are experiencing half this value. The solar radiation distribution is inhomogeneous on vertical planes, reaching the amount of 800 kWh/m^2 year on the unshaded, upper parts of the South façades. In this case, almost all the flat roofs can be equipped with solar modules without being visible from the public space. Pitched roofs are mainly characterized by a medium visibility, excepting some more visible fractions facing large squares or avenues; on the other hand, roof subdivisions towards narrow urban canyons or internal courtyards are globally less visible. By comparing the solar energy generation potential with the specific energy demand, it is possible to reach an effective load match respecting the required visibility constraints (see Table 8.1 and Table 8.2).
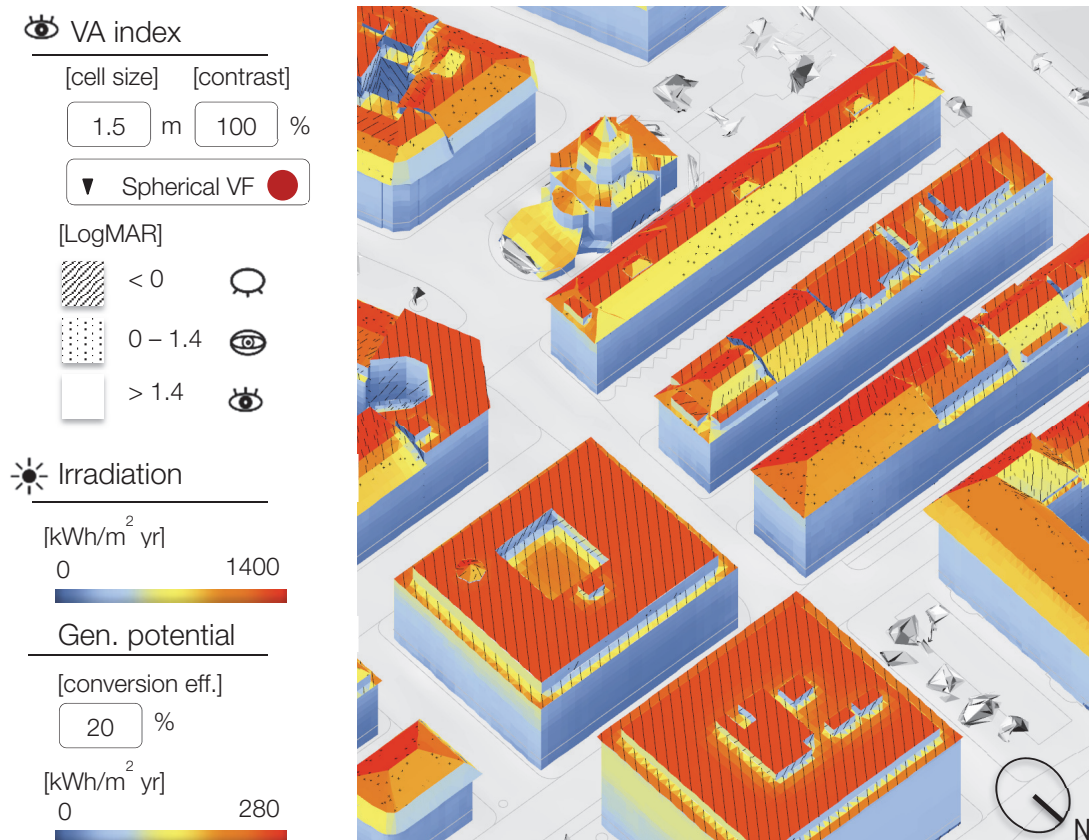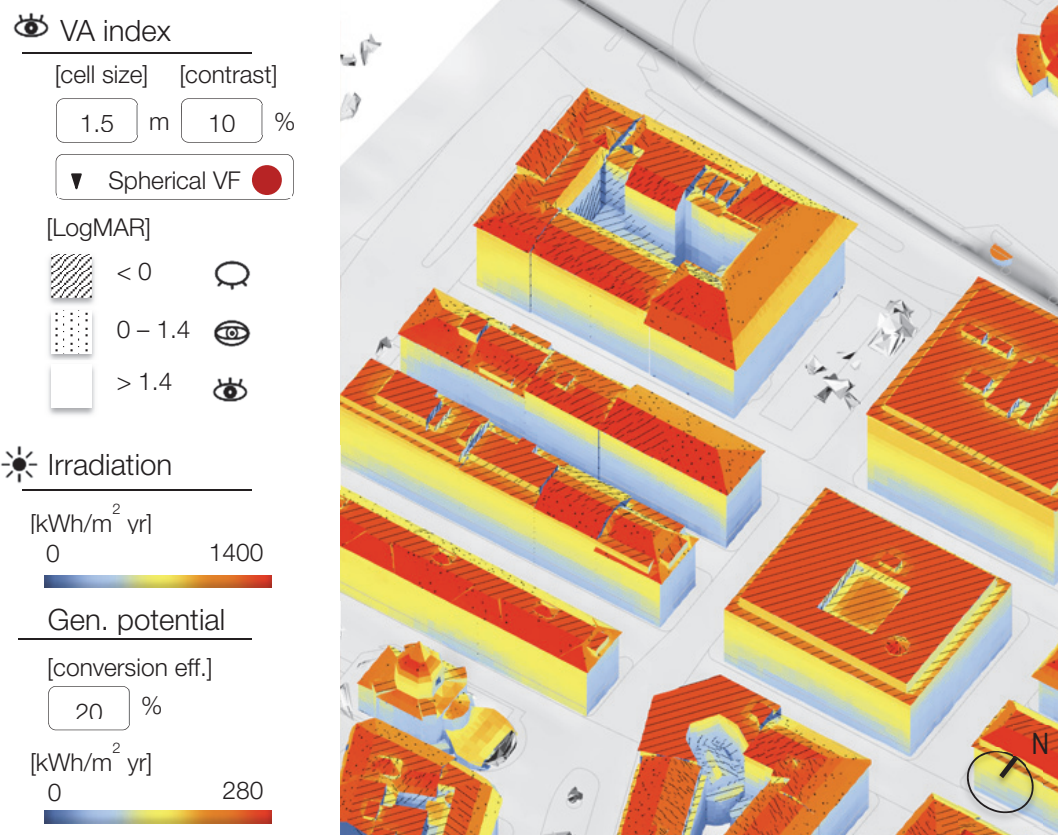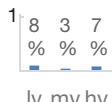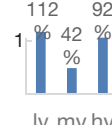
Figure 8.11 Hollande district, Geneva, Switzerland. 3D Cross mapping of visibility and solar radiation, aggregation per mesh subdivision.

(Used tool: Grasshopper for Rhino © elaboration on CC data from Système d'information du territoire à Genève - SITG)

Table 8.1 Hollande district, Geneva, Switzerland. Solar energy generation potential as a function of visibility class.

	low visibility	medium visibility	high visibility	TOTAL
surface [m²]	73'443	6'266	60'352	140'061
solar radiation [kWh / yr]	14'210'000	5'304'600	11'650'400	31'165'000
thermal potential (eff. 0.5) [kWh / yr]	7'105'000	2'652'300	5'825'200	15'582'500
electric potential (eff. 0.2) [kWh / yr]	2'842'000	1'060'920	2'330'080	6'233'000

Table 8.2 Hollande district, Geneva, Switzerland. Energy needs covering ratio as a function of end energy use.

Energy Reference Surface = 698'635 [m²]	heating	hot water	electricity
energy needs [kWh / yr]	85'634'347	6'330'854	30'810'523
Solar energy potential / needs ratio [% per visibility class*] *l=low,m=medium,h=high	1 8 3 7 % % % lv mv hv	112% 92% 1 42% lv mv hv	1 9 3 8 % % % lv mv hv

In the considered district, the solar radiation available on the low visible envelope area is equal to slightly less than half of the amount available on the whole envelope surface. For example, 10 GWh of annual thermal energy can roughly be produced on both the low and medium visibility envelope area, in comparison to the 20 GWh of solar radiation they benefit from: an energy conversion efficiency corresponding to solar thermal collectors of 50% is considered. This amount is sufficient to cover 11% of space heating needs of the whole district (without considering the heating system efficiency); hot water needs are fully satisfied with the sole use of the low visibility area (without considering the DHW system efficiency). Alternatively, 4 GWh of solar electricity can annually be generated on both the low and medium visibility envelope surface, considering a 20% energy conversion efficiency. This amount corresponds to 13% of the whole district needs (without considering system losses). Space heating needs as well as the Heated Floor Area are issued from the SITG open data building census (Système d'information du territoire à Genève). Hot water and electricity needs are issued from the national standard values according to the Swiss building codes (SIA 380/1 [215] and SIA 380/4 [216] respectively).

8.4 Conclusion and outlook

In this chapter, a method to implement selective attention in a photometric model with the purpose of visual amplitude assessment is presented. A proof of concept on a study area in Geneva is demonstrated by using the isovist drift magnitude and the Shannon entropy to determine respectively the main viewing direction and the gazing intensity distribution. This assumption is derived from previous experiences, referenced in the literature [94], [97]; it is not supported directly by a psychophysical validation. The objective is rather to outline a possible extension of the visual amplitude assessment methodology to more complex perceptual settings, which would include observers characterized by different behaviors.

A possible experimental set-up to investigate the validity of isovist drift and entropy as relevant variables for gazing models would involve the use of smartphones (Figure 8.12).
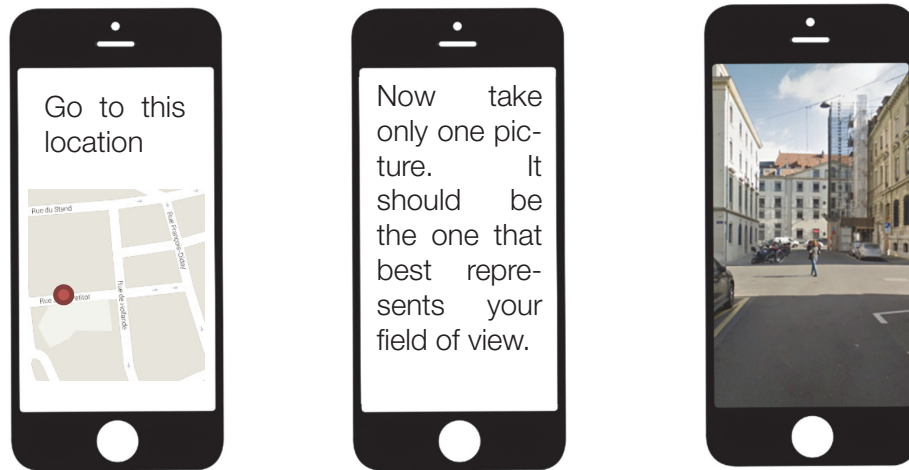
Figure 8.12 Possible experimental set-up for the validation of the isovist drift-entropy-driven gazing model.

(Author's own elaboration)

In particular, a group of observers would be sent to different viewpoint locations in the public space, characterized by different isovist drift and entropy values. Each subject would be asked to take a picture with his/her smartphone, i.e. the one that represents in the best way his/her field of view in his/her opinion. Only standard photographs without panoramic lenses and without processing by photocomposition software for 360 degrees views are allowed. The direction pointing to the center of the picture frame from the viewpoint is recorded and relative frequencies are determined for a set of direction bins, based on the subjects' responses. It is expected to find higher frequencies of photographs aiming in the direction of the street axis when the viewpoint is located in a narrow street, namely a deep urban canyon: this would confirm the validity of the isovist drift as indicator of the main viewing direction. Subsequently, the correlation between the frequency distribution of the aiming directions and the isovist entropy can be analyzed with an expected concentration along the main viewing direction, especially in narrow streets.

In Section 8.3, a cross mapping tool between the visual amplitude and the solar radiation suitable for neighborhood planning is introduced. A dynamic spherical gazing model is adopted for each viewpoint, the outcomes being returned at the level of mesh subdivisions. An intuitive tridimensional visualization allows an efficient navigation in the considered urban context and a

comprehensive representation of all envelope surfaces, which supports the decision-making process. The estimation of the building energy demand in the district indicates that slightly less than half of the total solar radiation available on the building envelopes reaches surfaces characterized by low visibility. Circa 10% of the space heating, or the electricity needs (alternatively), can be covered by means of the corresponding solar thermal collectors or PV solar panels, installed on a scarcely visible part of the building envelope. Exploiting also the medium visibility surface would allow to cover 12% to 13% of these energy needs. It seems legitimate to conclude that stakeholders can reasonably expect to produce a serious amount of solar energy by the way of building integrated solar modules without crucially affecting the public perception. At the same time, plenty of highly visible areas remain available for high-end solar refurbishments, which could also serve pilot and demonstration purposes.

Chapter 9   Conclusion and future outlook

The objective of this thesis is to provide a scale-dependent methodology to assess visibility of solar energy systems in urban areas and compare it with other relevant variables, such as urban sensitivity and the annual solar potential, to drive solar energy deployment strategies within buildings and urban sites.

With the specific aim to include it as a variable in a multi criteria method, a scale-adaptive visibility index is suggested, from the strategic broad territorial scale to the district level, and even the neighborhood or cluster of buildings. At each scale, this index is systematically overlapped at a variable level of detail on an urban sensitivity layer and on a spatial representation of the solar energy production potential.

At the broad territorial scale (1 : 100 000 – 1 : 30 000), a visual interest index is presented (Chapter 5), based on a census of relevant viewpoints and on the spatial density of photographs taken by visitors. The former top-down approach is expertise-driven and gathers punctual emerging visual prominences; the latter bottom-up approach is crowd-sourced and offers a uniform territorial assessment well-adapted to cities covered by a rich photographic database. Both seem to be reliable, representing complementary indicators of the "mass effect" component of visibility, i.e. the global public interest of a space, which can constitute a ponderation value for more detailed geometrical based analyses.

At the urban development planning stage (1 : 10 000 – 1 : 5000), a viewshed analysis is run on roofs of a whole metropolitan area from a discrete set of viewpoints sampled on the road axes (Chapter 6). Computational load has proven to be reasonable for a maximum distance of 500 m to the targeted object, which is compatible with practitioners' standards. Despite the globally scattered distribution of visible (by at least one viewpoint) and invisible surfaces, some general trends could be identified. Façades are not considered in the analysis at this stage, being assumed as visible by at least one viewpoint. The method seems robust enough to identify the most adapted buildings clusters corresponding to different solar planning strategies within a cautious scenario over-estimating visibility: trees and urban furniture are neglected at this stage.

Nevertheless, some non-negligible variations in visibility should be foreseen, mostly due to a simplified viewpoints sampling on the road axis used as a reference case.

At the detailed planning scale (1 : 2000 – 1 : 500), photometric models of visual field as well as ray-tracing techniques are explored to mimic human vision and identify the most perceived areas of building envelopes, including façades (Chapter 7). Obstructions from vegetation and urban furniture are considered. Results provide an average visibility assessment from a set of viewpoints, sampled on a fine grid on the public walkable space. The magnitude scale is based on solid angles to take into account the visual attenuation over distance of sight. This methodology seems valuable to compare distinct solar installation options on different envelope surfaces on a relative scale. Nevertheless, absolute values are affected by a moderate degree of uncertainty, in relation with: (i) the position and number of viewpoints, (ii) the selective attention of potential observers and their own movement, (iii) the size and layout of the solar modules, (iv) the visual contrast influenced by the meteorological conditions and the visible surface materials. As such, results cannot be considered to be absolutely rigorous on a perceptual basis, beyond purely geometrical aspects, corroborated with some psycho-physical and physiological considerations.

With the intention of overcoming such barriers, an improved methodology featuring an advanced viewpoints sampling technique and a selective attention model is suggested at the architectural scale (1 : 500 – 1 : 100) (Chapter 8): the focus of attention and its relative distribution is estimated according to some literature. Results demonstrate that different observers' behaviors can be successfully implemented in the algorithm, even though a psychophysical justification is yet to be found.

Concerning the solar radiation, different accuracy levels of the computation accompany the visibility indicator at the various scales: all methods are well-established and thoroughly validated in the scientific literature. At both the strategic and development planning scale an annual cumulative sky model is issued based on the latitude, the atmospheric transmittance and the optical path length, opportunely weighted by shading factors: the share of diffuse radiation is supposed to be constant and equal to 30%. This approach is sufficient to estimate coarse values of the annual solar radiation on the rough topography of the site (at the strategic scale) and to filter out roof areas below the economic viability threshold (at the development scale). At the detailed and architectural scale, the annual cumulative sky is deduced from measured

meteorological data, including direct normal and diffuse horizontal irradiance included in the International Weather File for Energy Calculations (IWEC). This method is adapted to formulate decisions on an annual basis but underestimates seasonal and daily fluctuations that include shading dynamics, as well as sun rays reflections (see [187]).
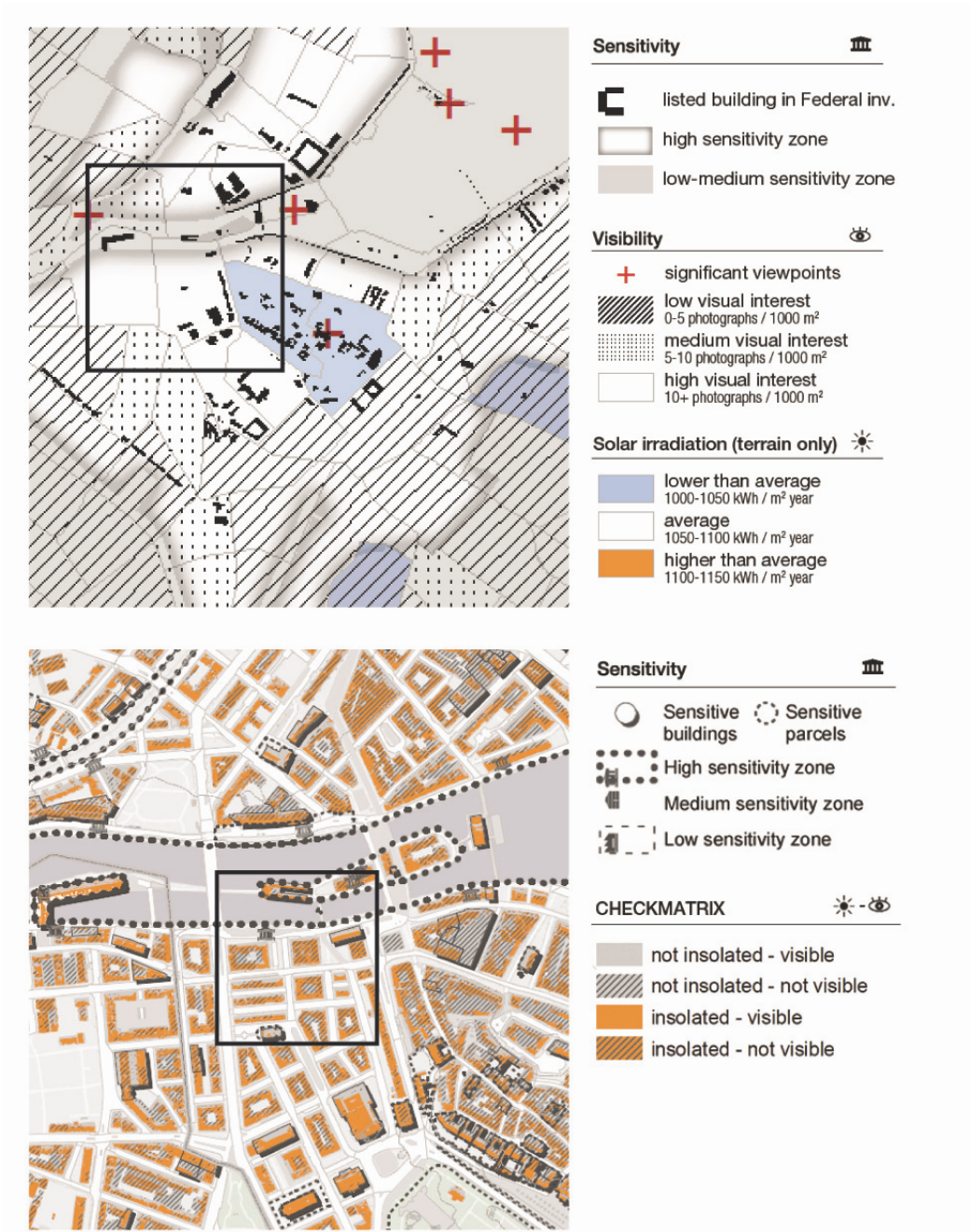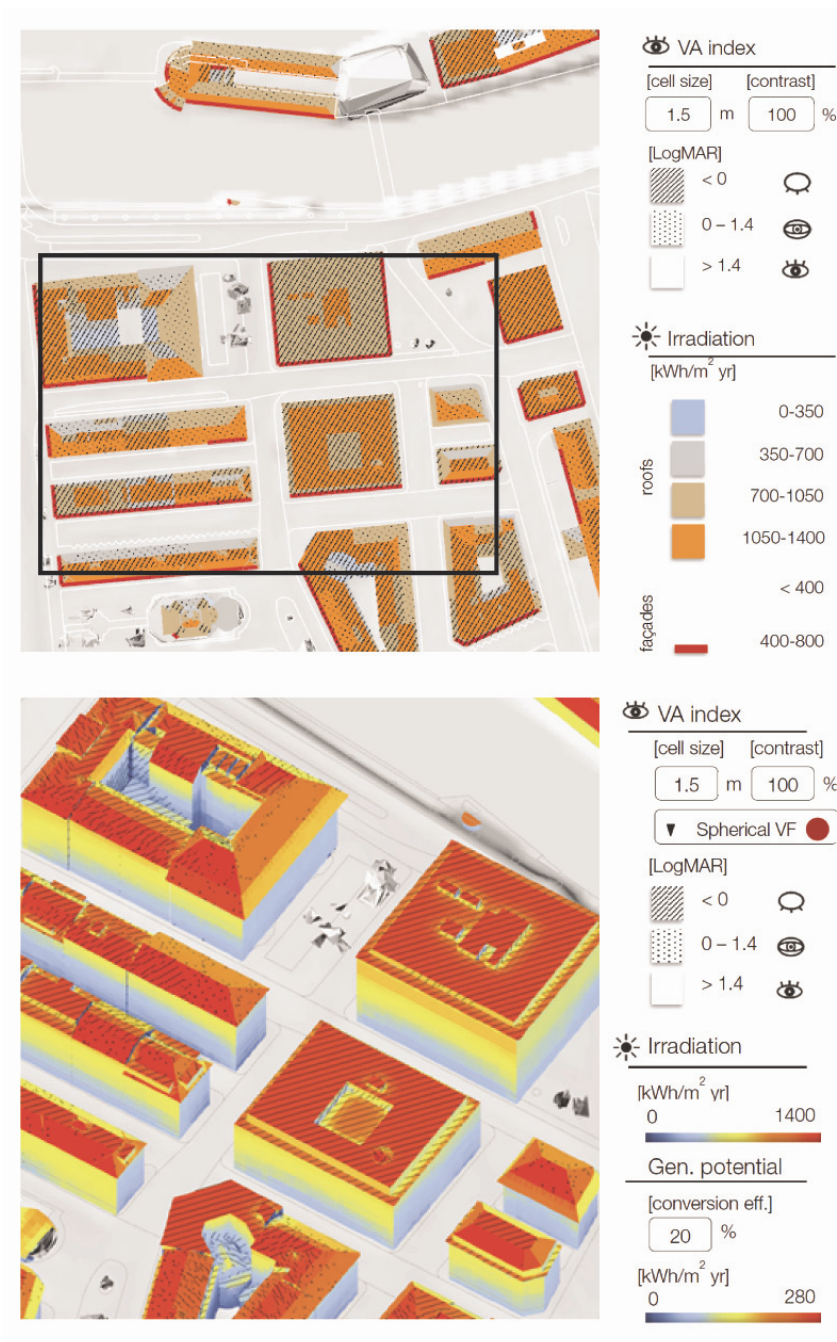
Figure 9.1 Comparison of cross-mapping representations at the various scales. From top to bottom: strategic planning, development planning, detailed planning, and architectural planning.

(Author's own elaboration)

By observing cross-mapping results at the various scales, a certain consistency can be recognized, both in terms of visibility and in terms of solar radiation potential (Figure 9.1). Only few differences can be highlighted between the development and the detailed planning scale due

to the shift to a full vector model that simplifies some roof shapes. Despite the different assessment methodologies summarized herewith, one may conclude that the whole scale-dependent approach is reliable and sound.

An open issue, which is recurrent across the whole thesis, is the psychophysical justification of some results and the empirical validation of visibility metrics, including benchmarking of thresholds. A possibility would be to set-up dedicated surveys proposed to a sample population, featuring different settings of solar modules. Viewpoints can be arranged both in a close and in a far perspective from the modules, both in open land and in urban environments: as such, the psychophysical reference used for this thesis [66], which is not specific to solar modules nor to urban contexts, would be enriched with new conclusions. With regards to selective attention modelling, the experimental toolset may also include eye-tracking devices and 360 degrees cameras, mounted on a backpack and brought by experimental subjects while making urban walks [217], [218]. The potential of eye-tracking studies in open spaces for urban studies is promising [213]: this would allow to study closer perspective, depth and movement effects on visitors' perception, visual comfort, as well as sense of safety. Much has to be done to unveil urban observers' behavior, the activities they perform while being in the public space and the consequent impact on attention, perception, emotions and sense of well-being.

Another aspect that would deserve further investigation is contrast. The relationship between lightness contrast and visual acuity at the basis of the current method [66, Fig. 10], should be translated into luminance contrast to model lighting conditions according to the physical principles of photometry. Contrast derived from textures, materials, light absorption and reflections from surfaces is yet to be thoroughly explored, with a great complexity added by the high spatial and temporal variability of these parameters. Different lighting conditions as a consequence of climatic and meteorological dynamics, artificial lighting and glare should be introduced in the raytracing approach which, despite its embryonal use within this thesis, may allow their implementation.

Further research should be focused on other forms of "visual pollution" [64] that may cumulate their effect with low-end solar modules, especially in highly anthropic environments such as urban contexts. One could enumerate advertisement, redundant road signs, technical equipment and fixtures for energy and water distribution, telecommunication devices and antennas, blinking and moving lights, chimneys (and relative smoke), mirrors and other reflective materials

as potential glare sources. All these objects may interfere with several human activities beyond touristic visiting and city sightseeing, sometimes inducing serious risks (e.g. for driving).

The outcomes of this thesis are mainly addressed to urban planners, energy consultants and stakeholders in the field of building preservation and renewable systems deployment. Architects, solar modules manufacturers as well as practitioners in general may benefit from this research too: practical aspects of this work are partially depicted in the appendix. More effort should be dedicated optimizing the current algorithm, make it more efficient in terms of computational resources and compatible with other datasets. Several graphical representations are suggested throughout all chapters and their compliance with users' ergonomics, conventions and expectations should be tested. The visual amplitude assessment methodology may lead to the development of a software tool with user interaction features, to input data and modify computation parameters through a proper Graphical User Interface (Figure 9.2).

Despite the several limitations, the author is convinced that the suggested approach could play a significant role in the framework of the Swiss Energy Strategy 2050, by stimulating the debate around the wise use of solar technologies deployed on buildings and their public perception.
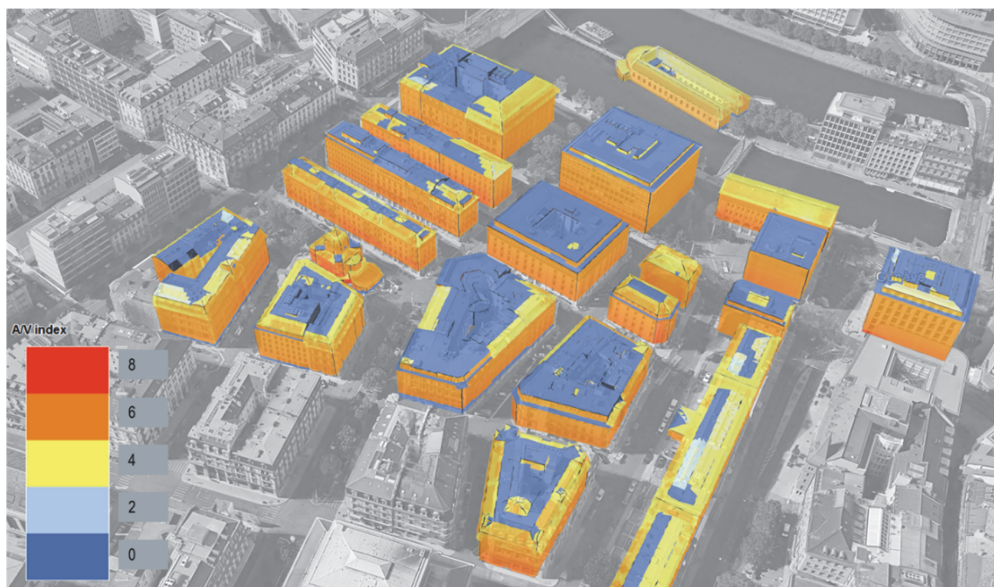
Figure 9.2 Draft of graphical user interface implemented in Google Earth ©.

(Used tool: Google Earth ©, Credits: Landsat Copernicus)

A. Appendix

This thesis has been supported by the Swiss Federal Office of Energy (SFOE), which is promoting innovative research in the domain of architectural integration of solar energy through the Swiss participation to the IEA SHC Task 51 'Solar Energy and Urban Planning' (International Energy Agency, Solar Heating and Cooling Program) [219]. This task was operational between 2013 and 2017, gathering experts from Academia, research institutions, public authorities as well as urban planners and building designers: the author had the opportunity to participate, as expert with his supervising team, to the activities of IEA SHC Task 51. This ideal situation fostered the information exchange and discussions with open-minded professionals, bringing practical inspiration to this thesis. Some of the relevant teamwork developed in this framework is presented in the following sections.

Another occasion to turn scientific competences into practice came from the NEST project at the EMPA Material Science and Technology research center in Dübendorf, a demonstrative building and research platform for outstanding applied science developments, prototypes and industrial products in the building and construction domain [220]. A partner consortium was constituted to design and build one unit of this building, denominated SolAce [221]: the Solar Energy and Building Physics Laboratory (LESO-PB) of EPFL is the scientific leader of this project. The author participated in the project steering committee and provided consultancy concerning the architectural design in general and the optimal integration of PV and solar thermal modules in particular. Few elements of this experience are mentioned herewith.

A.1 Consulting

A.1.1 Gasverket design project

Informal discussions within Task 51 offered the opportunity to test the visual amplitude assessment on an urban development project located in the city of Stockholm in its conceptual stage. The area is called Gasverket due to the industrial gas production plant that was operating on site until 2011 supplying gas to the Stockholm network. Many buildings were built at the end of the XIXth century by a local architect, Ferdinand Boberg, and designed according to high architectural standards. The main purpose of the detailed plan is to foster the conservation and

renovation of a fraction of the existing historically valuable buildings and exterior setting. The draft proposal allows the current part of the gasworks to offer new services, including a school, a gym, a tramway museum, a theater and a cultural center.

Figure A.1 Red brick building by Ferdinand Boberg in Gasverket district, Stockholm, Sweden.

(Credits: Holger Ellgaard, Wikimedia Commons)

The architectural firm developing the project wanted to install solar modules on some of the existing historical buildings, characterized by a red brick finish (Figure A.1): the latter sounded not appropriate to standard commercial modules showing highly reflective and colored cold tones. The aim was to guarantee a sustainable energy supply to the new development with building integrated technologies, without affecting the public image of the cultural heritage. As such, the architects wanted to reveal the different degrees of visibility of building envelope surfaces with high solar energy generation potential. Johan Dahlberg, from White Arkitekter, kindly provided this 3D model to the author. The public area around the ancient production site was selected for the visual amplitude analysis (Figure A.2). New buildings are not shown in these figures, their layout being still confidential, even though their volume has been considered as an obstruction. Only the buildings characterized by a 'satisfactory' incident solar radiation were retained as visual targets by the architects. The solar modules area for the assessment was fixed to 1.5 m x 1.5 m and employed as reference case.
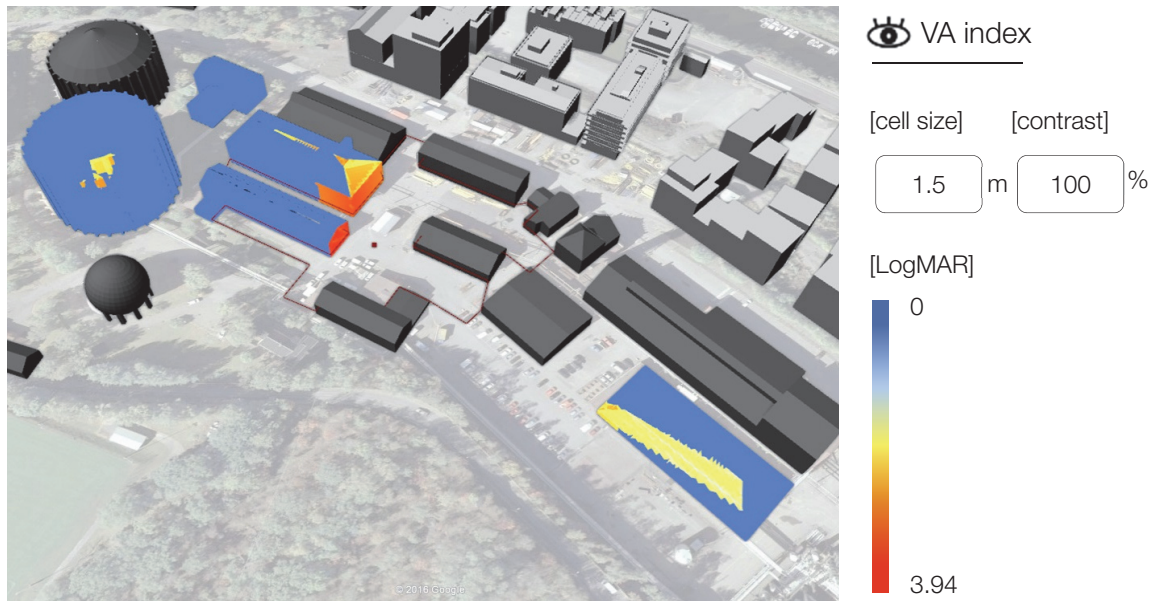
(a) Visual amplitude index from a single viewpoint in the center of the public space
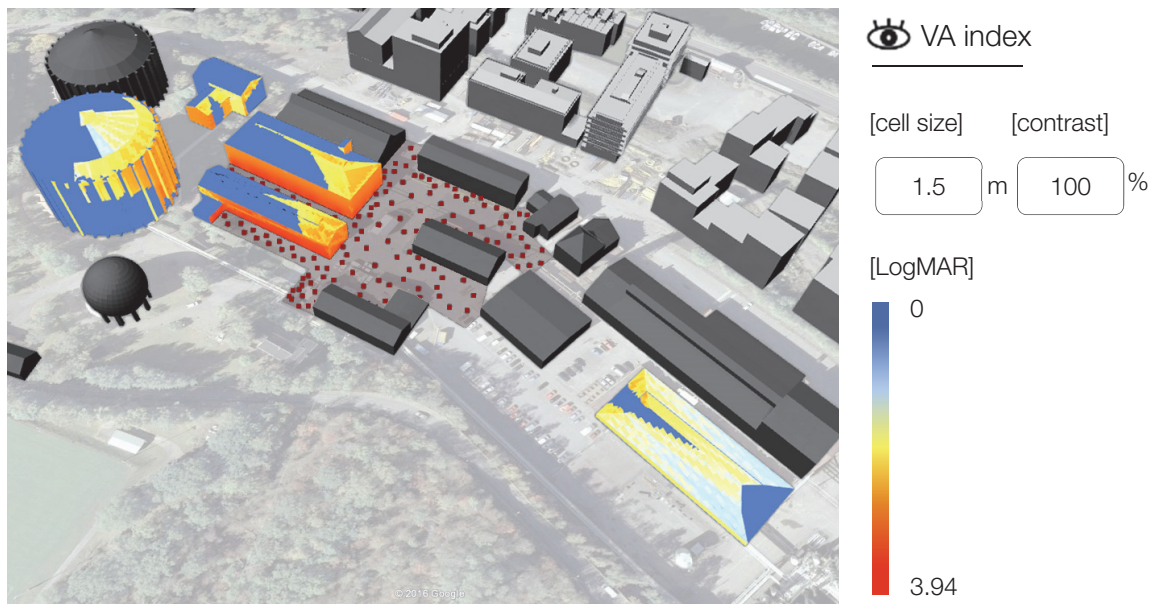
(b) Visual amplitude index from multiple random viewpoints sampled on the public space surrounding existing buildings

Figure A.2 Gasverket, Stockholm, Sweden. Visual amplitude index from one and multiple random viewpoints.

(Used tool: Grasshopper for Rhino © elaboration on data from White Arkitekter, Credits: Landsat Copernicus)

First, a single viewpoint located in the center of the square was used. The position of the viewpoint was modified 'on the fly' in order to highlight variations in the visual amplitude, to identify the most visible envelope subdivisions and to identify the most affected fractions of the public space (Figure A.2a). Subsequently, random viewpoints were distributed on the study area to

retrieve the global visual amplitude index (Figure A.2b). Results show that a considerable portion of South exposed slanted roofs is invisible from the sampled viewpoints, due to their low tilting angle in relation with their height above ground. Envelope fractions closer to the open square result in medium visual amplitudes, while the farthest building to the East presents medium to low values. Hence, the most adapted roof areas for a 'solar refurbishment' could be identified.

A.1.2 NEST SolAce unit

The NEST SolAce unit project was initiated in 2015 by EPFL researchers with the purpose of designing an energy positive module in annual terms, characterized by very low CO_2 emissions and centered on indoor comfort criteria. The goal in this prospect was to meet the highest standards of luminous, thermal, acoustic and air quality comfort, with a unitary and appealing aesthetic appearance. A field monitoring of the visual and non-visual effects of light will be carried-out in the unit, composed of a mixed-use space featuring offices and living areas. The construction materials were selected to generate the lowest impact on carbon emissions with the minimal embedded energy within their life cycle. All these objectives required a major effort in the conception phase in order to assess the global performance of the unit by means of computer simulations and foster appropriate design strategies.

(a) Highlighted lot of NEST unit SolAce. Credits: Landsat Copernicus

(b) Floor plan of the unit, showing the terrace in the middle. Credits: Lutz Architects ©

Figure A.3 NEST SolAce unit: context and conceptual floor plan.

(Used tool: Google Earth ©)

The assigned lot is composed of a 95 m² floor area on a cantilever structural concrete slab, with a three-orientations façade development: 23 m² facing South-East, 30 m² are facing South-West and 27 m² are facing South (Figure A.3). First, the space heating and electricity demands of the unit have been determined using validated software. At this point, a sound sizing and solar modules setting was needed to achieve a full coverage rate of the annual demand with solar energy. Both thermal and electricity storage facilities are available in the NEST building.
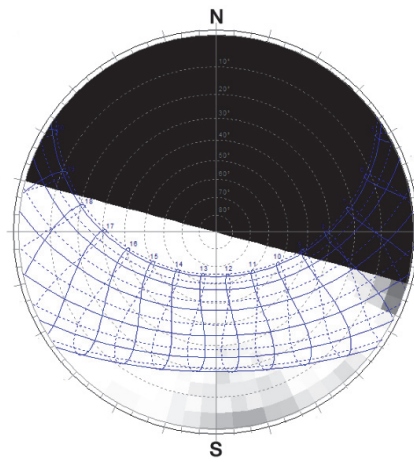
(a) stereographic sky projection
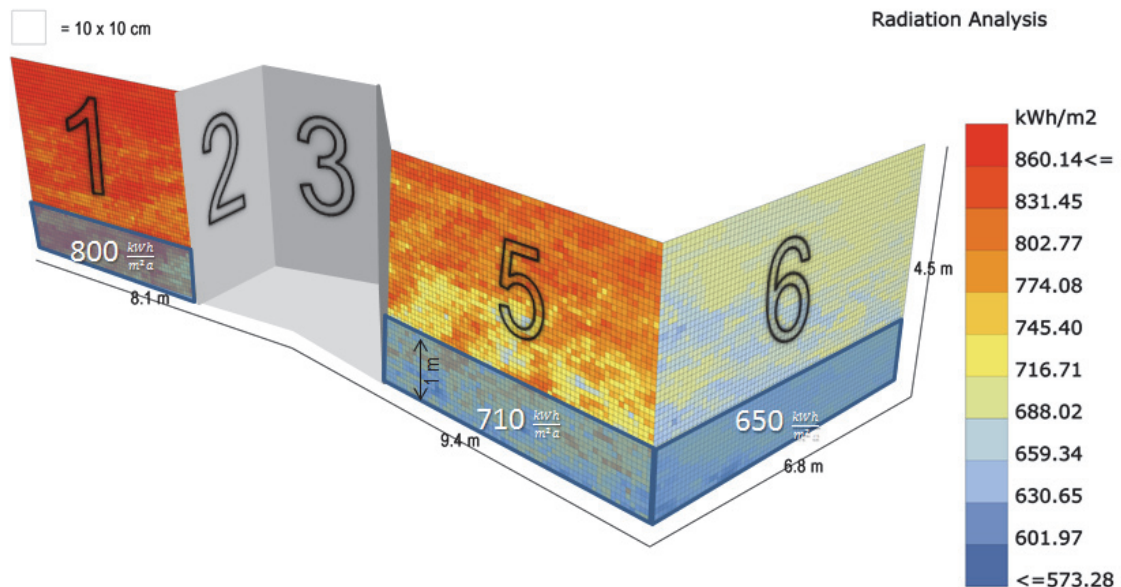
(b) Annual solar radiation diagram on façades

Figure A.4 NEST unit SolAce: solar radiation analysis

(Used tool: Grasshopper for Rhino © and Ladybug CC [121])

Unfortunately, the SolAce unit is located underneath an upper concrete floor: there is area available for an optimal building integrated solar energy production on the roof but it is occupied by another unit, the facades being the only remaining envelope surface for solar energy collection. The high visibility of solar modules on the façade of the unit was obvious, given the large open space that surrounds the building (Figure A.3a). As such, the annual solar radiation impinging on façades was assessed with the help of a tridimensional model of the unit, which includes its surrounding natural and built environment. From a preliminary analysis based on a stereographic sky diagram, it was found that some trees in front of the façade could possibly shade the solar modules (Figure A.4a). A more detailed simulation was performed with a backwards raytracing technique associated with a cumulative sky for Zürich Kloten, the closest location with available meteorological data (the calculation procedure is explained in Section 7.3). Results allowed for a detailed assessment of the annual solar radiation, which ranges from an average of 650 kWh/m^2 year on the South-Eastern façade to 800 kWh/m^2 year on the Southern façade: this value decreases to 710 kWh/m^2 year on the South-Western façade, partially shaded by trees (Figure A.4b). This preliminary analysis imposed the arrangement of windows in the upper part of the façade, up to the ceiling to benefit from most of daylight. Hence, solar modules were placed on a lower façade band of one meter height and on the opaque fraction of the South-Eastern façade. The visual amplitude index of the whole system was determined from a set of random viewpoints sampled with a 5 m spacing, on the internal streets of the EMPA campus surrounding the building. Considering the occlusions engendered by other buildings and trees, the returned visual amplitude index for the entire group of solar modules is 2.31 LogMAR. Given the high visibility of the considered surfaces and the demonstration character of the NEST SolAce unit, a high-end solar product was necessary to achieve a satisfactory architectural integration. Consequently, an innovative product made of nanostructured thin films on glass that reflects only a small band of the visible light spectrum was chosen (see [222], Figure 2.5 and Figure A.5): this luminous interference phenomenon induces a colored appearance on the solar modules with a very low impact on the glazing solar transmittance. Such glass can be applied on solar thermal collectors as well as laminated photovoltaic modules, to obtain a unitary aesthetic appearance: for the same purpose, non-energy productive parts of the façades can be cladded with the same glazing. A graphical rendering of the outcome is shown in Figure A.6. Considering an energy conversion efficiency equal to 0.5 for solar thermal collectors and to 0.12 for PV modules (including a performance factor of 0.8), the incident solar radiation would be sufficient to cover the energy needs of the unit and even

produce additional energy on an annual basis (Figure A.7). A small reduction of the energy conversion efficiency is foreseen due to the use of a colored glass, which prevents a portion of the solar spectrum from reaching the PV solar module.
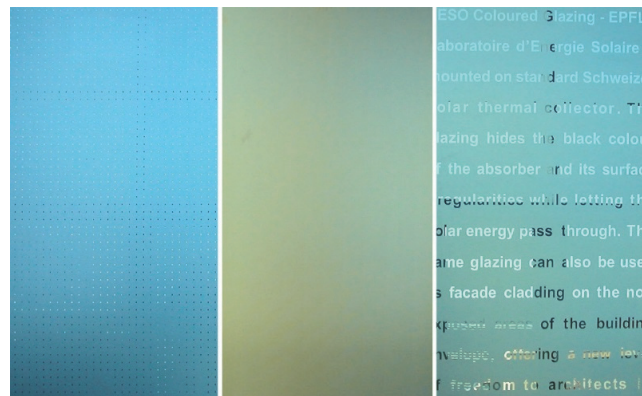
Figure A.5 Swissinso Kromatix ® special coating for colored solar modules

(Photo Credits: Maria Cristina Munari Probst ©)
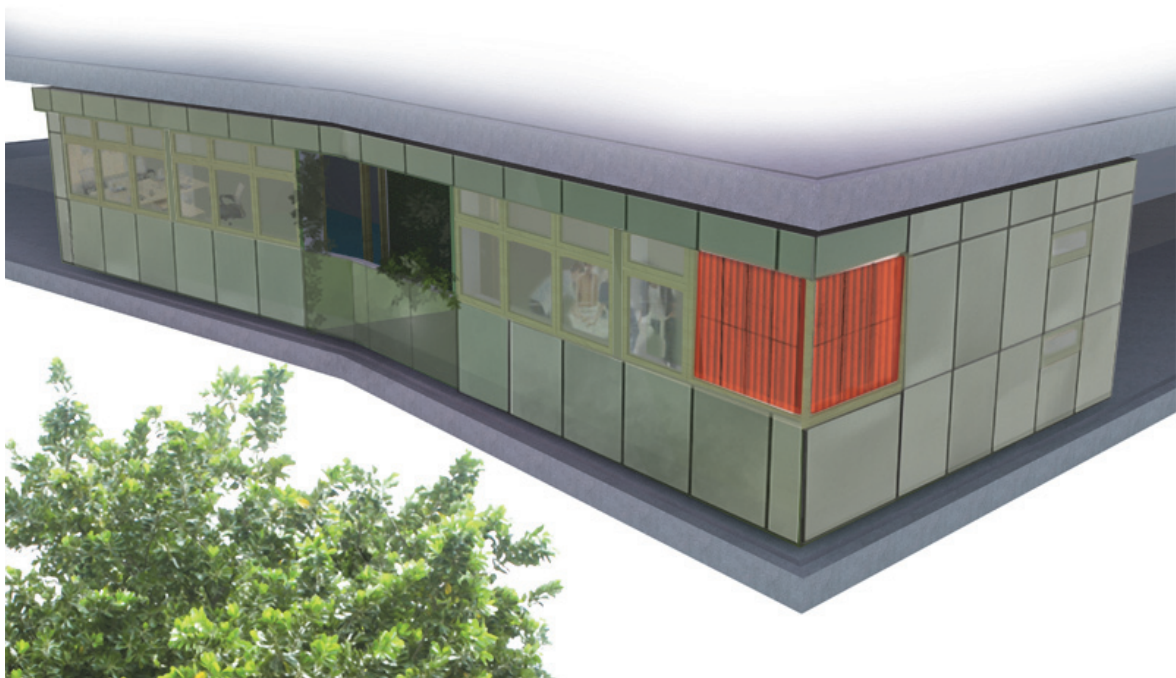
Figure A.6 NEST unit SolAce: preliminary project render

(Used tool: Archicad and Artlantis ©)
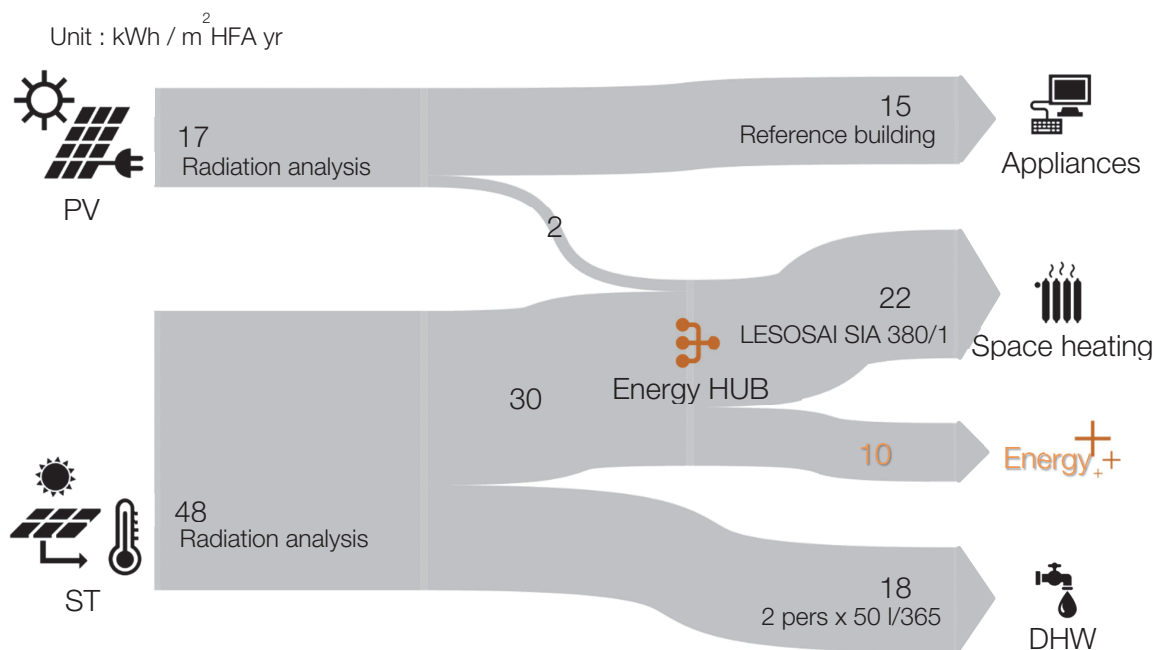
Figure A.7 NEST unit SolAce: Sankey diagram

(Used tool: Grasshopper for Rhino © and Ladybug CC [121])

Yearly electricity demand has been assumed from a highly performative office including lighting, appliances and ventilation, in conformity with the target value of the Swiss norm SIA 380/4 [216]; space heating and domestic hot water needs were calculated according to the Swiss norm SIA 380/1 [215]. An energy-hub is set-up in the building [10], providing an exchange platform for energy surplus injected to an appropriate storage facility and energy needs that are obtained from centralized generation (common to all the units). The heating system of the unit is composed of heating / cooling beams emitting from the ceiling.

A.2   Knowledge and Technology Transfer

Among the interesting outcomes of IEA SHC Task 51, there is a lot of dissemination material within the domain of architectural integration of solar systems. The LESO-QSV method for a wise architectural integration of solar modules [28], [223] has been adapted and tested by international experts on multiple case-studies, with support of its creators [224]. The author himself tested this novel method on a set of case studies, which have been accurately classified and rated using appropriate criteria (see Section 1.4 and Figure A.8a). General trends could be identified and analyzed according to the architectural integration strategy. The author updated accordingly the IEA website "Innovative solar products for building integration", a catalog of solar PV modules with characteristics fostering their integration in the building envelope with

high aesthetic standards (see [225], [226] and Figure A.8b). During the 3 years phase of market monitoring, 20 new product sheets were added to the database, while 8 products were withdrawn from retail and consequently archived in a dedicated section of the website. The reason is mainly the bankrupt of the manufacturing company, which shows a high market volatility in this field.

(a) Test examples of LESO-QSV rating on different categories of buildings

(b) Examples product sheets from the website "Innovative solar products for building integration"

Figure A.8 Dissemination activities

(Author's own elaboration)

The importance of education and training for an effective design of solar energy buildings, districts and cities was the object of a dedicated work package in the task [227]. The author

participated in the redaction of a review gathering relevant university-level courses in Switzerland, which was added to the main report. It is obvious, from the analyzed teaching activities, that the disciplines related to territorial and urban planning involve a broad range of renewable energies within their educational curriculum: those include demand, dispatch and supply characterization. A focus on the territorial scale enhances the need of a qualified expert addressing different spatial planning issues, from energy management to transport infrastructures and land use: currently a tailored educational program for this specific profile is lacking in Switzerland. Nevertheless, the creation of innovative transdisciplinary education programs covering geographical, technical, environmental and urban planning aspects partially tackles this challenge: new master courses, continuous education and master of advanced studies programs are leading in this direction. Within this framework, some disruptive teaching activities have been developed: early interactions between different backgrounds are experimented and the use of innovative decision support tools for envisioning urban scenarios empowers students with new approaches to design. The author contributed to teaching activities within this process, including the following:

i. The assistantship in interdisciplinary courses addressed to architects, civil and environmental engineers beyond traditional building physics lectures (e.g. EPFL course "Integration architecturale de l'Energie Solaire", Bachelor ENAC, Resp. Maria Cristina Munari Probst); among others, workshops addressed to the award-winning Swiss student team participating in the Solar Decathlon 2017 competition;

ii. The elaboration of guidelines on passive and active solar design principles for students in architecture;

iii. The promotion of essential tools to achieve effective solar design in professional practice, including the use of computational architecture.

B. Annexes

Index of Annexes

Annex I.   Strategic planning: Great Geneva area, Switzerland. Cross mapping of visual inter-
est (photographic locations) and sensitivity from ISOS maps.

Used tool: ArcGIS ArcMap © elaboration on CC data from Système d'information du territoire à Genève – SITG.

Original scale : 1 : 10 000

Fig. 2 : shooting locations of photos vs ISOS maps.
Geneva and Carouge metropolitan area

SCALE 1 : 10 000

significant viewpoints

photo shooting location

ISOS Maps.
Federal Inventory of
Swiss Heritage Sites of
national importance.

1	protected perimeters: built precincts which can be perceived as an entity ensembles:
I.1	coherent buildings clusters
XV	meaningful surrounding areas and environment

remarkable building

relevant building
or façade

perturbing element

Annex II.   Development planning: Geneva, Switzerland. Cross mapping of visibility, solar irra-
diation and sensitivity.

Used tool: ArcGIS ArcMap © elaboration on CC data from Système d'information du territoire à Genève – SITG.

Original scale : 1 : 5000

Detailed planning cross-mapping

Genève, Switzerland

Author: Pietro Floris

Legend

Annex III.   Detailed planning: Hollande district, Geneva, Switzerland. Cross mapping of visibility, solar irradiation and sensitivity.

Used tool: Grasshopper for Rhino © elaboration on CC data from Système d'information du territoire à Genève – SITG.

Original scale : 1 : 1000

VA index

[cell size] 1.5 m   [contrast] 100 %

[LogMAR]

> 1.4
0 – 1.4
< 0

Irradiation
[kWh/m² yr]

0-350
350-700
700-1050
1050-1400
< 400
400-800

façades   roofs

N
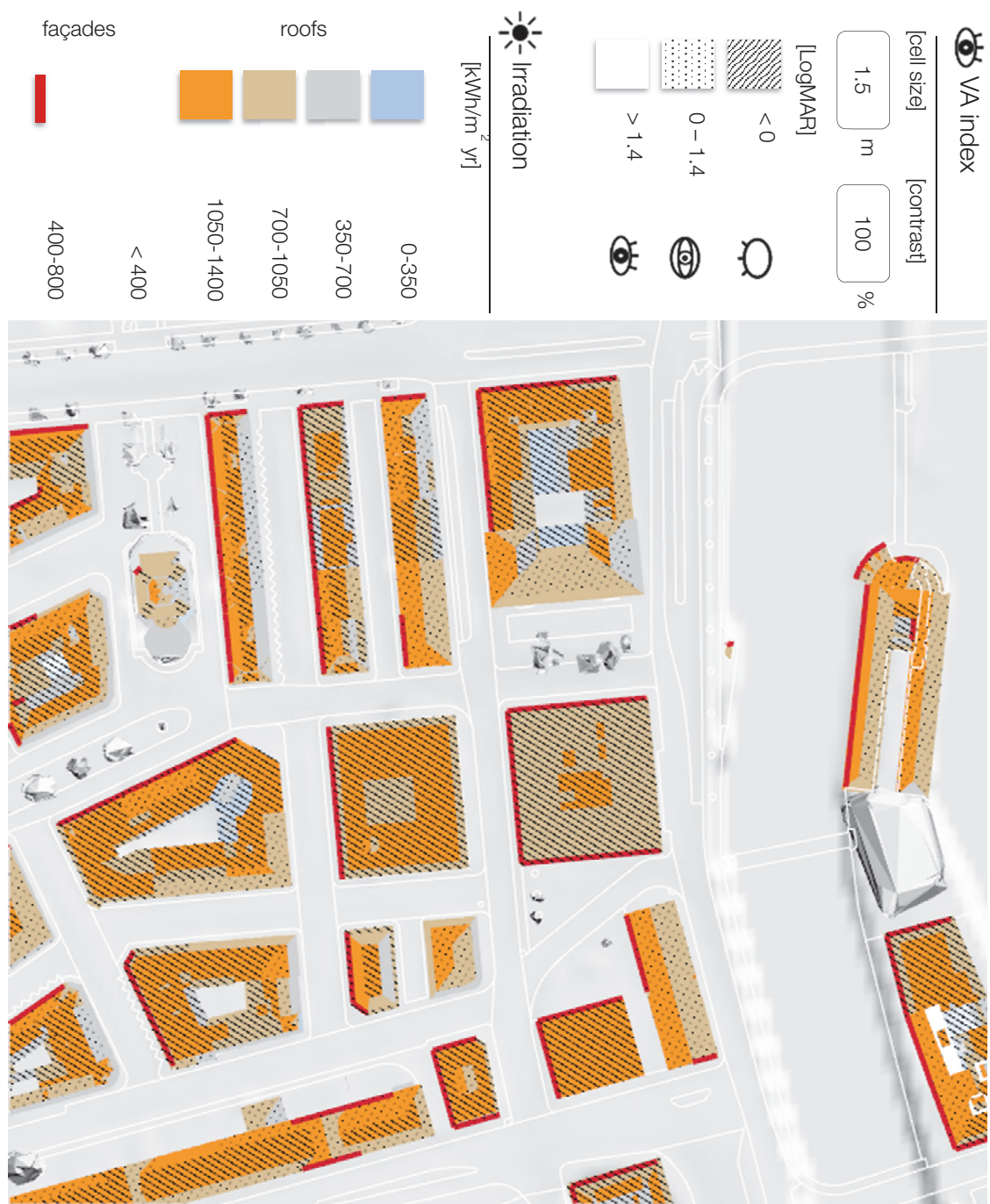
References

[1]   SFOE Swiss Federal Office of Energy, *Messaggio concernente il primo pacchetto di misure della Strategia energetica 2050 e l'iniziativa popolare «Per un abbandono pianificato dell 'energia nucleare (Iniziativa per l'abbandono del nucleare)»*. SFOE, Swiss Federal Office of Energy, 2013.

[2]   Swiss Parliament, *Loi sur l'énergie*. 1998.

[3]   Swiss Parliament, *Loi sur l'aprovisonnement en électricité*. 2007.

[4]   SFOE Swiss Federal Office of Energy, *Plan d'action pour les énergies renouvelables*. SFOE, Swiss Federal Office of Energy, 2008.

[5]   European Commission, *Une politique de l'énergie pour l'Europe*. European Commission, 2007.

[6]   SFOE Swiss Federal Office of Energy, "Schweizerische Statistik der erneuerbaren Energien - Ausgabe 2016," SFOE, Swiss Federal Office of Energy, 2016.

[7]   SFOE Swiss Federal Office of Energy, "Statistique globale Suisse de l'Energie 2016," SFOE, Swiss Federal Office of Energy, 2016.

[8]   European Parliament, *Directive 2010/31/EU of the European Parliament and of the Council on the energy performance of buildings (recast)*. European Parliament, 2010.

[9]   Swiss Parliament, *Ordinance on the Reduction of CO2 Emissions*. Swiss Parliament, 2012.

[10]   M. Geidl, G. Koeppel, P. Favre-Perrod, B. Klöckl, G. Andersson, and K. Fröhlich, "The Energy Hub: a powerful concept for future energy systems," in *3rd Annual Carnegie Mellon Conference on the Electricity Industry*, 2007.

[11]   BPIE Building Performance Institute Europe, "Principles for Nearly Zero Energy Buildings / Paving the way for effective implementation of policy requirements," 2011.

[12]   SFOE Swiss Federal Office of Energy, "Sécurité d'approvisionnement et développement de la concurrence sous la LApEl et l'OApEl," 2013.

[13]   United Nations, "World Urbanization Prospects," 2014.

[14]   I. Nolte and D. Strong, "Europe' s buildings under the microscope," 2011.

[15]   International Energy Agency IEA, "Potential for building integrated photovoltaics," 2002.

[16]   International Energy Agency IEA, "Technology Roadmap: Solar Photovoltaic Energy," 2014.

[17]   H. L. Zhang, T. Van Gerven, J. Baeyens, J. Degrève, and J. Ve, "Photovoltaics: reviewing the European Feed-in-Tariffs and changing PV efficiencies and costs.," *ScientificWorldJournal.*, vol. 2014, p. 404913, 2014.

[18]   J. J. Wang, Y. Y. Jing, C. F. Zhang, and J. H. Zhao, "Review on multi-criteria decision analysis aid in sustainable energy decision-making," *Renew. Sustain. Energy Rev.*, vol. 13, no. 9, pp. 2263–2278, 2009.

[19]   J. P. Huang, K. L. Poh, and B. W. Ang, "Decision analysis in energy and environmental modeling," *Energy*, vol. 20, no. 9, pp. 843–855, 1995.

[20]   G. H. Brundtland, "Our Common Future: Report of the World Commission on Environment and Development," 1987.

[21]   P. Zhou, B. W. Ang, and K. L. Poh, "Decision analysis in energy and environmental modeling: an update," *Energy*, vol. 31, no. 14, pp. 2604–2621, 2006.

[22]   S. D. Pohekar and M. Ramachandran, "Application of multi-criteria decision making to sustainable energy planning—A review," *Renew. Sustain. Energy Rev.*, vol. 8, no. 4, pp. 365–381, 2004.

[23]   L. A. Greening and S. Bernow, "Design of coordinated energy and environmental policies: Use of multi-criteria decision-making," *Energy Policy*, vol. 32, no. 6, pp. 721–735, 2004.

[24]   E. Løken, "Use of multicriteria decision analysis methods for energy planning problems," *Renew. Sustain. Energy Rev.*, vol. 11, no. 7, pp. 1584–1595, 2007.

[25]   P. S. Brandon, P. Lombardi, and G. Q. Shen, "Future Challenges in Evaluating and Managing Sustainable Development in the Built Environment," Wiley, 2017.

[26]   F. Cavallaro and L. Ciraolo, "A multicriteria approach to evaluate wind energy plants on an Italian island," *Energy Policy*, vol. 33, no. 2, pp. 235–244, 2005.

[27]   G. Dall'O', M. F. Norese, A. Galante, and C. Novello, "A multi-criteria methodology to support public administration decision making concerning sustainable energy action plans," *Energies*, vol. 6, no. 8, pp. 4308–4330, 2013.

[28]   M. C. Munari Probst and C. Roecker, "Solar energy promotion & urban context protection: LESO-QSV (Quality - Site - Visibility) Method," in *31th International PLEA Conference*, 2015.

[29]   Swiss Parliament, *Loi fédérale sur l 'aménagement du territoire*. Assemblée fédérale de la Confédération suisse, 2014, pp. 1–22.

[30]   J. Ducret, "Le bâtir écolo en butte à la liberté des communes," *24heures*, 12-Jan-2016.

[31]   M. C. Munari Probst and C. Roecker, "Urban acceptability of Building Integrated Solar Systems : LESO-QSV approach," in *Eurosun 2011*, 2011.

[32]   R. Krippner and T. Herzog, "Architectural aspects of solar techniques – Studies on the integration of solar energy systems," in *EuroSun 2000*, 2000.

[33]   M. C. Munari Probst, "Architectural Integration and Design of Solar Thermal Systems," EPFL Thesis n. 4258, 2009.

[34]   M. C. Munari Probst and C. Roecker, Eds., *Solar energy systems in architecture*, DA 2. IEA SHC Task 41, 2012.

[35]   J. Dahlberg and M. Lundgren, Eds., *Approaches, Methods and Tools for Solar Energy in Urban Planning*, DB4 ed. IEA SHC Task 51, 2018.

[36]   "Prize Årets Framtidsbyggare: Innovator of the year 2016. Sweden November 15th 2016." [Online]. Available: http://aretsframtidsbyggare.se/wp-content/uploads/2016/05/Pressmeddelande-Årets-Framtidsbyggare-161116.docx.

[37]   J. Smythies, "A Note on the Concept of the Visual Field in Neurology, Psychology, and Visual Neuroscience," *Perception*, vol. 25, no. 3, pp. 369–371, Mar. 1996.

[38]   J. Panero and M. Zelink, *Human dimension & interior space. A source book of design reference standard.*, Watson-Gup. New York, 1979.

[39]   P. Riordan-Eva and E. T. Cunningham, *Vaughan & Asbury's General Ophthalmology, 18th Edition*. McGraw-Hill Education, 2011.

[40]   C.-A. Roulet, *Santé et qualité de l'environnement intérieur dans les bâtiments*, 2e éd. mis. Lausanne: Presses Polytechniques et Universitaires Romandes, 2008.

[41]   B. Wandell, *Foundations of vision*, Sinauer As. Sunderland, Massachussets, 1995.

[42]   G. Wald, "The receptors of human color vision," *Science*, vol. 145, no. 3636, pp. 1007–16, Sep. 1964.

[43]   M. Burns and T. Lamb, "Visual Transduction by Rod and Cone Photoreceptors," in *The visual neuroscience*, no. 2003, 2003, pp. 215–233.

[44]   E. B. Goldstein, *Sensation and Perception*. 2009.

[45]   S. Kuffler, "Discharge patterns and functional organization of mammalian retina.," *J. Neurophysiol.*, vol. 16, no. 1, pp. 37–68, Jan. 1953.

[46]   B. A. Wandell, S. O. Dumoulin, and A. A. Brewer, "Visual Field Maps in Human Cortex," *Neuron*, vol. 56, no. 2, pp. 366–383, Oct. 2007.

[47]   A. D. Milner and M. A. Goodale, *The visual brain in action*. Oxford University Press, 2006.

[48]   Hunter Associates Laboratory, "CIE Standard Observers," *Appl. Note*, vol. 19, no. 10, 2008.

[49]   H. E. Bedell, "Spatial Acuity," in *The Psychophysical Measurement of Visual Function*, T. T. Norton, D. A. Corliss, and J. E. Bailey, Eds. Butterworth-Heinemann, 2002, p. 362.

[50]   G. T. Fechner, *Elemente der psychophysik*. Leipzig : Breitkopf und Härtel, 1860.

[51]   S. S. Stevens, "The surprising simplicity of sensory metrics.," *Am. Psychol.*, vol. 17, no. 1, pp. 29–39, 1962.

[52]   I. L. Bailey and J. E. Lovie, "New design principles for visual acuity letter charts.," *Am. J. Optom. Physiol. Opt.*, vol. 53, no. 11, pp. 740–5, Nov. 1976.

[53]   World Meteorological Organization, "Measurement of Visibility," in *Guide to Meteorological Instruments and Methods of Observation*, pp. 1–15.

[54]   E. Guerra, J. de Lara, A. Malizia, and P. Díaz, "Supporting user-oriented analysis for multi-view domain-specific visual languages," in *Information and Software Technology*, vol. 51, no. 4, 2009, pp. 769–784.

[55]   J. H. Seinfeld and S. N. Pandis, *Atmospheric Chemistry and Physics: From Air Pollution to Climate Change*. Wiley, 2016.

[56]   M. Stokes, M. Anderson, S. Chandrasekar, and R. Motta, "A Standard Default Color Space for the Internet - sRGB," 1996. [Online]. Available: https://www.w3.org/Graphics/Color/sRGB.html. [Accessed: 21-Dec-2017].

[57]   A. R. Robertson, "The CIE 1976 Color-Difference Formulae," *Color Res. Appl.*, vol. 2, no. 1, pp. 7–11, Mar. 1977.

[58]   R. L. De Valois, I. Abramov, and G. H. Jacobs, "Analysis of Response Patterns of LGN Cells," *J. Opt. Soc. Am.*, vol. 56, no. 7, p. 966, Jul. 1966.

[59]   R. Chiabrando, E. Fabrizio, and G. Garnero, "On the applicability of the visual impact assessment OAISPP tool to photovoltaic plants," *Renew. Sustain. Energy Rev.*, vol. 15, no. 1, pp. 845–850, 2011.

[60]   M. Mahy, L. Eycken, and A. Oosterlinck, "Evaluation of Uniform Color Spaces Developed after the Adoption of CIELAB and CIELUV," *Color Res. Appl.*, vol. 19, no. 2, pp. 105–121, Apr. 1994.

[61]   G. Garnero and E. Fabrizio, "Visibility analysis in urban spaces : a raster-based approach and case studies," *Environ. Plan. B Plan. Des.*, vol. 42, 2015.

[62]   M. Rodrigues, C. Montañés, and N. Fueyo, "A method for the assessment of the visual impact caused by the large-scale deployment of renewable-energy facilities," *Environ. Impact Assess. Rev.*, vol. 30, no. 4, pp. 240–246, 2010.

[63]   B. C. Chamberlain and M. J. Meitner, "A route-based visibility analysis for landscape management," *Landsc. Urban Plan.*, vol. 111, no. 1, pp. 13–24, 2013.

[64]   S. Chmielewski, D. J. Lee, P. Tompalski, T. J. Chmielewski, and P. Wężyk, "Measuring visual pollution by outdoor advertisements in an urban street using intervisibilty analysis and public surveys," *Int. J. Geogr. Inf. Sci.*, vol. 30, no. 4, pp. 801–818, Apr. 2016.

[65]   A. Minelli, I. Marchesini, F. E. Taylor, P. De Rosa, L. Casagrande, and M. Cenci, "An open source GIS tool to quantify the visual impact of wind turbines and photovoltaic panels," *Environ. Impact Assess. Rev.*, vol. 49, pp. 70–78, 2014.

[66]   H. Shang and I. D. Bishop, "Visual Thresholds for Detection, Recognition and Visual Impact in Landscape Settings," *J. Environ. Psychol.*, vol. 20, no. 2, pp. 125–140, 2000.

[67]   G. Humphrey, "The Psychology of the Gestalt.," *J. Educ. Psychol.*, vol. 15, no. 7, pp. 401–412, 1924.

[68]   I. Biederman, "Recognition-by-Components: A Theory of Human Image Understanding An Analogy Between Speech and Object Perception," *Psychol. Rev.*, no. 2, pp. 115–147, 1917.

[69]   R. Gregory, "Emmert's Law and the moon illusion," *Spat. Vis.*, vol. 21, no. 3, pp. 407–420, May 2008.

[70]   R. Xu, "Visual Impact Assessment of BIPV in facade retrofits using saliency models," EPFL, 2016.

[71]   R. Xu and S. Wittkopf, "Visual assessment of BIPV retrofit design proposals for selected historical buildings using the saliency map method," vol. 2, pp. 235–254, 2014.

[72]   D. Walther and C. Koch, "Modeling attention to salient proto-objects," *Neural Networks*, vol. 19, no. 9, pp. 1395–1407, Nov. 2006.

[73]   A. M. Treisman and G. Gelade, "A feature-integration theory of attention," *Cogn. Psychol.*, vol. 12, no. 1, pp. 97–136, Jan. 1980.

[74]   J. J. Gibson, *The perception of the visual world*, The Rivers. Cambridge, 1950.

[75]   S. Nijhuis, R. Van Lammeren, and F. Van der Hoeven, Eds., *Exploring the Visual Landscape*. Delft: IOS Press, Delft University Press, 2011.

[76]   K. Lynch, "The image of the environment - The city form," in *The Image of the City*, The Techno., Cambridge, 1960, p. Ch 1-3, App. A&B.

[77]   G. Cullen, *The Concise Townscape*, Architectu. 1961.

[78]   I. de Wolfe, K. Browne, and I. de Wolfe, *The Italian townscape*. London: Architectural Press, 1963.

[79]   E. N. Bacon, *Design of Cities*, Viking Pre. New York, 1974.

[80]   P. Thiel, "A Sequence-Experience Notation: For Architectural and Urban Spaces," *Town Plan. Rev.*, vol. 32, no. 1, pp. 33–52, 1961.

[81]   C. R. V Tandy, "The isovist method of landscape survey," in *Methods of Landscape Analysis*, H. C. Murray, Ed. London, 1967.

[82]   T. Higuchi, *The visual and spatial structure of landscapes*. Cambridge - Mass.& London: MIT Press, 1983.

[83]   K. Lynch, *Managing the sense of a region*. Cambridge - Mass.& London: MIT Press, 1976.

[84]   M. R. Travis, G. H. Elsner, W. D. Iverson, and C. G. Johnson, "VIEWIT: computation of seen areas, slope, and aspect for land-use planning," 1975.

[85]   M. Llobera, "Extending GIS-based visual analysis: the concept of visualscapes," pp. 25–48, 2003.

[86]   D. Wheatley, "Cumulative viewshed analysis," *Archaeol. Geogr. Inf. Syst. a Eur. Perspect.*, pp. 171–185, 1995.

[87]   M. Groß, "The analysis of visibility—Environmental interactions between computer graphics, physics, and physiology," *Comput. Graph.*, vol. 15, no. 3, pp. 407–415, Jan. 1991.

[88]   J. M. Domingo-Santos, R. F. de Villarán, I. Rapp-Arrarás, and E. C. P. de Provens, "The visual exposure in forest and rural landscapes: An algorithm and a GIS tool," *Landsc. Urban Plan.*, vol. 101, no. 1, pp. 52–58, 2011.

[89]   W. D. Iverson, "And That's About the Size of It: Visual Magnitude as a Measurement of the Physical Landscape," *Landscape Journal*, vol. 4. University of Wisconsin Press, pp. 14–22, 1985.

[90]   A. Grêt-Regamey, I. D. Bishop, and P. Bebi, "Predicting the scenic beauty value of mapped landscape changes in a mountainous region through the use of GIS," *Environ. Plan. B Plan. Des.*, vol. 34, no. 1, pp. 50–67, 2007.

[91]   D. Nutsford, F. Reitsma, A. L. Pearson, and S. Kingham, "Personalising the Viewshed: Visibility analysis from the human perspective," *Appl. Geogr.*, vol. 62, pp. 1–7, 2015.

[92]   M. L. Benedikt, "To take hold of space: isovists and isovist fields," *Environment and Planning B: Planning and Design*, vol. 6, no. 1. pp. 47–65, 1979.

[93]   C. Davies, R. Mora, and D. Peebles, "Isovists for Orientation: can space syntax help us predict directional confusion?," in *Proceedings of the Space Syntax and Spatial Cognition Workshop*, 2006.

[94]   T. Leduc and G. Chauvat, "Étude Comparée De Quatre Indicateurs Qualifiant Le Champ Visuel D'Un Piéton En Milieu Urbain," *Rev. Int. Géomatique*, vol. 25, no. 1, pp. 75–98, 2015.

[95]   M. Batty, "Exploring isovist fields: Space and shape in architectural and urban morphology," *Environ. Plan. B Plan. Des.*, vol. 28, no. 1, pp. 123–150, 2001.

[96]   A. Turner, M. Doxa, D. O'Sullivan, and A. Penn, "From isovists to visibility graphs: A methodology for the analysis of architectural space," *Environ. Plan. B Plan. Des.*, vol. 28, no. 1, pp. 103–121, 2001.

[97]   T. Leduc and O. Kontovourkis, "Towards a mixed approach combining visibility and mobility studies to analyze the Eleftheria Square, Nicosia (CY)," *3D Issues Urban Environ. Syst.*, no. 1, pp. 67–77, 2012.

[98]   A. E. Stamps, "Isovists, enclosure, and permeability theory," *Environ. Plan. B Plan. Des.*, vol. 32, no. 5, pp. 735–762, 2005.

[99]   R. Conroy-Dalton and N. Dalton, "OmniVista:an application for isovist field and path analysis," 2001.

[100]   P. Bartie, F. Reitsma, S. Kingham, and S. Mills, "Advancing visibility modelling algorithms for urban environments," *Comput. Environ. Urban Syst.*, vol. 34, no. 6, pp. 518–531, 2010.

[101]   S. Rana, "Isovist Analyst - An ArcView Extension for Planning Visual Surveillance," in *ESRI International User Conference*, 2006.

[102]   P. M. C. Christian Derix, Åsmund Gamlesæter, "3d Isovists and Spatial Sensations: two methods and a case study," in *EDRA 39th Annual Conference*, 2008.

[103]   E. Morello and C. Ratti, "A digital image of the city: 3D isovists in Lynch's urban analysis," *Environ. Plan. B Plan. Des.*, vol. 36, no. 5, pp. 837–853, 2009.

[104]   W. Suleiman, T. Joliveau, and E. Favier, "A New Algorithm for 3D Isovist," in *15th International Symposium on Spatial Data Handling Geospatial dynamics, geosimulation and exploratory visualization*, 2012.

[105]   R. C. Dalton and N. S. Dalton, "The problem of representation of 3D isovists," in *Proceedings of the 10th International Space Syntax Symposium*, 2015.

[106]   B. Hillier and J. Hanson, *The Social Logic of Space*, Cambridge. Cambridge, 1984.

[107]   T. Varoudis and S. Psarra, "Beyond two dimensions: Architecture through three-dimensional visibility graph analysis," *J. Sp. Syntax*, vol. 5, no. 1, 2014.

[108]   J. Peponis, J. Wineman, M. Rashid, S. Hong Kim, and S. Bafna, "On the description of shape and spatial configuration inside buildings: Convex partitions and their local properties," *Environment and Planning B: Planning and Design*, vol. 24, no. 5. pp. 761–781, 1997.

[109]   T. Leduc, F. Miguet, and V. Tourre, "Motion Perspectives Integration in the Qualification of the Urban Spaces: Towards a 2D- and a 3D-Enrichment of the S-Partition Method," in *Urban Design and Representation*, Cham: Springer International Publishing, 2017, pp. 69–82.

[110]   J. Krukar and C. Schultz, "Incorporating cognitively-motivated semantics ospace' and the architectural environment in 3D visibility analysis," in *Proceedings of the 11th Space Syntax Symposium*, 2017.

[111]   G. T. Johnson, I. D. Watson, G. T. Johnson, and I. D. Watson, "The Determination of View-Factors in Urban Canyons," *J. Clim. Appl. Meteorol.*, vol. 23, no. 2, pp. 329–335, Feb. 1984.

[112]   T. R. Oke, "Canyon geometry and the nocturnal urban heat island: Comparison of scale model and field observations," *J. Climatol.*, vol. 1, no. 3, pp. 237–254, Jul. 1981.

[113]   J. Wen, L. Liao, M. Mônica, and M. Cavaleri, "The Study of Sky View Factor in Urban Morphologies: Computational Tools and Methods of Analysis," in *PLEA 2014*, 2014.

[114]   J. Teller, "A spherical metric for the field-oriented analysis of complex urban open spaces," *Environ. Plan. B Plan. Des.*, vol. 30, no. 3, pp. 339–356, 2003.

[115]   D. Fisher-Gewirtzman, M. Burt, and Y. Tzamir, "A 3-D visual method for comparative evaluation of dense built-up environments," *Environ. Plan. B Plan. Des.*, vol. 30, pp. 575–587, 2003.

[116]   D. Shach-Pinsly, D. Fisher-Gewirtzman, and M. Burt, "Visual Exposure and Visual Openness: An Integrated Approach and Comparative Evaluation," *J. Urban Des.*, vol. 16, no. 2, pp. 233–256, 2011.

[117]   P. P. J. Yang, S. Y. Putra, and W. Li, "Viewsphere: A GIS-based 3D visibility analysis for urban design evaluation," *Environ. Plan. B Plan. Des.*, vol. 34, no. 6, pp. 971–992, 2007.

[118]   T. Ortner, J. Sorger, H. Steinlechner, G. Hesina, H. Piringer, and E. Groller, "Vis-A-Ware: Integrating Spatial and Non-Spatial Visualization for Visibility-Aware Urban Planning," *IEEE Trans. Vis. Comput. Graph.*, vol. 23, no. 2, pp. 1139–1151, Feb. 2017.

[119]   T. Lin, H. Lin, and M. Hu, "Three-dimensional visibility analysis and visual quality computation for urban open spaces aided by Google SketchUp and WebGIS," *Environ. Plan. B Plan. Des.*, 2015.

[120]   P. Suppes, "Is Visual Space Euclidean?," in *Models and Methods in the Philosophy of Science: Selected Essays*, Dordrecht: Springer Netherlands, 1993, pp. 373–393.

[121]   M. P. Mostapha Sadeghipour Roudsari and U. S. A. Adrian Smith + Gordon Gill Architecture, Chicago, "Ladybug: a Parametric Environmental Plugin for Grasshopper To Help Designers Create an Environmentally-Conscious Design," *13th Conf. Int. Build. Perform. Simul. Assoc.*, pp. 3129–3135, 2013.

[122]   D. Fisher-Gewirtzman, "Integrating 'weighted views' to quantitative 3D visibility analysis as a predictive tool for perception of space," *Environ. Plan. B Plan. Des.*, Nov. 2016.

[123]   A. Koltsova, B. Tunçer, and G. Schmitt, "Visibility Analysis for 3D Urban Environments," in *Computation and Performance - eCAADe 31*, 2013, vol. 2, pp. 375–384.

[124]   B. C. Arabacioglu, "Using fuzzy inference system for architectural space analysis," *Appl. Soft Comput.*, vol. 10, no. 3, pp. 926–937, Jun. 2010.

[125]   T. P. Lin, H. Lin, and M. Y. Hu, "3D visibility analysis in urban environment - cognition research based on VGE," in *ISPRS Annals of the Photogrammetry, Remote Sensing and Spatial Information Sciences*, 2013, vol. II, no. November, pp. 27–29.

[126]   P. E. Lizcano, C. Manchado, V. Gomez-Jauregui, and C. Otero, "Virtual reality to assess visual impact in wind energy projects," in *Advances on Mechanics, Design Engineering and Manufacturing*, Eynard B., Nigrelli V., Oliveri S., Peris-Fajarnes G., and Rizzuti S., Eds. Springer, Cham, 2017, pp. 717–725.

[127]   K. Chamilothori, J. Wienold, and M. Andersen, "Adequacy of Immersive Virtual Reality for the Perception of Daylit Spaces: Comparison of Real and Virtual Environments," 2018.

[128]   M. Ayadi, L. Suta, M. Scuturici, S. Miguet, and C. Ben Amar, "A Parametric Algorithm for Skyline Extraction," in *Advanced Concepts for Intelligent Vision Systems*, 2016, pp. 604–615.

[129]   R. Kaplan and S. Kaplan, *The experience of nature : a psychological perspective*. Cambridge University Press, 1989.

[130]   W. E. Dramstad, M. S. Tveit, W. J. Fjellstad, and G. L. A. Fry, "Relationships between visual landscape preferences and map-based indicators of landscape structure," *Landsc. Urban Plan.*, vol. 78, no. 4, pp. 465–474, Nov. 2006.

[131]   J. Teller and M. Ginzarly, "Deriving cultural heritage values : the use of social media," in *Delli Aspetti de Paesi*, 2016, no. November.

[132]   I. D. Bishop and D. R. Miller, "Visual assessment of off-shore wind turbines: The influence of distance, contrast, movement and social variables," *Renew. Energy*, vol. 32, no. 5, pp. 814–831, Apr. 2007.

[133]   Swiss Parliament, *Loi fédérale sur la protection de l'environnement*. 1983.

[134]   European Parliament, *Directive 2014/52/EU of the European Parliament and of the Council of 16 April 2014 amending Directive 2011/92/EU on the assessment of the effects of certain public and private projects on the environment*. European Parliament, 2014.

[135]   D. Apostal, J. Palmer, M. Pasqualetti, R. Smardon, and R. Sullivan, *The renewable energy landscape : preserving scenic values in our sustainable future*. London: Routledge, Taylor & Francis Group, 2017.

[136]   C. Cassatella, "Linee guida per l'analisi, la tutela e la valorizzazione degli aspetti scenico-percettivi del paesaggio," Torino, 2014.

[137]   K. Rezakhanlou and E. Frei, "Etude d'integration des panneaux solaires dans la zone ville et villages / Commune de Lutry," 2011.

[138]   J. P. Hurtado, J. Fernández, J. L. Parrondo, and E. Blanco, "Spanish method of visual impact evaluation in wind farms," *Renew. Sustain. Energy Rev.*, vol. 8, no. 5, pp. 483–491, 2004.

[139]   L. A. Fernandez-Jimenez, M. Mendoza-Villena, P. Zorzano-Santamaria, E. Garcia-Garrido, P. Lara-Santillan, E. Zorzano-Alba, and A. Falces, "Site selection for new PV power plants based on their observability," *Renew. Energy*, vol. 78, pp. 7–15, 2015.

[140]   A. Scognamiglio, "'Photovoltaic landscapes': Design and assessment. A critical review for a new transdisciplinary

design vision," *Renew. Sustain. Energy Rev.*, vol. 55, pp. 629–661, Mar. 2016.

[141] M. C. Munari Probst and C. Roecker, *Architectural integration and design of solar thermal systems*. Lausanne: EPFL Press, 2011.

[142] I. Zanetti, K. Nagel, and D. Chianese, "Concepts for Solar Integration. Development of Technical and Architectural Guidelines for Solar System Integration in Historical Buildings," in *25th European Photovoltaic Solar Energy Conference and Exhibition / 5th World Conference on Photovoltaic Energy Conversion*, 2010, pp. 5105–5109.

[143] F. Frontini, M. Manfren, and L. C. Tagliabue, "A Case Study of Solar Technologies Adoption: Criteria for BIPV Integration in Sensitive Built Environment," *Energy Procedia*, vol. 30, pp. 1006–1015, 2012.

[144] A. del C. Torres-Sibille, V.-A. Cloquell-Ballester, V.-A. Cloquell-Ballester, and M. A. Artacho Ramírez, "Aesthetic impact assessment of solar power plants: An objective and a subjective approach," *Renew. Sustain. Energy Rev.*, vol. 13, pp. 986–999, 2009.

[145] T. Rose and A. Wollert, "The dark side of photovoltaic — 3D simulation of glare assessing risk and discomfort," *Environ. Impact Assess. Rev.*, vol. 52, pp. 24–30, 2015.

[146] R. Chiabrando, E. Fabrizio, and G. Garnero, "The territorial and landscape impacts of photovoltaic systems: Definition of impacts and assessment of the glare risk," *Renew. Sustain. Energy Rev.*, vol. 13, pp. 2441–2451, 2009.

[147] J. A. Jakubiec and C. F. Reinhart, "Authors : Abstract Disability glare , visual impairment due to extreme brightness or contrast , can be caused by intense reflections from new constructions nearby existing transportation or building infrastructure . A case study analysis is performed of a," *Transp. Res. Rec. J. Transp. Res. Board*, vol. 2449, no. 1, pp. 114–122, 2014.

[148] J. B. Graham, J. R. Stephenson, and I. J. Smith, "Public perceptions of wind energy developments: Case studies from New Zealand," *Energy Policy*, vol. 37, no. 9, pp. 3348–3357, Sep. 2009.

[149] E. Strantzali and K. Aravossis, "Decision making in renewable energy investments: A review," *Renew. Sustain. Energy Rev.*, vol. 55, pp. 885–898, 2016.

[150] R. Wüstenhagen, M. Wolsink, and M. J. Bürer, "Social acceptance of renewable energy innovation: An introduction to the concept," *Energy Policy*, vol. 35, no. 5, pp. 2683–2691, 2007.

[151] P. Haurant, P. Oberti, and M. Muselli, "Multicriteria selection aiding related to photovoltaic plants on farming fields on Corsica island: A real case study using the ELECTRE outranking framework," *Energy Policy*, vol. 39, no. 2, pp. 676–688, 2011.

[152] G. Di Giovanni and P. Bonomo, "Analysis of the levels of PV integrability and definition of a performance scheme to control a BIPV project," in *SB11 Helsinki World Sustainable Building Conference*, 2011.

[153] G. Higgs, R. Berry, D. Kidner, and M. Langford, "Using IT approaches to promote public participation in renewable energy planning: Prospects and challenges," *Land use policy*, vol. 25, no. 4, pp. 596–607, Oct. 2008.

[154] S. Izquierdo, M. Rodrigues, and N. Fueyo, "A method for estimating the geographical distribution of the available roof surface area for large-scale photovoltaic energy-potential evaluations," *Sol. Energy*, vol. 82, no. 10, pp. 929–939, 2008.

[155] K. Fath, J. Stengel, W. Sprenger, H. R. Wilson, F. Schultmann, and T. E. Kuhn, "A method for predicting the economic potential of (building-integrated) photovoltaics in urban areas based on hourly Radiance simulations," *Sol. Energy*, vol. 116, pp. 357–370, 2015.

[156] J. Kanters, M. Wall, and E. Kjellsson, "The Solar Map as a Knowledge Base for Solar Energy Use," *Energy Procedia*, vol. 48, pp. 1597–1606, Jan. 2014.

[157] R. L. Knowles, *Sun rhythm form*. Cambridge, Mass: MIT Press, 1981.

[158] I. G. Capeluto and E. Shaviv, "Modeling the design of urban fabric with solar right considerations," in *ISES*, 1997.

[159] E. Morello and C. Ratti, "Sunscapes: 'Solar envelopes' and the analysis of urban DEMs," *Comput. Environ. Urban Syst.*, vol. 33, no. 1, pp. 26–34, Jan. 2009.

[160] A. Vartholomaios, "The residential solar block envelope: A method for enabling the development of compact urban blocks with high passive solar potential," *Energy Build.*, vol. 99, pp. 303–312, Jul. 2015.

[161]   J. Dahlberg, M. Lundgren, and M. Snow, Eds., *Current Status of Solar Energy in Urban Planning*, DA1-DB1 ed. IEA SHC Task 51, 2018.

[162]   City of New York, *Building Zone Resolution*. 1916.

[163]   Greater London Authority, "London View Management Framework SPG," London, 2012.

[164]   Atelier Parisien d'Urbanisme, "La fabrique du paysage métropolitain," Paris, 2014.

[165]   UNESCO, "Recommendation on the historic urban landscape," Paris, 2011.

[166]   Leporello, "Explications relatives à l'Inventaire Fédéral des Sites construits d'importance nationale (ISOS)," 2011.

[167]   Service des Bâtiments, "Recensement architectural du canton de Vaud," Lausanne, 2002.

[168]   A. Dubey, N. Naik, D. Parikh, R. Raskar, and C. A. Hidalgo, "Deep Learning the City: Quantifying Urban Perception At A Global Scale," in *ECCV 2016*.

[169]   A. Danalet, "Activity choice modeling for pedestrian facilities," EPFL Thesis n. 6806, 2015.

[170]   F. Girardin, A. Vaccari, A. Gerber, A. Biderman, and C. Ratti, "Quantifying urban attractiveness from the distribution and density of digital footprints *," *Int. J. Spat. Data Infrastructures Res.*, vol. 4, pp. 175–200, 2009.

[171]   F. Orsi and D. Geneletti, "Using geotagged photographs and GIS analysis to estimate visitor flows in natural areas," *J. Nat. Conserv.*, vol. 21, no. 5, pp. 359–368, 2013.

[172]   T. Tammet, A. Luberg, and P. Järv, "Sightsmap: Crowd-Sourced Popularity of the World Places," in *Information and Communication Technologies in Tourism 2013: Proceedings of the International Conference in Innsbruck, Austria, January 22-25, 2013*, 2013, pp. 314–325.

[173]   J. C. García-Palomares, J. Gutiérrez, and C. Mínguez, "Identification of tourist hot spots based on social networks: A comparative analysis of European metropolises using photo-sharing services and GIS," *Appl. Geogr.*, vol. 63, pp. 408–417, 2015.

[174]   E. Fischer, "Geneva map of tourists vs local residents photographs," 2015. [Online]. Available: https://www.mapbox.com/labs/twitter-gnip/locals/#14/46.2147/6.1323. [Accessed: 07-Mar-2018].

[175]   A. Mislove, H. S. Koppula, K. P. Gummadi, P. Druschel, and B. Bhattacharjee, "Growth of the flickr social network," in *Proceedings of the first workshop on Online social networks - WOSP '08*, 2008, p. 25.

[176]   B. W. Silverman, *Density estimation for statistics and data analysis*, CRC press. 1986.

[177]   M. De Smith, M. Goodchild, and P. Longley, *Geospatial analysis. A Comprehensive guide to Principles, Techniques and Software tools*. The Winchelsea Press, 2015.

[178]   P. Fu and P. M. Rich, *The Solar Analyst 1.0 Manual*. Helios Environmental Modeling Institute (HEMI), 2000.

[179]   Swiss Federal Council, *Ordonnance sur la protection des biens culturels en cas de conflit armé, de catastrophe ou de situation d'urgence*. 2014.

[180]   P. Florio, M. C. Munari Probst, A. Schüler, and J.-L. Scartezzini, "Visual prominence vs architectural sensitivity of solar applications in existing urban areas: an experience with web-shared photos.," in *CISBAT 2017*, 2017.

[181]   P. Florio, M. C. Munari Probst, C. Roecker, A. Schüler, and J.-L. Scartezzini, "Assessing visibility in multi-scale urban planning: a contribution to a method enhancing social acceptability of solar energy in cities," *Forthcoming*.

[182]   R. Van der Ham and J. Idding, "De landschapstypologie naar visuele kenmerken. Methoden en gebruik.," 1971.

[183]   Grand Conseil de la République et canton de Genève, *Loi sur la protection des monuments, de la nature et des sites (LPMNS)*. 1976.

[184]   Service des monuments et des sites, *Répertoire des immeubles classés, immeubles à l'inventaire, ensembles XIXe/XXe s., autres immeubles protégés*. Genève, 1989.

[185]   E. Zanchetta, "Potentiel photovoltaïque en façade Etude de cas : District Jonction , Genève," Lausanne, 2016.

[186]   N. Mohajeri, D. Assouline, B. Guiboud, and J.-L. Scartezzini, "Does roof shape matter? Solar PV integration on Roofs,"

in *Sustainable Built Environment (SBE) Regional Conference Zurich 2016.*, 2016, pp. 130–135.

[187]   J. A. Jakubiec and C. F. Reinhart, "A method for predicting city-wide electricity gains from photovoltaic panels based on LiDAR and GIS data combined with hourly Daysim simulations," *Sol. Energy*, vol. 93, pp. 127–143, 2013.

[188]   E. Paliou, D. Wheatley, and G. Earl, "Three-dimensional visibility analysis of architectural spaces: Iconography and visibility of the wall paintings of Xeste 3 (Late Bronze Age Akrotiri)," *J. Archaeol. Sci.*, vol. 38, no. 2, pp. 375–386, 2011.

[189]   M. Bern and P. Plassmann, "Mesh Generation," *Handb. Comput. Geom.*, pp. 291–332, 2000.

[190]   A. Van Oosterom and J. Strackee, "The Solid Angle of a Plane Triangle," *IEEE Trans. Biomed. Eng.*, vol. BME-30, no. 2, pp. 125–126, Feb. 1983.

[191]   U. Schiefer, H. Wilhelm, and W. Hart, *Clinical neuro-ophthalmology : a practical guide*. Springer, 2007.

[192]   J. Grobbel, J. Dietzsch, C. A. Johnson, R. Vonthein, K. Stingl, R. G. Weleber, and U. Schiefer, "Normal Values for the Full Visual Field, Corrected for Age- and Reaction Time, Using Semiautomated Kinetic Testing on the Octopus 900 Perimeter," *Transl Vis Sci Technol.*, vol. 5, no. 2, p. 2, 2016.

[193]   M. Luckiesh and S. K. Guth, "Brightnesses in visual field at borderline between comfort and discomfort.," *Illum. Eng.*, vol. 44, no. 11, pp. 650–70, Nov. 1949.

[194]   J. A. Jakubiec, "The Use of Visual Comfort Metrics in the Design of Daylit Spaces," MIT, 2014.

[195]   ANSI/IESNA, *IESNA LM-63-02: Standard File Format for the Electronic Transfer of Photometric Data*. 2002, pp. 1–17.

[196]   International Standards Organization (ISO), *ISO 8596:2017(en), Ophthalmic optics — Visual acuity testing — Standard and clinical optotypes and their presentation*. 2017.

[197]   International Council of Ophtalmology, "Visual acuity measurement standard," *Ital. J. Ophthalmol. II*, pp. 1–15, 1988.

[198]   World Health Organisation, "International Classification of Diseases - 10," 1994.

[199]   G. J. Ward, "The RADIANCE Lighting Simulation and Rendering System," in *SIGGRAPH conference*, 1994.

[200]   C. Ratti, "Building form and environmental performance: archetypes, analysis and an arid climate," *Energy Build.*, vol. 35, no. 1, pp. 49–59, Jan. 2003.

[201]   NASA Earth Observatory, "Normalized Difference Vegetation Index (NDVI)," *Measuring Vegetation (NDVI & EVI)*, 2015. [Online]. Available: https://earthobservatory.nasa.gov/Features/MeasuringVegetation/measuring_vegetation_2.php. [Accessed: 09-Apr-2018].

[202]   G. Peronato, E. Rey, and M. Andersen, "3D-modeling of vegetation from LiDAR point clouds and assessment of its impact on façade solar irradiation," in *ISPRS - International Archives of the Photogrammetry, Remote Sensing and Spatial Information Sciences*, 2016, vol. XLII-2/W2, pp. 67–70.

[203]   M. Llobera, "Modeling visibility through vegetation," *Int. J. Geogr. Inf. Sci.*, vol. 21, no. 7, pp. 799–810, 2007.

[204]   C. Magalhaes Carneiro, "Extraction of Urban Environmental Quality Indicators using LiDAR-Based Digital Surface Models," EPFL, 2011.

[205]   R. Perez, R. Seals, and J. Michalsky, "All-weather model for sky luminance distribution—Preliminary configuration and validation," *Sol. Energy*, vol. 50, no. 3, pp. 235–245, Mar. 1993.

[206]   D. Robinson and A. Stone, "Irradiation modelling made simple: the cumulative sky approach and its applications," in *PLEA*, 2004, pp. 19–22.

[207]   G. Ward and I. Ashdown, "Gendaymtx command: Radiance documentation," 2000.

[208]   M. Herrera, S. Natarajan, D. A. Coley, T. Kershaw, A. P. Ramallo-González, M. Eames, D. Fosas, and M. Wood, "A review of current and future weather data for building simulation," *Build. Serv. Eng. Res. Technol.*, vol. 38, no. 5, pp. 602–627, Sep. 2017.

[209]   ASHRAE, "Complete Listing of the 3012 IWEC2 Weather Files," 2015. [Online]. Available: https://www.ashrae.org/File Library/Technical Resources/Bookstore/IWECStationList_1477-RP_Final_Report_20111019-2.pdf. [Accessed: 19-

Apr-2018].

[210] P. R. Tregenza, "Subdivision of the sky hemisphere for luminance measurements," *Light. Res. Technol.*, vol. 19, no. 1, pp. 13–14, Mar. 1987.

[211] F. Biljecki, H. Ledoux, J. Stoter, and G. Vosselman, "The variants of an LOD of a 3D building model and their influence on spatial analyses," *ISPRS J. Photogramm. Remote Sens.*, vol. 116, pp. 42–54, Jun. 2016.

[212] F. Biljecki, H. Ledoux, and J. Stoter, "An improved LOD specification for 3D building models," *Comput. Environ. Urban Syst.*, vol. 59, pp. 25–37, Sep. 2016.

[213] P. Kiefer, I. Giannopoulos, M. Raubal, and A. Duchowski, "Eye tracking for spatial research: Cognition, computation, challenges," *Spat. Cogn. Comput.*, vol. 17, no. 1–2, pp. 1–19, Jan. 2017.

[214] J. Appleton, *The experience of landscape*. London: Wiley, 1975.

[215] *SIA 380/1 L'énergie thermique dans le bâtiment*. Switzerland: SIA, Société Suisse des Ingénieurs et des Architectes, 2009.

[216] SIA, *SIA 380/4 L'énergie électrique dans le bâtiment*. Switzerland: SIA, Société Suisse des Ingénieurs et des Architectes, 2006.

[217] D. Griego, S. Kuliga, M. Bielik, M. Standfest, V. K. Ojha, S. Schneider, R. Koenig, D. Donath, and G. Schmitt, "ESUM Urban Sensing Handbook: Component, Assembly and Operational Guide: Sensor backpack & 360° Videos," 2017.

[218] R. Camponovo, P. Gallinelli, and P. Thomann, "moodCity – Qualifier l'environnement urbain : un outil d'aide à l'urbanisme climatique," in *18th Status-Seminar "Forschen für den Bau im Kontext von Energie und Umwelt,"* 2014, no. September, pp. 1–8.

[219] International Energy Agency IEA, "IEA Task 51 - Solar Energy in Urban Planning." [Online]. Available: http://task51.iea-shc.org/.

[220] Swiss Federal Institute for Materials Science and Technology EMPA and Swiss Federal Insitute for Acquatic Research EAWAG, "NEST – Exploring the Future of Buildings." [Online]. Available: https://www.empa.ch/web/nest/overview.

[221] "SolAce unit at NEST." [Online]. Available: https://www.empa.ch/web/nest/solace.

[222] A. Schüler, C. Roecker, J. Boudaden, P. Oelhafen, and J.-L. Scartezzini, "Potential of quarterwave interference stacks for colored thermal solar collectors," *Sol. Energy*, vol. 79, no. 2, pp. 122–130, Aug. 2005.

[223] M. C. Munari Probst and C. Roecker, "Criteria and policies to master the visual impact of solar systems in urban environments : the LESO-QSV method," *Build. Environ.*, 2018.

[224] G. Lobaccaro, C. Lindkvist, M. Wall, and A. Wyckmans, Eds., *Illustrative Prospective of Solar Energy in Urban Planning*. IEA SHC Task 51, 2017.

[225] M. C. Munari Probst, L. Deschamps, and C. Roecker, "Innovative solar products for architectural integration: a joint IEA tasks 41 and 51 website," in *ISES Eurosun 2014*, 2014, no. September, pp. 16–19.

[226] M. C. Munari Probst, C. Roecker, and L. Deschamps, "Innovative solar products for building integration." [Online]. Available: http://solarintegrationsolutions.org/.

[227] T. Siems, K. Simon, and K. Voss, Eds., *State-of-the-Art of Education on Solar Energy in Urban Planning Part 1 - Approaches and Methods in Education*. IEA SHC Task 51, 2017.

Curriculum Vitae

Personal information

First name / Surname

Pietro Florio
Italian, born June 9th, 1987

Address(es)
🇨🇭 av. de Longemalle 16, 1020 Renens (CH)
🇮🇹 corso Alberto Picco 56, 10131 Torino (IT)

Mobile 🇨🇭 0041 787210057
🇮🇹 0039 3381445104

E-mail(s)
pietro.florio@epfl.ch
pietroflorio@gmail.com

Highlights

- Architectural background enriched with thorough research expertise in Building Physics and Computational Architecture with high communicative and visualization impact
- Practice oriented career, experience in design, construction sites, building energy assessment and certification
- Business development & strategy consultant in the field of social and green economy. Project management
- Experience with policy-making, policy design and policy assessment

Work experience

Dates MAY 2014 →

Position PhD assistant

Employer EPFL – Ecole Polytechnique Fédérale de Lausanne;
LESO-PB – Solar Energy and Building Physics Laboratory
LE 0 02 (Bâtiment LE), Station 18, CH-1015 Lausanne (VD) (Switzerland)

Activities
- Commitment as an **Expert within the Task 51 "Solar Energy and Urban Planning"** of the SHC – Solar Heating and Cooling Program by the IEA – International Energy Agency;
- **Architectural project manager**, NEST SolAce project (EMPA, Swiss Federal Laboratories for Material Science and Technology)
- **Visibility and visual impact assessment** of renewables, architectural integration of solar modules
- **Teaching assistantship in Building Physics**, Solar Energy and Architecture classes for bachelor students in Architecture.

Dates JUNE 2013 - NOVEMBER 2013

Position Research assistant

Employer CSTB – Centre Scientifique et Technique du Bâtiment
Public establishment with industrial and commercial aims under the patronage of the *Ministère de l'Égalité des Territoires et du Logement* and of the *Ministère de l'Écologie, du Développement Durable et de l'Énergie*
14, boulevard Isaac Newton, 77420 Champs-sur-Marne (77) (France)

Activities
- Collaboration with the **French National Energy Poverty Observatory** (ONPE);
- Benchmark of **European public policies** coping the exclusion from the energy supply and the price raise, concerning in particular low incomes (energy poverty);
- International workshops attendance and redaction of a national public report;
- **Research partner** of the project "Against Energy Poverty" in collaboration with **Leroy Merlin Italy** and **Caritas Italy**, to provide low income households with domestic energy saving devices
- **Energy consumptions and energy expenditure models** of a statistical sample of France;

Dates NOVEMBER 2009 - MAY 2013

Position Assistant, designer

Employer Eng. Alessandro Bernini – Engineering firm
via Sassari, 18, 10152 Torino (Italy)

Activities safety in constructions, safety on work places (Decree 81/08); energy saving and certifying (ACE, Decree 192/05 and Regional Law Piemonte 13/07). On-site surveys in the post-event structural tests during the earthquake emergency phase.

Dates	OCTOBER 2010 - MAY 2011
Position	**Assistant, designer**
Employer	<u>Eco Energy Home design studio Eng Giuseppe Dammacco</u> – Engineering firm via Bernardo Vittone, 26, 10023 Chieri (TO) (Italy)
Activities	developing a project of a standard sustainable house
Dates	NOVEMBER 2008 - DECEMBER 2008
Position	**Intern, archivist**
Employer	<u>Archivio Edilizio della Città di Torino (Building Commission Archive of Municipality of Turin)</u> piazza San Giovanni, 5, 10122 Torino (Italy)
Activities	understanding archive complexity and classification, organising files; digital classification of files, search and consultation service.

Education and training

Dates	MAY 2014 - ONGOING
Qualification	Philosophy Doctorate in **Energy**
Institution	EPFL – Ecole Polytechnique Fédérale de Lausanne; EDOC Doctoral School route Cantonale, CH-1015 Lausanne (Switzerland)
Competence	Thesis Title: *Visibility evaluation of solar energy applications in urban sites for architectural integration "criticity" assessment* Supervisors: Jean-Louis Scartezzini, Maria Cristina Munari Probst
Dates	FEBRUARY 2013 - JUNE 2013
Qualification	IFTS - **Green Building High Technician – HVAC System Specialist**
Institution	ENGIM Piemonte corso Palestro 14, 10122 Torino (Italy)
Competence	Post-graduate diploma
Dates	SEPTEMBER 2009 - SEPTEMBER 2012
Qualification	Master of Science in **Architecture**
Institution	Politecnico di Torino, Facoltà di Architettura II viale Mattioli, 39, 10125 Torino (Italy)
Competence	Thesis Title: *Energy retrofit of school buildings through Building Automation Technologies* Supervisors: Valentina Serra, Marco Filippi, Enrico Fabrizio Grade: **110/110** Italian national context participation "Think Green, be Efficient" by Schneider Electric ® Attendance to the "13th International Conference of the International Building Performance Simulation Association – IBPSA 2013"
Dates	SEPTEMBER 2006 -JULY 10
Qualification	Bachelor of Science in **Architecture for design process**
Institution	Politecnico di Torino, Facoltà di Architettura II viale Mattioli, 39, 10125 Torino (Italy)
Competence	*French castles during the Renaissance period. A case study: Gaillon* Supervisor: Mauro Luca De Bernardi Grade: **102/110**
Dates	FEBRUARY 2009 - JULY 2009
Qualification	LLP programme **Erasmus**
Institution	ENSAN - Ecole Nationale Superièure d'Architecture de Normandie 27, rue Lucien Fromage, 76161 Darnétal (France)
Dates	SEPTEMBER 2001 - JULY 2006
Qualification	**Scientific Diploma**
Institution	Liceo Scientifico Statale Piero Gobetti (High School Piero Gobetti) via Maria Vittoria 39bis, 10123 Torino (Italy)
Competence	Grade: 98/100

	Publications
Dates	Forthcoming
Title	**Matching visual impact, solar energy production potential and energy system optimization for an enhanced solar integration: an experience with a novel pre-design tool**
Authors	Florio, P; Coccolo, S; Perera, A.T.D; Scartezzini J.-L. (LESO-PB, Laboratoire d'Energie Solaire et Physique du Bâtiment, EPFL)
Venue	PLEA 2018, 10-12 December 2018 – Hong Kong
Dates	Forthcoming
Title	**Assessing visibility in multi-scale urban planning: a contribution to a method enhancing social acceptability of solar energy in cities**
Authors	Florio, P; Roecker, C.; Munari Probst, M.C.; Schüler, A.; Scartezzini, J.-L. (LESO-PB, Laboratoire d'Energie Solaire et Physique du Bâtiment, EPFL)
Dates	SEPTEMBER 2017
Title	**Visual prominence vs architectural sensitivity of solar applications in existing urban are-as: An experience with web-shared photos**
Authors	Florio, P.; Roecker, C.; Munari Probst, M.C.; Schüler, A.; Scartezzini, J.-L. (LESO-PB, Laboratoire d'Energie Solaire et Physique du Bâtiment, EPFL)
Journal	Energy Procedia 2017 vol. 122, proc. of CISBAT 2017, 6-8 September 2017 – Lausanne (Switzerland)
Dates	DECEMBER 2016
Title	**Visibility of Building Exposed Surfaces for the Potential Application of Solar Panels: A Photometric Model**
Authors	Florio, P.; Roecker, C.; Munari Probst, M.C.; Scartezzini, J.-L. (LESO-PB, Laboratoire d'Energie Solaire et Physique du Bâtiment, EPFL)
Venue	Eurographics Workshop on Urban Data Modelling and Visualisation, 8 December 2016 – Liège (Belgium)
Dates	FEBRUARY 2015
Title	**Estimation of the Energy Performance Certificate of a housing stock characterised via qualitative variables through a typology approach-based model: a fuel poverty evaluation tool**
Authors	Florio, P.; Teissier, O. (CSTB – Centre Scientifique et Technique du Bâtiment, DESH – Département d'Economie et de Sciences Humaines)
Journal	Energy & Buildings vol. 89, 15
Dates	OCTOBER 2013
Title	**Smart schools: estimation of the obtainable energy savings**
Authors	Florio, P.; Cantamessa, P.; Monetti, V.; Becchio, C., Filippi, M. (DENERG – Dipartimento di Energia, Politecnico di Torino); Fabrizio, E. (DISAFA – Dipartimento di Scienze Agrarie, Forestali e Alimentari, Università di Torino)
Venue	AICARR (Associazione Italiana del Condizionamento dell'Aria, Riscaldamento e Refrigerazione), 31° convegno nazionale di Bologna, 17 October 2013 - Bologna - SAIE BolognaFiere II
Dates	AUGUST 2013
Title	**Dynamic simulation of BACS (Building Automation and Control Systems) for the energy retrofitting of a secondary school**
Authors	Becchio, C.; Cantamessa, P.; Florio, P.; Monetti, V.; Filippi, M. (DENERG – Dipartimento di Energia, Politecnico di Torino); Fabrizio, E. (DISAFA – Dipartimento di Scienze Agrarie, Forestali e Alimentari, Università di Torino)
Venue	IBPSA (International Building Performance Simulation Association) 13th Building Simulation International Conference, 25-28 August 2013 - Chambery (France)

Contributions to **IEA SHC Task 51 Reports**	
Dates	Forthcoming
Title	**Approaches, Methods and Tools for Solar Energy in Urban Planning**
Editors	Dahlberg, J.; Lundgren, M.
Deliverable	DB 4, IEA SHC Task 51
Dates	2017
Title	**State-of-the-Art of Education on Solar Energy in Urban Planning Part 1 - Approaches and Methods in Education**
Editors	Siems, T. ; Simon, K.; Voss, K.
Deliverable	DD 1, IEA SHC Task 51
Dates	2017
Title	**Illustrative Prospective of Solar Energy in Urban Planning**
Editors	Lobaccaro, G.; Lindkvist, C.; Wall, M.; Wyckmans, A.
Deliverable	DC 1, IEA SHC Task 51

Volunteering	

- **Peer reviewer** of Elsevier Solar Energy J., Sustainable Cities and Societies J.
- **Scout leader** at Italian Scout Association AGESCI
- **Volunteer, A/V technician** at Arsenale della Pace – SerMiG
- **Volunteer** at XX Winter Olympics – Torino 2006

Honors and Awards	

- **Scholarship Postgrad Talent Award 2013 – CRT Foundation**

Personal skills and competences	

Mother tongue(s) — **Italian**

Other languages, Self-assessment
European level (*)

	Understanding			Speaking				Writing	
	Listening		Reading		Spoken interaction		Spoken production		
English	C1	Proficient user	C2	Proficient user	B2	Proficient user	C1	Proficient user	C1	Proficient user
French	C2	Proficient user	C2	Proficient user	C1	Proficient user	C1	Proficient user	C1	Proficient user
German	A2	Basic user	A2	Basic user	A2	Basic user	A2	Basic user	A2	Basic user

(*) Common European Framework of Reference (CEF) level

Social skills and competences — team spirit established over 6 years of scouting experience and through several years of volunteering activities in social field. Work in contact with weak social groups (immigrants, indigents): two years of experience managing a dormitory shelter in a volunteer staff. Participation in a survey on the homeless population promoted by the Municipality of Turin for statistical purposes.

Organisational skills and competences — organisation and planning attitude; **teaching experience** at undergraduate level; good logistical skills.

Technical skills and competences — strategies for **green design**, **energy analysis of buildings** (certification, assessment, audit); planning at all levels; **international policy-making** elements concerning energy and consumer protection; **fundamentals of statistical analysis**; principles of degradation analysis of buildings, principles of structural design. Design and stage construction for live orchestral performances; assisting the management of an audio mixing console.

Computer skills and competences

- installation of hardware components of a desktop PC; advanced management of a **Windows PC** (configuration, installation, assembly, troubleshooting);
- professional knowledge of **CAD software and 3D rendering** (Autodesk Autocad, Autodesk Revit Architecture, Autodesk 3ds, Graphisoft Archicad, SketchUp, Rhino and Grasshopper);
- advanced knowledge of **energy calculation and raytracing software** (DOE EnergyPlus, DesignBuilder, NREL Openstudio, Autodesk Ecotect, DIVA with Radiance, Logical Termolog EPIX 2, LESOSAI).
- advanced knowledge of **Adobe Creative Suite CS5** (especially Photoshop, Illustrator, InDesign);
- advanced use for research purposes of **parametric design software** (Rhino Grasshopper) and **GIS tools** (ArcGIS, ArcMap, ArcScene, QGis);
- basic user in **statistical analysis software** (STATA, SAS, R) and **python programming**;
- configuration of a **simple computer network** with routers and gateways; advanced knowledge of **Microsoft Office** suite;
- practice in surfing the **internet** and in managing its features (configuration of browsers, Internet Explorer, Mozilla Firefox, Outlook Express, FTP, P2P)

Artistic skills and competences — elementary reading of the staff sheet music, **acoustic guitar playing** at professional level, participation in the guitar band "Guitars for Peace", with a self-produced 8 tracks CD and various live performances; interest for philosophical and theological issues

Driving licence — **B (cars)**

I authorize the processing of any personal data contained in my curriculum vitae.